The Effects of CPAP Tube Reverse Flow

by

Chutu Li

A thesis submitted to
Auckland University of Technology
in partial fulfilment of the requirements for the degree of
Master of Engineering (ME)

November 2008

School of Engineering

Primary Supervisor: Professor Ahmed Al-Jumaily

In memory of my grandparents,

Lingzhi Li and Jiezhi Zeng

Acknowledgement

Abstract

CPAP is the most common treatment for moderate to severe sleep apnea in adults. Despite its efficacy, patients' safety, comfort and compliance are issues to be considered and improved in CPAP design. The issues include condensation, carbon dioxide in inhaled air, humidity and temperature of inhaled air.

When a CPAP user breaths deeply, there will be some air not fully expelled and may be driven back into the heated air delivery tube (HADT). An interest has existed in what impacts this so called reverse flow may bring about to the CPAP use. The main objectives of this research are to quantify the reverse flow and its influence on carbon dioxide re-breathing, delivered humidity to the patient and condensation in the HADT.

Within this thesis, two computer models of the CPAP system have been constructed on Simulink™ in the Matlab™ environment. One is about the CPAP fluid dynamic performance and carbon dioxide re-breathing and the other is on thermodynamic performance. The models can predict the dynamic behaviour of the CPAP machine. They are able to mimic the breath induced airflow fluctuation, and flow direction changes over wide real working ranges of ambient conditions, settings and coefficients. These models can be used for future analysis, development, improvement and design of the machine.

The fluid dynamic and thermodynamic models were experimentally validated and they have proved to be valuable tool in the work.

The main conclusions drawn from this study are:

- Reverse flow increases when breath load increases and pressure setting decreases.
- Reverse flow does not definitely add exhaled air to the next inhalation unless the reverse flow is relatively too much.
- Mask capacity does not influence the reverse flow.
- The exhaled air re-breathed is mainly due to that stays in the mask, therefore larger mask capacity increases the exhaled air re-breath and the percentage of exhaled air in next inhalation drops when the breath load increases.

- Deep breathing does not significantly change the total evaporation in chamber.

- When deep breathing induced reverse flow occurs, condensation occurs or worsens in the HADT near the mask. This happens only when the humidity of the airflow from the CPAP is much lower than that of the exhaled air and the tube wall temperature is low enough for condensation to occur.

- The deep breathing and reverse flow do not significantly influence the average inhaled air temperature.

- The overall specific humidity in inhaled air is lower under deep breathing.

- Mask capacity does not influence the thermal conditions in the HADT and the inhaled air specific humidity. Also the mask capacity does not significantly influences the inhaled air temperature.

Table of Contents

List of Figures

List of Tables

Statement of Originality

"I hereby declare that this submission is my own work and that, to the best of my knowledge and belief, it contains no material previously published or written by another person nor material which to a substantial extent has been accepted for the qualification of any other degree or diploma of a university or other institution of higher learning, except where due acknowledgment is made in the acknowledgments."

……………………….. (signed)

…………………….. (date)

Nomenclature

Symbol	Meaning of the symbol	Unit
A	Area	m^2
A_{BH}	Smallest cross sectional area in each bias vent hole	m^2
A_{Bw}	Interface area between chamber base and water	m^2
A_{C1i}	Wall 1 inner cylindrical surface area	m^2
A_{C23oR}	The sum of 3/4 of wall 2 area and full wall 3 area	m^2
A_{CB}	Area of the chamber base	m^2
A_{Co}	Connecting opening cross sectional area	m^2
A_{Dcs}	Cross sectional area at the connecting duct inlet and outlet	m^2
A_{Mi}	Mask inner surface area	m^2
A_R	The radiation area on chamber wall 1 outer surface	m^2
A_{Tcs}	Cross sectional area of HADT	m^2
A_{Tli}	HADT internal surface area for each lump	m^2
A_{Toc}	Convectional area of HADT lump outer surface	m^2
A_{ws}	Water surface area	m^2
c	Specific heat	$J/(kg \cdot K)$
c_C	Specific heat of chamber wall material (High-density Polyethylene)	$J/(kg \cdot K)$
c_{Ca}	Average specific heat of chamber air	$J/(kg \cdot K)$
c_{Da}	Average specific heat of airflow in connecting duct	$J/(kg \cdot K)$
c_{Ma}	specific heat of air in the mask	$J/(kg \cdot K)$

c_{MW}	Specific heat of mask wall material (Polycarbonate)	$J/(kg \cdot K)$
c_T	Specific heat of HADT wall material (Polyethylene)	$J/(kg \cdot K)$
c_{Ta}	specific heat of air in HADT	$J/(kg \cdot K)$
c_{Tan}	specific heat of the air in lump n of HADT	$J/(kg \cdot K)$
c_w	specific heat of water	$J/(kg \cdot K)$
C_d	Discharge coefficient for each bias vent hole	Decimal
C_{Caiv}	Absolute humidity at the chamber inlet	kg/m^3
C_{Mav}	Absolute humidity of mask inlet	kg/m^3
C_{Msv}	Saturated absolute humidity level at mask inner surface temperature	kg/m^3
C_{sv}	Absolute humidity of saturated air at water surface interface film	kg/m^3
C_{Tav}	Absolute humidity of airflow in a HADT lump	kg/m^3
C_{Tsv}	Saturated Absolute humidity level at a HADT lump wall temperature	kg/m^3
C_v	Absolute humidity	kg/m^3
C_{Erb}	Percentage of the exhaled air re-breathed within a total inhalation	Percentage
C_{El30}	Exhaled air concentration in flow from lump 30 of the HADT	Decimal
C_{ME}	Concentration of exhaled air in the mask	Decimal
C_{MEet}	Concentration of exhaled air during exhalation phase	Decimal
C_{MEiO}	Concentration of exhaled air in the mask at the beginning of inhalation phase	Decimal
C_{MEit}	Concentration of exhaled air during inhalation phase	Decimal

C_{MFeO}	Concentration of fresh air in the mask at the beginning of exhalation phase	Decimal
C_{MFet}	Concentration of fresh air during exhalation phase	Decimal
C_O	Initial concentration of the former fluid in a container	Decimal
C_t	Former fluid concentration dynamically varying with time in the container	Decimal
d	Specific humidity of moist air	Decimal
d_{Ca}	Specific humidity of air in humidifier chamber	Decimal
d_{inh}	Overall (average) specific humidity within a total inhalation	Decimal
d_M	Specific humidity of air in the mask	Decimal
d_∞	Specific humidity of ambient air (also that of the inlet to chamber)	Decimal
D	Diameter	m
D_D	Connecting duct diameter at the connecting duct inlet	m
D_{Ti}	HADT inner diameter	m
D_{RF}	Distance of reverse flow	m
D_{wa}	Mass diffusivity of water molecules from fluid water into air	m
f	Friction factor of the conduit inner surface	Decimal
f_D	Equivalent friction factor on the duct inner surface	Decimal
f_T	Friction factor on HADT inner surface	Decimal
g	Gravitational acceleration	m/s^2
Gr	Grashof number	
Gr_{C2i}	Grashof number at chamber wall 2 inner surface	
h	Heat convection coefficient	$W/(m^2 \cdot K)$

h_{fg}	Latent heat of evaporation	J/kg
h	Specific enthalpy of a gaseous mixture	J/kg
h_i	Specific enthalpy of individual component in a gaseous mixture	J/kg
h_{va}	Thermal enthalpy brought in by evaporated water vapour	J/kg
H	Height of a surface	m
ΔH	Increased enthalpy gained by air flowing through the blower	J/kg
k	Thermal conductivity	$W/(m \cdot K)$
k_{Al}	Thermal conductivity of Aluminium	$W/(m \cdot K)$
k_C	Chamber wall material thermal conductivity (High-density polyethylene)	$W/(m \cdot K)$
k_{ma}	Thermal conductivity of moist air	$W/(m \cdot K)$
k_w	Water thermal conductivity	$W/(m \cdot K)$
k_{ev}	Water surface mass convection (evaporation) coefficient	m/s
k_{evn}	Natural mass convection (evaporation) coefficients	m/s
k_{evf}	Forced mass convection (evaporation) coefficients	m/s
k_{ec}	condensation-to-evaporation coefficient	Decimal
l_{CB}	Thickness of the Chamber base	m
l_{C1i}	Wall 1 height (water height level)	m
L_D	Connecting duct length	m
L_T	HADT length	m
l_{Tl}	HADT lump length	m
m	Mass	kg
m_{C1}	Mass of chamber wall 1	kg

m_{C23}	Mass of wall 2 and 3 together	kg
m_{Ca}	Average air mass in chamber	kg
m_{cv}	Fluid mass of a controlled volume	kg
m_{Cw}	Mass of water in humidifier chamber	kg
m_{store}	Air mass in a container	kg
m_i	Mass of individual component in the mixture	kg
m_{Ma}	Mass of air in the mask	kg
m_{MW}	Mass of mask wall	kg
m_{Mec}	Net condensation or evaporation within a breath cycle in the mask	kg
m_{MecN}	Total amount of condensation occurred within a breath cycle in the mask (the negative part of $\dot{m}_{Mec}$)	kg
m_{MecP}	Total amount of evaporation or evaporation potentiality within a breath cycle in the mask (the positive part of $\dot{m}_{Mec}$)	kg
m_{Tlec}	Net condensation or evaporation within a breath cycle in an HADT lump	kg
m_{TlecN}	Total amount of condensation occurred within a breath cycle in an HADT lump(the negative part of $\dot{m}_{Tlec}$)	kg
m_{TlecP}	Total amount of evaporation or evaporation potentiality within a breath cycle in an HADT lump (the positive part of $\dot{m}_{Tlec}$)	kg
m_{Tl}	Mass of one lump HADT wall	kg
m_{Tla}	Air mass in one HADT lump	kg
M_a	Molar mass of air	kg
$\dot{m}_C$	Mass flow rate in chamber	kg/s

$\dot{m}_{BV}$	Bias vent mass flow rate	*kg/s*
$\dot{m}_{cndns}$	condensation rate	*kg/s*
$\dot{m}_{D}$	Air mass flow rate through connecting duct	*kg/s*
$\dot{m}_{ev}$	Evaporation rate on chamber water surface	*kg/s*
$\dot{m}_{in}$	Mass flow rate toward a container	*kg/s*
$\dot{m}_{out}$	Mass flow rate away from a container	*kg/s*
$\dot{m}_{Mec}$	Mask inner surface condensation or evaporation rate	*kg/s*
$\dot{m}_{Tlec}$	HADT lump inner surface condensation or evaporation rate	*kg/s*
$\dot{m}_{P}$	Patient's respiratory mass flow rate	*kg/s*
$\dot{m}_{T}$	Air mass flow rate in HADT	*kg/s*
n_{BH}	Number of bias vent holes	
Nu	Nusselt number	
Nu_{Bwn}	Natural convection Nusselt number from chamber base to water	
Nu_{C2ni}	Natural convection Nusselt number at the inner surface of wall 2	
Nu_{C2fi}	Forced convection Nusselt number at the inner surface of wall 2	
Nu_{C2mi}	mixed convection Nusselt number at chamber wall 2 inner surface	
Nu_{C3ni}	mixed convection Nusselt number at chamber wall 3 inner surface	
Nu_{C2no}	Natural convection Nusselt number at chamber wall 2 outer surface	
Nu_{C3no}	Natural convection Nusselt number at chamber wall 3 outer surface	

Nu_{Cp}	Nusselt number for chamber water surface parallel flow	
Nu_{dir}	Nusselt number for direct impact on chamber water surface	
Nu_{Ti}	Forced convectional Nusselt number at HADT inner surface	
Nu_{To}	Nusselt number of natural convection on HADT outer surface	
Nu_{wsn}	Chamber water surface natural convection Nusselt number	
Nu_{wsf}	Total water surface forced convection Nusselt number	
Nu_{wsm}	Water surface mixed convection Nusselt number	
P	Pressure	
P_o	Standard atmospheric air pressure (101325 Pascals)	Pascal
P_{Ao}	Pressure at air delivery unit outlet	Pascal
P_C	Pressure in chamber	Pascal
P_M	Pressure in the mask	Pascal
P_{set}	CPAP pressure setting	cmH2O
ΔP	Pressure drop or pressure gap	Pascal
ΔP_{mn}	minor pressure drop	Pascal
ΔP_{total}	Total pressure drop along the whole tubing system with frictional and minor losses included	Pascal
$\Pr$	Prandtl number	
$\Pr_a$	Prandtl number of air	
$\Pr_w$	Prandtl number of water	
$\dot{q}$	Volumetric flow rate	m^3/s
$\dot{q}_C$	Volumetric chamber air flow rate	m^3/s
$\dot{q}_P$	Patient's respiratory volumetric flow rate	m^3/s

$\dot{Q}_{Bw}$	Heat flow from heating plate to water through chamber base	W
$\dot{Q}_{C1i}$	Heat flow rate from the chamber water to wall 1 inner surface	W
$\dot{Q}_{C1o}$	Heat flow rate to ambient on chamber wall 1 outer surface	W
$\dot{Q}_{C1oR}$	Radiation heat transfer on chamber wall 1 outer surface	W
$\dot{Q}_{C1st}$	Heat storage in chamber wall 1	W
$\dot{Q}_{C23i}$	Heat flow rate from chamber air to wall 2 and 3	W
$\dot{Q}_{C23o}$	Heat dissipation rate to the ambient through wall 2 and 3 outer surfaces	W
$\dot{Q}_{C23St}$	Heat storage in wall 2 and 3	W
$\dot{Q}_{Cai}$	Heat energy brought into chamber by inlet	W
$\dot{Q}_{Cao}$	Heat energy brought away from chamber by outlet	W
$\dot{Q}_{CaSt}$	Heat storage in the chamber air	W
$\dot{Q}_{CwSt}$	Heat storage in chamber water	W
$\dot{Q}_{ev}$	Latent heat transfer rate removed from water by evaporation	W
$\dot{Q}_{HE}$	Heat flow from heating element to heating plate top surface	W
$\dot{Q}_{Hp\infty}$	Total heat dissipation from heating plate rim	W
$\dot{Q}_{Mast}$	Heat storage in the in-mask air	W
$\dot{Q}_{Mi}$	Heat energy brought into the mask by inlet	W
$\dot{Q}_{Mic}$	Convection heat transfer rate on mask inner surfaces	W
$\dot{Q}_{Mo}$	Heat energy brought away from the mask by outlet	W
$\dot{Q}_{Moc}$	Convectional heat transfer rate on mask outer surfaces	W

$\dot{Q}_{Mor}$	Radiation heat transfer rate on mask outer surfaces	W
$\dot{Q}_{Mwst}$	Heat storage in mask wall	W
$\dot{Q}_{Tastn}$	Heat storage in the air at HADT lump n	W
$\dot{Q}_{Ticn}$	convectional heat flow at HADT lump n inner surface	W
$\dot{Q}_{Tin}$	Heat energy brought into lump n by inlet	W
$\dot{Q}_{Thn}$	Thermal energy provided by HADT heating to each lump	W
$\dot{Q}_{Tocn}$	convectional heat flow at HADT lump n outer surface	W
$\dot{Q}_{Ton}$	Heat energy brought away from an HADT lump by outlet	W
$\dot{Q}_{Torn}$	Radiation heat flow at HADT lump n outer surface	W
$\dot{Q}_{TWstn}$	Heat storage in the wall of HADT lump n	W
$\dot{Q}_{va}$	The sharable heat energy carried into chamber air by evaporated water molecules	W
$\dot{Q}_{wa}$	Convectional heat flow rate from chamber water into chamber air	W
r_{C1o}	Chamber wall 1 inner average radius	m
r_{C1i}	Chamber wall 1 outer average radius	m
R_{ugc}	Universal gas constant (8.31 $J/K{\cdot}mole$)	
Re	Reynolds number	
Re_{C2i}	Reynolds number at chamber wall 2 inner surface	
Re_{Ti}	Reynolds number of HADT flow	
Ra	Rayleigh number	
Ra_w	Rayleigh number of water	
Ra_{wsa}	Rayleigh number of air on water surface	

Ra_{To}	Rayleigh number on HADT outer surface	
R	Thermal resistance	K/W
R_{Bwn}	Chamber base-water interface thermal resistance	K/W
R_{C1i}	Natural convection thermal resistance on chamber wall 1 inner surface	K/W
R_{C1cyl}	conductive resistance through the cylindrical wall 1 of the chamber	K/W
R_{C1o}	Total thermal resistance at the wall 1 outer surface	K/W
R_{C1oC}	Convectional thermal resistance on wall 1 outer surface	K/W
R_{C1oR}	Radiation thermal resistance on wall 1 outer surface	K/W
R_{C23i}	Mixed convection thermal resistance on wall 2 and 3 inner surface	K/W
R_{C2cyl}	conductive resistance through the cylindrical wall 2 of the chamber	K/W
R_{C3}	conductive resistance through chamber wall 3	K/W
R_{C23}	conductive thermal resistance through chamber wall 2 and wall 3	K/W
R_{C23no}	natural convection thermal resistance on wall 2 and wall 3 outer surfaces	K/W
R_{C23R}	radiation thermal resistance on wall 2 and wall 3 outer surfaces	K/W
R_{C23o}	Total thermal resistance on wall 2 and wall 3 outer surfaces	K/W
R_{HS}	Resistance from ceramic to heating plate outer surface	K/W
R_{Hpw}	Total thermal resistance from heating plate top to chamber water	K/W
R_{ws}	Convection thermal resistance on water surface	K/W

R_{Mic}	Mask inner surface convectional thermal resistance	K/W
R_{Moc}	Convectional thermal resistance on the mask outer surface	K/W
R_{Ticn}	Forced convectional thermal resistance at HADT lump inner surface	K/W
R_{Toc}	HADT lump outer surface natural convection resistance	K/W
R_{Torn}	HADT lump outer surface radiation thermal resistance	K/W
s	Distance the air flows over	m
Sc_a	Schmidt number for air	
t_l	Varying transport delay for air flowing through an HADT lump	s
T^*	Temperature	$°C$ or K
T_o	A specific standard temperature for diffusivity calculation (256 K)	
T_f	Film temperature	$°C$
T_s	Surface temperature	$°C$
T_{fl}	Fluid temperature	$°C$
T_{DewPt}	dew point	$°C$
T_∞	Ambient temperature	$°C$
T_w	Chamber water temperature	$°C$
ΔT_{ADUa}	Air temperature increase after flowing through air delivery unit	$°C$
T_{C1}	Chamber wall 1 temperature	$°C$
T_{C1i}	Chamber wall 1 inner surface temperature	$°C$
T_{C1o}	Chamber wall 1 outer surface temperature	$°C$ or K

T_{Ca}	Chamber air temperature	$°C$
T_{Cai}	Chamber inlet air temperature	$°C$
T_{CBu}	Chamber base upper surface temperature	$°C$
T_{C23}	Temperature of chamber wall 2 and 3	$°C$
T_{C23i}	Temperature of chamber wall 2 and 3 inner surface	$°C$
T_{C23o}	Temperature of chamber wall 2 and 3 outer surface	$°C$ or K
T_{HE}	Heating element temperature (also its setting temperature)	$°C$
T_{Hp}	Heating plate outer and upper surface temperature	$°C$
T_{Ma}	Air temperature in the mask	$°C$
T_{Mi}	Mask inlet air temperature	$°C$
T_{MW}	Mask wall temperature	$°C$
T_{Tan}	Air temperature in lump n	$°C$
$T_{Ta(n-1)}$	Air temperature in lump n-1	$°C$
T_{TWn}	HADT wall temperature of lump n	$°C$
T_{inh}	average temperature of inhaled air	$°C$
u	Fluid flow velocity	m/s
u_D	Air flow velocity at the connecting duct inlet and outlet (both have same diameter)	m/s
u_C	Characteristic velocity on chamber water surface and inner surfaces	m/s
u_T	Air flow velocity in HADT	m/s
$\tilde{u}(t)$	fluctuating Air flow velocity in HADT for transport delay calculation	m/s
u_{MW}	Characteristic airflow velocity over mask inner surfaces	m/s

V	Capacity of the container	m^3
V_{Ca}	Chamber air capacity	m^3
V_{Ma}	Capacity of the mask	m^3
V_{Tl}	Internal capacity of a tube lump (also the volume of air in this lump)	m^3
w_{nose}	Average width of human nose	m
w_{P1i}	Inner width of mask triangular plate	m
β	Volumetric expansion coefficient of fluid	$1/K$
β_a	Volumetric expansion coefficient of air	$1/K$
β_w	Volumetric expansion coefficient of water	$1/K$
δ	Characteristic length	m
δ_{Bw}	Characteristic length	m
δ_{C1}	Wall 1 characteristic length (wall 1 height)	m
δ_{ws}	Characteristic length of water surface	m
δ_{Ti}	Characteristic length	m
δ_{To}	HADT outer surface characteristic length	m
ε	Emissivity of the material	Decimal
$\lambda_n(t)$	Airflow property fluctuation at lump n	
$\lambda_{n-1}(t)$	Airflow property fluctuation at lump n-1	
$\lambda_1(t)$	Airflow property fluctuation at lump 1	
$\lambda_{30}(t)$	Airflow property fluctuation at lump 30	
$\lambda_C(t)$	Airflow's property fluctuation in chamber	
$\lambda_M(t)$	Airflow's property fluctuation in the mask	

ν	Kinetic viscosity of fluid	m^2/s
ν_a	Kinetic viscosity of air	m^2/s
ν_w	Kinetic viscosity of water	m^2/s
ρ	Density of fluid	kg/m^3
ρ_{Da}	Average air density in connecting duct	kg/m^3
ρ_{Ma}	Average air density in the mask	kg/m^3
ρ_{Ta}	Average air density in HADT	kg/m^3
σ	Stefan-Boltzmann constant $(5.67 \times 10\text{-}8 W/m^2 \cdot K^4)$	

Chapter 1 Introduction

1.1 Background

About one third of human being's life is spent in sleeping. A good sleep can help people refresh from their awake-time tiredness physically, mentally and emotionally. It increases people's energy level and reduces people's feeling of depression [1]. However, world widely, hundreds of millions of people are suffering from sleep disorder problems. These sleep disorders include sleep apnea, narcolepsy and various forms of insomnia [2].

Sleep apnea is a sleep disorder in which people repeatedly stop breathing during sleep. The stop may last for more than 10 seconds [3]. Sleep apnea can be categorized as central sleep apnea, obstructive sleep apnea and mixed apnea which is a combination of the two [2]. Obstructive sleep apnea (OSA) is caused by muscle relaxation during sleep (see Figure 1.1).
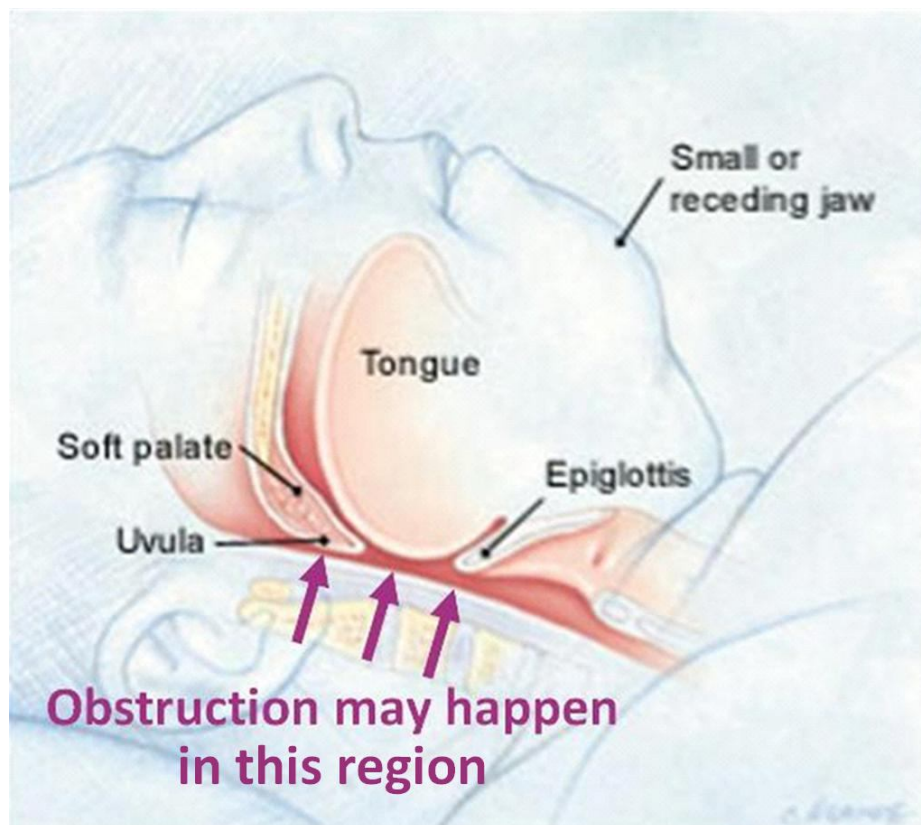
Figure 1.1 Obstructive sleep apnea [4]

When such relaxation happens somewhere from the soft palate, uvula to trachea, breathing can be obstructed. Central sleep apnea is related to the hypo-function of the central nervous system. Central sleep apnea is caused by the muscles controlling breathing fail to do so because they either do not get signal from brain or the brain does not send signal to them, or the signal gets interrupted. In this case, the airway may stay open, but the diaphragm and chest muscles stop working, thus normal breathing stops. The most common sleep apnea is the obstructive sleep apnea. When OSA happens, the muscles of the diaphragm and chest work harder to overcome the extra friction in the upper airway. Such effort may wake up the sufferer and makes sleeping of low-quality or even totally deprived [5-7].

When breathing stops, the blood Oxygen level decreases and the heart needs to work harder for Oxygen supply. Blood pressure rises and sometimes heart beats irregularly which may cause cardiovascular problems and even deaths [6]. Poor sleep is also found to cause increase traffic accidents [5-7].

1.2 OSA Treatments

Obstructive sleep apnea can be alleviated by weight loss and be treated by surgery, oral appliances (mechanical devices inserted into the mouth) and a breathing-assistance device [8]. Types of these treatments are reviewed below.

1.2.1 Oral Appliances

Two kinds of appliances are used for the treatment.

A. Mandibular Repositioning Device (MRD)

Figure 1.2 Mandibular repositioning device[9]

The MRD is worn in user's mouth while sleeping and pulls the lower jaw forward thus moves the base of the tongue forward and allows a wider space in the airway and behind the soft palate so to remove or alleviate the obstruction [10].

B. Tongue Retaining Device (TRD)

Figure 1.3 tongue retaining device[10]

This Tongue Retaining Device uses a flexible polyvinyl material fitting to the user's teeth and dental arches and the tongue is held forward by the negative pressure created in the vacuum bulb on the front of the appliance. This prevents the tongue from collapsing the airway [10].

1.2.2 Surgeries

A. Uvulopalatopharyngoplasty (UPPP) surgery

Uvulopalatopharyngoplasty (UPPP) is an surgical operation that removes excess tissue such as uvula, soft palate, Excess throat tissue, tonsils, and adenoids in the throat to make the airway wider. UPPP may stop snoring, but apnea episodes may continue [11].

B. Laser-Assisted Uvulaplasty (LAUP)

Laser-assisted uvulopalatoplasty (LAUP) is a procedure using lasers to execute surgery for those with mild sleep-related breathing disorders such as loud, habitual snoring, upper airway resistance syndrome, mild obstructive sleep apnea. It is reported that the effecting rate of LAUP for treating sleep apnea is not high. The American Academy of Sleep Medicine has not approved LAUP for treating sleep apnea [12].

C. Nasal Surgery

Nasal surgery is a procedure reducing the turbinate size, correcting the deviated septum or enlarging the nasal valve so to improve nasal breathing. However nasal surgery alone usually does not reach significant achievement in treating moderate to severe obstructive sleep apnea. Nasal surgery is sometimes used to enhance a patient's tolerance toward CPAP therapy [13].

D. Jaw Surgery

Jaw surgery is the most invasive surgical procedure used to treat obstructive sleep apnea. The surgical procedure may be limited to pulling the tongue forward (genioplasty). An extensive procedure may need moving both the upper jaw and/or lower jaw forward [4]. In severe cases of OSA, this treatment has a success rate of over 90%. [14].

1.2.3 Breathing-Assistance Devices

A. Continuous positive airway pressure (CPAP)

CPAP (Figure 1.4) is a machine firstly pioneered in treating OSA in early 1980s [15] and is now the most common treatment for moderate to severe sleep apnea in adults [16]. It usually consists of a blower (air pressure generator), a humidifier, an air delivery tube and a mask. There should be bias vent holes on the mask base or near the mask for expelling the exhaled air so to make sure air received by the patient is fresh. The machine provides continuous pressurized air flow from its blower (air delivery unit) into the OSA patient's upper airway pneumatically splinting the OSA patient's airway open [17, 18] (Figure 1.6). The air pressure should be adjusted to be just enough to avoid patient's airway from becoming narrowed or blocked [16].

Figure 1.4 CPAP machine
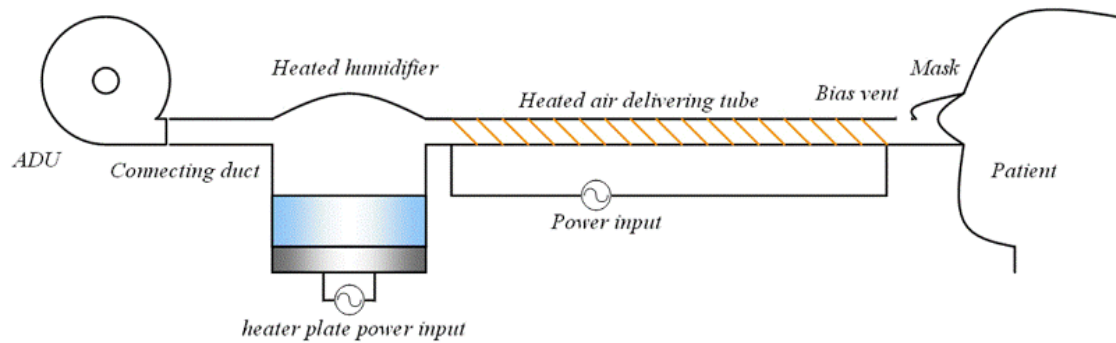
Figure 1.5 Schematic diagram of a CPAP system in use [19]
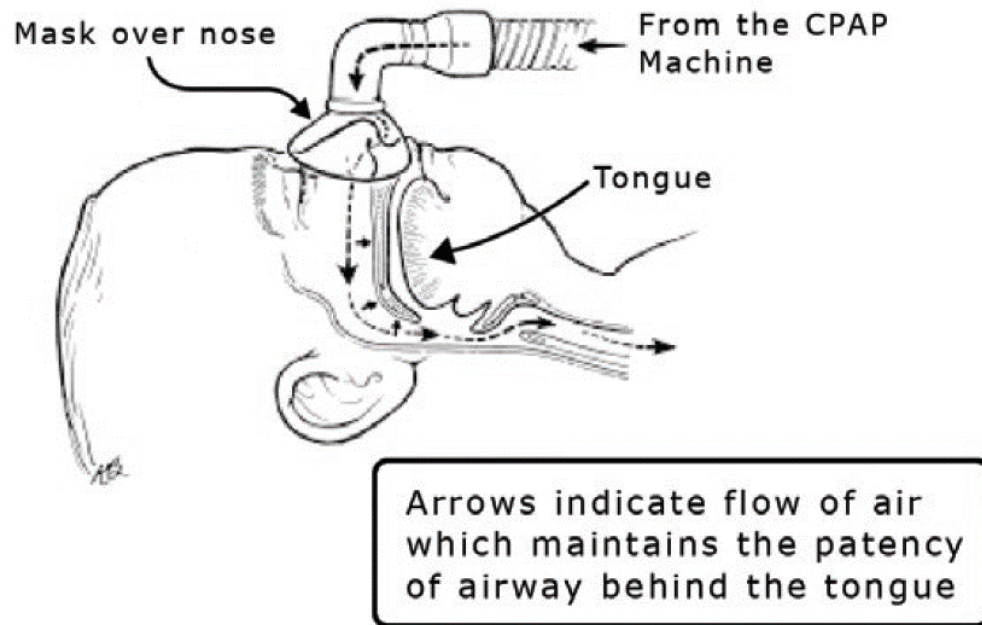
Figure 1.6 CPAP treatment of sleep apnea[20]

B. Bi-level positive airway pressure (Bi-PAP)

Bi-PAP was introduced into use in the 1990s. A problem with CPAP is that the patient has to exhale against the extra pressure. However, with Bi-PAP, pressure can be set at a higher level for inhalation and lower for exhalation. This is helpful for the patient's exhalation and makes it easier for compliance. Bi-PAP is more expensive than CPAP [21].

C. A-PAP

The Auto-adjustable-CPAP or Automatic-CPAP [22] prototype was firstly developed in the early 1990s [23]. When in use, it is firstly set to a low pressure level which reduces the extra pressure comparing to CPAP. There is a sensor in the APAP. Once the sensor detected a "specific pressure characteristics of air" which indicates an obstruction is happening, the machine will automatically raise the pressure to keep the patient's upper airway open. When obstruction is absent, the pressure drops gradually to the minimum pressure. This keeps the overall average pressure much lower than traditional CPAP and makes the patient more comfortable [24].

6

1.3 Literature survey

A literature survey was carried out on CPAP, the inhaled air quality requirement under such pressurized respiration and mathematical modelling of the machine.

1.3.1 Delivered air quality and the problem of condensation when using CPAP

When using CPAP, besides the provision of pressure, there are other conditions to consider for patients' safety, comfort and compliance. There are:

1.3.1.1 CPAP pressure consideration

When a CPAP is used for remedy, its pressure should be set high enough to have the remedy effect and should not be too high to disturb patient's sleep and increase mouth leak [25].

1.3.1.2 Carbon dioxide limit in inhaled air

The Occupational Safety and Health Administration (OSHA) standard for carbon dioxide is an eight-hour time-weighted average (TWA) of 5,000 ppm (0.5% of weight) with a short term 15-minute average limit of 30,000 ppm (3% of weight) [26]. They are 0.325% and 1.95% by volume respectively.

The average carbon dioxide (CO_2) content of exhaled air is 3.7% CO_2 by volume [27], which is equivalent to about 5% CO_2 by weight. This is 10 times the limit. This means if assuming CO_2 concentration in the exhaled air is evenly distributed, the exhaled air should be no more than 9% in inhalation.

Another phenomenon observed is that at the lower pressure settings, there is higher CO_2 percentage in the inhaled air [28]. This also becomes a limitation when considering the possibility of higher pressure induced sleep disturbance and mouth leak [29]. More discussions are in below sub-sections.

1.3.1.3 Humidity and temperature of inhaled air

The American National Standards Institute suggested a minimum absolute humidity of 10 mg/L at no lower than 22°C for non-intubated patients [30]. The 10 mg/L is equivalent to air at 22°C and 50% relative humidity which means that the normal room

condition is acceptable for the air inhaled using CPAP. Usually, when air is inhaled through the nose, it is warmed up to about 36°C and humidified to above 97% of saturation at this temperature before it reaches the trachea [31]. The cooler and dryer incoming airflow takes heat and moisture from the upper airway lining although the heat and moisture will be but only partly restored to the lining during exhalation [32]. This creates the dryness in the nose, mouth, throat and even nasal mucosal blood flux when there is mouth leak thus reduces the comfort and compliance. Mouth leak means a portion of the air directly flows out from mouth taking away heat and moisture without restoration [32, 33]. So, although the minimum humidity can be low to 10 mg/L, considering the higher temperature and higher humidity level can reduce the deprivation of heat and moisture from upper airway lining thus increase the patients' comfort and compliance [34], and more over the mouth leak which worsens the situation needs a compensation, a higher temperature and humidity level in the CPAP airflow is more agreeable [35]. It has been reported that heated humidification did ease and even get rid of these symptoms and uncomfortableness [32, 34].

1.3.1.4 Condensation in tube and its undesirability

Humidified air increases the comfort and compliance. However, airflow with higher humidity may create condensation on its way. When condensation occurs in the air delivery tube, the built-up condensate on the inner surface of the tube can increase pressure drop and reduce the pressure in the mask [36]. The exhaled air is usually at 33°C and almost saturation [30]. When the exhaled air cools down in the system, it can also contribute condensation to wherever it can reach.

So a CPAP not only provides a pressurized airflow to splint airway open but it is also required to provide a safe and comfortable airflow. Moreover, these requirements should be satisfied under different combinations of conditions over wide respective working ranges. Development and design require analytical investigation. Mathematical models have been used besides experimental investigation for this purpose.

1.3.2 Former models

Available mathematical models have been reviewed. These models are briefed below.

White [37] built a mathematical model simulating the airflow through air delivery tube connecting the humidifier chamber and the mask. The model was used to simulate the

CPAP fluid dynamic performance with patient breathing load. The author concluded that the breathing system model can closely mimic the prototype system's dynamic behaviour and give an excellent result of steady state mask pressure.

Zhen [38] used an empirical equation to express the discharge coefficient of a typical orifice. The condensation in the mask was also modelled. The condensation was considered as film condensation and the mask wall temperature and the saturation temperature comparison was taken as the determination of condensation. A sinusoidal wave is used to simulate the breath load. The author stated that low velocity zone in the mask has higher possibility of condensation.

Sun [19] built a model to simulate the thermodynamics of the CPAP. His model can dynamically simulate the "switch-on" of the machine and its ramping-up to steady state over a range of ambient conditions as well as the machine setting conditions.

Comments on these models:

White's model used linearized relationships. The linear relationships may bring errors when extrapolating the range, especially when deep breathing is introduced and the fluctuating velocity goes to negative. The equation for orifice discharge coefficient used by Zhen has a narrow range of reasonably constant value in Reynolds number from 900 to 2500. Sun's model copes well with the complicated thermal dynamic performance of the CPAP machine, however, the model can only simulate steady flow conditions.

An interest exists in the fluid dynamic and thermodynamic performances of the CPAP machine in "real" use with the patient's breathe is added in and airflow fluctuates. To develop such a model will be very helpful for future analysis and development, improvement and design of the machine.

1.4   Objectives

In some circumstances such as low CPAP pressure and/or high exhaling process, some of the exhaled air will travel back into the HADT. The distance the exhaled air can reach is defined as the distance of the reverse flow. This fully saturated air at about 33°C could produce condensation and raise the carbon dioxide concentration in the next inhalation. This project attempts to set up general mathematical model(s) simulating these phenomena. This will be helpful for future CPAP design and control, and

eventually beneficial to the users by reducing condensation and carbon dioxide inhalation. The model should be able to cope with changes within a certain range of variations of ambient conditions, settings and coefficients.

The main objectives of this research are to

- Quantify the reverse flow under combinations of pressure setting and breathe load
- The influence of the reverse flow on carbon dioxide re-breathing, delivered humidity to the patient and condensation in the HADT.

To accomplish this, the following tasks will be undertaken:

1. Understand the CPAP system, its working principles and working conditions.
2. Use laws of physics to mathematically model the relevant components of the CPAP system.
3. Based on the mathematical model, build a software model of the CPAP system on Simulink™ in the Matlab™ environment.
4. Validate the Simulink™ model simulation through experiments.
5. Use the validated model(s) to study the factors which influence the fluid dynamics and thermodynamics of the CPAP system, the reverse flow and the consequential influences on exhaled air inhalation, delivered humidity and condensation.

Chapter 2 Mathematical Modelling of Fluid Dynamics

2.1 Introduction

The CPAP machine type chosen for analyse is CPAP HC600 manufactured by Fisher & Paykel Healthcare Co. Ltd. (Figure 2.1). This chapter is to analyse and understand the physics of the machine's operation then build up a mathematical model to simulate its working and predict the required outputs.

Geometry and physical characteristics of the machine components will be used to obtain correct values of parameters. Physical laws, mainly of fluid mechanics, will be used to develop differential equations to describe the relationships and simulate the dynamic situation. The machine's components will be analysed sequentially. The model's inputs include machine settings and patient's breathe load.

Figure 2.1 CPAP HC600 by Fisher and Paykel Healthcare Co. Ltd.

The model is analysed based on sea level conditions. The specific heat is assumed constant due to the low range of temperature between 5 ~ 65°C.

Based on the geometry and measured highest flow rate of about 53 L/min. through the bias vent holes at the highset pressure setting, the airflow velocity through the holes is calculated as no more than 60 m/s which is the highest velocity in this system. Thus the air flow velocities in this model are all below 1/3 of the speed of sound for considering air compressibility [39]. Furthermore, comparing with the atmospheric pressure, the working pressure is also very low. Therefore an incompressible fluid is assumed.

2.2 System overview
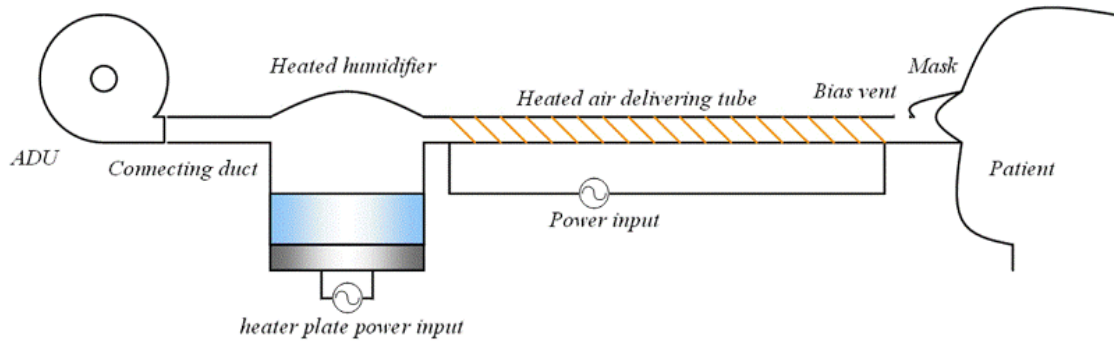
Figure 2.2 CPAP system

Figure 2.2 shows the schematic diagram of a CPAP system in use. The components of the CPAP machine include an air delivery unit (ADU), a connecting duct, a humidifier, a heated air delivery tube (HADT), an elbow with bias vent holes and a mask.

ADU provides and maintains a proper positive pressure to the mask and then to patient's upper airway. The connecting duct guides the air flow into the humidifier chamber. The humidifier which has a heating plate underneath receives the air and adds water vapour to the air by heating and evaporating the water in the chamber. The HADT connects the humidifier and delivers humidified air to the mask. To prevent condensation in the tube, the HADT is heated by embedded wire winding along inside the tube wall. There is an elbow with bias vent holes locating between the HADT and the mask. These holes are for purging exhaled air to provide patient fresh air. The mask is an interface between the machine and the patient.

This project will provide two models. One is for analysing the re-breath of exhaled air with higher CO_2 concentration level while the other is for thermodynamic analysis.

2.3 Fluid dynamic analysis

This section is based on the assumption that the thermal conditions do not significantly influence the fluid dynamic performance. On the other hand, exhaled air transportation analysis and thermal analysis will be based on the air flow. This section is to analyse the CPAP fluid dynamic performance starting with a generic relevant conduit internal flow and container mass balance analyses.

2.3.1 Conduit internal flow and container mass balance analyses

2.3.1.1 Internal flow analysis

In this section an expression for the fluid velocity is developed. Figure 2.3 shows a controlled volume of fluid in the simplest internal flow situation. A constant cross sectional area circular smooth tube and a constant fluid density are assumed.
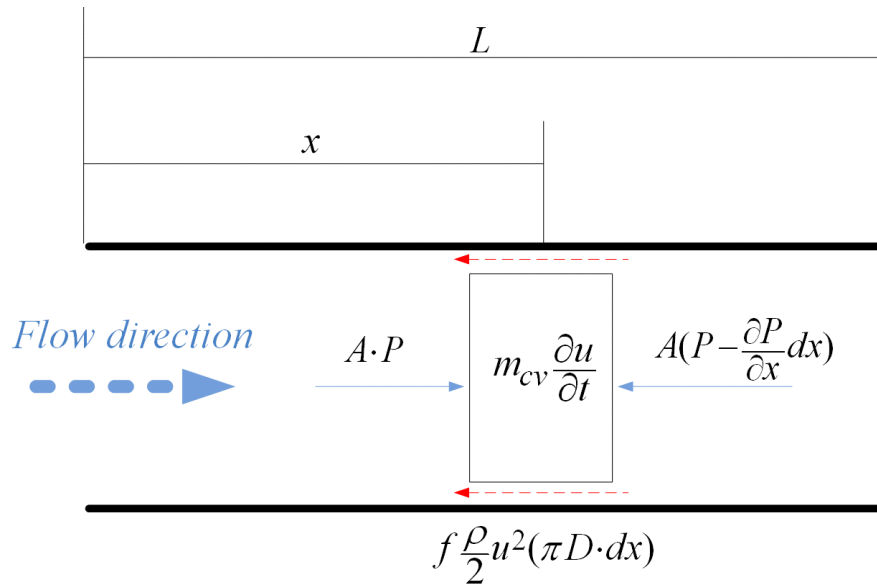
Figure 2.3 Controlled volume analysis of tube flow

Based on Newton's second law, for the controlled volume:

$$\Sigma F = m_{cv} a \tag{2.1}$$

The forces exerting on the controlled volume include axial pressure generating forces on both ends and frictional force on the interface between the tube wall and the control volume. Thus the equation above can be expanded to:

$$F_{left} - F_{right} - F_f = m_{cv} a \tag{2.2}$$

13

Apply this equation to the fluid element in Figure 2.3 leads to:

$$\frac{\partial P}{\partial x} - 2f\frac{\rho}{D}u^2 = \rho \cdot a \qquad (2.3)$$

Since the change in the velocity may be expressed as $du = \frac{\partial u}{\partial x}dx + \frac{\partial u}{\partial t}dt$ which will give an acceleration of $a = \frac{du}{dt} = \frac{\partial u}{\partial x}\frac{dx}{dt} + \frac{\partial u}{\partial t} = u\frac{\partial u}{\partial x} + \frac{\partial u}{\partial t}$. Assuming incompressible fluid simplifies the velocity and acceleration to be independent to position along the conduit. Thus the partial differentiate $\frac{\partial u}{\partial x} = 0$ and acceleration becomes:

$$a = \frac{du}{dt} \qquad (2.4)$$

Thus Eq. (2.3) can be written as:

$$\frac{dP}{dx} = 2f\frac{\rho}{D}u^2 + \rho \cdot \frac{du}{dt} \qquad (2.5)$$

dP is the pressure drop across the controlled volume at any time. Integration of Eq. (2.5) along the conduit length gives the pressure drop on the whole conduit:

$$\Delta P = \int_L (2f\frac{\rho}{D}u^2 + \rho \cdot \frac{du}{dt})dx = (2f\frac{\rho}{D}u^2 + \rho \cdot \frac{du}{dt})L \qquad (2.6)$$

Where ΔP is the instantaneous fluctuating pressure drop over the conduit of length L as a result of velocity fluctuation.

For the model to be able to cope with positive and negative velocity i.e. reverse flow, term u^2 in Eq. (2.6) may be rewritten as $u \cdot |u|$, so u alone can be used to determine the sign of this item and $u \cdot |u|$ together for value. Rearranging Eq. (2.6) gives:

$$\frac{du}{dt} = \frac{\Delta P}{\rho \cdot L} - \frac{2f}{D}u \cdot |u| \qquad (2.7)$$

This equation is to calculate the internal flow velocity fluctuation along the changing pressure drop.

If there are minor pressure drops, their sum can be written as:

$$\Delta P_{mn} = \rho g h_{mn} = \Sigma(\frac{\rho \cdot k_i}{2} u^2) \tag{2.8}$$

Where k is the minor head loss coefficient which is experimentally determined. Adding this to the right side of Eq. (2.6) gives:

$$\Delta P_{total} = 2fL\frac{\rho}{D}u^2 + \Sigma(\frac{\rho \cdot k_i}{2}u^2) + \rho \cdot L\frac{du}{dt} \tag{2.9}$$

Where ΔP_{total} is the total pressure drop along the whole tubing system with frictional and minor losses included. Therefore:

$$\frac{du}{dt} = \frac{\Delta P_{total}}{\rho \cdot L} - (\frac{2f}{D} + \frac{\Sigma k_i}{2L}) \cdot u \cdot |u| \tag{2.10}$$

This equation can be used to calculate the internal flow velocity fluctuation in tubing system with minor losses.

2.3.1.2   Mass balance

For the volumetric components, the mass balance can be described by:

$$\frac{dm_{store}}{dt} = \Sigma\dot{m}_{in} - \Sigma\dot{m}_{out} \tag{2.11}$$

The volumetric components in the CPAP system are the humidifier chamber and the mask.

2.3.2   Air Delivery Unit

The series HC600 CPAP uses a centrifugal blower as its pressure generator which is designed to provide a pressure range from 4 to 20 cm water-height (cmH_2O). Pulse Width Modulation (PWM) method is used for regulating the ADU power. The PWM is controlled by a Proportional Integral and Derivative (PDI) controller.
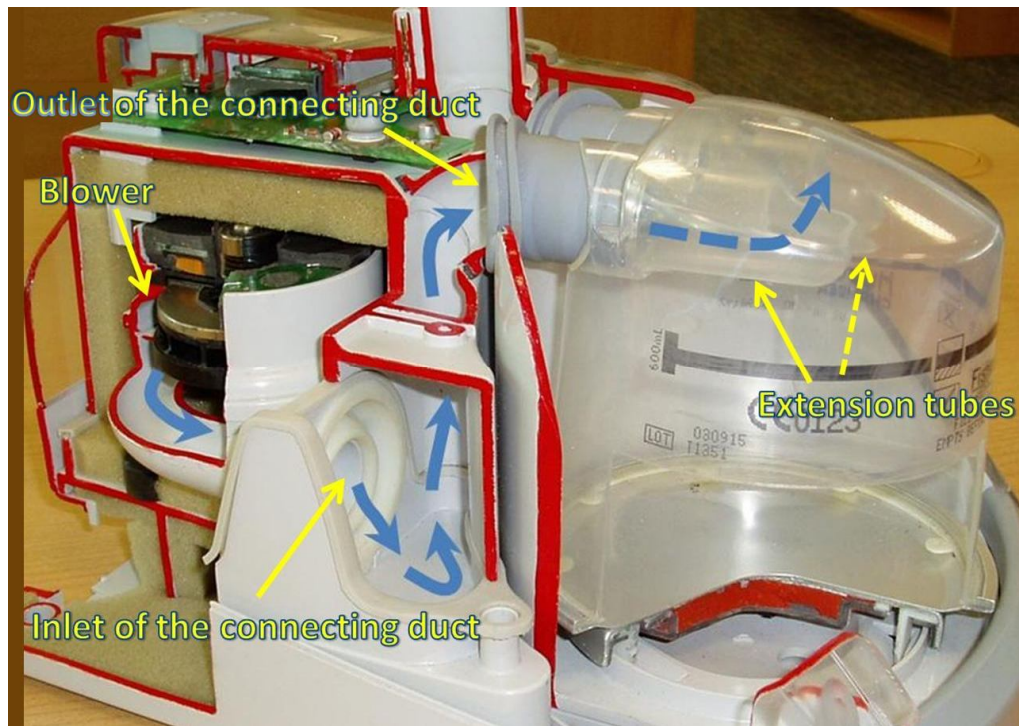
Figure 2.4 The blower and the connecting duct

The ADU is assumed to be a zero order element with no time delay. The pressure at the outlet of the blower is mainly controlled by the motor impeller rotating speed but also influenced by flow rate [40, 41]. So it is necessary to model the pressure variation with varying flow rate when the patient's breathing is added in. Since the analysis of the blower is beyond the scope of this project, an experiment was conducted to determine the relationship of ADU outlet pressure with its pressure setting and volumetric flow rate. Also the reverse flow will be investigated.
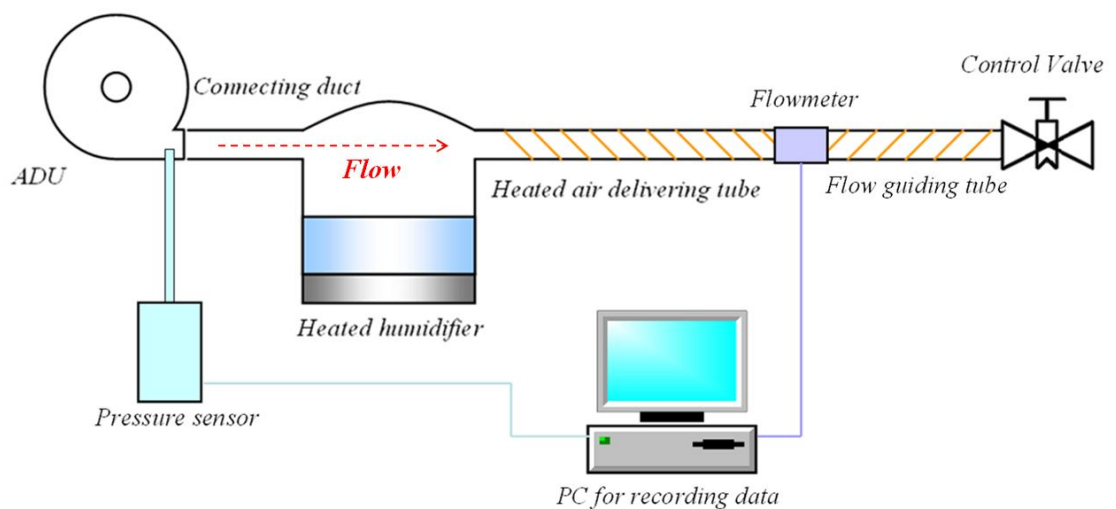
Figure 2.5 Experimental set up for positive direction flow ADU outlet pressure measurement

Figure 2.6 Pressure sensor - Honeywell Precision Pressure Transducer

Figure 2.7 Flowmeter - NDD Ultrasonic Flow Sensor

The experimental set up for measuring the ADU outlet pressure for positive flow rate is shown in Figure 2.5. The pressure sensor used was a Honeywell Precision Pressure Transducer PPT0001DWW2VA-A (Figure 2.6) and the flow meter was NDD Ultrasonic flow sensor (Figure 2.7). Figure 2.8 shows the details of how the pressure sensor was connected to the ADU outlet. A valve was installed at the end to control the flow without affecting the velocity profile inside the system.
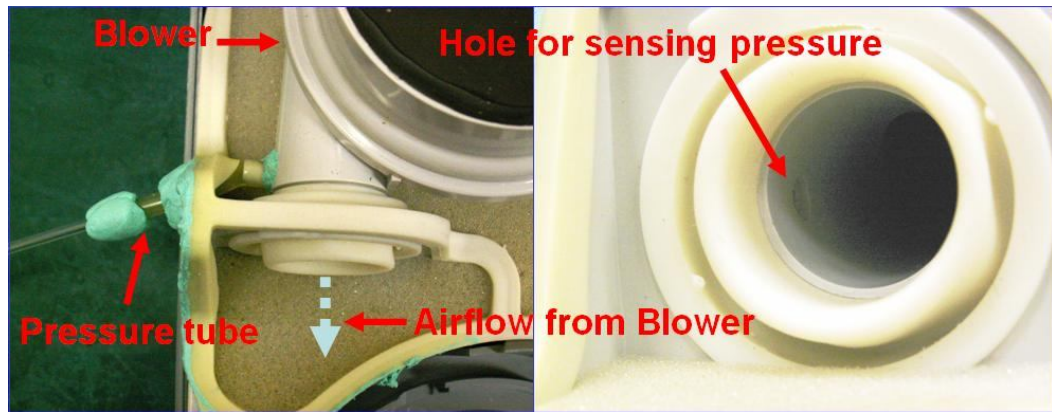
Figure 2.8 Measuring pressure at the blower outlet

For measuring the ADU outlet pressure during reverse flow, two other CPAPs were used to generate a stronger opposite flow toward the CPAP under investigation (Figure 2.9). To avoid the reading error in flowmeter, the control valve is connected downstream of the flowmeter by a connecting tube. Figure 2.10 shows the method of connecting two CPAPs which together provide a pressure stronger than the CPAP under measurement.
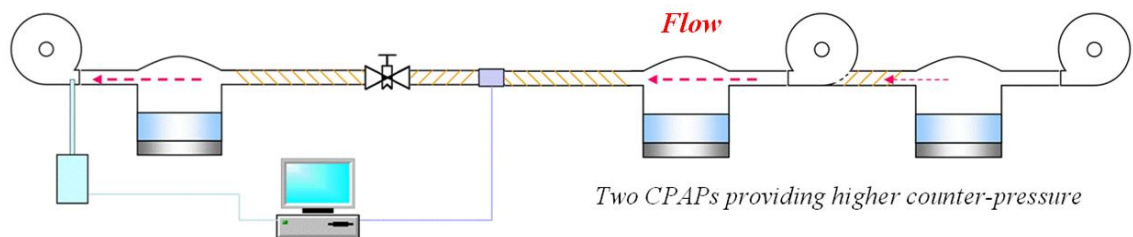
Figure 2.9 Experimental set up for ADU outlet pressure measurement with reverse flow
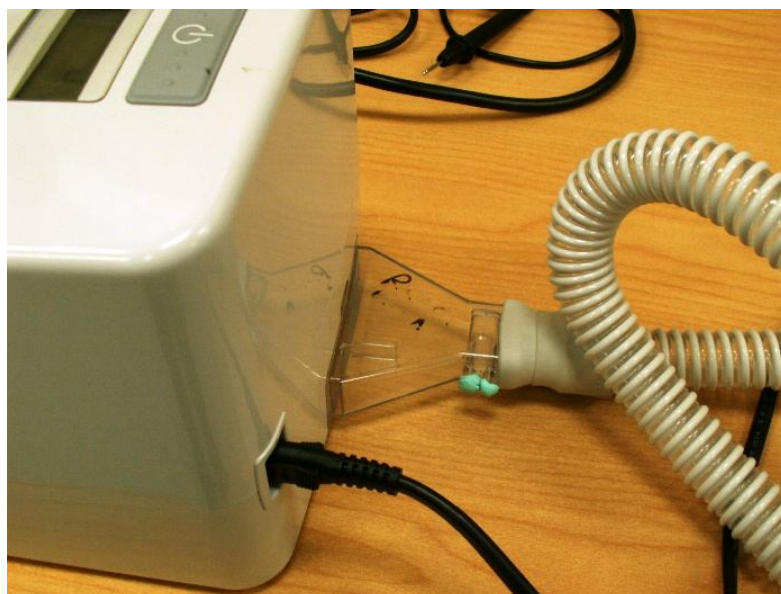
Figure 2.10 Connecting adapter between two CPAPs

The pressure readings were taken after the pressure sensor calibration. These data were corrected to produce stagnation pressure. The related test results and data process are in Appendix I.

From the test results and curve fitting, an expression for the ADU outlet pressure may be written as:

$$P_{Ao} = (-0.0961P_{set} - 0.5932)u_D{}^3 + (0.9124P_{set} - 1.2827)u_D{}^2$$

$$+ (-0.1791P_{set} - 8.9763)u_D + (95.555P_{set} + 38.95) \qquad (2.12)$$

Where P_{set} is CPAP pressure setting in cmH$_2$O and u_D is the airflow velocity at the connecting duct inlet and outlet.

The curves fitted from Eq. (2.12) and the data from tests are shown in Figure 2.11.
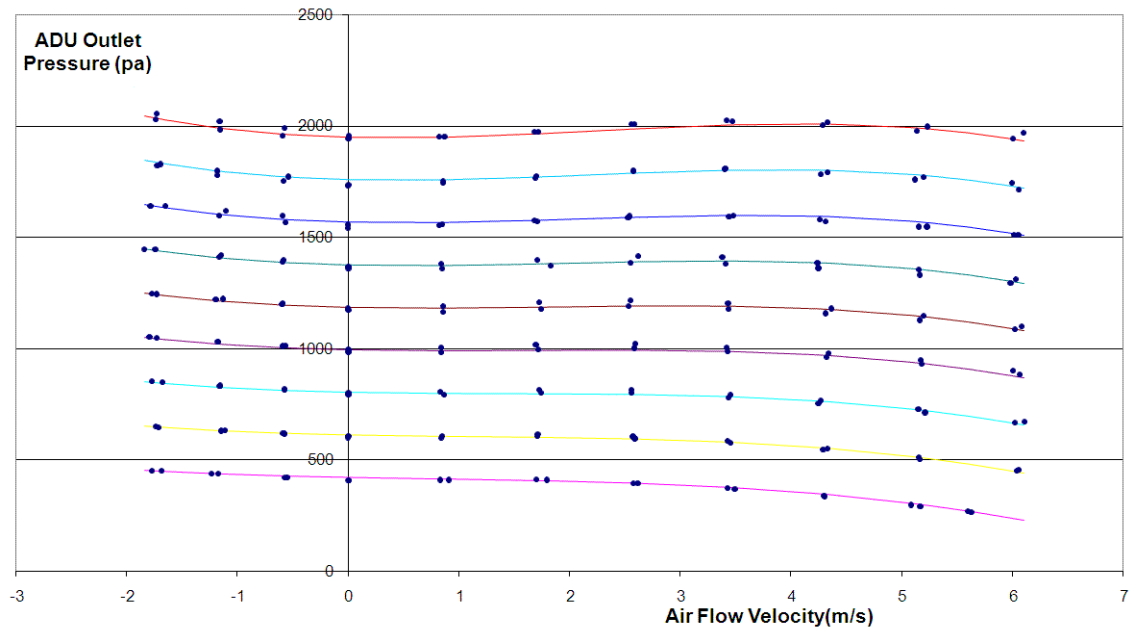
Figure 2.11 ADU outlet pressure at different pressure settings and different flow rate

Blower characteristics are normally described by relationship between the pressure and volumetric flow rate. In this modelling, for compatibility with other calculations, the flow rate is converted into airflow velocity at the blower outlet (also the connecting duct inlet). This velocity is calculated from measured volumetric airflow rate divided by the cross sectional area at the outlet of the blower which has a diameter of 19.2 mm.

The four main components of the CPAP system after the blower are the connecting duct between the blower and chamber, the chamber, the HADT and the mask. They can be categorized as length-wise and volumetric components. These four components will be analysed in the following subsection.

2.3.3   Connecting Duct

The connecting duct is a chain of tunnels in several parts and its role is to guide the compressed air flow from ADU outlet into the chamber. The whole connecting duct has a complicated inner shape (see Figure 2.4) which makes it difficult to model in details.

Setting a control volume around the fluid in this duct and considering friction, bends and other losses leads to:

$$\frac{du_D}{dt} = \frac{P_{Ao} - P_C}{\rho_{Da} \cdot L_D} - \frac{2f_D}{D_D} u_D \cdot |u_D| \qquad (2.13)$$

The diameter at the duct's inlet and outlet are both 19.2 mm. the air density in the connecting duct ρ_{Da} is assumed of an average value 1.18 kg/m^3 which is for an average air at 25°C and 50% relative humidity (RH) in this duct. L_D, the connecting duct length is determined as 20 cm along the centre line of the duct.

The data used for curve fitting were based on steady flow tests. Figure 2.12 is a sketch of the experimental setup. The two thin tubes of the pressure sensor gave a reading of the pressure difference between ADU outlet and the chamber. A static and stagnant pressure compensation was also applied. The flow rate was measured at the tube end and it was controlled by a valve connected downstream of the flowmeter by a connecting tube.
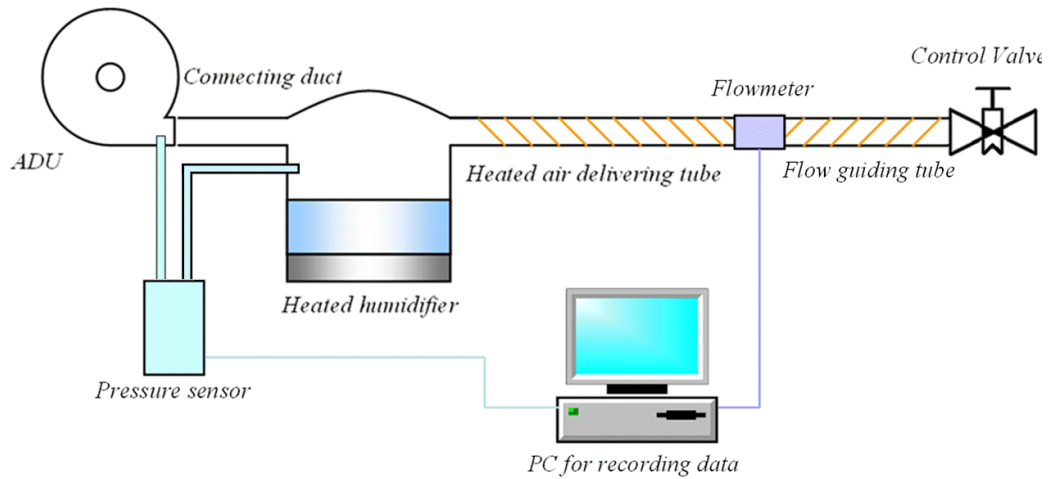
Figure 2.12 Experimental set up for connecting duct air flow velocity and pressure drop measurement

The Honeywell Precision Pressure Transducer was used to test the pressure drop. The pressure tube connecting to the higher pressure port (P1) of the pressure sensor was placed at the ADU outlet same as when testing the ADU outlet pressure. The pressure tube connecting to the lower pressure port (P2) of the pressure sensor was inserted in the chamber. Thus the reading from the pressure transducer would be the pressure difference between the two locations. Figure 2.13 shows locations where pressure tubes were placed.
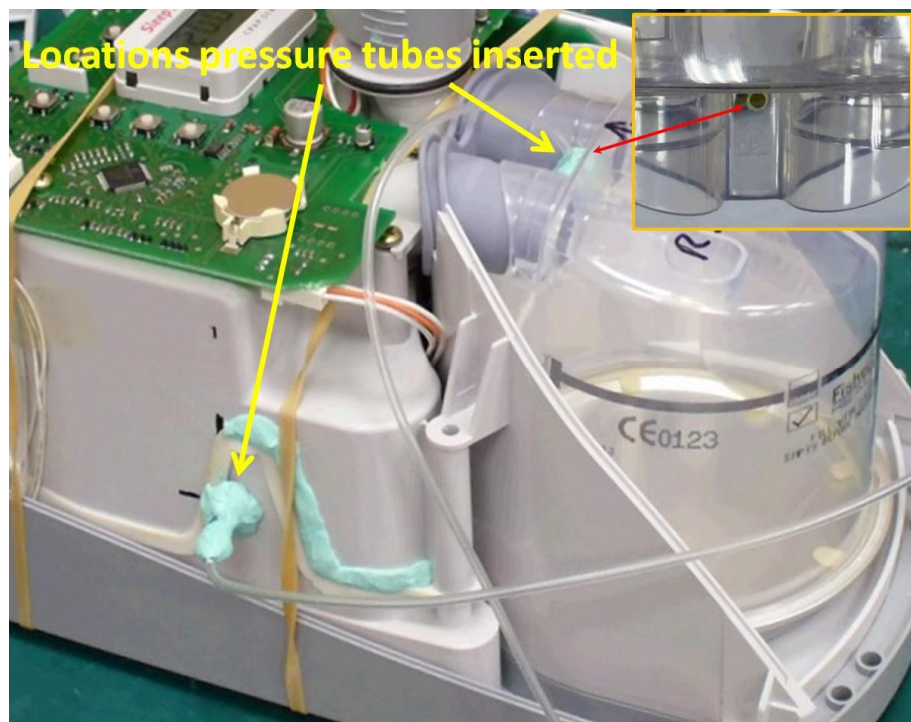
Figure 2.13 Pressure tubes inserted for measuring pressure drop on the connecting duct

The friction factor for the duct may take the form as [42]:

$$f = \frac{k_f}{\mathrm{Re}^a}$$ (2.14)

Regressing the data from experiment gave $a = 0.1679$ and $k_f = 0.4226$ for air flow through the duct (see Figure 2.14 and see Appendix II for calculation details).
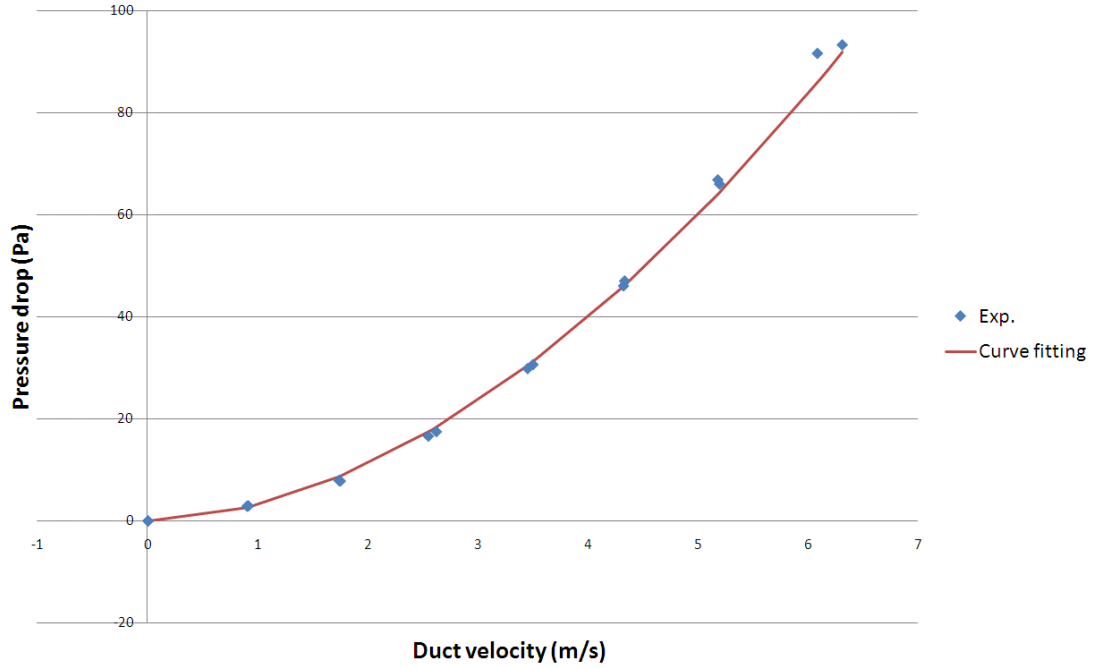
Figure 2.14 Connecting duct pressure drop vs. airflow velocity

Thus the relationship of the velocity and pressure drop along the connecting duct can be expressed as:

$$\frac{du_D}{dt} = \frac{P_{Ao} - P_C}{\rho_{Da} \cdot L_D} - \frac{0.8451}{D_D(\frac{D_D \rho_{Da}}{\eta_{Da}})^{0.1679}} u_D \cdot |u_D|^{0.8321}$$ (2.15)

The minor head losses were incorporated in the equivalent friction factor f_D. When the pressure at ADU outlet is known, the instantaneous pressure in the chamber may be calculated by rearranging Eq. (2.15) into:

$$P_C = \rho_{Da} \cdot L_D[\frac{P_{Ao}}{\rho_{Da} \cdot L_D} - \frac{0.8451}{D_D(\frac{D_D \rho_{Da}}{\eta_{Da}})^{0.1679}} u_D \cdot |u_D|^{0.8321} - \frac{du_D}{dt}]$$ (2.16)

22

2.3.4 Chamber air space mass balance

The chamber is filled with an amount of water when in use. Due to evaporation, the amount of water reduces and the air space increases. However, for simplification, the model assumes a fixed 206 ml as the air space.

The air mass balance in the chamber may be expressed as:

$$\frac{dm_{Ca}}{dt} = \dot{m}_D + \dot{m}_{ev} - \dot{m}_T \tag{2.17}$$

Since the evaporation rate is very small compared to that of inlet and outlet mass flow rates, omitting it will not significantly change the pressure and flow rate in the chamber.

Eq. (2.17) may be expanded by using the state equations:

$$\frac{dm_{Ca}}{dt} = \frac{M_a V_{Ca}}{R_{ugc} T_{Ca}} \frac{dP_C}{dt} \tag{2.18}$$

$$\dot{m}_D = \rho_{Da} A_{Dcs} u_D \tag{2.19}$$

$$\dot{m}_T = \rho_{Ta} A_{Tcs} u_T \tag{2.20}$$

Where M_a is the molar mass of air in kilogram, R_{ugc} is universal gas constant and T_{Ca} is chamber air temperature in K. Substituting Eq.(2.18), (2.19) and (2.20) into Eq. (2.17) and rearranging gives an expression for calculating the fluctuating flow velocity in the connecting duct:

$$u_D = \frac{M_a V_{Ca}}{R_{ugc} T_{Ca} \rho_{Da} A_{Dcs}} \left(\frac{dP_C}{dt} + \frac{R_{ugc} T_{Ca}}{M_a V_{Ca}} \rho_{Ta} A_{Tcs} u_T \right) \tag{2.21}$$

2.3.5 Heated Air Delivery Tube
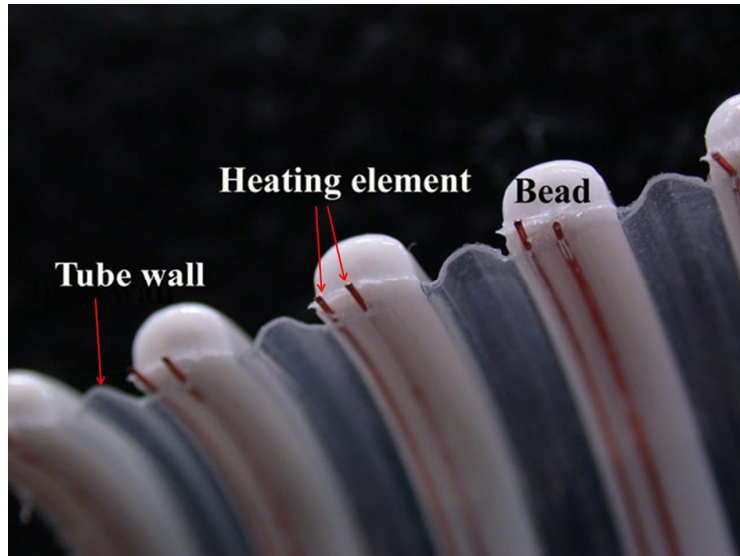
Figure 2.15 Corrugated wall of the HADT [19]

The HADT is a corrugated tube 1.725 m in length. The corrugation of its wall is shown in Figure 2.15.

The HADT and the mask fluid dynamic model are shown in Figure 2.16. The minor losses at the ends of the HADT are neglected for simplification. Since the density variation of air flow in the HADT is small, an average density of 1.142 kg/m^3 is assumed for simplification. The average density is based on the mean working conditions in the HADT as 30°C air temperature, 80% relative humidity and 12 cmH$_2$O ADU pressure setting.
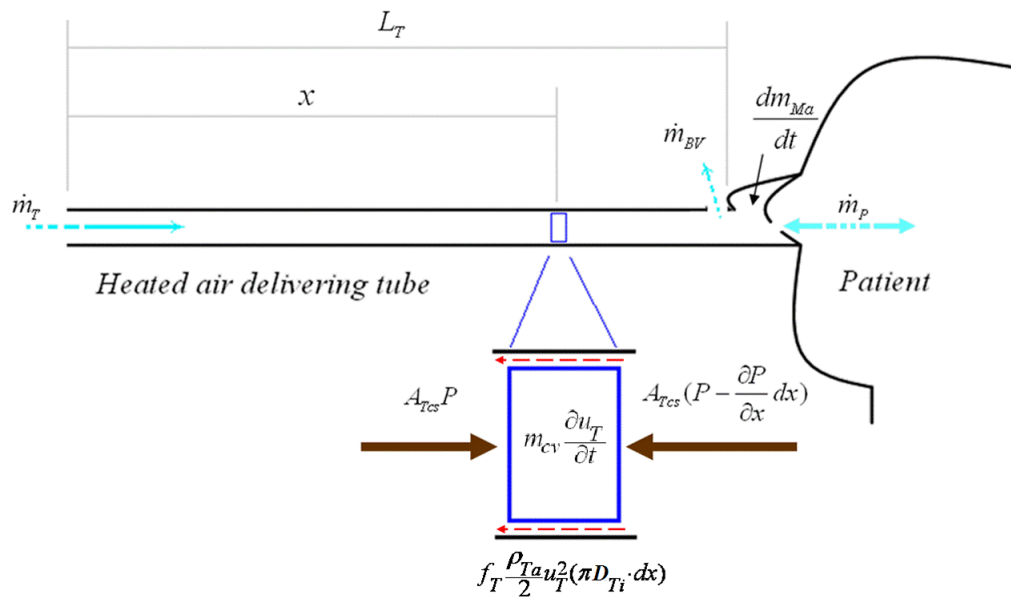
Figure 2.16 controlled volume analysis of airflow in HADT

From the above analysis, the pressure drop along the HADT, which is also the pressure difference between the chamber and the mask, can be expressed as:

$$\Delta P = P_C - P_M = (2 f_T \frac{\rho_{Ta}}{D_{Ti}} u_T^2 + \rho_{Ta} \cdot \frac{du_T}{dt}) L_T \qquad (2.22)$$

The HADT inner wall is corrugated. However, since the relative roughness is small, the pitch is long and the Reynolds number is no more than 10^5. This inner surface friction may not be too much different from a smooth tube. Darcy-Weisbach friction factor may be applicable [42]:

$$f_T = \frac{0.3164}{\text{Re}_{Ti}^{0.25}} \qquad (2.23)$$

After substituting Eq. (2.23) in, Eq. (2.22) can be rearranged as follow to calculate pressure in the mask:

$$P_M = \rho_{Ta} \cdot L_T [\frac{P_C}{\rho_{Ta} \cdot L_T} - \frac{0.6328}{D_{Ti}(\frac{D_{Ti}\rho_{Ta}}{\eta_{Ta}})^{0.25}} u_T \cdot |u_T|^{0.75} - \frac{du_T}{dt}] \qquad (2.24)$$

2.3.6   Mask air mass balance

The mask is the interface for patient to use the CPAP machine. The mask is strapped tightly onto patient's face to prevent leakage. When a patient inhales, air flows into the mask through an elbow with bias vent holes and gets mixed with air already in the mask before being inspired into the patient's upper airway. When the patient exhales, exhaled air from patient gets mixed before leaving the mask. One of the objectives for this project is to investigate the influence of mask capacity on the CPAP machine's performance.

Figure 2.17 Nasal mask type "FlexFit™407" and Full face mask type "FlexFit™432"

Two types of mask are considered in this investigation. One is a nasal mask type "FlexFit407" and another is a full face mask type "FlexFit432" (Figure 2.17). In reality, when using a full face mask and the patient breaths with both nose and mouth, the breath load should be larger than that of using the nasal mask. However, for comparison, the model considers the breath loads the same whether using nasal mask or full face mask. Furthermore, for the full face mask "FlexFit432", its bias vent holes are not on the elbow but on the mask base. Another feature is that the FlexiFit^{TM}432 mask has an accessory called "Non-rebreathing valve". There are two pieces of flaps in this valve which open when the airflow is from the CPAP and close when airflow is from the mask. This one-way valve actually prevents the reverse flow occurring (Figure 2.18). The different location of the bias vent holes may influence the mixing process in the mask and the "Non-rebreathing valve" may influence the system fluid dynamics. However, in this thesis we are interested in the influence of mask capacity, the different masks are considered as only different in their capacity.
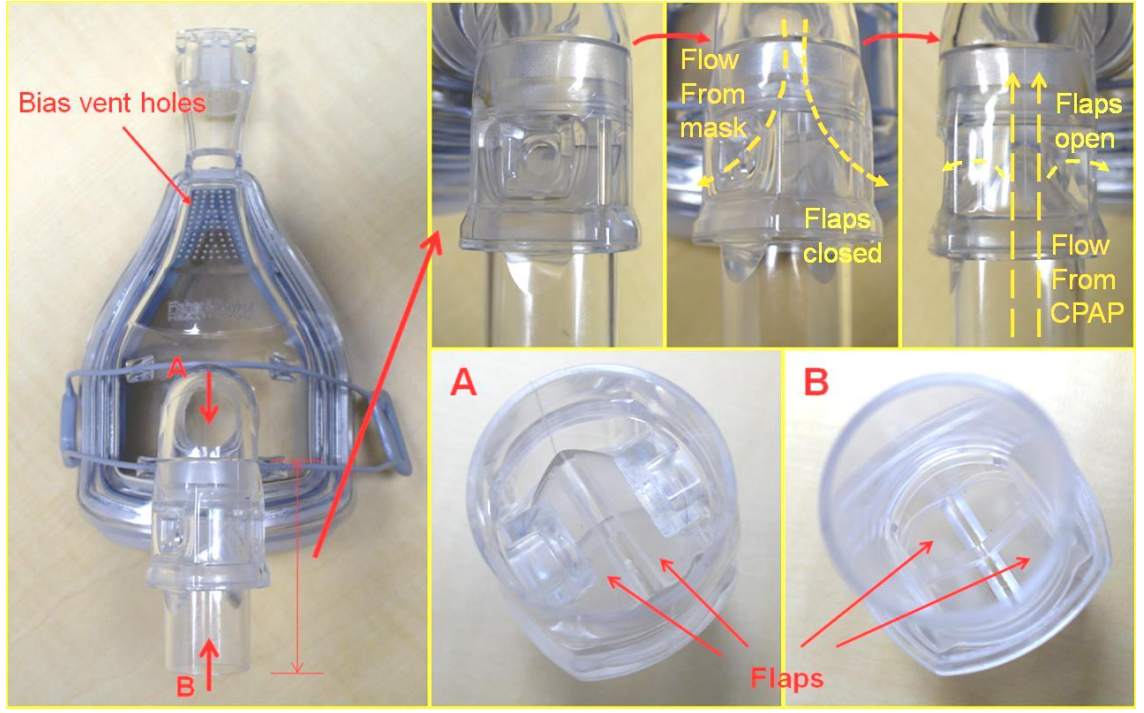
Figure 2.18 Full face mask and the non-rebreathing valve

For simplicity, a full face mask is assumed as 1.5 times in all one dimensional sizes of the nasal mask except wall thickness which is the same for both masks. Correspondingly, the full face mask capacity is 3.375 times ($1.5^3 = 3.375$) of the nasal mask capacity (The real full face mask capacity is about 3.3 times of that of the nasal mask).

The air mass balance in the mask leads to:

$$\frac{dm_{Ma}}{dt} = \dot{m}_T + \dot{m}_P - \dot{m}_{BV} \tag{2.25}$$

Where $\dot{m}_P$ is the patient's respiratory mass flow rate. The patient's normal respiratory mass flow rate curve is provided by Fisher and Paykel Healthcare Company [37]. The air mass flow rate in HADT can be calculated by Eq. (2.20). Mass change rate in the mask may be calculated by:

$$\frac{dm_{Ma}}{dt} = \frac{M_a V_{Ma}}{R_{ugc} T_{Ma}} \frac{dP_M}{dt} \tag{2.26}$$

The bias vent is an array of small holes on an elbow connecting the HADT and the mask. There are 46 holes on this elbow and the diameter at the narrowest point for each

hole is 0.65 mm (0.00065 m). The bias vent flow rate can be calculated by using following equation [43, 44]:

$$\dot{m}_{BV} = \sqrt{2\rho_{Ma}} C_d (A_{BH} \cdot n_{BH}) \sqrt{|P_M|} \cdot sign(P_M) \qquad (2.27)$$

Where C_d is the discharge coefficient for each bias vent hole, A_{BH} is the smallest cross sectional area in each hole and n_{BH} is the number of bias vent holes. using $\sqrt{|P_M|} \cdot sign(P_M)$ in the equation instead of simply $\sqrt{P_M}$ attributes to the fact that if the patient's inhalation is too strong and the tube flow can not provide enough air to fill the mask, pressure in the mask might be lower than the ambient pressure and air around the mask might enter the mask through these holes.
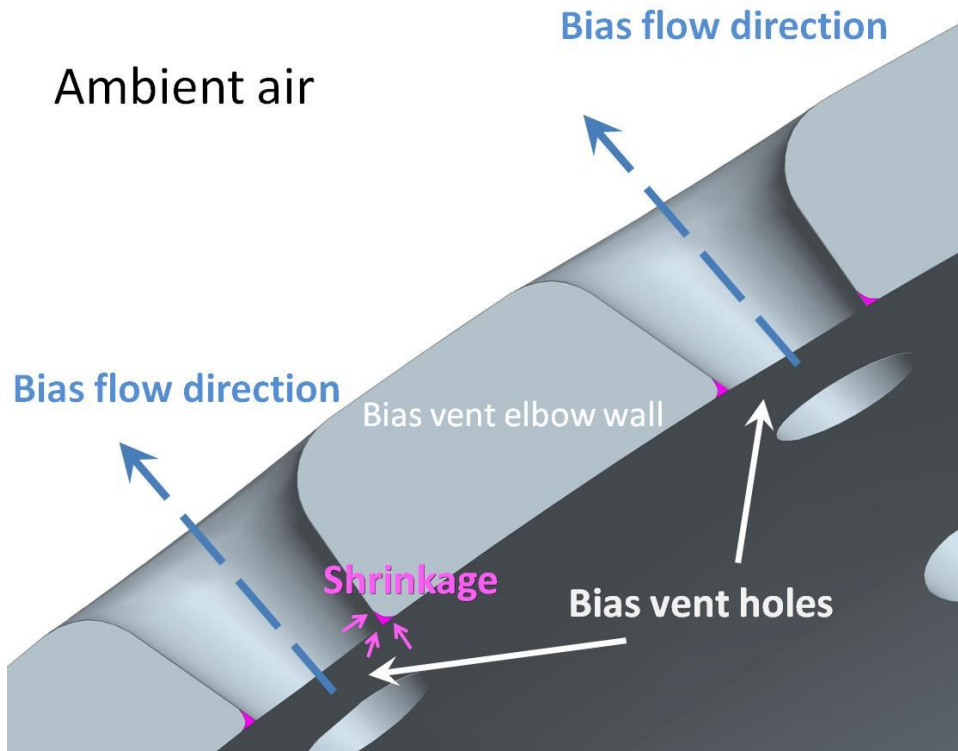
Figure 2.19 The shape of bias vent holes

This axial cross-sectional picture (Figure 2.19) shows that the bias vent holes are somewhat cone-shaped. Considering shrinkage of plastic after moulding, the sharp angles may become rounded so the shape of each hole is similar to a Venturi tube. A typical value of 0.985 as Venturi tube's discharge coefficient is chosen for these bias vent holes [45].

Inserting Eq. (2.26) and Eq. (2.27) into Eq. (2.25) and rearranging gives an expression for calculating the fluctuating flow velocity in HADT:

$$u_T = \frac{1}{\rho_{Ta} A_{Tcs}} [\frac{M_a V_{Ma}}{R_{ugc} T_{Ma}} \frac{dP_M}{dt} - \dot{m}_P + 0.985\sqrt{2\rho_{Ma}}(A_{BH} \cdot n_{BH})\sqrt{|P_M|} \cdot sign(P_M)] \quad (2.28)$$

2.4 Reverse flow and air transportation

2.4.1 Reverse flow calculation

Reverse flow occurs when the volumetric flow rate of the patient's exhalation is greater than the bias vent flow rate so the pressure in the mask increases. When it is higher than that in the humidifier chamber, some of the air will be pushed back into the HADT. Reverse flow can be calculated by integrating the possible negative part of the HADT velocity in each breath cycle:

$$D_{RF} = \int u_T dt \quad (2.29)$$

Where $u_T < 0$, and integration range is repetitive within $n \cdot t_c < t < (n+1) \cdot t_c$ for each breath cycle while $n = 0,1,2,...$

Flow and reverse flow in the HADT is simplified by assuming that they displace each other. Although mixing near the interface of fresh air and exhaled air produces a gradient of concentration, it is not expected to significantly influence the condensation and CO_2 in the re-breath.

2.4.2 Varying transport delay analysis

For dynamic and reverse flow situations, tube air flow velocity is fluctuating with time and can be negative when reverse flow occurs. That is to say, within a breath cycle, air is mainly flowing from the chamber towards the mask then the patient. However, for a short fraction of time within the cycle, air is pushed back by exhalation from the mask towards the chamber. For analysing and mimicking the humid air, the HADT is divided into 30 lumps with each lump of 5.75 cm (1.725 m/30). Due to the varying airflow velocity, time for air flowing over one lump's length is also fluctuating. This fluctuating time may be derived as follow:

Time for passing a very small distance under varying velocity can be expressed as:

$$dt = \frac{ds}{\tilde{u}(t)} \qquad (2.30)$$

The in-tube airflow fluctuating velocity is a function of time. Inserting $s = \tilde{u}(t) \cdot t$ into Eq. (2.30) and integrating it yields:

$$t_l = \int_{l_{Tl}} \frac{d[\tilde{u}(t) \cdot t]}{\tilde{u}(t)} \qquad (2.31)$$

Where t_l is the varying transport delay for air flowing through a lump-long distance. For simplicity, a numerical approximation is applied to calculate the varying transportation time:

$$t_l = \Sigma \Delta t = \Sigma \frac{\Delta s}{\tilde{u}(t)} \qquad (2.32)$$

In this simulation, Δs is taken as 1/10 of a lump length l_{Tl}, i.e. 5.75 mm which is small enough and may give a good approximation for this varying time span.

2.4.3   The effect of flow direction on air property transportation

When reverse flow occurs, the exhaled air with high concentration of CO_2 reaches the tube lumps. During a breath cycle, the fresh air also flows through these lumps thus the CO_2 concentration at a certain lump fluctuates. This fluctuation will also be transported along the channel.

The transport of a fluid variable may be expressed by a simple expression as:

$$\lambda_n(t) = \lambda_{n-1}(t - t_l) \qquad (2.33)$$

when $u_T > 0$ and:

$$\lambda_n(t) = \lambda_{n+1}(t - t_l) \qquad (2.34)$$

when $u_T < 0$.

Where $\lambda_n(t)$ is the airflow property fluctuation at lump n, $\lambda_{n-1}(t)$ the airflow property fluctuation at lump $n-1$.

This indicates that if the variable is of a wave form λ, it may experience a phase shift when transporting from one lump to another as indicated in Eq.(2.33) and Eq.(2.34).

As for airflow in the mask, the direction of transportation is controlled by patient's respiration. Similar to the tube flow analysis, during the inhalation phase which is considered positive flow, the transportation delay from last lump of the HADT (lump 30) to the mask is:

$$\lambda_M(t) = \lambda_{30}(t - t_l) \tag{2.35}$$

Therefore when there is reverse flow, there is air comes from the mask into lump 30, air properties in lump 30 in this phase will be:

$$\lambda_{30}(t) = \lambda_M(t - t_l) \tag{2.36}$$

Where $\lambda_{30}(t)$ and $\lambda_M(t)$ are the airflow's property fluctuation at lump 30 and the mask respectively.

As for transportation between the chamber and HADT lump 1:

$$\lambda_1(t) = \lambda_C(t - t_l) \tag{2.37}$$

when $u_T > 0$ and:

$$\lambda_C(t) = \lambda_1(t - t_l) \tag{2.38}$$

when $u_T < 0$.

Where $\lambda_C(t)$ and $\lambda_1(t)$ are the airflow's property fluctuation in the chamber and at lump 1 respectively.

2.5 Exhaled air re-breathing

This section is to analyse the re-breath of the exhaled air based on the fluid dynamics model from previous section.

When there is no reverse flow, the exhaled air still fills and stays in the mask and will be inhaled by the next inhalation. When reverse flow occurs, on top of that staying in the mask, part of the exhaled air pushed-back in the HADT, may re-enter the mask when next inhalation starts and be inhaled also.

For calculating the exhaled air re-breathing, it is necessary to consider the mixing procedure of the fresh air and the exhaled air in the mask.

There are two idealized models for mixing. One is displacement while the other is perfect mixing.

When displacement occurs in the mask, a new species of fluid enters it and pushes the previous fluid out of it. The gradual decrease of the amount of the previous species in the mask can be expressed as:

$$C_t V_M = C_O V_M - \int \dot{q}_P dt \quad 0 < C_O < 1, \ 0 < C_t < 1 \quad (2.39)$$

Where C_O is the concentration of the previous species in the mask at the beginning of the mixing, C_t is its gradually diluted concentration, $\dot{q}_P$ is the patient's respiratory volumetric flow rate and V_M is capacity of the mask. Thus concentration (or ratio) of the previous fluid in the mask can be expressed as:

$$C_t = C_O (1 - \frac{\int \dot{q}_P dt}{V_M}) \quad 0 < C_O < 1, \ 0 < C_t < 1 \quad (2.40)$$

As for perfect mixing, the new species of fluid enters the mask and gets fully mixed with the previous fluid and the mixture flows out with a continuously changing ratio of these two species. The concentration of the previous fluid in the mask will decrease based on expression as [46]:

$$C_t = C_O \cdot e^{-\frac{\int \dot{q}_P dt}{V_M}} \quad 0 < C_O < 1, \ 0 < C_t < 1 \quad (2.41)$$

However in reality, mixing turns out to be somewhere between these two extremities, i.e. the concentration of a fluid material may decrease following a certain combination of the two expressions above. A ratio of 1:1 was chosen for the ratio of displacement to perfect mixing for the mixing in the mask. Such combined mixing may be expressed as:

$$C_t = C_O[0.5(1 - \frac{\int \dot{q}_P dt}{V_M}) + 0.5e^{-\frac{\int \dot{q}_P dt}{V_M}}] \qquad (2.42)$$
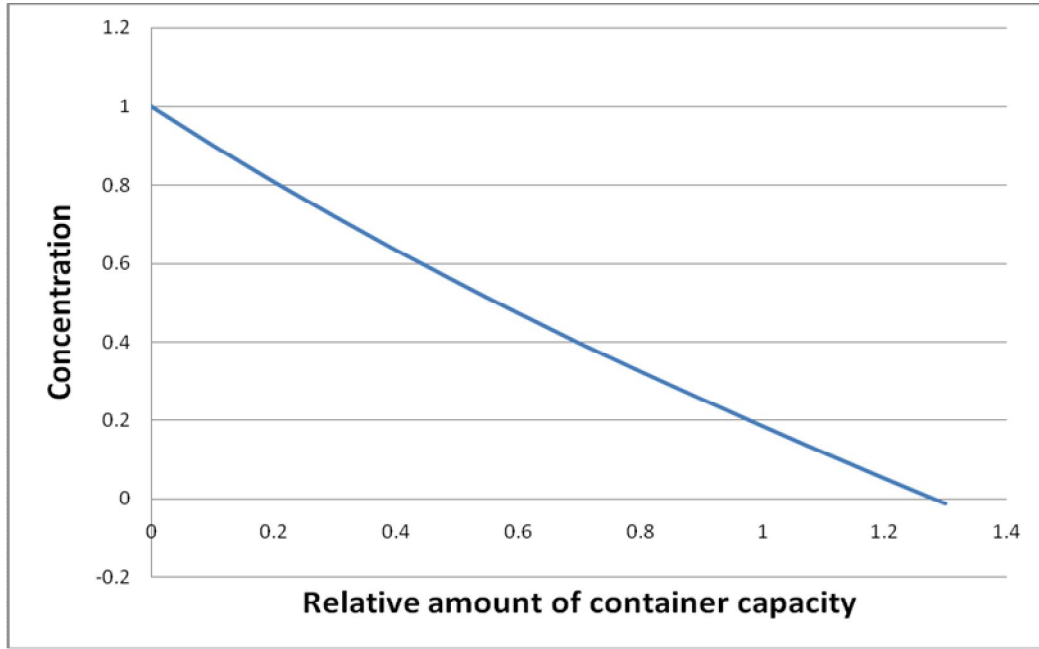
Figure 2.20 Diluting curve in the mask

A graph based on Eq. (2.42) is shown in Figure 2.20 which means that if mixing can be expressed as so, then when another species of fluid flows in, the former fluid will be totally replaced after the inlet amount reaches about 1.3 times of the mask capacity.

Mixing of exhaled air with fresh air in the mask may occur twice in a respiratory cycle, one starts at the beginning of inhalation and the other starts at the beginning of exhalation. When the exhalation phase begins, the concentration of fresh air already-in-mask decreases following the expression as:

$$C_{MFet} = C_{MFeO}[0.5(1 - \frac{\int \dot{q}_P dt}{V_M}) + 0.5e^{-\frac{\int \dot{q}_P dt}{V_M}}] \qquad (2.43)$$

While the concentration of exhaled air in the mask increases as:

33

$$C_{MEet} = 1 - C_{MFeO}[0.5(1 - \frac{\int \dot{q}_P dt}{V_M}) + 0.5e^{-\frac{\int \dot{q}_P dt}{V_M}}] \qquad (2.44)$$

On the other hand, at the beginning of the inhalation phase, if the air coming from HADT is fully fresh, the concentration of exhaled air decreases as:

$$C_{MEit} = C_{MEiO}[0.5(1 - \frac{\int \dot{q}_P dt}{V_M}) + 0.5e^{-\frac{\int \dot{q}_P dt}{V_M}}] \qquad (2.45)$$

However if the air from HADT is not fully fresh because of reverse flow, the concentration of exhaled air may decrease as:

$$C_{MEit} = C_{MEiO}[0.5(1 - \frac{\int \dot{q}_P(1 - C_{El30})dt}{V_M}) + 0.5e^{-\frac{\int \dot{q}_P(1 - C_{El30})dt}{V_M}}] \qquad (2.46)$$

Where C_{El30} is the exhaled air concentration in flow from lump 30 of the HADT. The integration of Eq. (2.46) will give out a value smaller than that of Eq.(2.45) so the concentration of the exhaled air in the mask will decrease at a lower rate. Nevertheless, the concentration of exhaled air in the mask is decreasing during inhalation phase.

Percentage of exhaled air re-breathed within a total inhalation can be calculated by:

$$C_{Erb} = 100\% \times \frac{\int C_{ME} \cdot \dot{q}_P dt}{\int \dot{q}_P dt} \qquad (2.47)$$

with integration only over the inhalation phase.

2.6   Closure of the fluid dynamic mathematical modelling

The mathematical equations have been developed for the fluid dynamics of the CPAP in this chapter. These mathematical equations will be converted into Simulink™ model. The model will be capable of simulating the breath induced airflow fluctuation in the system, the reverse flow, the transportation of fluid through the HADT with a varying-time delay, the mixing of fresh air and exhaled air in the mask and the re-inhalation of exhaled air.

Chapter 3   Mathematical Modelling of Thermodynamic Section

3.1   Introduction

The main purpose of this chapter is to analyse the thermal performance of the CPAP machine. The physical laws of thermodynamics and heat transfer will be used to develop governing equations simulating the dynamic system. This will give the dynamic fluctuating outputs of evaporation in the chamber, temperature changes and condensations in HADT and the mask. The model can also provide steady state outputs. Thus it can be used to compare between steady state outputs and breathing-introduced fluctuating outputs. When using a CPAP machine, all the components and water will be at the ambient temperature prior to switching it on. When the machine is switched on, the temperatures will move through a transient phase, until steady-state is achieved. This thermodynamic model developed in this thesis does not account for this warm-up period. The breathing-introduced fluctuating situation is a steady-state-based situation.

The system inputs include ambient air conditions, mask size, pressure, heating element setting, HADT heating setting and patient's breathe load.

Several generic assumptions and simplifications for the thermodynamic model are listed below.

- The ambient air is simplified as quiescent.
- Air is incompressible [39], however, the density can be considered different due to different temperature and different pressure at different locations.
- The water in the chamber is considered quiescent [19].

3.2   Airflow in ADU

As mentioned in the fluid dynamic analysis, the ADU is a centrifugal blower and is simplified as a zero order device. Due to inefficiency, some of the electric energy will be wasted in the form of heat losses. The heat raises the temperature at the blower and its vicinity and also raises the temperature of airflow passing through it. Compression of air in the blower may also increase the temperature. Factors influencing the airflow

temperature changes may be the efficiency of the blower at different pressure settings, the flow rate, the insulation conditions and the thermal capacity of the airflow. Because of the complexity in blower, first principle analysis is beyond the scope of this project. The main concern of the project is to determine the airflow temperature changes. An experiment was performed to measure the temperature change at various pressure settings for steady flow. Since breathing induced velocity fluctuation is fast compared to temperature changes and after flowing through ADU the airflow will mix in the chamber, it is reasonable to assume the outlet temperature from the ADU as a mean temperature and ignore the effect of the fluctuation.

In greneral, the enthalpy of a fluid mixture is the sum of the enthalpies of its components [47]. Therefore the specific enthalpy of the mixture can be expressed as:

$$h = \frac{\Sigma m_i h_i}{m} \qquad (3.1)$$

Specific heat of a mixture is the weighed sum of its components' specific heat [48]. Here in this project, the ratio of vapour mass to the mass of the total moist air is used as the definition of specific humidity. It can be expressed as $d = \frac{m_{vapor}}{m_{vapor} + m_{dry\_air}}$ [42].

Because the average temperature of the airflow in this project is about 30°C, the values of 1006 J/kg·K and 1865 J/kg·K were respectively chosen for the specific heat of dry air and vapour [49]. The specific heat of moist air may be expressed as:

$$\frac{\Delta H}{\Delta T} = c = 1006(1-d) + 1865d \qquad (3.2)$$

Thus an expression can be obtained to calculate the air temperature increase after receiving certain amount of enthalpy:

$$\Delta T_{ADUa} = \frac{\Delta H}{1006(1-d) + 1865d}(°C) \qquad (3.3)$$

For obtaining the relationship between enthalpy increase and CPAP pressure setting, experiments were conducted to measure the temperature at the blower outlet at different pressure settings with interval of 2cmH$_2$O.

An Environment Control Chamber (Vötsch C4-340 by Vötsch Industrial Technic Co. Ltd.) was used to provide steady ambient inputs at Fisher and Paykel Co. Ltd. (Figure 3.1). During the tests, drifts of ±0.5ºC in temperature and ±2% in relative humidity were observed as the maximum deviation.

Figure 3.1 CPAP in the Vötsch C4-340 Environment Control Chamber for testing
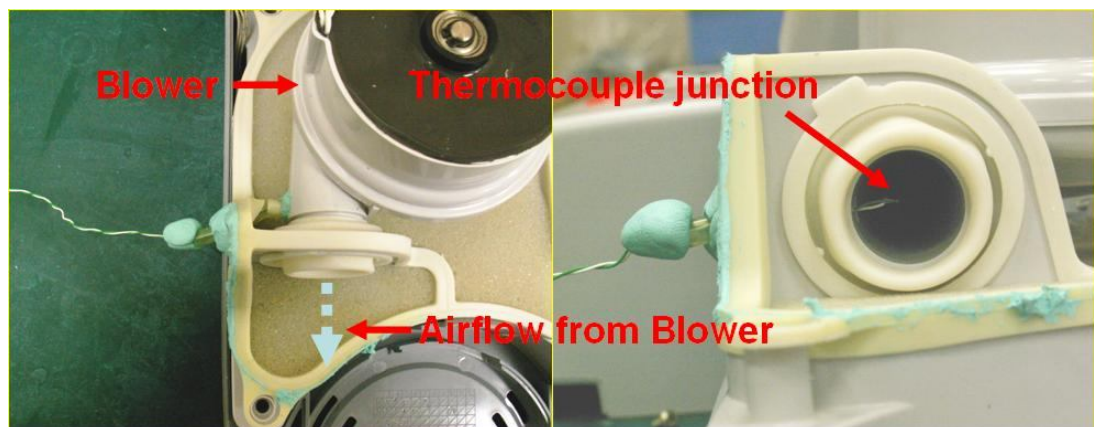
Figure 3.2 Air temperature at the blower outlet measurement
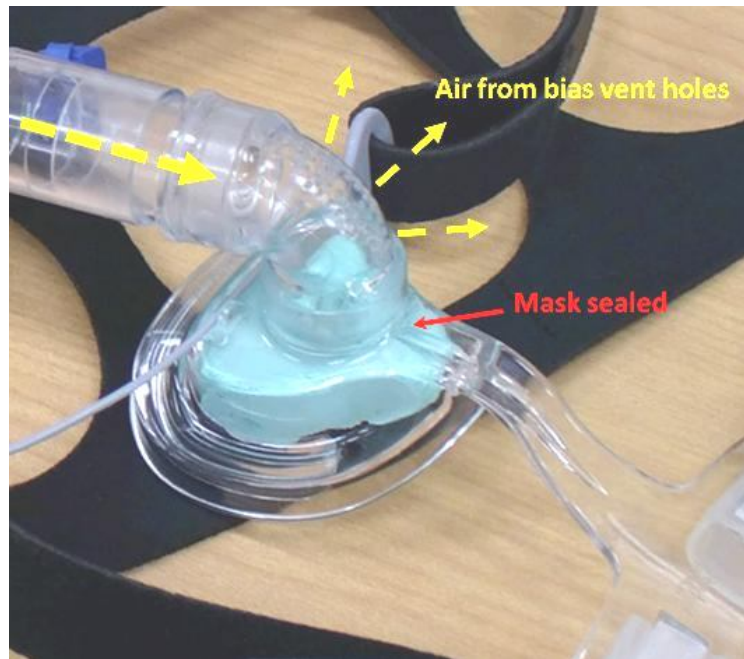
Figure 3.3 Airflow only comes out from bias vent holes

The thermocouple was inserted at the blower outlet as shown in Figure 3.2. Elbow with bias vent holes was used to control the flow rate (Figure 3.3). It is assumed that the thermal energy gain of air in the ADU is unaffected by the inlet air conditions. Repeating the tests under three different ambient conditions as listed below:

- Temperature 10°C and relative humidity 50% for cold and dry condition
- Temperature 20°C and relative humidity 70% for most common room condition
- Temperature 35°C and relative humidity 90% for hot and humid condition

Averaged results from these tests gave the relationship between pressure setting and enthalpy increase in Figure 3.4 (see Appendix III for details of the data process).
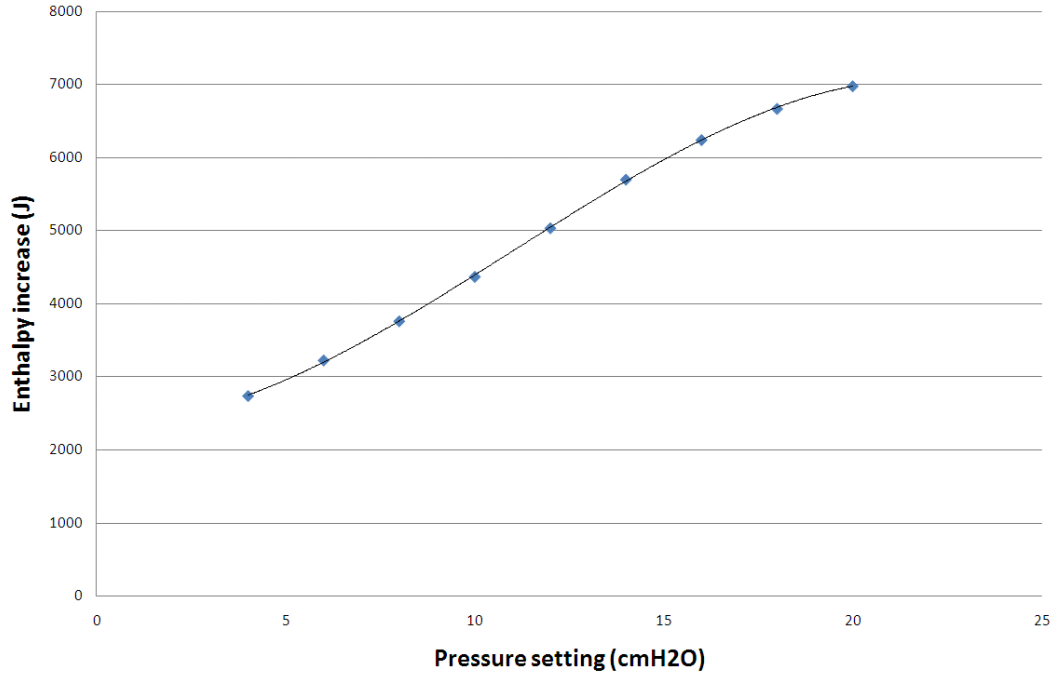
Figure 3.4 Thermal enthalpy gain of airflow between CPAP inlet and the chamber

The resulted curve fit may be expressed as:

$$\Delta H = -0.943 P_{set}^3 + 31.094 P_{set}^2 - 14.6048 P_{set} + 2372.5 \qquad (3.4)$$

The correlation of $R^2 = 0.999$ shows excellent fit.

Therefore for airflow within the range of 10~35°C and RH up to 90%, its temperature increase after flowing through the ADU may be calculated by inserting Eq. (3.4) into Eq. (3.3):

$$\Delta T_{ADUa} = \frac{-0.943 P_{set}^3 + 31.094 P_{set}^2 - 14.6048 P + 2372.5}{1006(1-d) + 1865d} \qquad (3.5)$$

The temperature of chamber inlet from ADU thus becomes:

$$T_{Cai} = T_\infty + \Delta T_{ADUa} = T_\infty + \frac{-0.943 P_{set}^3 + 31.094 P_{set}^2 - 14.6048 P + 2372.5}{1006(1-d) + 1865d} \qquad (3.6)$$

39

3.3 Chamber water heat balance

In this section, an expression for the water temperature is derived.
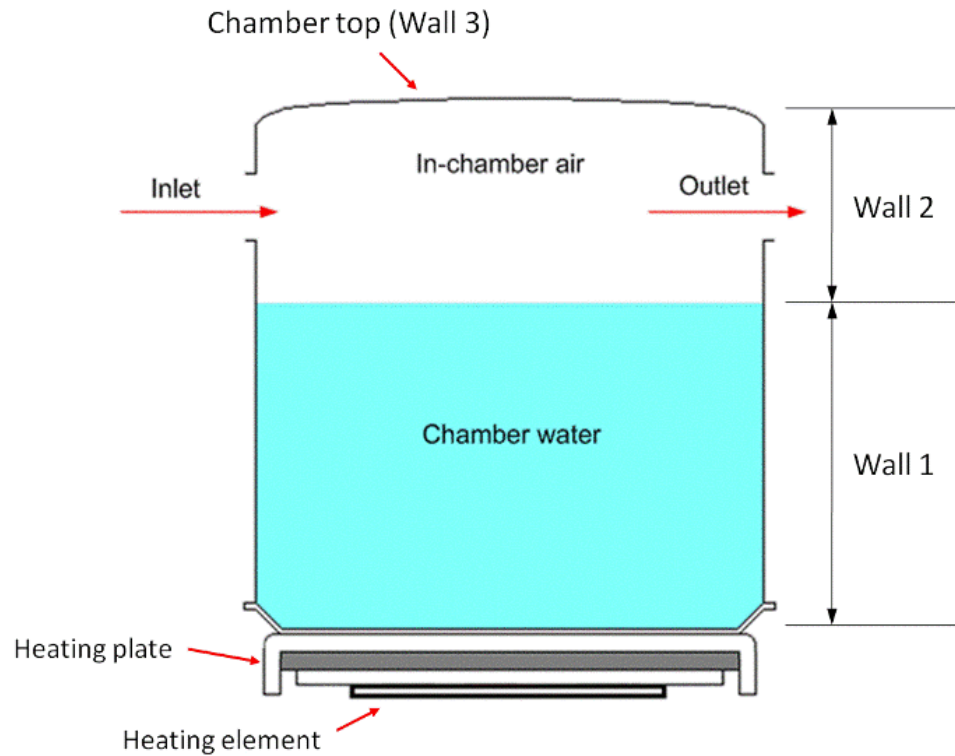
Figure 3.5 Humidifier diagram

Figure 3.5 is a diagram of a CPAP humidifier. The humidifier consists of a chamber with an Aluminium base. The chamber heating system consists of heating element, ceramic, 3M thermal tape and the heating plate at the top contacting the chamber base to provide heat to the chamber water. The heating element is printed on one side of a ceramic substrate (50 x 50 mm) (See Figure 3.6). The heating element transfers electrical power from the Pulse Width Modulation (PWM) power regulator into thermal energy which flows through the ceramic substrate, the 3M thermal tape and the heating plate. On the outer surface of the heating plate, part of the thermal energy dissipates into ambient through the rim of the plate and another part goes upward to the chamber base. The humidifier chamber has an 806 ml capacity with a maximum water level of 600 ml. Air flows through the upper part of the chamber over the water surface.
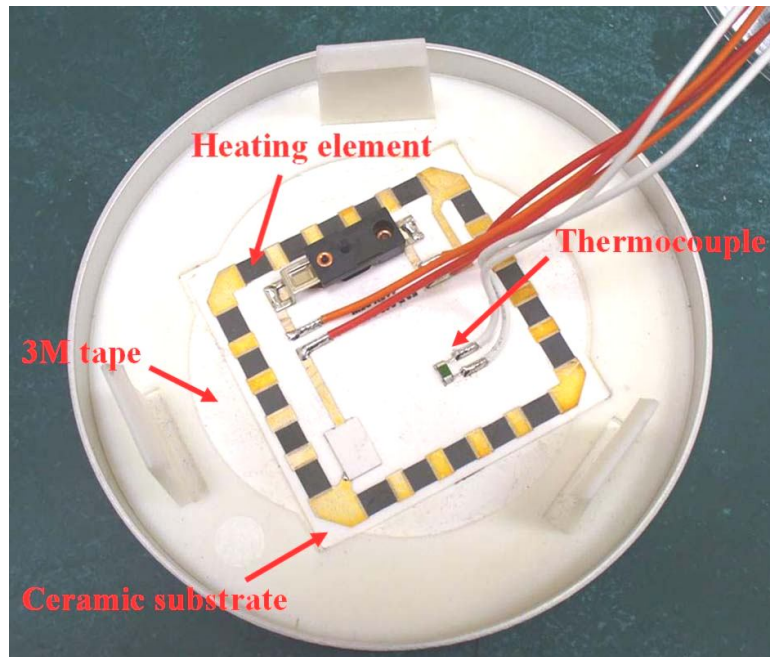
Figure 3.6 Heating element beneath heating plate

Figure 3.7 is a flow chart describing the humidifier's working principles and thermal balance. When the water is heated, the airflow will be heated and humidified by the heated water beneath. The airflow is humidified due to evaporation from the water. The evaporation is a secondary effect [19] achieved by water heating. The CPAP machine is designed to control the heating element temperature. The factors influencing water temperature may include heating element temperature setting, ambient air temperature and humidity, pressure setting, air flow rate and air flow velocity over the water surface as well as flow pattern and flow direction on the surface. Evaporation rate also influences heat taken away from the water thus influence water temperature. Chamber geometry, size, structural lay-out and material of mask are also related factors.
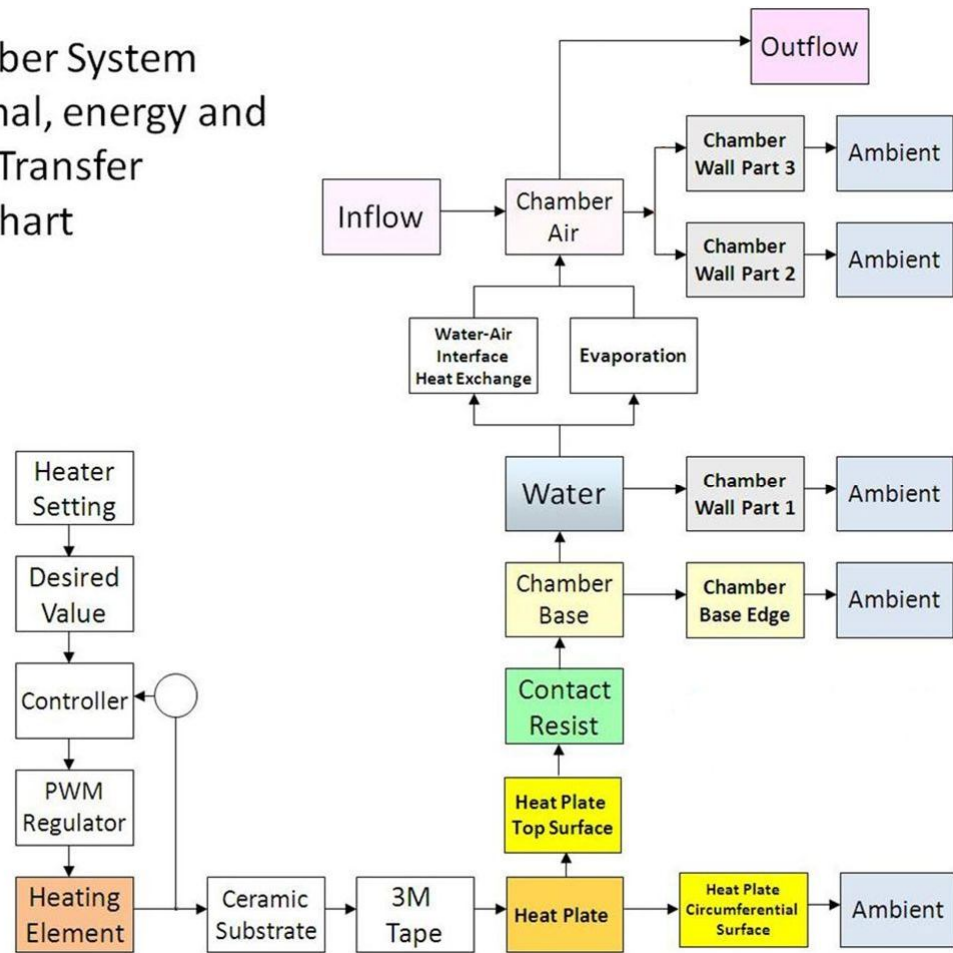
Figure 3.7 Humidifier thermal balance flow chart

The chamber geometry design is aimed at higher heat and mass (vapour) transfer rate from the water to the airflow. The high Nusselt number and mass convection (evaporation) coefficient are caused by creating turbulent flow, letting air to have a longer contact with water and trying to avoid airflow shortcuts from chamber inlet directly to outlet.
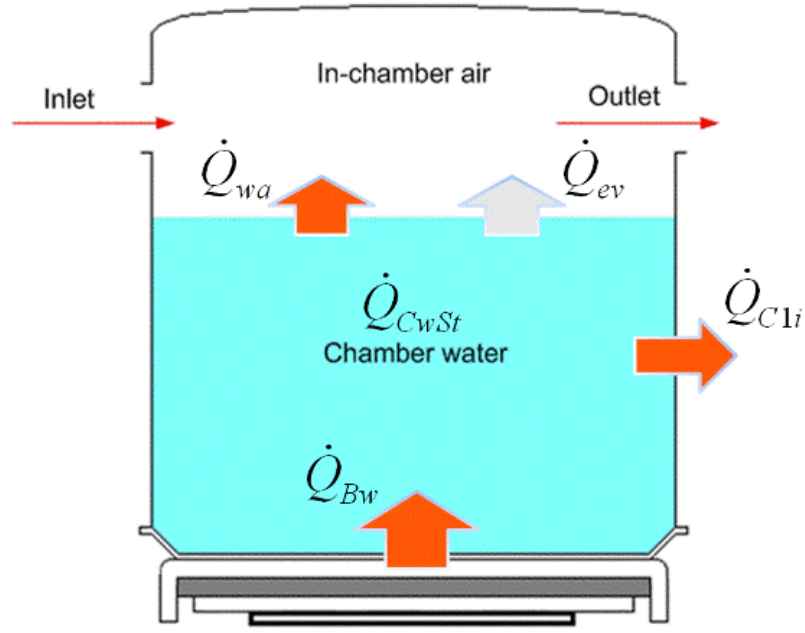
Figure 3.8 Chamber water heat balance

Figure 3.8 shows the chamber water heat balance. Heat flows into the water from heating element by the chamber base. Some of the heat delivers to the water dissipates to ambient through the chamber wall (the part below water) and some transfers to the air in the chamber's upper part by heat transfer and mass transfer (evaporation). The evaporation heat loss is an effective latent heat loss from the water. The heat balance for this process can be written as:

$$\dot{Q}_{Bw} = \dot{Q}_{CwSt} + \dot{Q}_{C1i} + \dot{Q}_{wa} + \dot{Q}_{ev} \tag{3.7}$$

However, since the model is to simulate the steady-state situation, the water temperature is assumed not changing with time. Also, the water temperature is considered stable regardless of the airflow fluctuation because of the comparatively fast fluctuation pace and the large thermal capacity of the water. Therefore, after neglecting $\dot{Q}_{Cwst}$, Eq. (3.7) can be expanded to:

$$\frac{T_{Hp} - T_w}{R_{Hpw}} = \frac{T_w - T_{C1i}}{R_{C1i}} + \frac{T_w - T_{Cai}}{R_{ws}} + k_{ev} A_{ws} (C_{sv} - C_{Caiv}) h_{fg} \tag{3.8}$$

Where C_{sv} is the absolute humidity in saturated air at water surface [42]. Equations and calculations for the parameters in Eq. (3.7) will be analysed and derived in the following sections.

43

3.3.1 Heat flow from the heating element to water

The heating element is surrounded by the heating plate. The heat generated in heating element flows to the heating plate via ceramic substrate and a 3M tape. Since constant settings and ambient conditions are assumed, further assumption is made that the temperature in the heating element, ceramic substrate, 3M tape and heating plate will remain unchanged. When reaching the top of the heating plate the heat will travel to the chamber with some dissipation to the ambient. It is necessary to analyse the balance at the heating plate top for obtaining the heat flow from heating plate toward the water through the chamber base.

3.3.1.1 Chamber base upper surface temperature

In this section, the temperature on chamber base upper surface is discussed and determined.

The heat flow to water can be written as:

$$\dot{Q}_{Bw} = \frac{T_{Hp} - T_w}{R_{Hpw}} \tag{3.9}$$

Where R_{Hpw} is the total thermal resistance from heating plate top to the water. This includes heating plate and chamber base thermal contact resistance, chamber base conductive resistance and chamber-water interface natural convection thermal resistance. The thermal contact resistance between the heating plate surface and the chamber base was calculated to be 9.32×10^{-3} (K/W) [19] and chamber base conductive resistance can be calculated by [47]:

$$R = \frac{l_{CB}}{k_{Al} \cdot A_{CB}} \tag{3.10}$$

The thermal contact resistance, chamber base conductive resistance and the total are listed in Table 3.1.

Table 3.1 Thermal resistance from heating plate to chamber base top

Components	l (m) (Thichness)	k [W/m·K] (Thermal conductivity)	A (m²) (Area)	R (K/W) (Thermal resistance)
Contact thermal resistance				9.32×10^{-3}
Chamber base thermal resistance (Aluminium)	0.0006	237[50]	0.01135	0.22×10^{-3}
Total thermal resistance from plate top to base top				9.54×10^{-3}

In this project, the thermal conductivities of all solid components are considered constant within the working temperature range.

As the water in the chamber is considered quiescent, the resistance on the base-water interface is modelled as natural convection from a horizontal circular hot plate to the water.

In general, thermal resistance on convectional interface is [47]:

$$R = \frac{1}{h \cdot A} \qquad (3.11)$$

Heat convection coefficient can be expressed as [50]:

$$h = \frac{k}{\delta} Nu \qquad (3.12)$$

Where k is thermal conductivity of fluid, δ is characteristic length and Nu is Nusselt number.

Nusselt number for such natural convection may be determined by [47]:

$$Nu = C \cdot Ra^n \qquad (3.13)$$

Where Ra is Rayleigh number which may be expressed as [47]:

$$Ra = Gr \cdot \text{Pr} = \frac{g\beta\delta^3\Delta T}{v^2} \text{Pr} \qquad (3.14)$$

Where Gr is Grashof number and Pr is Prandtl number, β the volumetric expansion coefficient of the fluid and v the kinetic viscosity of the fluid.

Values of β and v are evaluated at interface film temperature which is defined as [50]:

$$T_f = \frac{T_s + T_{fl}}{2} \tag{3.15}$$

The average Rayleigh number for this interface is 5.462×10^6 [19]. This gives $C = 0.54$ and $n = 1/4$ for fluid above hot plate [47] (see Appendix XIX for values of C and n of different situations). Thus, Eq. (3.11) can be rewritten as:

$$R_{Bwn} = \frac{1}{0.54 \dfrac{k_w \cdot A_{Bw}}{\delta_{Bw}} [\dfrac{g\beta_w \delta_{Bw}^3 (T_{CBu} - T_w)}{v_w^2} \Pr_w]^{\frac{1}{4}}} \tag{3.16}$$

Where β_w, v_w and $\Pr_w$ are evaluated at the film temperature $\dfrac{T_{CBu} + T_w}{2}$ while $\delta_{Bw} = \dfrac{\pi D_{Bw}}{4}$ for circular interface [50].

The total resistance from heating plate to the water bottom is:

$$R_{Hpw} = 0.00954 + \frac{1}{0.54 \dfrac{k_w \cdot A_{Bw}}{\delta_{Bw}} [\dfrac{g\beta_w \delta_{Bw}^3 (T_{CBu} - T_w)}{v_w^2} \Pr_w]^{\frac{1}{4}}} \tag{3.17}$$

Where the value 0.00954 is the thermal resistance from the heating plate top to the chamber base top as shown in Table 3.1.

The average thermal resistance from heating plate top to the water (including the interface between the chamber base and water) is 0.2711K/W [19]. Thus the chamber base upper surface temperature can be calculated based on the ratio below:

$$\frac{T_{Hp} - T_{CBu}}{T_{Hp} - T_W} = \frac{0.00954}{0.2711} \doteq 0.035 \tag{3.18}$$

This shows that the chamber base upper surface temperature is close to the heating plate temperature. Thus, T_{CBu} is assumed the same as T_{Hp} which will be discussed below.

3.3.1.2   Heat balance at the outer surface of the heating plate
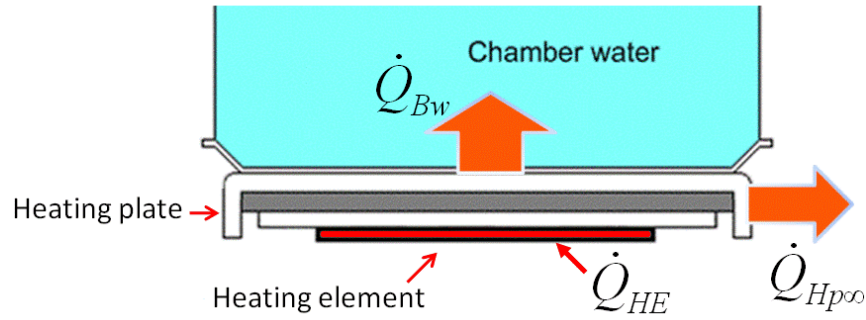
Figure 3.9 Heating plate heat balance

The heat generated by the heating element transfers to the heating plate (Figure 3.5). The thermal conduction resistance for each of these components can be expressed as:

$$R = \frac{l}{k \cdot A} \tag{3.19}$$

The overall resistance from heating element to heating plate is added up in table below:

Table 3.2 Overall resistance from heating element to heating plate [19]

Component	l(m) (Thickness)	k[W/(m·K)] (Thermal conductivity)	A(m²) (Area)	R(K/W) (Thermal resistance)
Ceramic substrate	0.000635	24	0.0025	0.01058
3M thermal conductive tape	0.00025	0.6	0.00567	0.07349
Aluminium heating plate	0.0012	237	0.01033	0.00049
Total from Ceramic to Plate				0.08456

The heat balance on the top of the heating plate can be written as (Figure 3.9):

$$\dot{Q}_{HE} = \dot{Q}_{Bw} + \dot{Q}_{Hp\infty} \tag{3.20}$$

$$\dot{Q}_{HE} = \frac{T_{HE} - T_{Hp}}{R_{HS}} \tag{3.21}$$

Because of the assumption that the ambient air is quiescent, the model is simplified to have only natural convection on all the outer surface area. For the outer circumferential vertical surface of the heating plate, the rim (Figure 3.9), Sparrow and Gregg have demonstrated that a vertical cylinder can be considered as flat vertical plate for the

Nusselt number. This may be applied when the ratio of D/H is large enough and the wall curvature will not significantly influence its convection boundary layer [51, 52]:

$$D/H \geq \frac{35}{Gr^{1/4}} \tag{3.22}$$

Where D is the diameter of the vertical cylindrical surface (the rim of the heating plate) and H is its height. For this rim, the average Grashof number is 2765 and the criterion is satisfied. Therefore the rim can be considered as flat vertical plate for Nusselt number calculation. The Prandtl number of the air is taken as a constant of 0.711 over the working temperature range of the CPAP machine [50]. The average Rayleigh number for the rim is about 2000, hence:

$$Nu = 0.59 Ra^{1/4} \tag{3.23}$$

is chosen [47]. The resistance on it can be calculated by:

$$R_{Hp\infty} = \frac{1}{0.59 \frac{A \cdot k_{ma}}{\delta} Ra^{1/4}} \tag{3.24}$$

Where the characteristic length δ is the rim height 0.009 m and k_{ma} is thermal conductivity of moist air.

Now, Eq.(3.20) leads to:

$$\frac{T_{HE} - T_{Hp}}{R_{HS}} = \frac{T_{Hp} - T_w}{R_{Hpw}} + \frac{T_{Hp} - T_\infty}{R_{Hp\infty}} \tag{3.25}$$

Therefore:

$$T_{Hp} = \left(\frac{1}{R_{HS}} + \frac{1}{R_{Hpw}} + \frac{1}{R_{Hp\infty}} \right)^{-1} \cdot \left(\frac{T_{HE}}{R_{HS}} + \frac{T_w}{R_{Hpw}} + \frac{T_\infty}{R_{Hp\infty}} \right) \tag{3.26}$$

T_{Hp} will be used in calculating R_{Bwn} as well as the heat from heating plate to the water $\dot{Q}_{Bw}$.

3.3.2 Heat flow from chamber water into ambient air via wall 1, $\dot{Q}_{C1i}$
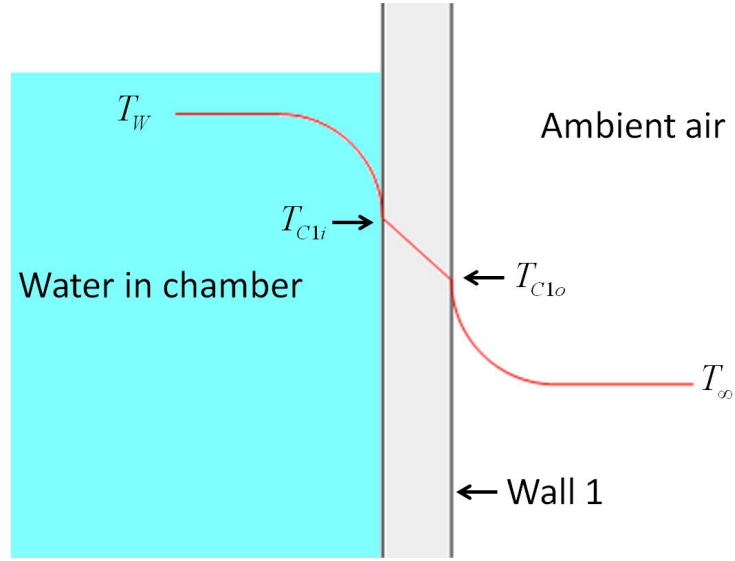
Figure 3.10 Temperature at wall 1

Due to the water high temperature, heat from the chamber water dissipates toward ambient through chamber wall (Figure 3.10). The chamber wall under water level is a vertical cylinder (wall 1). Based on Eq.(3.22), the chamber inner wall can be simplified as a vertical flat plate. On the inner surface there is only natural convection from water to the chamber wall. On its outer surface, since the chamber, specifically the lower hotter part, is well surrounded by the CPAP case, the radiation dissipation is neglected for simplification. Thus it is assumed that there is only natural convection on the chamber outer surfaces. The heat balance at wall 1 may be written as:

$$\dot{Q}_{C1i} = \dot{Q}_{C1st} + \dot{Q}_{C1o} \qquad (3.27)$$

However, since the water temperature and the ambient air temperature are simplified as constant during operation. Thus $\dot{Q}_{C1st}$ is neglected and Eq. (3.27) can be changed to:

$$\frac{T_w - T_{C1i}}{R_{C1i}} = \frac{T_{C1o} - T_\infty}{R_{C1o}} \qquad (3.28)$$

The heat dissipation into the ambient at the outer surface also equals to the conductive heat flow through the chamber wall. Thus:

$$\frac{T_{C1i} - T_\infty}{R_{C1cyl} + R_{C1o}} = \frac{T_{C1o} - T_\infty}{R_{C1o}} \qquad (3.29)$$

49

Therefore:

$$T_{C1o} = \frac{R_{C1cyl} \cdot T_\infty + R_{C1o} \cdot T_{C1i}}{R_{C1cyl} + R_{C1o}}$$ (3.30)

Substituting Eq. (3.30) into Eq. (3.28) gives:

$$T_{C1i} = (\frac{1}{R_{C1i}} + \frac{1}{R_{C1cyl} + R_{C1o}})^{-1} \cdot (\frac{T_w}{R_{C1i}} + \frac{T_\infty}{R_{C1cyl} + R_{C1o}})$$ (3.31)

T_{C1i} will be used to determine water and wall 1 interface film temperature and water properties on this surface which are temperature dependent. T_{C1i} will also be used to calculate the heat flow rate through wall 1 inner surface. Due to the high thermal conductivity and thickness of the wall, the difference between T_{C1i} and T_{C1o} is not significant. To simplify the computation, T_{C1i} is used to replace T_{C1o} in outer surface resistance calculation. Resistances in this equation can be determined as follows.

The conductive resistance through the cylindrical wall R_{C1cyl} can be written as [47]:

$$R_{C1cyl} = \frac{\ln(\frac{r_{C1o}}{r_{C1i}})}{2\pi l_{C1i} k_C}$$ (3.32)

The Sparrow and Gregg's criterion is also satisfied for both wall 1 inner surface and outer surface. Thus Eq. (3.23) is also applied here.

Now R_{C1i}, R_{C1o} and R_{C1cyl} are all determined and T_{C1i} now can be calculated by Eq.(3.31).

3.3.3 Heat transfer from the chamber water into chamber air $\dot{Q}_{wa}$

Heat transfer rate from the water to the chamber air is:

$$\dot{Q}_{wa} = \frac{T_w - T_{Cai}}{R_{ws}}$$ (3.33)

Where T_{Cai} is the chamber inlet air temperature. When airflow is from ADU to the chamber, T_{Cai} depends on ambient air temperature and humidity also on enthalpy gain

through ADU which is a function of pressure setting as empirically calculated in section 3.2. However, when reverse flow occurs, the air flowing into the chamber is the air from the HADT re-entering the chamber with its already heated and humidified properties.

The CPAP air flow rate may have a wide range from 0 to 100 L/min. as well as reverse flow. Therefore, both natural and forced convections need to be considered.

Natural convection Nusselt number over this horizontal round water surface can be calculated using the same values of C=0.54 and n=1/4 as that at the water bottom.
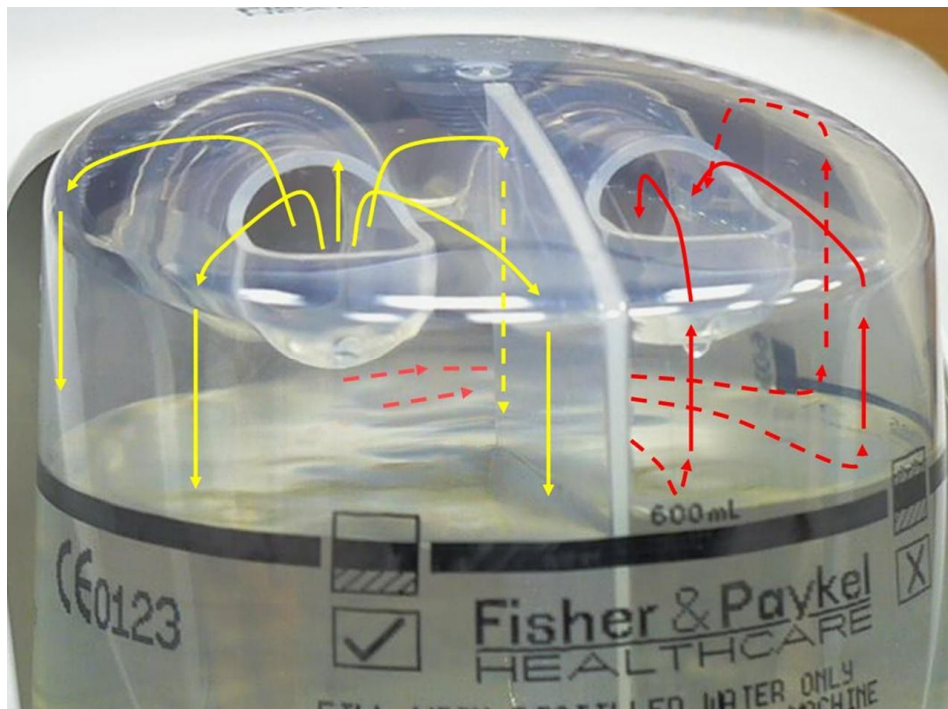
Figure 3.11 Airflow direction in the chamber

Flow pattern in the chamber is considered as turbulent [19]. Figure 3.11 shows the inlet and outlet air directions. When air flows into the chamber, it blows upward towards the chamber top then scatters and may return to directly impact onto the water surface. After touching the water surface, the air may flow horizontally over the surface to the other half of the chamber through the lower half of the opening which connects the two halves of the chamber. In the outlet half, the airflow may surf over the water surface then flow upward and finally leaves the chamber from outlet.

The impact of the inlet air on the water surface occurs only in the inlet half of the chamber. For chamber wall 2 and wall 3 surrounding the chamber air part, air is modelled as a single pass air flow over each of them.
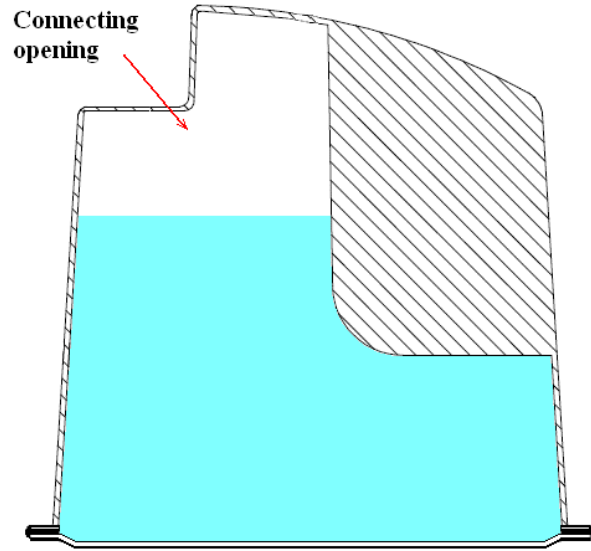
Figure 3.12 connecting opening in the chamber

The air flow velocity in the chamber is simplified as a characteristic velocity based on the volumetric air flow rate through the lower half of the opening (see Figure 3.12). When the water is filled to 600 ml, the area of this opening is about 16 cm^2.

$$u_C = \frac{\dot{q}_C}{0.5 A_{Co}}$$
(3.34)

Where A_{Co} is the connecting opening cross sectional area. When reverse flow occurs, the inlet is from the HADT.

The volumetric chamber air flow rate is considered the same as the chamber inlet flow rate. Thus for forced convection at water-air interface, the Nusselt number may be separately calculated as direct impact and parallel flow.

For air flowing directly toward a surface, Nusselt number may be calculated by [50]:

$$Nu_{dir} = 0.23 \, \mathrm{Re}_{ws}^{0.73} \, \mathrm{Pr}_a^{1/3}$$
(3.35)

While for airflow over a surface [50]:

$$Nu_{Cp} = 0.037 \, \mathrm{Re}_{ws}^{0.8} \, \mathrm{Pr}_a^{1/3}$$
(3.36)

Where Re_{ws} is the Reynolds number of air flow on the chamber water surface.

It is assumed that the direct impact covers half of the water surface and horizontal surface flow over the other half, the forced convection Nusselt number for the total water surface may be expressed as:

$$Nu_{wsf} = 0.5(Nu_{dir} + Nu_{Cp}) \tag{3.37}$$

Where Nu_{wsf} is total water surface forced convection Nusselt number.

The mixed convection on such surface may be calculated as follow [50, 53]:

$$Nu_{wsm} = (Nu_{wsn}^3 + Nu_{wsf}^3)^{1/3} = [Nu_{wsn}^3 + (0.5Nu_{dir} + 0.5Nu_{Cp})^3]^{1/3} \tag{3.38}$$

So thermal resistance on the chamber water surface is:

$$R_{ws} = \frac{1}{\dfrac{A_{ws} \cdot k_{ma}}{\delta_{ws}} Nu_{wsm}} = \frac{1}{\dfrac{A_{ws} \cdot k_{ma}}{\delta_{ws}} [Nu_{wsn}^3 + (0.5Nu_{dir} + 0.5Nu_{Cp})^3]^{1/3}} \tag{3.39}$$

Where A_{ws} is the water surface area. Thus the heat transfer from water to chamber air can be determined when the water temperature is known.

3.3.4   Heat lost from the chamber water into chamber air by evaporation $\dot{Q}_{ev}$

Evaporation rate on a horizontal surface may be calculated by [54]:

$$\dot{m}_{ev} = k_{ev} A_{ws} (C_{sv} - C_{Caiv}) \tag{3.40}$$

When the flow is from the ADU to the chamber, this inlet has the same specific humidity as ambient air but may have different level of absolute humidity due to temperature and pressure differences between the chamber and the ambient. When the flow is reversed, then the inlet is the air re-entering chamber from HADT and the absolute humidity is that of the re-entering air from the HADT. The absolute humidity can be calculated from the specific humidity as:

$$C_v = \frac{[28.966(1-d) + 18.01d]d \cdot P}{8.31T} \tag{3.41}$$

Where P is pressure in kPa and T is air temperature in K.

The water surface saturated absolute humidity C_{sv} can also be calculated by using Eq. (3.41) but using the saturated humidity at the water temperature.

The corresponding thermal energy removed from the water to chamber air by evaporation is:

$$\dot{Q}_{ev} = k_{ev} A_{ws} (C_{sv} - C_{Caiv}) h_{fg} \tag{3.42}$$

Where h_{fg} is the latent heat with unit of (J/kg) which depends on temperature of water where the vapour comes from [54]:

$$h_{fg} = 2257000 + 4182(100 - T_w) \tag{3.43}$$

For the mass convection (evaporation) coefficient k_{ev}, an analogy to heat convection is applied [55]:

$$k_{evn} = \frac{0.54(Gr \cdot Sc_a)^{1/4}}{\delta} D_{wa} \tag{3.44}$$

$$k_{evf} = \frac{0.5(0.23\,\mathrm{Re}_{ws}^{0.73}\,Sc_a^{1/3} + 0.037\,\mathrm{Re}_{ws}^{0.8}\,Sc_a^{1/3})}{\delta} D_{wa} \tag{3.45}$$

Where Sc_a is Schmidt number for molecular diffusivity of water vapour in air and D_{wa} is the mass diffusivity of water molecules from fluid water into air.

D_{wa}, may be expressed as [56]:

$$D_{wa} = 1.97 \times 10^{-5} (\frac{P_o}{P})(\frac{T}{T_o})^{1.685} \tag{3.46}$$

Where P_o is the standard atmospheric air pressure (101325 Pascals) and T_o is a specific standard temperature (256 K) for mass diffusivity empirical equation. However, since the mass diffusivity does not change very much within the working range, for simplifying the computation, an average value of 2.71×10^{-5} m^2/s calculated from Eq. (3.46) is used for chamber evaporation.

Schmidt number for molecular diffusivity of water vapour in air is defined as [56]:

$$Sc_a = \frac{v_a}{D_{wa}} \qquad (3.47)$$

Analogous to the convective heat transfer, the mixed mass convection may be expressed as:

$$k_{ev} = (k_{evn}^3 + k_{evf}^3)^{1/3} \qquad (3.48)$$

Thus, Eq. (3.40) and Eq. (3.42) for the evaporation rate and the thermal energy carried away by evaporation can be determined.

Based on all the analysis in this section and the inlet temperature calculation as well as the flow rate and pressure conditions analysed in chapter 2, Eq. (3.8) can be determined and the water temperature can now be calculated:

$$T_w = (\frac{1_w}{R_{Hpw}} + \frac{1}{R_{C1ni}} + \frac{1}{R_{ws}} + m_w c_w \frac{d}{dt})^{-1} \cdot$$

$$[\frac{T_{Hp}}{R_{Hpw}} + \frac{T_{C1i}}{R_{C1ni}} + \frac{T_{Cai}}{R_{ws}} - k_{ev} A_{ws} (C_{sv} - C_{Caiv}) h_{fg}] \qquad (3.49)$$

3.4 Chamber-air heat balance

The chamber-air heat balance is used to find the chamber air temperature under various combinations of ambient conditions and CPAP machine settings. The chamber air temperature is influenced by chamber water temperature, ambient air temperature, ambient air humidity, pressure setting, and air flow velocity over water surface as well as flow pattern and flow direction at the interface. Evaporation rate is also a factor influencing the heat brought in from the water by vapour molecules. There is also heat loss through the chamber walls surrounding the air space. When a patient's breathing is added in while the other conditions and settings remain the same, the heat transfer rate and evaporation rate on water surface will fluctuate and their average value will also be somewhat different from those of steady state. However, due to its large heat capacity, the water temperature may be considered constant.

3.4.1　Governing equation
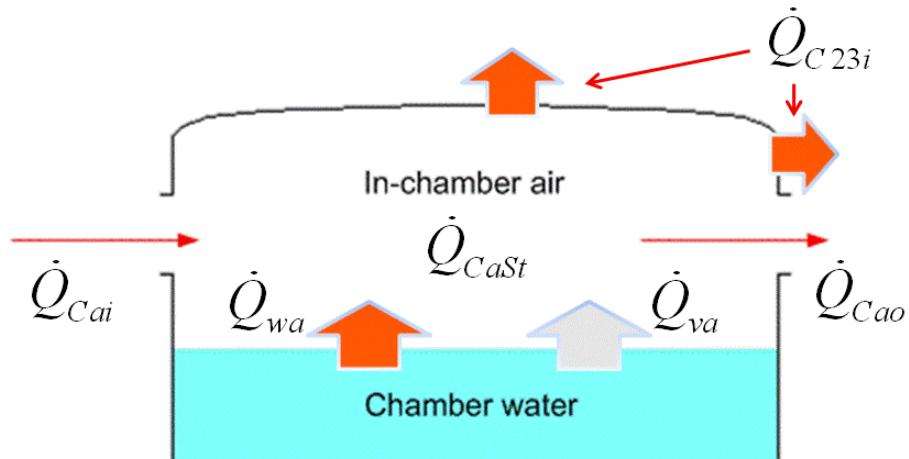
Figure 3.13 Chamber air heat balance

Figure 3.13 shows the chamber air heat balance. Thermal energy added into chamber air comes in by means of inlet, heat convection and evaporation from the water below it. Such acquired thermal energy is transferred to enthalpy by means of increasing the chamber air temperature i.e. change of heat storage in chamber air. The thermal energy is carried out by the outlet and dissipation to ambient through the chamber walls surrounding the air space. For simplification, the upper part of the vertical chamber wall (wall 2) and the top part of the chamber (wall 3) are assumed to have the same temperature (see Figure 3.5). It is further assumed that the outlet from the chamber has the same thermal properties as the chamber air. Note that when the flow is from ADU toward the patient, the inlet is from ADU via the connecting duct and outlet goes into HADT. However, during reverse flow, the inlet is the air re-entering the chamber from HADT and outlet is the air pushing back into the connecting duct from the chamber. The governing equation of the chamber-air thermal balance may be expressed as:

$$\dot{Q}_{Cai} + \dot{Q}_{wa} + \dot{Q}_{va} = \dot{Q}_{Cao} + \dot{Q}_{CaSt} + \dot{Q}_{C23i} \qquad (3.50)$$

$\dot{Q}_{wa}$ is the same as it is in Eq. (3.7) for heat balance in the water. Equations for the remaining terms in Eq. (3.50) will be analysed and derived in following subsections.

3.4.2　Heat carried into chamber air by evaporated molecules

The heat brought into chamber air by the evaporated water molecules is the same as that analysed in the water heat balance analysis in section 3.3. However, as long as this vapour does not condense, the latent heat will be kept in these water vapour molecules

and keep them in gaseous status. Only a part of the thermal energy brought from the water will participate the chamber air thermal energy sharing. Thus the sharable energy brought into chamber air by evaporated water can be expressed as [54]:

$$h_{va} = 4182 \times T_w \qquad (3.51)$$

Where h_{va} is the sharable thermal energy brought in by evaporated water in J/kg.

3.4.3 Thermal energy brought in at the chamber inlet

The energy brought in by air inlet when air flows from the ADU is:

$$\dot{Q}_{Cai} = \dot{m}_D c_{Da} T_{Cai} \qquad (3.52)$$

Where:

$$\dot{m}_D = A_{Dcs} \rho_{Da} u_D \qquad (3.53)$$

Also according to Eq. (3.6), $T_{Cai} = T_\infty + \Delta T_{ADUa}$. So Eq. (3.52) may be expanded to:

$$\dot{Q}_{Cai} = c_{Da} A_{Dcs} \rho_{Da} u_D (T_\infty + \Delta T_{ADUa}) \qquad (3.54)$$

However, when reverse flow occurs the inlet is from the HADT. The energy brought in is:

$$\dot{Q}_{Cai} = \dot{m}_T c_{Ta} T_{Cai} \qquad (3.55)$$

Here the inlet temperature T_{Cai} is the air temperature in HADT lump 1.

3.4.4 Thermal energy at the outlet

Same as the inlet calculation above, the outlet also needs to consider the flow direction. When reverse flow occurs the air flows into the chamber from HADT and flows out toward ADU.

3.4.5 Heat storage in chamber air

The heat storage in the chamber air may be expressed as:

$$\dot{Q}_{CaSt} = m_{Ca} c_{Ca} \frac{dT_{Ca}}{dt} \qquad (3.56)$$

3.4.6 Heat transfer from chamber air into ambient via wall 2 and 3

The flow pattern through the chamber is very complicated. The situation is simplified by assuming that the air flow in the chamber flows only once over all the chamber inner surfaces [19]. It is further assumed that the flow produces a characteristic velocity over all the surfaces which is defined by Eq. (3.34) as $u_C = \frac{\dot{q}_C}{0.5 A_{Co}}$.

Note that the water surface is dropping while the CPAP is in use due to evaporation. However neglecting this change will not influence the objectives of the project. Also due to flow velocity may range widely from 0 to 100 L/min., both natural and forced convections need to be included. To calculate T_{C23i}, the temperature at the inner surface of wall 2 and wall 3, energy balance at the inner surface is carried out below.

The heat transfer toward the chamber wall 2 and 3 at their inner surfaces is converted to wall heat storage and heat dissipation into ambient:

$$\dot{Q}_{C23i} = \dot{Q}_{C23St} + \dot{Q}_{C23o} \qquad (3.57)$$

Since the breathing induced airflow fluctuating is very short comparing to the chamber wall temperature change, the wall 2 and wall 3 temperature is simplified as constant therefore $\dot{Q}_{C23St}$ is neglected. Thus Eq. (3.57) can be changed as:

$$\frac{T_{Ca} - T_{C23i}}{R_{C23i}} = \frac{T_{C23o} - T_\infty}{R_{C23o}} \qquad (3.58)$$

Same as the analysis of wall 1 thermal balance, inner surface temperature of wall 2 and 3 can be calculated as:

$$T_{C23i} = \left(\frac{1}{R_{C23i}} + \frac{1}{R_{C23} + R_{C23o}}\right)^{-1} \cdot \left(\frac{T_{Ca}}{R_{C23i}} + \frac{T_\infty}{R_{C23} + R_{C23o}}\right) \qquad (3.59)$$

Where R_{C23} is the conductive thermal resistance of wall 2 and wall 3 together. Heat transfer through the walls includes mixed convection at inner surface, conduction

through the walls and natural convection at outer surface. These resistances will be analysed below.

3.4.6.1 Mixed convectional thermal resistance R_{C23i}

At the inner surfaces of chamber wall 2 and 3, the flow is considered to be always turbulent. Nusselt number for forced convection at the inner surface of wall 2 and wall 3 can be considered as airflow over these surfaces and be calculated the same as the water surface flow by Eq.(3.36).

The Nusselt number for natural convection over the vertical wall 2 can be calculated by using Eq. (3.23). The mixed convection Nusselt number at this surface can be:

$$Nu_{C2mi} = (Nu_{C2ni}^3 + Nu_{C2fi}^3)^{1/3} \qquad (3.60)$$

The inner surface of wall 3, which is the chamber top, is simplified as a horizontal round plate with cooler surface facing down (see Appendix XIX for Nusselt number coefficient values). Nusselt number for mixed convection on wall 3 inner surface can be calculated same as Eq. (3.60). So the total mixed convectional thermal resistance over the two inner surfaces can be calculated as:

$$R_{C23i} = \cfrac{1}{\cfrac{A_{C2i} \cdot k_{ma}}{\delta_{C2i}} Nu_{C2mi} + \cfrac{A_{C3i} \cdot k_{ma}}{\delta_{C3i}} Nu_{C3mi}} \qquad (3.61)$$

3.4.6.2 The conductive thermal resistance through the chamber wall 2 and 3

The conductive resistance of wall 2 can be calculated the same as wall 1. Wall 3 is simplified as a flat round plate. The over all conductive thermal resistance of chamber wall 2 and 3 surrounding the air part of the chamber can be:

$$R_{C23} = \frac{R_{C2cylinder} \cdot R_{C3}}{R_{C2cylinder} + R_{C3}} \qquad (3.62)$$

3.4.6.3 The thermal resistance at outer surfaces of wall 2 and 3

For simplification, the heat dissipation at the outer surfaces of the chamber upper part is also considered natural convection only. The overall natural convection thermal resistance on these two outer surfaces together can be calculated as:

$$R_{C23no} = \frac{1}{\dfrac{A_{C2o} \cdot k_{ma}}{\delta_{C2o}} Nu_{C2no} + \dfrac{A_{C3o} \cdot k_{ma}}{\delta_{C3o}} Nu_{C3no}}$$

(3.63)

Now Eq. (3.59) for T_{C23i} can be calculated by plugging in all the items derived in equations from Eq. (3.60) to Eq. (3.63).

As all the variables in the governing equation (3.58) have been derived and obtainable, T_{Ca} can now be calculated by rearranging Eq. (3.58) into:

$$T_{Ca} = \frac{c_{Cai} T_{Cai} \dot{m}_{Cai} + \dfrac{T_w - T_{Cai}}{R_{ws}} + k_{ev} A_{ws} (C_{sv} - C_{Caiv}) h_{fg} + \dfrac{T_{C23i}}{R_{C23i}}}{m_{Ca} c_{Ca} \dfrac{d}{dt} + c_{Ca} \dot{m}_{Cao} + \dfrac{1}{R_{C23i}}}$$

(3.64)

Where C_{Caiv} is the chamber inlet absolute humidity. When reverse flow occurs, the chamber inlet is from the HADT, thus c_{Cai}, T_{Cai}, $\dot{m}_{Cai}$ and C_{Caiv} should be those of the airflow from HADT.

The specific humidity of outlet from the chamber is considered as the same as that of the air in the chamber. Humidity balance in the chamber may be considered as inlet vapour plus evaporated vapour equals to outlet vapour:

$$d_{Ca} \dot{m}_C = d_\infty \cdot \dot{m}_C + \dot{m}_{ev}$$

(3.65)

Therefore:

$$d_{Ca} = \frac{d_\infty \cdot \dot{m}_C + \dot{m}_{ev}}{\dot{m}_C}$$

(3.66)

Where d_{Ca} is the specific humidity of the chamber air and $\dot{m}_C$ the mass flow rate in the chamber and may be considered as the average of connecting duct mass flow rate and HADT mass flow rate. $\dot{m}_{ev}$ can be calculated by Eq. (3.40).

3.5 HADT heat balance

After the airflow is heated and humidified in the chamber, it continues flowing toward patient through the HADT. When there is reverse flow, the airflow may firstly be stopped and then reverse toward the chamber from the mask. No matter which direction the air flows, if there is no heat added in, the air cools down because of heat transfer into the ambient through the HADT wall.

When the air temperature drops down below its dew point, the specific humidity will drop because of condensation. If this occurs, the built-up condensate in the HADT can increase pressure drop in it thus reduce the pressure in the mask [36]. Also cooler air with lower specific humidity continuously blows into patient's upper airway may make the patient uncomfortable. To avoid these, the HADT has embedded copper wire to provide heat to the tube wall so to heat up or maintain airflow temperature. The tube heating will be turned on when it is needed and its heating level is adjustable. Figure 3.14 shows the HADT wall.
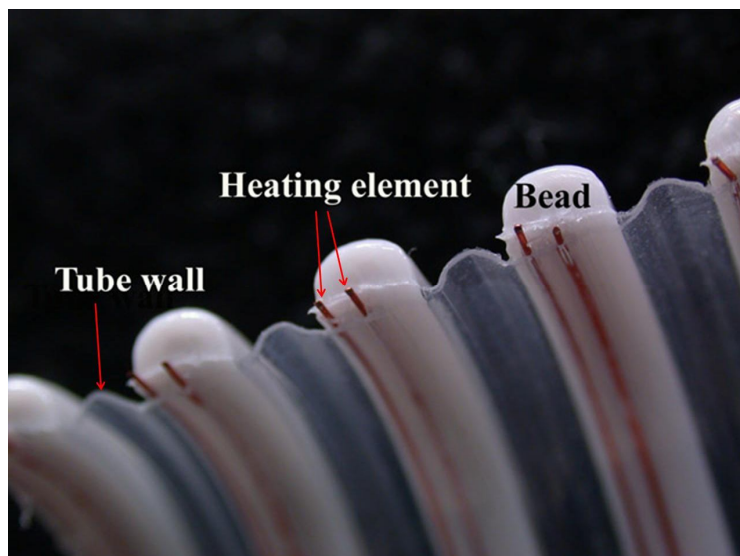
Figure 3.14 Heated air delivery tube wall [19]

HADT thermal balance analysis is to determine the temperature change of the air and the potentiality for condensation along the HADT under various combinations of

ambient conditions and CPAP machine settings. The main factors influencing the condensation may be the inlet temperature and humidity level, ambient air temperature and humidity, tube heating setting and air flow rate. Tube size, shape, surface conditions and tube wall temperature are also factors. The thermal contact resistance between the copper heating wire and the HADT wall is simplified as zero, the thermal capacitance of the copper wire is also neglected. The axial conduction along the HADT wall and the airflow are both neglected. The HADT is a thin and long tube exposed in the ambient and the surface area is large compared with its volume, neglecting the radiation from its outer surface may bring significant error. Thus heat dissipation at its outer surface is considered as both natural convection and radiation.

Heat balances are applied to each lump and to the wall as follows.

The equation for air is:

$$\dot{Q}_{Tin} - \dot{Q}_{Ton} + \dot{Q}_{Ticn} = \dot{Q}_{Tastn} \qquad (3.67)$$

Also assuming the HADT wall temperature is stable, the equation for HADT lump wall is:

$$\dot{Q}_{Thn} = \dot{Q}_{Tocn} + \dot{Q}_{Torn} + \dot{Q}_{Ticn} \qquad (3.68)$$

$\dot{Q}_{Thn}$, the thermal energy provided by tube heating to each HADT lump, is the total energy from copper wire divided by the number of lumps, n in all these subscriptions represents the lump number. Expressions for these items are to be derived in following sub-sections.

3.5.1   Heat energy brought in and out by inlet and outlet

The heat energy brought into the lump by inlet can be expressed as:

$$\dot{Q}_{Tin} = c_{Tan} T_{Ta(n-1)} A_{Tcs} \rho_{Ta} u_T \qquad (3.69)$$

While the heat energy brought away from the lump by outlet can be expressed as:

$$\dot{Q}_{Ton} = c_{Tan} T_{Tan} A_{Tcs} \rho_{Ta} u_T \qquad (3.70)$$

$T_{Ta(n-1)}$ is also considered as inlet temperature of the lump under inspection. T_{Tan}, air temperature in this lump, is also considered as inlet temperature of next lump.

However, when reverse flow occurs, air flows from bigger numbered lump toward smaller numbered lump. The last lump receives air from the mask and the air in lump 1 flows back into the chamber.

3.5.2 Convection at HADT lump inner surface

The HADT internal convection is considered forced convection only because its small internal dimension does not give much space for natural convection to develop. Nusselt number for internal forced convection can be expressed as [57]:

$$Nu_{Ti} = 0.052 \, \text{Re}_{Ti} \sqrt{\text{Pr}_a} \cdot \sqrt{f_T} \tag{3.71}$$

f_T is the Darcy-Weisbach friction factor explained in chapter 2 which gives $\sqrt{f_T} = \dfrac{0.5625}{\text{Re}_{Ti}^{0.125}}$. Thus Nusselt number above becomes:

$$Nu_{Ti} = 0.02925 \, \text{Re}_{Ti}^{0.875} \, \text{Pr}_a^{0.5} \tag{3.72}$$

Therefore the convectional resistance on HADT lump inner surface is:

$$R_{Ticn} = \frac{1}{0.02925 \, \text{Re}_{Ti}^{0.875} \, \text{Pr}_a^{0.5} \dfrac{k_{ma} A_{Tli}}{\delta_{Ti}}} \tag{3.73}$$

3.5.3 Convection at HADT lump outer surface

The HADT may be modelled as a horizontal cylinder and the natural convectional thermal resistance at an HADT lump outer surface may be expressed as [55]:

$$R_{Toc} = \frac{1}{1.02 \dfrac{k_{ma} A_{Toc}}{\delta_{To}} Ra_{To}^{0.148}} \tag{3.74}$$

However, the HADT outer surface is corrugated (Figure 3.15). The corrugation increases the surface area as well as the convection. A_{Toc} in Eq. (3.74) is the corrugated

outer surface area of the lump which is about 196% of its cylindrical basic surface area (See Appendix IV for calculation details).

Corrugated outer surface
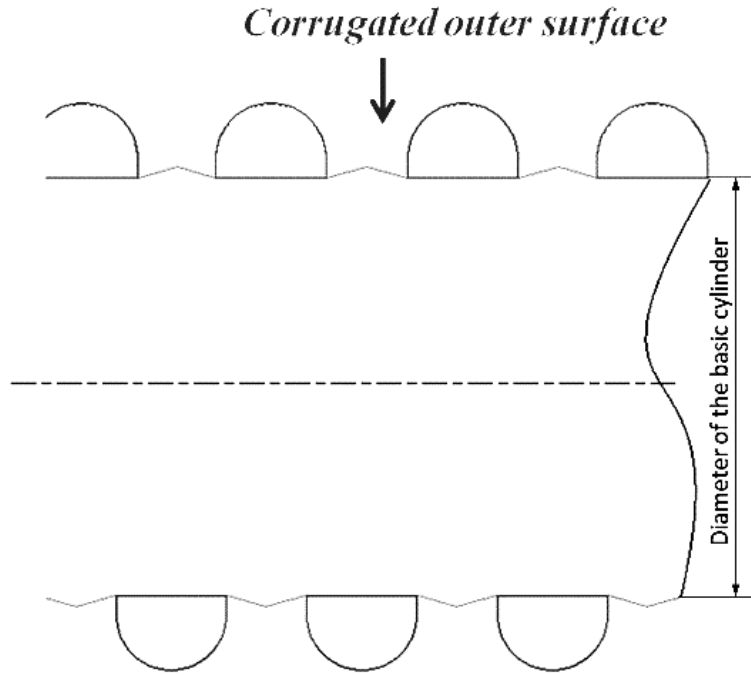
Figure 3.15 the corrugated HADT outer surface

3.5.4 Radiation at HADT outer surface

The radiation heat transfer on the surface of a body can be expressed as [58]:

$$\dot{Q}_{Br} = \frac{T - T_\infty}{R_{Br}} = A\sigma\varepsilon(T^4 - T_\infty^4) \qquad (3.75)$$

Where $\dot{Q}_{Br}$ is the radiation heat transfer rate, R_{Br} the radiation thermal resistance, σ is the Stefan-Boltzmann constant (5.67×10^{-8} W/m^2·K^4) and ε the emissivity of the surface.

The radiation heat dissipation rate at an HADT lump outer surface can be calculated as:

$$\dot{Q}_{Torn} = \frac{T_{TWn} - T_\infty}{R_{Torn}} \qquad (3.76)$$

Where R_{Torn} is radiation thermal resistance at the HADT outer surface of the lump and can be expressed as:

64

$$R_{Torn} = \frac{1}{\varepsilon \delta A_{Tlor}(T_{TWn} + T_{\infty})(T_{TWn}^2 + T_{\infty}^2)} \qquad (3.77)$$

Where A_{Tlor} is outer surface area of a lump for radiation calculation. The emissivity of the tube wall (Polyethylene) is given as 0.85 [59]. The outer surface temperature can be replaced by the HADT wall temperature as discussed above.

Due to view factor for radiation [55], the basic cylindrical diameter of the HADT outer surface 19.3 mm (0.0193 m) is chosen as the area for the surface radiation calculation.

3.5.5 Heat storage in air of the lump

$\dot{Q}_{Tastn}$, heat storage in this air lump, may be calculated as:

$$\dot{Q}_{Tastn} = m_{Tla} c_{Tan} \frac{dT_{Tan}}{dt} = (\rho_{Ta} V_{Tl}) c_{Tan} \frac{dT_{Tan}}{dt} \qquad (3.78)$$

Where m_{Tla} is air mass in this lump and V_{Tl} is the internal capacity of a HADT lump which is also the volume of air in this lump.

Substituting above expressions into Eq. (3.67) and rearranging gives:

$$T_{Tan} = \frac{A_{Tcs} \rho_{Ta} c_{Tan} u_T T_{Ta(n-1)} + \dfrac{T_{TWn}}{R_{Ticn}}}{m_{Tla} c_{Tan} \dfrac{d}{dt} + A_{Tcs} \rho_{Ta} c_{Tan} u_T + \dfrac{1}{R_{Ticn}}} \qquad (3.79)$$

Substituting above expressions into the Eq. (3.68) and rearranging gives:

$$T_{TWn} = \frac{\dot{Q}_{Thn} + \dfrac{T_{Tan}}{R_{Ticn}} + \dfrac{T_{\infty}}{R_{Tocn}} + \dfrac{T_{\infty}}{R_{Torn}}}{\dfrac{1}{R_{Ticn}} + \dfrac{1}{R_{Tocn}} + \dfrac{1}{R_{Torn}}} \qquad (3.80)$$

This pair of equations now can be used to calculate air temperature and HADT wall temperature as well as the heat balance of the inspected HADT lump.

3.6 HADT wall inner surface condensation analysis

One of the objectives of this thesis is to analyse and predict whether and where along the HADT condensation will occur under a certain condition and setting combination and to compare such condensation between steady flow and breath-added situations.

There are three types of condensation namely direct contact condensation, homogenous condensation and surface condensation [58]. The direct contact condensation does not apply to this CPAP machine. For the condensation in the HADT, when the tube heating is off, the airflow temperature inside the HADT is higher than the HADT wall temperature, so the surface condensation will always occur prior to the homogenous condensation. When the tube heating is on, usually there will be no condensation. Even there is homogenous condensation, it will be hard for condensate to form on the HADT wall inner surface because of entrainment. Therefore, it is reasonable to only consider surface condensation in this thesis.

3.6.1 General comparison of condensation and evaporation

When moist air flows over a surface, if its humidity level is lower than the saturated humidity level at surface temperature, the air will take in water molecules from the surface. In another words, this airflow has a potentiality of vaporization. Evaporation rate on such a surface is determined by the difference of absolute humidity level in the moist airflow and the Absolute humidity level saturated at surface temperature as well as mass convection coefficient and surface area as mentioned before:

$$\dot{m}_{ev} = k_{ev}A(C_{sv} - C_{av}) \tag{3.81}$$

On the other hand, if the moist airflow touches a surface and the surface temperature is lower than the air's dew point, some of the water will condense on the surface. That is to say condensation is converse to evaporation [52]. From Marek [60], under same conditions, condensation rate is about 1.2 times of evaporation rate. This means it is practical to use the same evaporation rate calculation equation to calculate both evaporation and condensation if the conditions for evaporation and condensation do not vary significantly.

However, it is necessary to point out that the calculation of condensation based on evaporation equation can predict where the condensation will occur and compare the

condensation severity but cannot calculate the actual amount of condensate built-up in a period of time. This is because once condensate starts to build up, the thermal conditions on the surface changes and the condensation rate will be no longer the same [42].

3.6.2 Condensation within the HADT

When there is no patient's breathing, the CPAP machine is working in a steady state and provides a steady flow. The condensation in the HADT can be predicted by comparing the dew point temperature of the airflow to the local HADT wall (the local lump) temperature. If the wall temperature is lower than the airflow dew point, condensation will occur on the inner surface of the wall. By data regression between 5°C ~60°C [61], dew point can be expressed as below (see Appendix V for regression details):

$$T_{DewPt} = 17.222 \ln d + 93.343 (°C) \tag{3.82}$$

Where d is specific humidity defined in chapter 3.

The condensation can also be predicted by comparing relative humidity of the airflow in the HADT to the saturated relative humidity at the local HADT wall temperature. If the airflow relative humidity is higher than the wall temperature saturated relative humidity, there will be water vapour spared out from the airflow onto the HADT wall.

With the patient's breathing, the humidity of airflow in the HADT is fluctuating. The surface temperature may be higher or lower than the dew point. The condensation under such fluctuation can only be calculated by humidity comparison. Net condensation within a breath cycle can be used to predict the condensation build-up. The evaporation rate in a lump of the HADT may be expressed as:

$$\dot{m}_{ev} = k_{ev} A_{Tli} (C_{Tsv} - C_{Tav}) \tag{3.83}$$

Where C_{Tsv} is the saturated absolute humidity level at the local HADT wall temperature and C_{Tav} is the absolute humidity of airflow through the lump.

Analogous to heat convection, the mass convection coefficient k_{ev} may be expressed as:

$$k_{ev} = \frac{0.02925\,\mathrm{Re}_{Ti}^{0.875}\,Sc_a^{0.5}}{\delta} D_{wa} \qquad (3.84)$$

Based on the conditions here, an average value of 2.67×10^{-5} m^2/s for D_{wa} is used for simplifying the computation.

Based on the analysis above, condensation rate at the same place can be expressed as:

$$\dot{m}_{cndns} = 1.2 \cdot k_{ev} A_{Tli}(C_{Tsv} - C_{Tav}) \qquad (3.85)$$

$\dot{m}_{cndns}$ is condensation rate and quantitatively equals to 120% of evaporation rate but with opposite sign because $C_{Tsv} < C_{Tav}$ when condensation is occurring.

Eq. (3.83) and Eq. (3.85) can be combined as:

$$\dot{m}_{Tlec} = k_{ec}k_{ev}A_{Tli}(C_{Tsv} - C_{Tav}) \qquad (3.86)$$

Where $\dot{m}_{Tlec}$ is HADT lump inner surface condensation or evaporation rate, k_{ec} may be named as condensation-to-evaporation coefficient. When $C_{Tsv} > C_{Tav}$, evaporation may occur and $k_{ec} = 1$. When $C_{Tsv} < C_{Tav}$, condensation occurs and $k_{ec} = 1.2$.

Integration of positive part of $\dot{m}_{Tlec}$ within a breath cycle gives the cycle-wise total amount of potential evaporation and integration of negative part of $\dot{m}_{Tlec}$ within a breath cycle gives that of condensation.

$$m_{TlecP} = \int k_{ev} A_{Tli}(C_{Tsv} - C_{Tav})dt \qquad \text{when } C_{Tsv} - C_{Tav} > 0 \qquad (3.87)$$

And:

$$m_{TlecN} = 1.2\int k_{ev} A_{Tli}(C_{Tsv} - C_{Tav})dt \qquad \text{when } C_{Tsv} - C_{Tav} < 0 \qquad (3.88)$$

$$m_{Tlec} = m_{TlecP} + m_{TlecN} \qquad (3.89)$$

The sum of the two integrals gives the net condensation or evaporation within a breath cycle on inner surface of this lump. If the sum is positive, it means there is no condensation remaining within a whole breath cycle. It may mean that there is no

condensation has occurred at all or it may also be possible that condensation occurred but the condensate has already dried up by incoming warmer and drier airflow.

3.7 Mask heat balance

Figure 3.16 Nasal mask type "FlexFit™407" and Full face mask type "FlexFit™432"

Two types of mask are taken into investigation. One is nasal mask type "FlexFit407" and another is full face mask type "FlexFit432" (Figure 2.17).
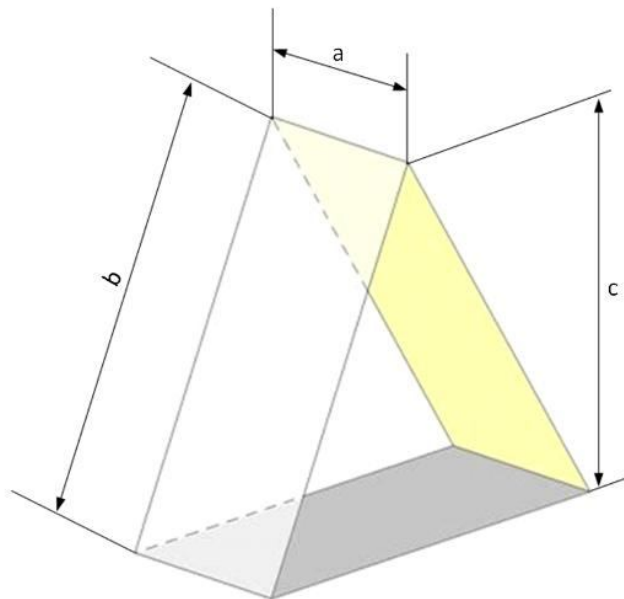
Figure 3.17 Simplified mask geometry

The dimensions in Figure 3.17 are listed below.

a = Mask height (width of rectangular side plates)

b = Length of rectangular side plates (width of triangular plate)

c = Length of triangular plate

The geometry of the masks is simplified as simple triangular shaped [19] as shown in Figure 3.17. For easiness in modelling and easy model use, the full face mask is simplified as 1.5 times in all one dimensional sizes except wall thickness is the same as that of the nasal one. Correspondingly, the full face mask volume is 3.375 times ($1.5^3 = 3.375$) of the nasal mask volume and the weight ratio is 2.25 ($1.5^2 = 2.25$). Place an average-sized human nose of 3.8 cm in width at the centre in the mask [62] and assume the air flows over each of the mask internal surfaces once only. By using the velocity over the rectangular surface as characteristic velocity, the airflow velocity on the mask inner surfaces can be expressed as:

$$u_{MW} = \frac{\dot{m}_P / \rho_{Ma}}{\frac{1}{2}(w_{P1i} - w_{nose})l_{P1i}}$$
(3.90)

Where w_{nose} is the average width of human nose.

The real full face mask has bias vent holes on itself. For comparison of the mask size effect, the full face mask is modelled same as nasal mask with no bias vent holes on itself but connected to a holed elbow for ventilation.

The technique of thermal balance in the mask is same as that of HADT lump and a pair of governing equations may be expressed as follow. For heat energy balance of air in the mask:

$$\dot{Q}_{Mi} - \dot{Q}_{Mo} - \dot{Q}_{Mic} = \dot{Q}_{Mast}$$
(3.91)

For heat energy balance of mask wall based on the assumption of stable mask wall temperature:

$$\dot{Q}_{Mic} = \dot{Q}_{Moc} + \dot{Q}_{Mor}$$
(3.92)

The inlet is the air from HADT during inhalation phase and is exhaled air from patient during exhalation phase. For simplification, it is assumed that there are only natural convectional on mask outer surface. Air mass in the mask is also simplified as constant. Similar to HADT lump analysis, Eq. (3.91) and Eq. (3.92) can be expanded and rearranged respectively:

$$T_{Ma} = \frac{c_{Ma}\dot{m}_P T_{Mi} + \dfrac{T_{MW}}{R_{Mic}}}{c_{Ma}m_{Ma}\dfrac{d}{dt} + c_{Ma}\dot{m}_P + \dfrac{1}{R_{Mic}}} \tag{3.93}$$

$$T_{MW} = \frac{\dfrac{T_{Ma}}{R_{Mic}} + \dfrac{T_{\infty}}{R_{Moc}}}{\dfrac{1}{R_{Mic}} + \dfrac{1}{R_{Moc}}} \tag{3.94}$$

T_{Mi}, the inlet air temperature, is the temperature of air from HADT lump 30 when in inhalation phase and temperature of exhaled air at 33°C in exhalation phase [30].

Since the rectangular side walls of the masks are of silicon seal and foam cushion (Figure 3.18), these walls are simplified as insulated therefore the heat exchange with the ambient is considered only occurs at the triangular wall. However, condensation may still occur on the inner surfaces of the rectangular walls. Temperature on these rectangular inner surfaces is assumed as the same as the average temperature of the air in the mask.
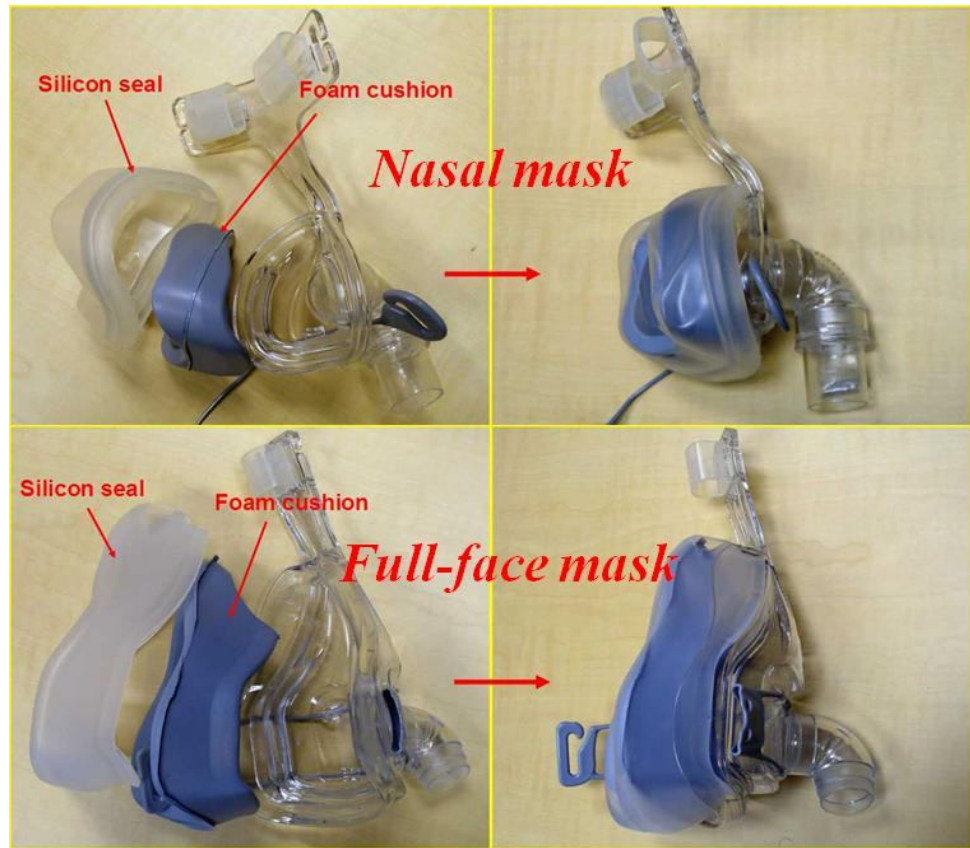
Figure 3.18 Silicon seal and foam cushion of the masks

3.8   Mask inner surface condensation

Similar to the analysis of condensation and evaporation in HADT, the mask inner surface condensation or evaporation rate may be expressed as:

$$\dot{m}_{Mec} = k_{ec} k_{ev} A_{Mi} (C_{Msv} - C_{Mav})$$

(3.95)

Integration is again used here for calculating the net condensation or evaporation.

$$m_{MecP} = \int k_{ev} A_{Mi} (C_{Msv} - C_{Mav}) dt \qquad \text{when } C_{Msv} - C_{Mav} > 0 \qquad (3.96)$$

And:

$$m_{MecN} = 1.2 \int k_{ev} A_{Mi} (C_{Msv} - C_{Mav}) dt \qquad \text{when } C_{Msv} - C_{Mav} < 0 \qquad (3.97)$$

$$m_{Mec} = m_{MecP} + m_{MecN}$$

(3.98)

Also, there will be net condensation build up if the sum of the two integrals is negative within a breath cycle.

3.9 Average temperature of inhaled air

The average temperature of inhaled air can be calculated as below and the integration only integrates over the inhalation phase.

$$T_{inh} = \frac{\int T_{Ma} \cdot \dot{q}_P dt}{\int \dot{q}_P dt} \qquad (3.99)$$

3.10 Average specific humidity of inhaled air

The average specific humidity within a total inhalation can be calculated as below and the integration only integrates over the inhalation phase.

$$d_{inh} = \frac{\int d_M \cdot \dot{q}_P dt}{\int \dot{q}_P dt} \qquad (3.100)$$

Where d_{inh} is the overall specific humidity within a total inhalation and d_M is the specific humidity of air in the mask.

3.11 Closure of the thermodynamic mathematical modelling

The mathematical equations have been developed for the thermodynamics of the CPAP in this chapter. These mathematical equations will be converted into Simulink^{TM} model. The model will be capable to simulate and calculate the breathing induced airflow fluctuation in the system, the reverse flow, the dynamic fluctuations of the evaporation rate in the chamber, the transportation of fluid through the HADT with a varying-time delay, the condensation in HADT and the mask, the mixing of air, the specific humidity and temperature of the inhaled air.

Chapter 4 SIMULINK™ Modelling

4.1 Introduction

In this chapter, the process of simulating the mathematical models into computational models is explained. Each part of the CPAP mathematical model that was set up in chapter two and three is to be built up as a separate subsystem in Simulink™ model in the Matlab™ environment. The computational models are basically Simulink™ block diagram expressional version of the equations derived in previous chapters. However there will be some adjustments because of computational easiness which will be explained when there is such. The project will provide two Simulink™ models one for fluid dynamic and exhaled air rebreathing analysis and another for thermodynamic analysis. The two models are to be explained in details in this chapter.

4.2 Computational model of fluid dynamics and exhaled air re-breathing

This model is used to calculate the reverse flow and exhaled air re-breath. The model consists of a fluid dynamic section which further contains several subsystems, HADT lumps with lump-delay subsystem, reverse flow calculation subsystem and mask mixing subsystems.

The whole model consists of a fluid dynamic subsystem, 30 lump airflow delay subsystems, a mask mixing subsystem and an exhaled air and CO_2 calculation subsystem.

The inputs to the model are listed in Table 4.1:

Table 4.1 Inputs to the fluid dynamics model

Input	Unit
Pressure setting	cmH_2O
Breath magnitude ratio	N. D.*
Mask capacity ratio	N. D.
Human nose in-mask space occupancy factor	N. D.

* N. D. means no dimension applicable.

The outputs are listed in Table 4.2:

Table 4.2 Inputs of the fluid dynamics model

Output	Unit
Breath load	(gram per breath cycle)
Pressures at ADU outlet, chamber and mask	Pa
Flow velocity in the connecting duct	m/s
Flow velocity in HADT	m/s
Backflow (reverse flow) (Graph output, curve)	m
Backflow (reverse flow) (Display output, Maximum distance)	m
Exhaled air level in lumps	Normalized (0~1)
Exhaled air level in the mask	Normalized (0~1)
Percentage of exhaled air in next inhalation	Percentage
Percentage of CO_2 in next inhalation	Percentage

The block diagram and the Simulink[TM] model of the whole system are shown in Figure 4.1 and Figure 4.2 respectively:
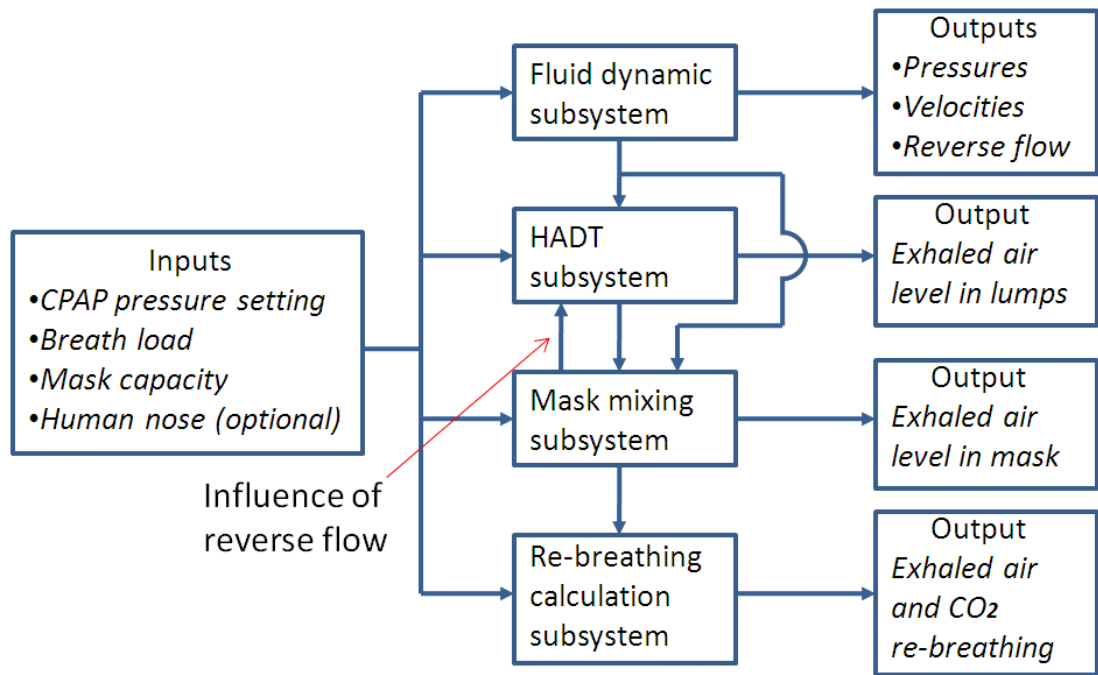
Figure 4.1 Block diagram of CPAP fluid dynamic and exhaled air re-breath analyses model
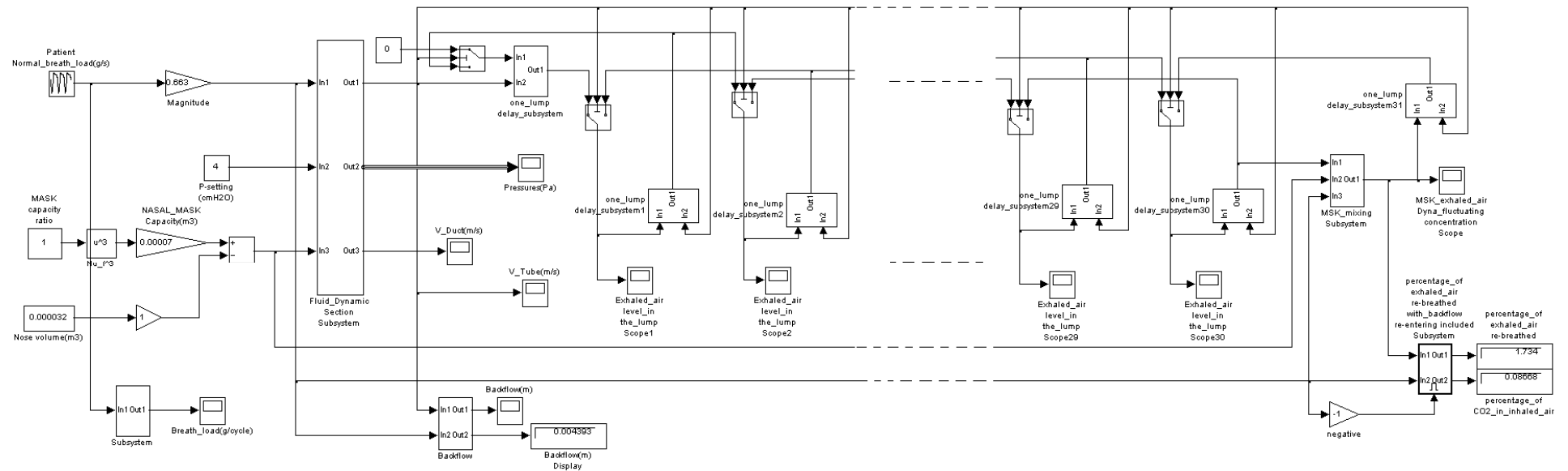
Figure 4.2 Simulink^{TM} model for fluid dynamic and exhaled air re-breathing analysis

4.2.1 The overall fluid dynamic section

Figure 4.3 shows the overall fluid dynamic section. Its inputs are listed in Table 4.3:

Table 4.3 Inputs to the overall fluid dynamic section subsystem

Input port number	Input	Unit
1	Patient's breath load	g/s
2	ADU pressure setting	cmH$_2$O
3	Mask capacity	m^3

The fluid dynamic section mainly provides tube flow velocity which will be used to calculate reverse flow and exhaled air mixing. The mask capacity is adjustable for analyse of mask size influence on reverse flow and exhaled air re-breath. For the inputs to the "Fluid Dynamic Section Subsystem", the block "Normal Breath Load (g/s)" provides a repeating sequence of breath load curve to the model and the block "Ratio to Normal Breath" is a gain block the value of which should be zero to simulate the steady flow situation, should be 1 when the breathing is normal and be 2 to simulate patient's deep breathing.

On the right side of the picture, the fluid dynamic section consists of ADU-outlet pressure subsystem and subsystem of the CPAP machine fluid dynamic section from ADU outlet to the mask.
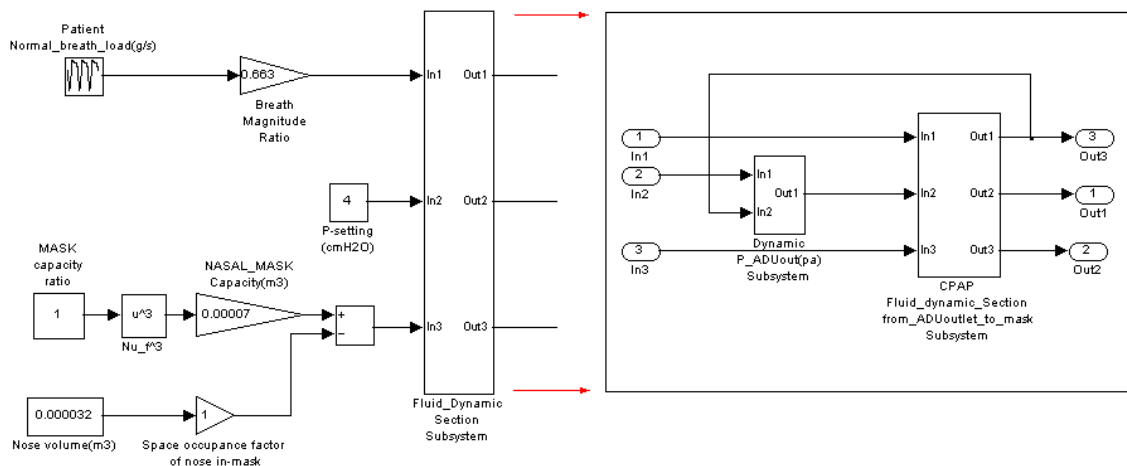
Figure 4.3 Overall Fluid Dynamic Section Subsystem

The outputs from this fluid dynamic section subsystem are in Table 4.4:

Table 4.4 Outputs from the overall fluid dynamic section subsystem

Output port number	Output	Unit
1	Tube airflow velocity	m/s
2	Bus output of pressures at ADU outlet in the chamber and the mask	Pascal
3	Connecting duct airflow velocity	m/s

Details inside these diagrams are explained below.

4.2.1.1   ADU outlet pressure subsystem

Figure 4.4 is the model of ADU-outlet pressure subsystem created based on Eq. (2.12).

Inputs are listed in Table 4.5.

Table 4.5 Inputs to the ADU outlet pressure subsystem

Input port number	Input	Unit
1	ADU pressure setting	cmH$_2$O
2	Connecting duct airflow velocity	m/s
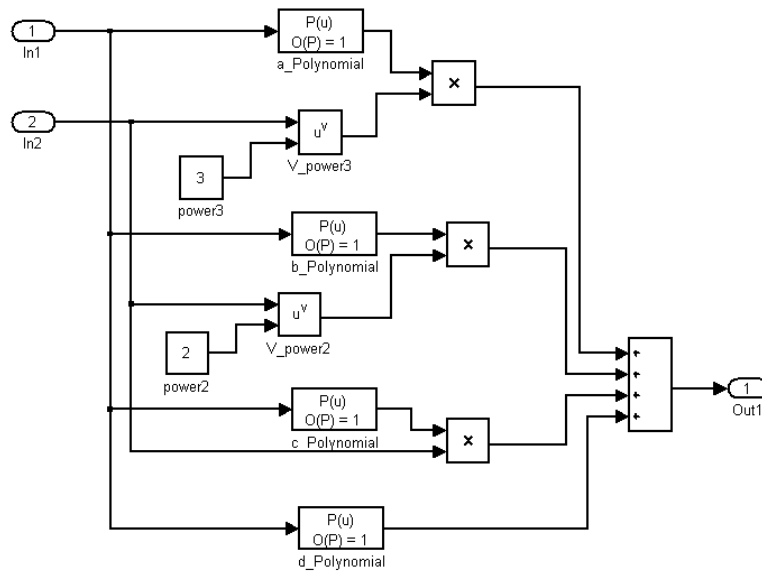
Figure 4.4 ADU outlet pressure subsystem

The connecting duct airflow velocity is obtained from the "CPAP machine fluid dynamic section from ADU outlet to mask" subsystem. The polynomial blocks represent the bracketed first ordered polynomials in Eq. (2.12).

79

The output of this subsystem is the pressure at ADU outlet which will vary along with the fluctuation of the airflow velocity during dynamic simulation.

4.2.1.2   The CPAP fluid dynamic section after ADU outlet

Figure 4.5 shows the inside structure of CPAP fluid dynamic section after ADU outlet. Inputs to this section subsystem are listed in Table 4.6:

Table 4.6 Inputs to the CPAP fluid dynamic section after ADU outlet

Input port number	Input	Unit
1	Patient's breath load	g/s
2	ADU outlet pressure	Pascal
3	Mask capacity	m^3
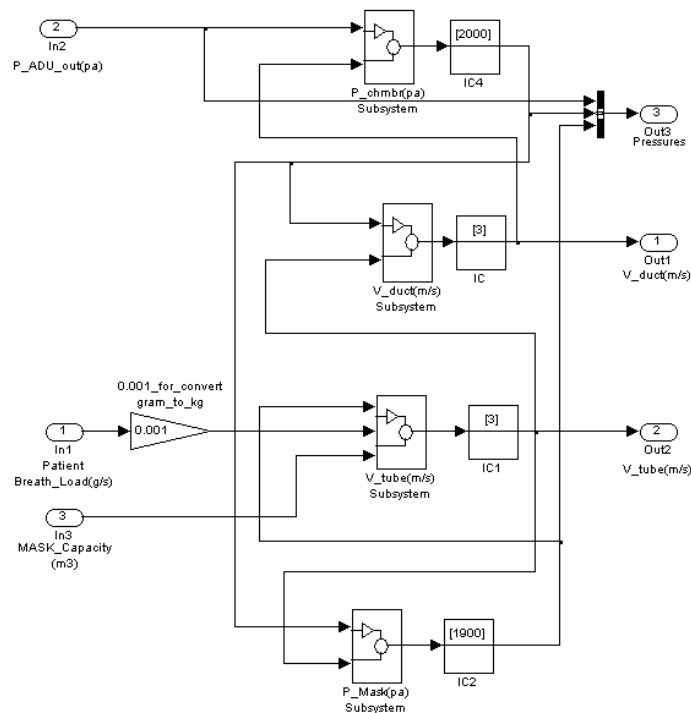
Figure 4.5 CPAP Fluid Dynamic Section after ADU Outlet

The section mainly consists of four subsystems:

- Chamber pressure subsystem
- Connecting duct airflow velocity subsystem
- HADT airflow velocity subsystem
- Mask pressure subsystem

80

Gain block after input 1 is to convert patient's breath load from g/s to kg/s for unifying dimensions. The IC blocks (stands for "Initial Condition") are here to give initial conditions to the system so to make the model has a stable start thus runs well. Such IC blocks will often be used in this model and thermodynamic model without further mentioning. The outputs are listed in Table 4.7.

Table 4.7 Outputs from the CPAP fluid dynamic section after ADU outlet

Output port number	Output	Unit
1	connecting duct airflow velocity	m/s
2	airflow velocity in HADT	m/s

The connecting duct airflow velocity will be used to calculate dynamic ADU outlet pressure. The airflow velocity in HADT will be used for reverse flow and exhaled air mixing and re-breath calculations.

(See Appendix VII for details of these subsystems)

4.2.2   Reverse flow calculation subsystem

The reverse flow calculation subsystem in Figure 4.6 is created from Eq. (2.29). The inputs are listed in Table 4.8 below:

Table 4.8 Inputs to the reverse flow calculation subsystem

Input port number	Input	Unit
1	Airflow velocity in HADT	m/s
2	Breath load for integration control	

The upper part of this subsystem provides a graph of the reverse flow to a scope block via output 1 and the lower part provides the reading of maximum distance of the reverse flow to a display block via output 2. The subsystem output gives a positive reading for reverse flow.
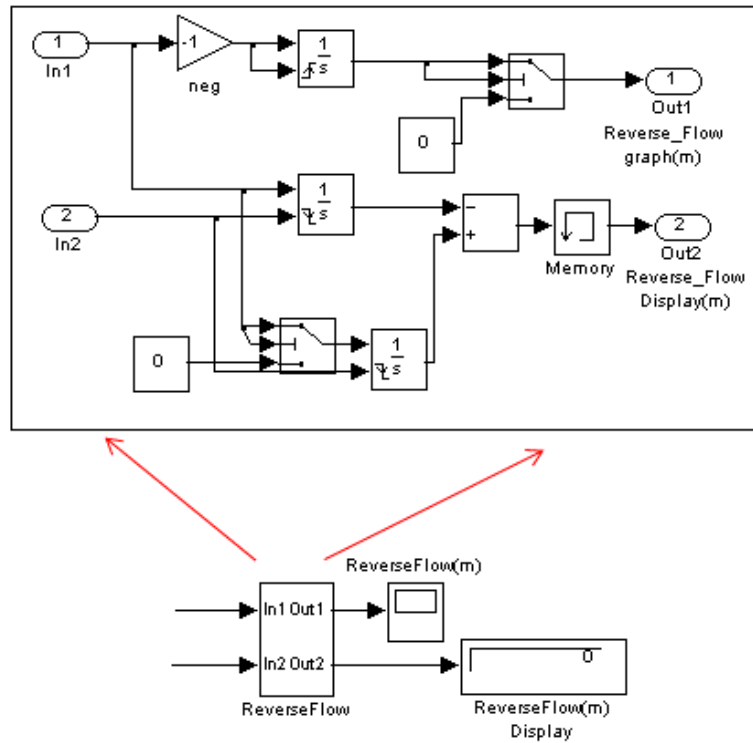
Figure 4.6 – Reverse flow Calculation Subsystem

4.2.3 Varying transport delay subsystem

Transport of fluid mass and its properties from one lump to another takes time. Figure 4.7 shows the varying transport delay subsystem created from Eq. (2.32). Enlarged part in the right upper corner of Figure 4.7 is the inside algorithm in one of the ten subsystems. The algorithm represents $\Delta t = \dfrac{\Delta s}{\tilde{v}(t)}$ and ten of such together consists of a "one lump delay subsystem" which gives the fluctuating time of air flowing through a lump.

Input one is the signal input. For this fluid dynamic and CO_2 model, it is the exhaled air concentration level in fluid flow from neighbouring lump. Input two is fluid flow velocity. The fluid flow velocity is used to calculate the amount of time delay which will be put into the variable transport delay block to suspend the input signal such amount of time. Output is the delayed signal which will be delivered to the next lump as signal input.

82
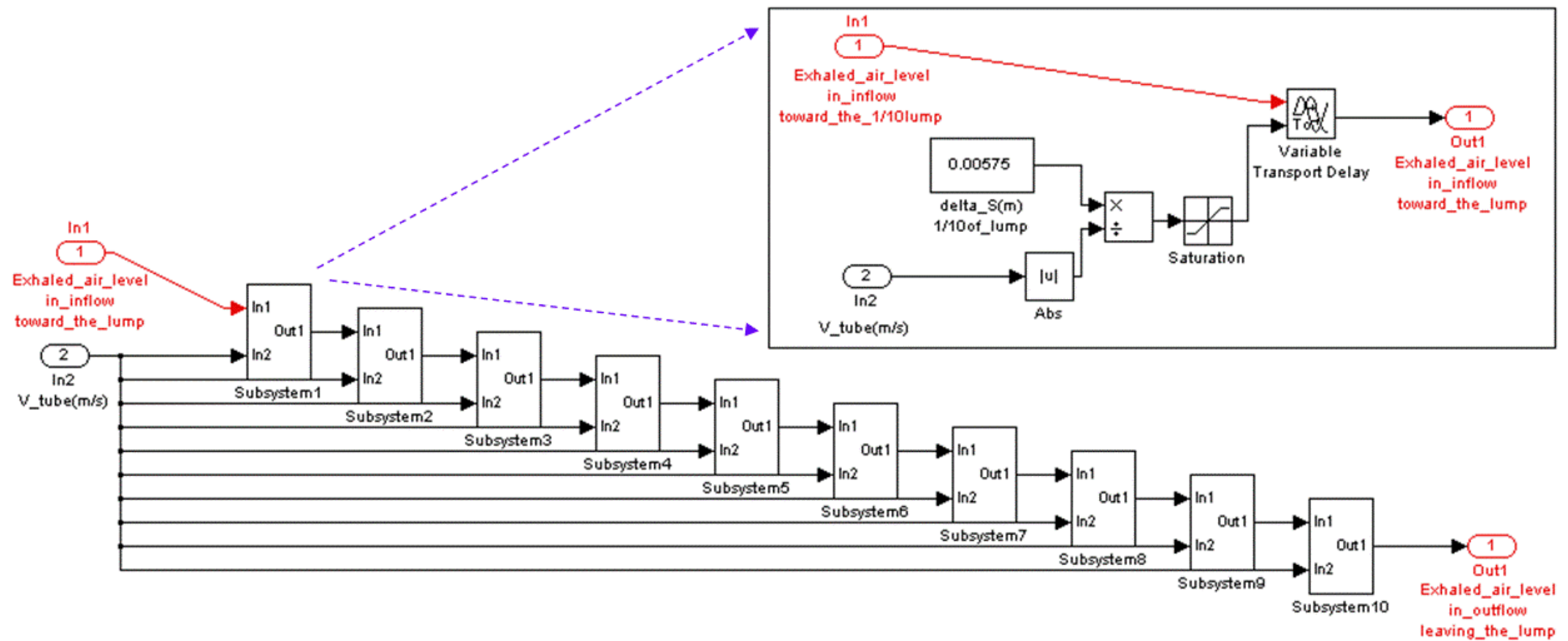
Figure 4.7 Varying Transport Delay Subsystem

4.2.4   Control of positive and negative direction of the flow

Controls of positive and negative directions of the flow are based on Eq. (2.33) and Eq. (2.34) for transport between HADT lumps; based on Eq. (2.35) and Eq. (2.36) for transport between lump 30 and the mask; based on Eq. (2.37) and Eq. (2.38) for transport between the chamber and HADT lump 1.
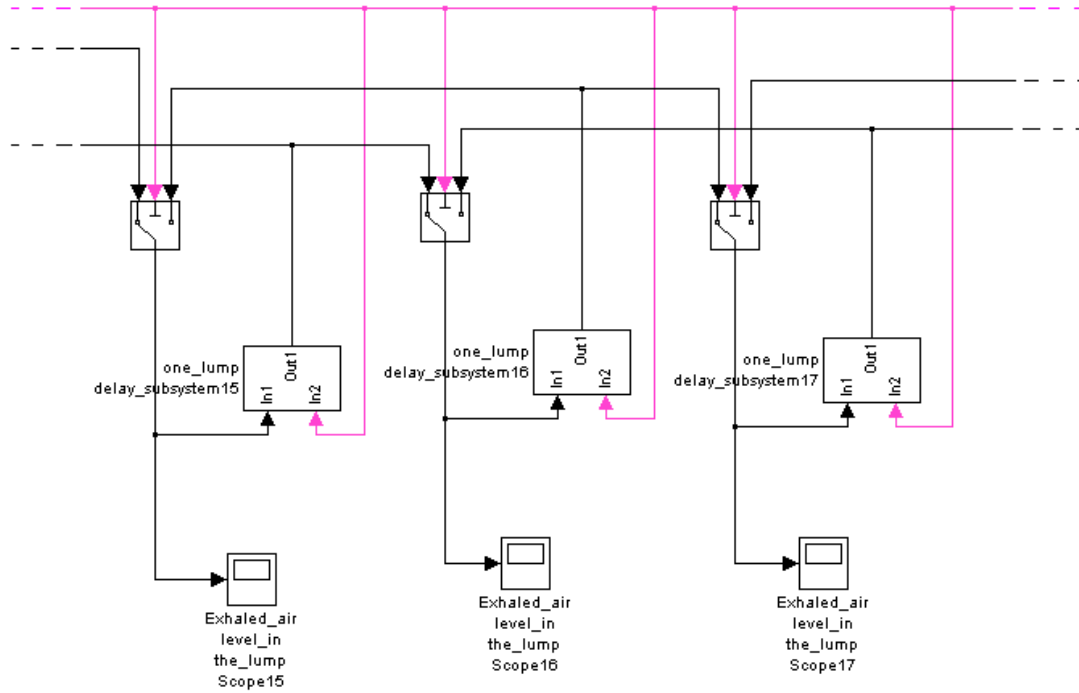
Figure 4.8 - Positive and Negative Flow Direction Control

The control of positive and negative directions of the flow and its transportation is achieved by using switch blocks. The central port of the switch block is the control port to which the input is tube velocity. The criteria for passing the first (left) input is set as when the input to the control port is equal or greater than zero. When there is positive direction flow, the in-tube velocity is positive and the signal comes into a lump from the left port of the switch block which means the air and its properties is transported in from upstream (chamber side). When the velocity is negative the air is transported into the lump from downstream (the mask side). Figure 4.8 shows the switches used for linking the "one lump delay subsystems" which representing the corresponding lumps. The air flowing into the lump will flow out to whether up or down stream neighbouring lumps after a variable time delay calculated by the "one lump delay subsystem" described in subsection 4.2.3. The pink input is the airflow velocity in HADT and the black inputs as well as the outputs from switch block and the delay subsystem is the signal of the exhaled air level.

84

4.2.5 Mask mixing calculation subsystem

The mask mixing subsystem shown in Figure 4.9 is created from Eq. (2.46). As mentioned before, the provided breath-load takes flow in inhalation phase as negative when the air is taken away from the mask by breathing. Oppositely, the exhalation phase is considered positive since exhalation adds air into the mask. Inputs are listed in Table 4.9 below.

Table 4.9 Inputs to the mask mixing calculation subsystem

Input port number	Input	Unit
1	The patient's breath load	g/s
2	Mask capacity	m^3
3	Exhaled air level in airflow from lump 30	In decimal
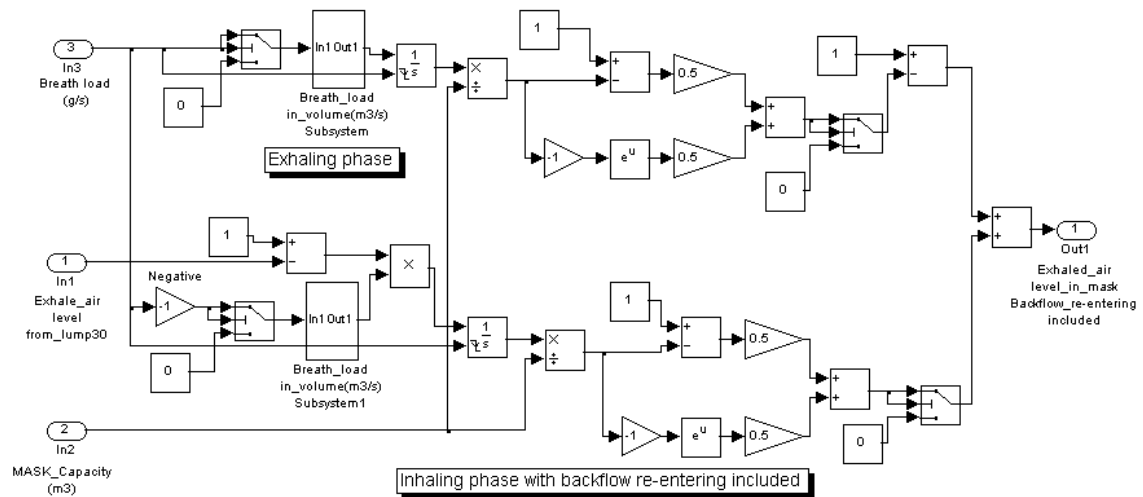
Figure 4.9 - Mask Mixing Calculation Subsystem

The upper part of the subsystem gives the mixing algorithm for exhalation phase. For calculating the mixing procedure during the exhalation phase, the integration should only take in the exhalation part and the integration starts at each cycle's beginning of exhalation phase. These are controlled by switch block and integration block. The switch block restrains the integration within exhalation phase and the integration block with a falling external-reset-setting resets the integration at the beginning of each exhalation.

The lower part of the subsystem gives the mixing algorithm for inhalation phase. The level of exhaled air re-entering the mask from lump 30 is added in from input port 3. So the integration from the lower part includes the influence of the reverse flow's re-

entering the mask. The sum-up of the two parts gives the value of C_t. According to Eq. (2.46), C_t is the fluctuating concentration of exhaled air in the mask in a full breath cycle which is the value of output 1.

4.2.6 The percentage of exhaled air being re-breathed

Figure 4.10 shows the "Percentage of exhaled air re-breathed with reverse flow re-entering included Subsystem" which is created based on Eq. (2.47). This subsystem is enabled and the "Enable" block is controlled by the breath load. During exhalation phase, the input to the "Enable" is smaller than zero and the subsystem is disabled so it only calculates during the inhalation phase. This gives the correct answer and also accelerates the model's running. Inputs are listed in Table 4.10 below.

Table 4.10 Inputs to the percentage of exhaled air being re-breathed subsystem

Input port number	Input	Unit
1	Concentration of exhaled air in the mask	In decimal
2	Breath load	g/s
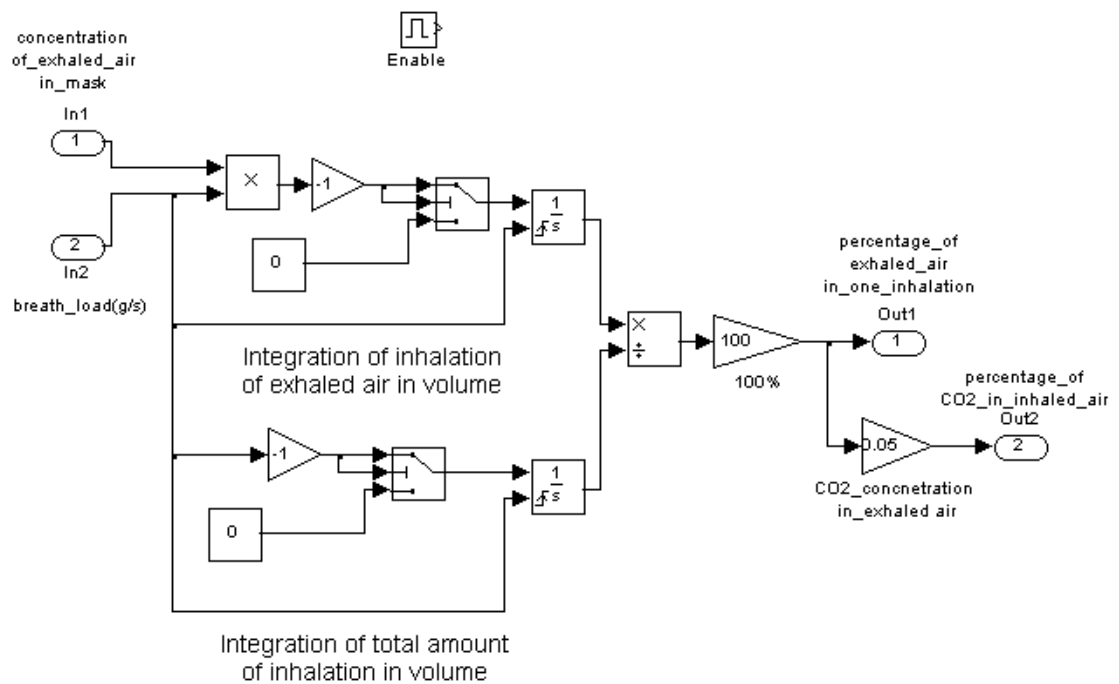
Figure 4.10 - Subsystem for Percentage of Exhaled Air Re-breathed

Output 1 is volumetric percentage of exhaled air being retaken in one inhalation load. Output 2 is the percentage of CO_2 in one inhalation.

4.3   Computational model of thermal dynamic analyses

This model is used to calculate dynamic condensation in HADT when different load of breath is added and reverse flow occurs. The model also compares the result with the condensation when breathing is not added and thus flow is steady. Like the fluid and CO_2 model, this thermal dynamic model requires fluid dynamic section and lump-delay subsystems.

This model consists of three main parts. They are ADU and chamber part, lumped HADT part and mask part. They are to be described in following sub-sections. As explained in chapter 3, considering all the wall temperatures are much stable when the airflow temperature is fluctuating and for shortening the model ramping time, the Simulink^{TM} model uses steady state calculation for all the wall temperatures and the chamber water temperature. These steady state (constant) wall temperatures are input to the dynamic fluctuating subsystems for calculating the fluctuating airflow properties. Thus, all the chamber part, HADT lump parts and the mask part consist of a steady state subsystem and a dynamic fluctuating subsystem.

The inputs required are listed in Table 4.11 below:

Table 4.11 Inputs to the thermodynamic model

Input block	Unit
Breath magnitude ratio	
Mask capacity ratio	
Human nose in-mask space occupancy factor	
Pressure setting	cmH$_2$O
Heat element temperature setting	°C
HADT tube heating	W
Ambient temperature	°C
Ambient relative humidity	In decimal

The outputs are listed in Table 4.12 below:

Table 4.12 Outputs from the thermal dynamic model

Output	Unit
Steady state outputs	
Chamber water temperature	°C
Steady state chamber air temperature	°C
Steady state evaporation rate	kg/s
Steady state chamber air specific humidity	Decimal
Steady state air temperature at HADT lump	°C
HADT lump wall temperature	°C
Gap between lump wall temperature and airflow dew point	°C
Mask wall temperature	°C
Steady state mask air temperature	°C
Dynamic outputs	
Dynamically fluctuating chamber air specific humidity	Decimal
Averaged dynamic chamber air specific humidity	Decimal
Dynamically fluctuating evaporation rate in the chamber	kg/s
Averaged dynamic evaporation rate in the chamber	kg/s
Dynamically fluctuating chamber air temperature	°C
Averaged dynamic chamber air temperature	°C
In-HADT flow velocity comparison between steady flow and fluctuating flow	m/s
Dynamically fluctuating air specific humidity at HADT lump	Decimal
Dynamically fluctuating air temperature at HADT lump	°C
Dynamically fluctuating condensation/evaporation rate at HADT lump	kg/s
Net condensation/evaporation rate at HADT lump in a breath cycle	kg/s
Dynamically fluctuating air specific humidity in the mask	Decimal
Dynamically fluctuating air temperature in the mask	°C
Dynamically fluctuating condensation/evaporation rate in the mask	kg/s
Net condensation/evaporation rate in the mask over a breath cycle	kg/s
Averaged specific humidity in inhaled air	kg/s
Averaged temperature of inhaled air	°C

The block diagram of the whole thermodynamic system is shown in Figure 4.11 and the Simulink[TM] model is shown in Figure 4.16 and Figure 4.13.
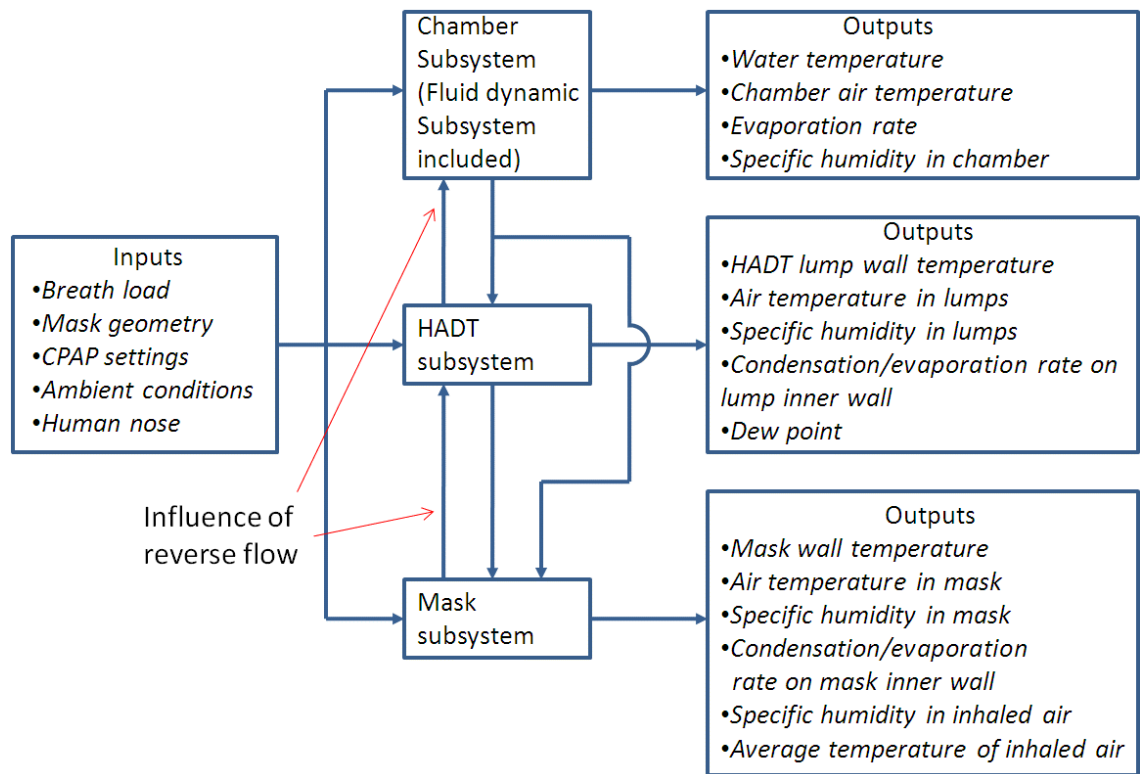
Figure 4.11 Block diagram of CPAP thermodynamic analyses model
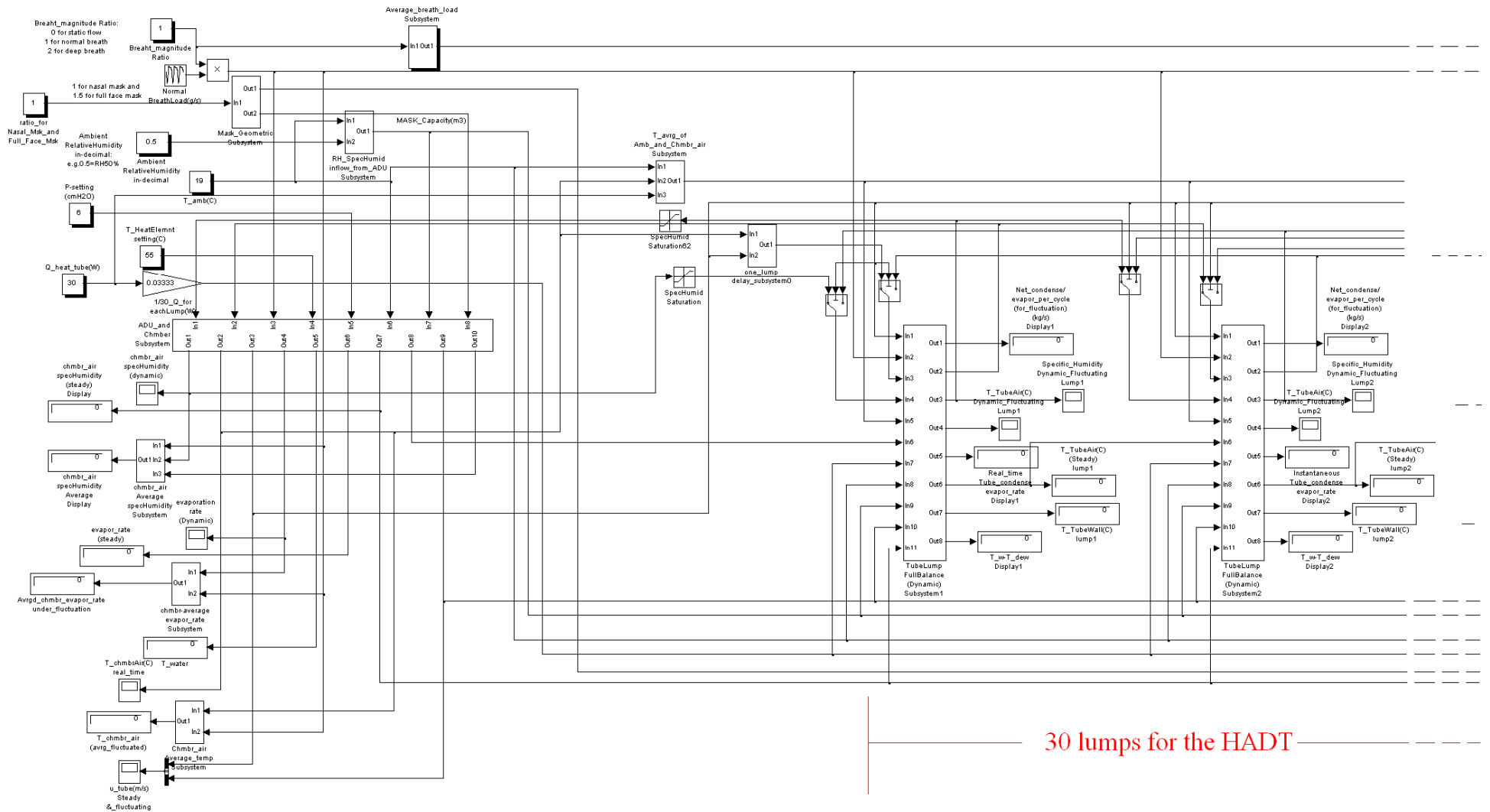
Figure 4.12 SimulinkTM model for thermodynamic analysis (part A)

90
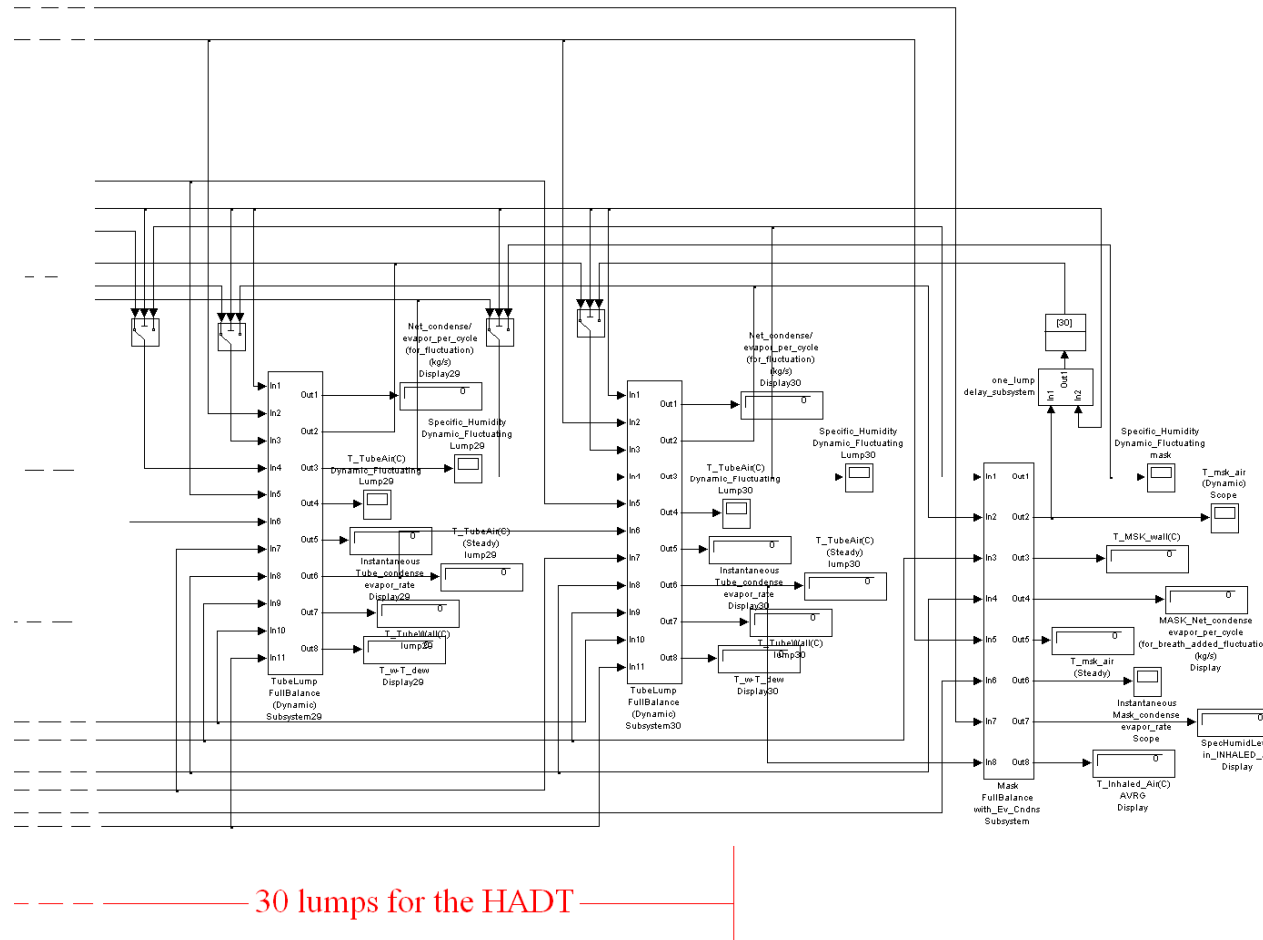
Figure 4.13 Simulink^{TM} model for thermodynamic analysis (part B)

91

4.3.1 Thermal section of ADU and chamber part

The ADU and chamber part is created based on sections 3.2, 3.3 and 3.4, chapter 3. This part is the most complicated. There are two main subsystems in this part. One is whole chamber steady state subsystem and another is the dynamic chamber-air thermal balance subsystem. The whole chamber steady state subsystem is mainly to provide the water temperature to be used by chamber-air subsystem. The dynamic chamber-air subsystem is for obtaining dynamic fluctuating air flow velocity, chamber air temperature and specific humidity. The air flow velocity, airflow temperature and humidity are properties of the airflow provided to the patient through the long HADT and the mask. These properties will be key factors for the analysis and comparison of condensation in the HADT and the mask. Details in these two subsystems will be shown and described later.

The inputs are listed in Table 4.13 below.

Table 4.13 Inputs to the thermal section of ADU and chamber part

Input port number	Input	Unit
1	Specific humidity of air from HADT due to reverse flow	In decimal
2	Temperature of air from HADT due to reverse flow	°C
3	Breath load	g/s
4	Heat element temperature setting	°C
5	CPAP pressure setting	cmH_2O
6	Ambient air temperature	°C
7	Ambient air specific humidity	In decimal
8	Mask capacity	m^3
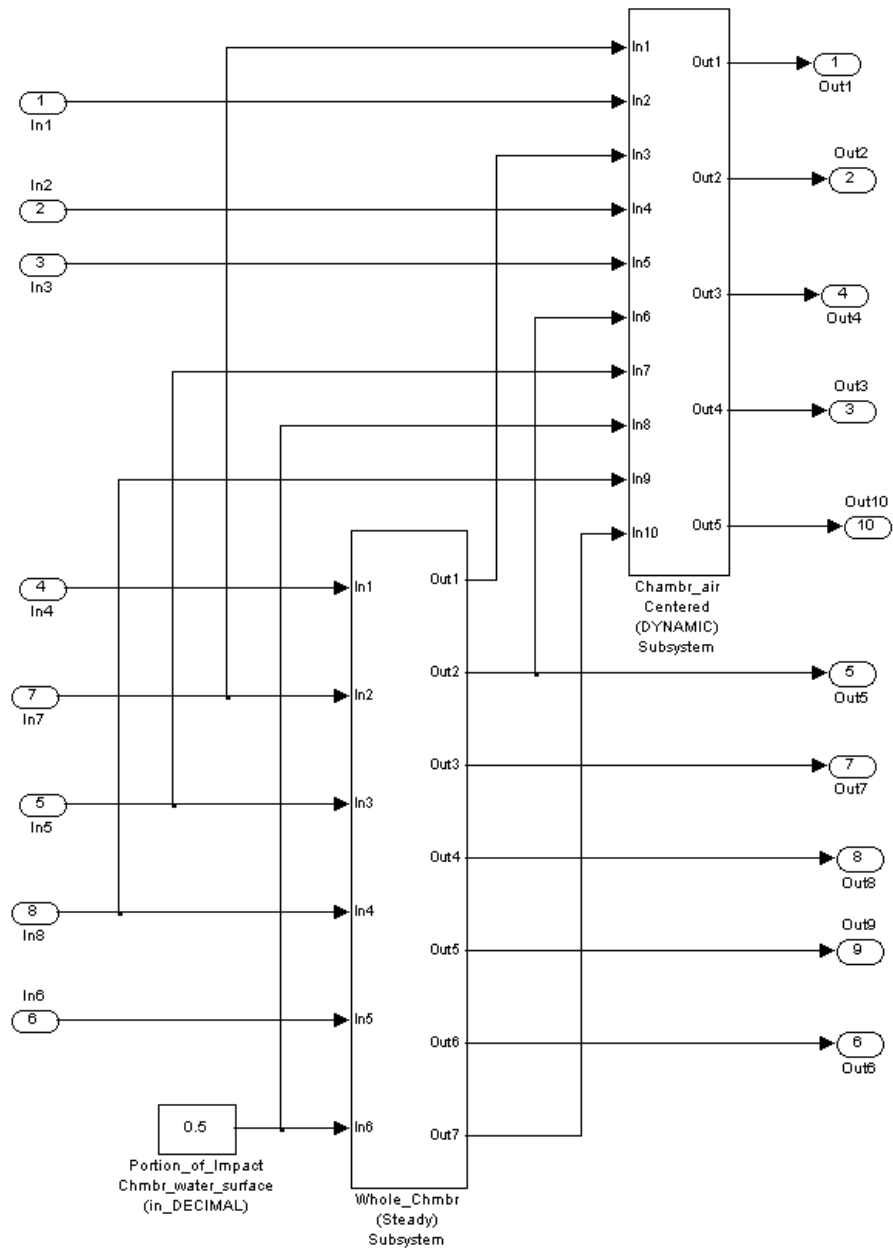
Figure 4.14 ADU and chamber part subsystem

The outputs are listed in Table 4.14 below.

Table 4.14 Outputs from the thermal section of ADU and chamber part

output port number	output	Unit
1	Fluctuating specific humidity in the chamber	In decimal
2	Fluctuating air temperature in the chamber	°C
3	Fluctuating airflow velocity in HADT	m/s
4	Fluctuating evaporation rate	kg/s
5	Water temperature	°C

6	Steady state evaporation rate	kg/s
7	Steady state specific humidity in the chamber	In decimal
8	Steady state air temperature in the chamber	°C
9	Steady state airflow velocity in HADT	m/s
10	Average of fluctuating airflow velocities in HADT and the connecting duct	m/s

The average velocities of airflow in HADT and the connecting duct are used to calculate the flow rate in the chamber.

4.3.1.1   Whole chamber steady state subsystem

The Whole chamber steady state subsystem consists of 5 subsystems.

- Fluid dynamic section subsystem (for steady flow)
- Temperature of chamber inlet from ADU subsystem
- Water thermal balance subsystem
- Chamber-air steady state thermal balance subsystem
- Chamber air specific humidity subsystem

The "Fluid dynamic section subsystem (for steady flow)" is basically the same as the one in "Fluid dynamic and exhaled air re-breath model". The only difference is that the breath load input to it is always zero thus makes this subsystem always provide steady flow velocity and steady pressures. The inputs are listed in Table 4.15 below.

Table 4.15 Inputs to the whole chamber steady state subsystem

Input port number	Input	Unit
1	Heat element temperature setting	°C
2	Ambient air specific humidity	In decimal
3	CPAP pressure setting	cmH_2O
4	Mask capacity	m^3
5	Ambient air temperature	°C
6	Portion of direct impact area to total water surface area	In decimal
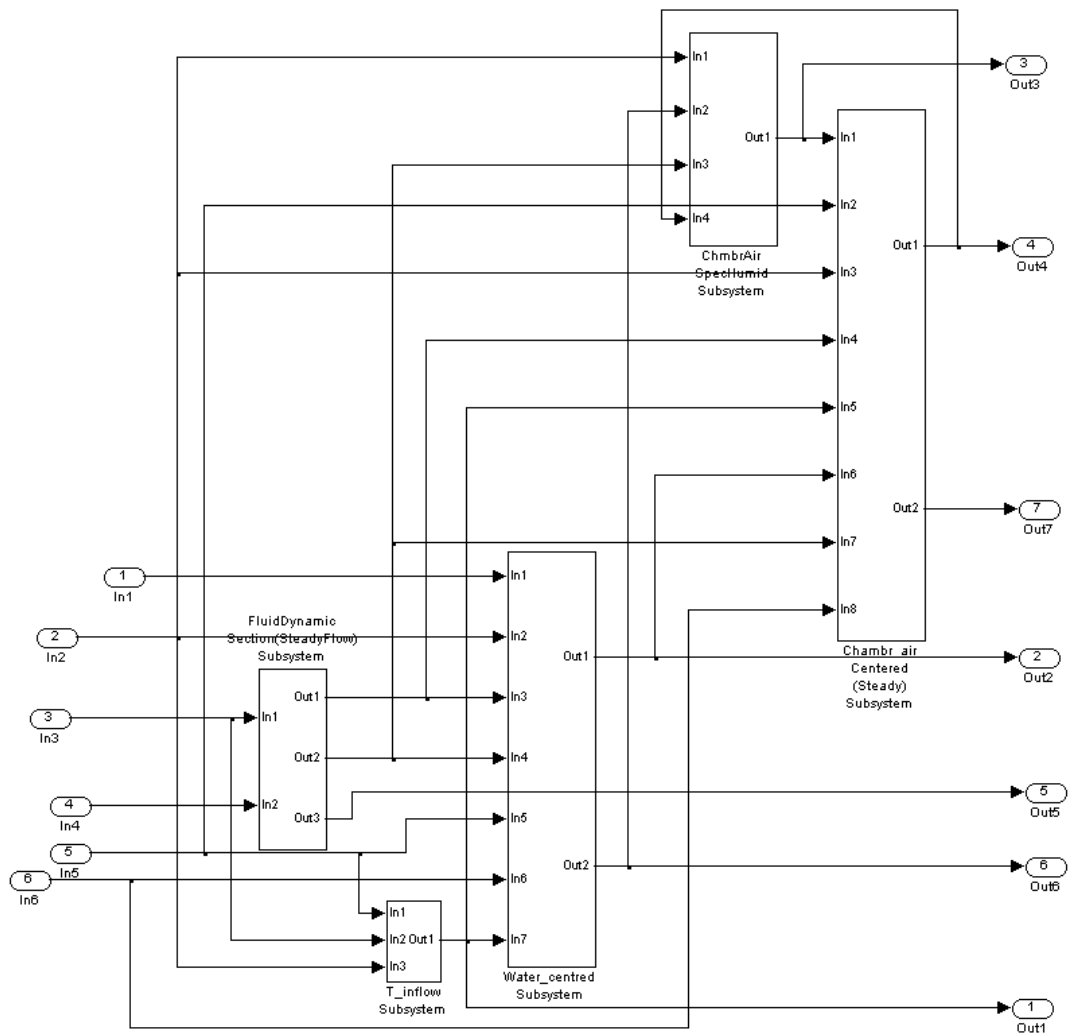
Figure 4.15 Whole chamber steady state subsystem

The outputs are listed in Table 4.16 below.

Table 4.16 Outputs from the whole chamber steady state subsystem

output port number	output	Unit
1	Temperature of inlet to the chamber from ADU	°C
2	Water temperature	°C
3	Steady state specific humidity in the chamber	In decimal
4	Steady state air temperature in the chamber	°C
5	Steady state airflow velocity in HADT	m/s
6	Steady state evaporation rate	kg/s
7	Temperature of wall 2 and 3	°C

(See Appendix VIII for details of these subsystems)

4.3.1.2 Dynamic chamber-air thermal balance subsystem

The Dynamic chamber-air thermal balance subsystem consists of 3 subsystems. They are listed below:

- Fluid dynamic section subsystem (for dynamic fluctuating flow)
- Chamber air specific humidity subsystem
- Chamber-air fluctuating thermal balance subsystem

The "Fluid dynamic section subsystem (for dynamic fluctuating flow)" is the same as the one in the Fluid dynamic and exhaled air re-breath model. The Chamber air specific humidity subsystem is the same as the one described in Appendix VIII. The differences are that the inputs are all fluctuating and its input of "specific humidity of inlet" is from a switch block. The block provides specific humidity of inlet from the blower when flow direction is from the blower and from the HADT lump 1 when the flow is reverse. For the Chamber-air fluctuating thermal balance subsystem, it is basically the same as the steady state chamber-air thermal balance subsystem described in Appendix VIII. The differences are also that the inputs are all fluctuating and the inlet specific humidity and inlet temperature are from the blower when flow is positive and from the HADT lump 1 when the flow is reverse.

The inputs are listed in Table 4.17 below.

Table 4.17 Inputs to the dynamic chamber-air thermal balance subsystem

Input port number	Input	Unit
1	Ambient air specific humidity	In decimal
2	Specific humidity of air from HADT due to reverse flow	In decimal
3	Temperature of inlet to the chamber from ADU	°C
4	Temperature of air from HADT due to reverse flow	°C
5	Breath load	g/s
6	Water temperature	°C
7	CPAP pressure setting	cmH$_2$O
8	Portion of impact area to total water surface area	In decimal
9	Mask capacity	m^3
10	Temperature of wall 2 and 3	°C
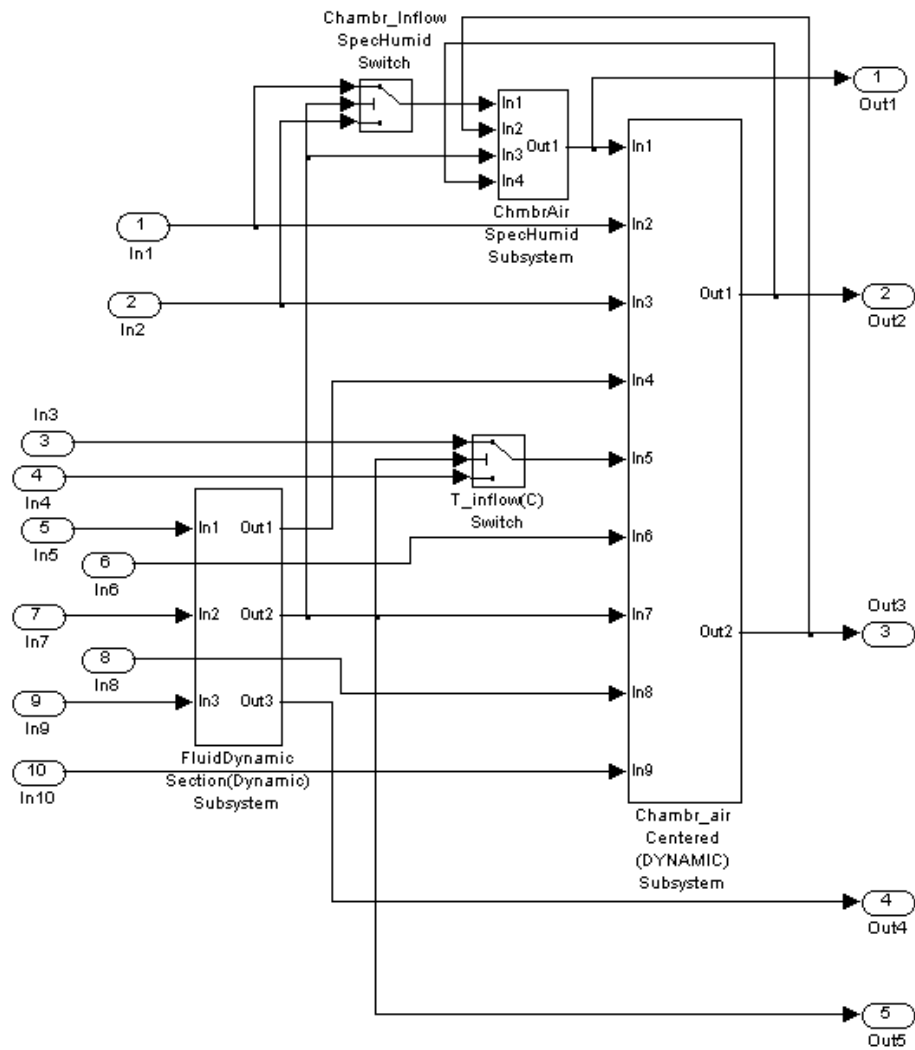
Figure 4.16 Dynamic chamber-air thermal balance subsystem

The outputs are listed in Table 4.18 below.

Table 4.18 Outputs from the dynamic chamber-air thermal balance subsystem

output port number	output	Unit
1	Fluctuating specific humidity in the chamber	In decimal
2	Fluctuating air temperature in the chamber	°C
3	Fluctuating evaporation rate	kg/s
4	Fluctuating airflow velocity in HADT	m/s
5	Average of fluctuating airflow velocities in HADT and the connecting duct	m/s

4.3.2 HADT lump thermal balance subsystem

For each lump, there are two subsystems, one is the HADT lump steady state subsystem and the other is the HADT lump air dynamic thermal balance and condensation

subsystem. The HADT lump steady state subsystem is used to provide steady state HADT wall temperature and steady state airflow temperature at the HADT lump. The constant lump wall temperature is also output to calculate the dew point so to determine the steady state condensation. The HADT lump air dynamic thermal balance and condensation subsystem is to calculate the dynamically fluctuating airflow temperature, the dynamic condensation/evaporation rate and the transportation delay of the airflow and its properties.

The inputs are listed in Table 4.19 below.

Table 4.19 Inputs to the HADT lump thermal balance subsystem

Input port number	Input	Unit
1	Fluctuating airflow velocity in HADT	m/s
2	Breath load	g/s
3	Temperature of air flowing into the lump	°C
4	Specific humidity of air flowing into the lump	In decimal
5	Initial in-tube air temperature	°C
6	Steady state inlet temperature	°C
7	Tube heating power to each lump (1/30 of the total)	W
8	Ambient air temperature	°C
9	Ambient air specific humidity	In decimal
10	Steady state airflow velocity in HADT	m/s
11	Chamber outlet steady state specific humidity	In decimal

The air flowing into the lump is from its neighbouring lump. When the inspected lump is lump 1, the flow comes from the chamber.
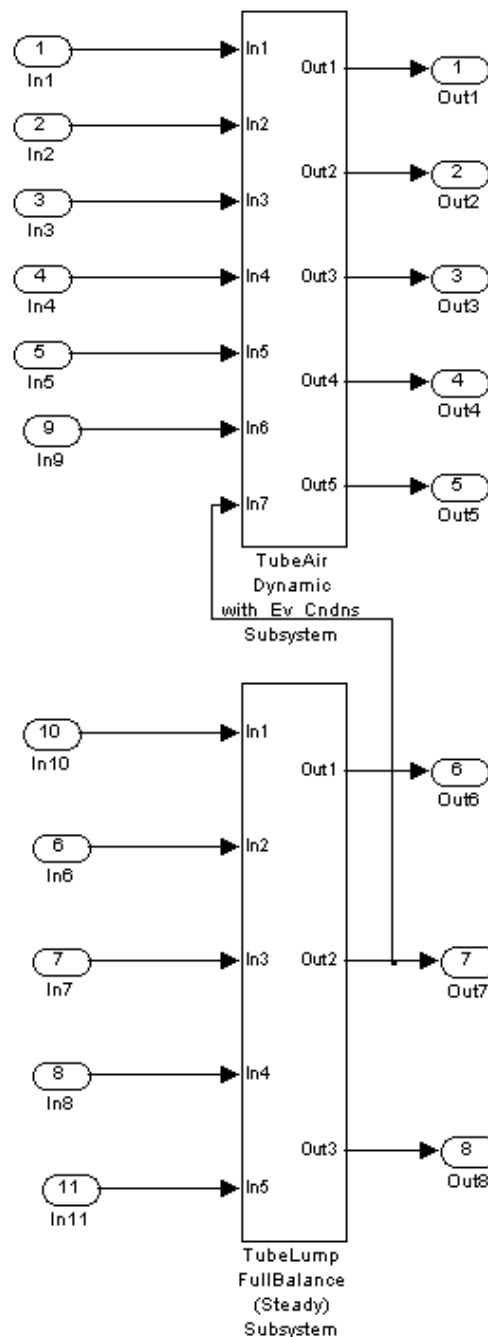
Figure 4.17 HADT lump thermal balance subsystem

The outputs are listed in Table 4.20 below.

Table 4.20 Outputs from the HADT lump thermal balance subsystem

output port number	output	Unit
1	Net condensation/evaporation rate (over a breath cycle)	kg/s
2	Air temperature of outlet from the lump	°C
3	Specific humidity of outlet from the lump	In decimal
4	Fluctuating temperature of air in the lump	°C

5	Fluctuating condensation/evaporation rate	kg/s
6	Steady state temperature of air in the lump	°C
7	HADT wall temperature at the lump	°C
8	Temperature gap between HADT lump wall and steady state air flow at the lump	°C

The two subsystems are shown and described below.

4.3.2.1 Steady state HADT lump full thermal balance subsystem

The steady state HADT lump full thermal balance subsystem consists of three subsystems. They are the HADT lump wall temperature subsystem, the steady state HADT air temperature subsystem and the flow dew point and HADT lump wall temperature gap subsystem.

Inputs to this subsystem are listed in Table 4.21 below.

Table 4.21 Inputs to the steady state HADT lump full thermal balance subsystem

Input port number	Input	Unit
1	Steady state airflow velocity in HADT	m/s
2	Steady state inlet temperature	°C
3	Tube heating power to each lump (1/30 of the total)	W
4	Ambient air temperature	°C
5	Chamber outlet steady state specific humidity	In decimal
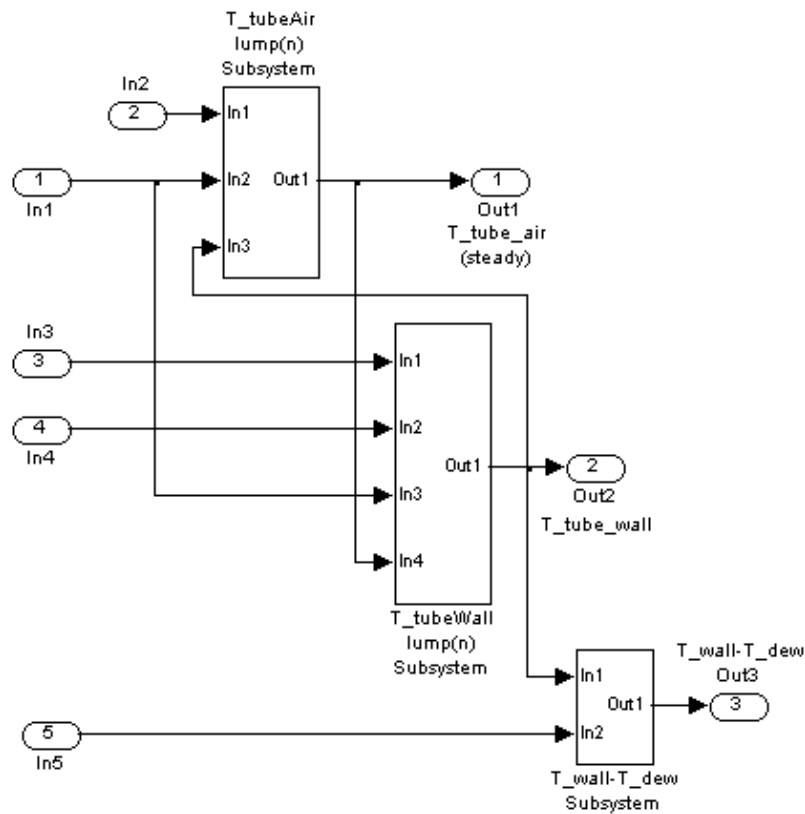
Figure 4.18 Steady state HADT lump full thermal balance subsystem

The outputs are listed in Table 4.22 below.

Table 4.22 Outputs from the steady state HADT lump full thermal balance subsystem

output port number	output	Unit
1	Steady state temperature of air in the lump	°C
2	HADT wall temperature at the lump	°C
3	Temperature gap between HADT lump wall and steady state air flow at the lump	°C

The HADT wall temperature at this lump will be used in the HADT lump air dynamic thermal balance and condensation subsystem of the same lump. The Steady state temperature of air in the lump will be sent to the next lump subsystem as inlet temperature.

(See Appendix IX for details of these subsystems)

4.3.2.2   HADT lump air dynamic fluctuating thermal balance and condensation
subsystem

This subsystem contains two subsystems. One is the dynamic fluctuating lump air
thermal balance subsystem and the other is the dynamic fluctuating lump air
temperature subsystem.

Inputs to this subsystem are listed in Table 4.23 below:

**Table 4.23 Inputs to the HADT lump air dynamic fluctuating thermal balance and condensation
subsystem**

Input port number	Inputs	Unit
1	Fluctuating airflow velocity in HADT	m/s
2	Breath load	g/s
3	Temperature of air flowing into the lump	°C
4	Specific humidity of air flowing into the lump	In decimal
5	Initial in-tube air temperature	°C
6	Ambient air specific humidity	In decimal
7	HADT wall temperature at the lump	°C
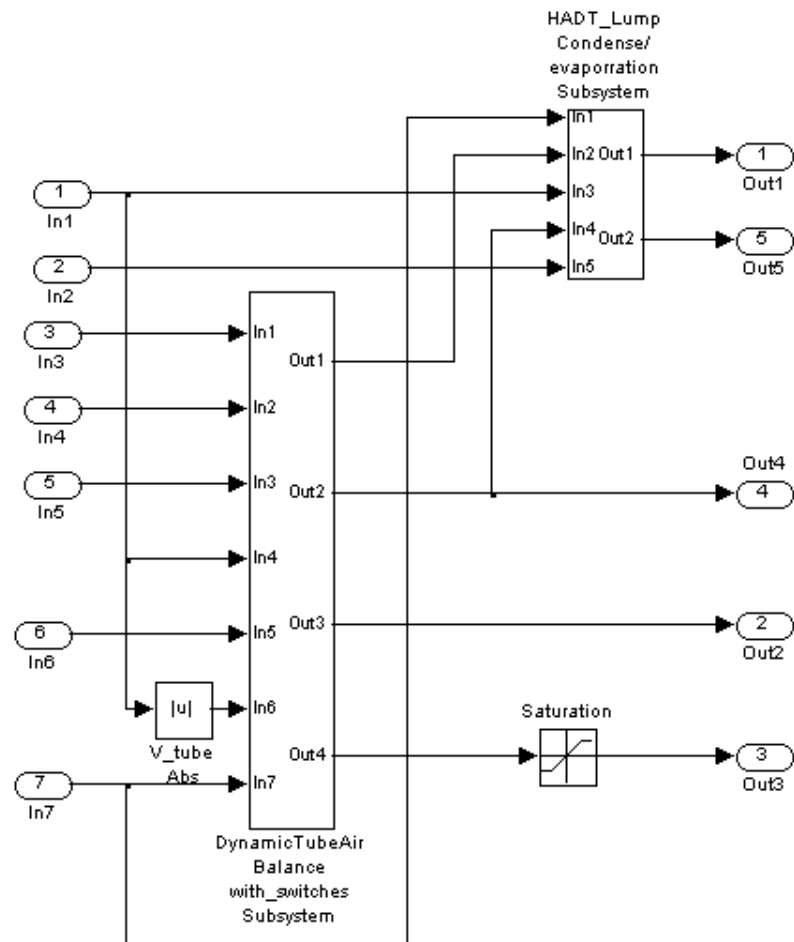
Figure 4.19 HADT lump air dynamic fluctuating thermal balance and condensation subsystem

The outputs are listed in Table 4.24 below.

Table 4.24 Outputs from the HADT lump air dynamic fluctuating thermal balance and condensation subsystem

output port number	output	Unit
1	Net condensation/evaporation rate (over a breath cycle)	kg/s
2	Air temperature of outlet from the lump	°C
3	Specific humidity of outlet from the lump	In decimal
4	Fluctuating temperature of air in the lump	°C
5	Fluctuating condensation/evaporation rate	kg/s

(See Appendix X for details of these subsystems)

4.3.3 Mask thermal balance subsystem

The mask thermal balance subsystem is to obtain the air temperature, mask wall temperature and condensation possibility in the mask. Same as for HADT lump mentioned before, this calculation is good for predicting whether condensation will occur under certain given combination of conditions. It is also good for comparison of condensation between different level of breath load added scenarios when other conditions remaining the same. The calculated condensation is the condensation rate when condensation just starts but not the amount of condensate build-up in a certain period of time.

The inputs are listed in Table 4.25 below.

Table 4.25 Inputs to the mask thermal balance subsystem

Input port number	Input	Unit
1	Specific Humidity of airflow from HADT lump 30	In decimal
2	Temperature of airflow from HADT lump 30	°C
3	Ambient air specific humidity	In decimal
4	Ambient air temperature	°C
5	Breath load	g/s
6	Mask Geometric parameters (multiplex)	N/A
7	Average mass flow rate in the mask	g/s
8	Steady state airflow temperature from HADT lump 30	°C
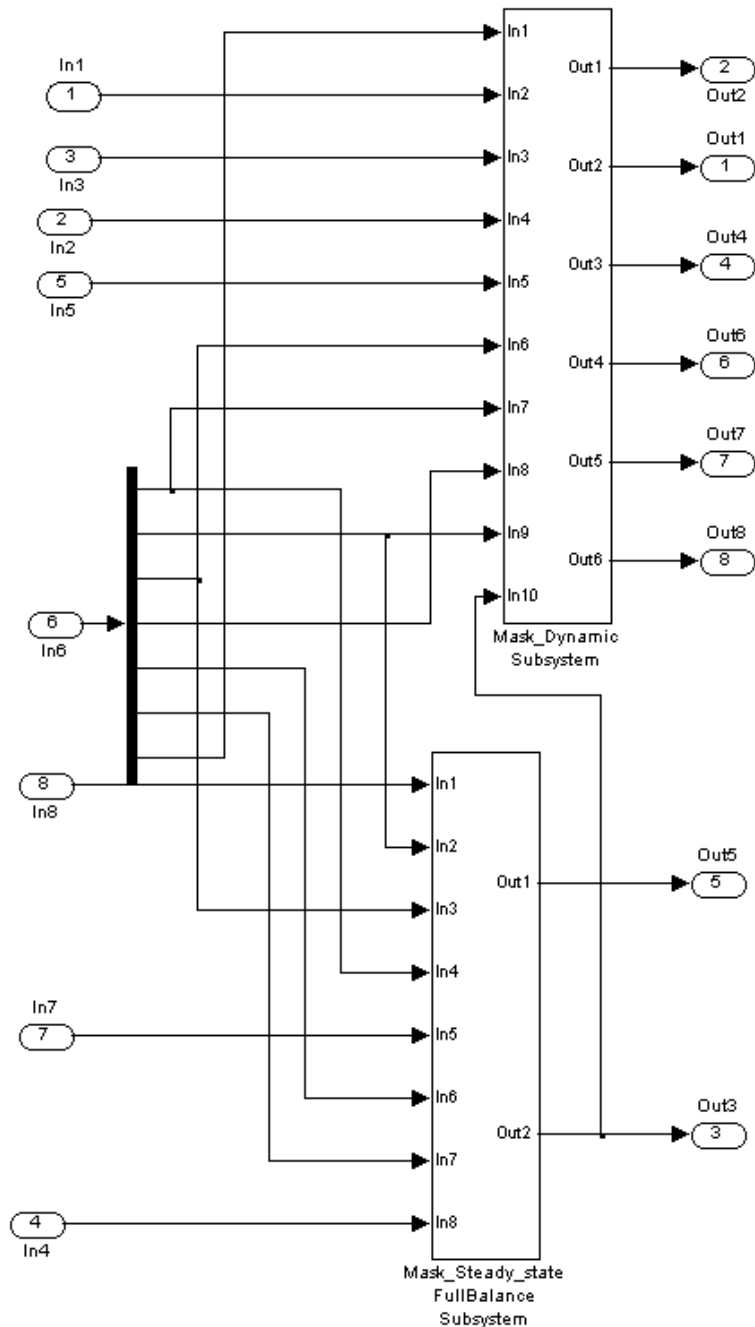
Figure 4.20 Mask thermal balance subsystem

The outputs are listed in Table 4.26 below.

Table 4.26 Outputs from the mask thermal balance subsystem

Output port number	Output	Unit
1	Fluctuating specific humidity of air in the mask	In decimal
2	Fluctuating air temperature in the mask	°C
3	Temperature of mask wall with heat dissipation	°C
4	Net condensation/evaporation in a breath cycle	kg/s

5	Steady state air temperature in the mask (for reference)	°C
6	Real time condensation/evaporation rate	kg/s
7	Average specific humidity in inhaled air	In decimal
8	Average temperature of inhaled air	°C

4.3.3.1   Steady state mask full thermal balance subsystem

The steady state mask full thermal balance subsystem is mainly for obtaining the mask wall temperature used in further calculation. It can also output the steady state air temperature in the mask for reference.

The inputs are listed in Table 4.27 below.

Table 4.27 Inputs to the steady state mask full thermal balance subsystem

Input port number	Input	Unit
1	Steady state airflow temperature from HADT lump 30	°C
2	Length of the triangular plate inner surface	m
3	Half width of the triangular plate inner surface	m
4	Mask inner height	m
5	Average mass flow rate in the mask	g/s
6	Length of the triangular plate outer surface	m
7	Half width of the triangular plate outer surface	m
8	Ambient air temperature	°C
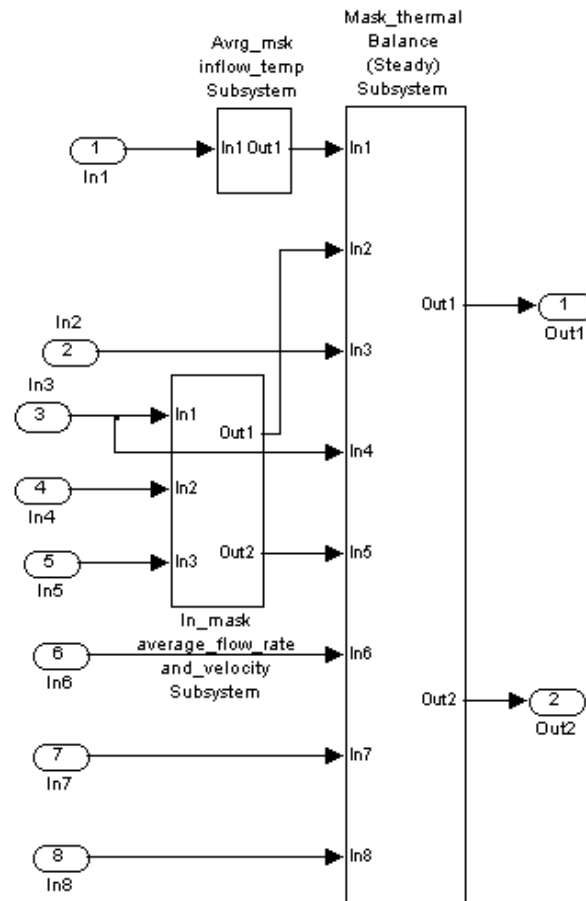
Figure 4.21Steady state mask full thermal balance subsystem

The outputs are listed in Table 4.28 below.

Table 4.28 Outputs from the steady state mask full thermal balance subsystem

output port number	output	Unit
1	Steady air temperature in the mask (for reference)	°C
2	Temperature of mask wall with heat dissipation	°C

(See Appendix XI for details of these subsystems)

4.3.3.2   Mask air dynamic fluctuating thermal balance and condensation subsystem

The purpose of this mask dynamic thermodynamic subsystem is to obtain the dynamically fluctuations of air temperature and specific humidity in the mask as well as the temperature and specific humidity of inhaled air. It contains four subsystems which will be shown and explained below.
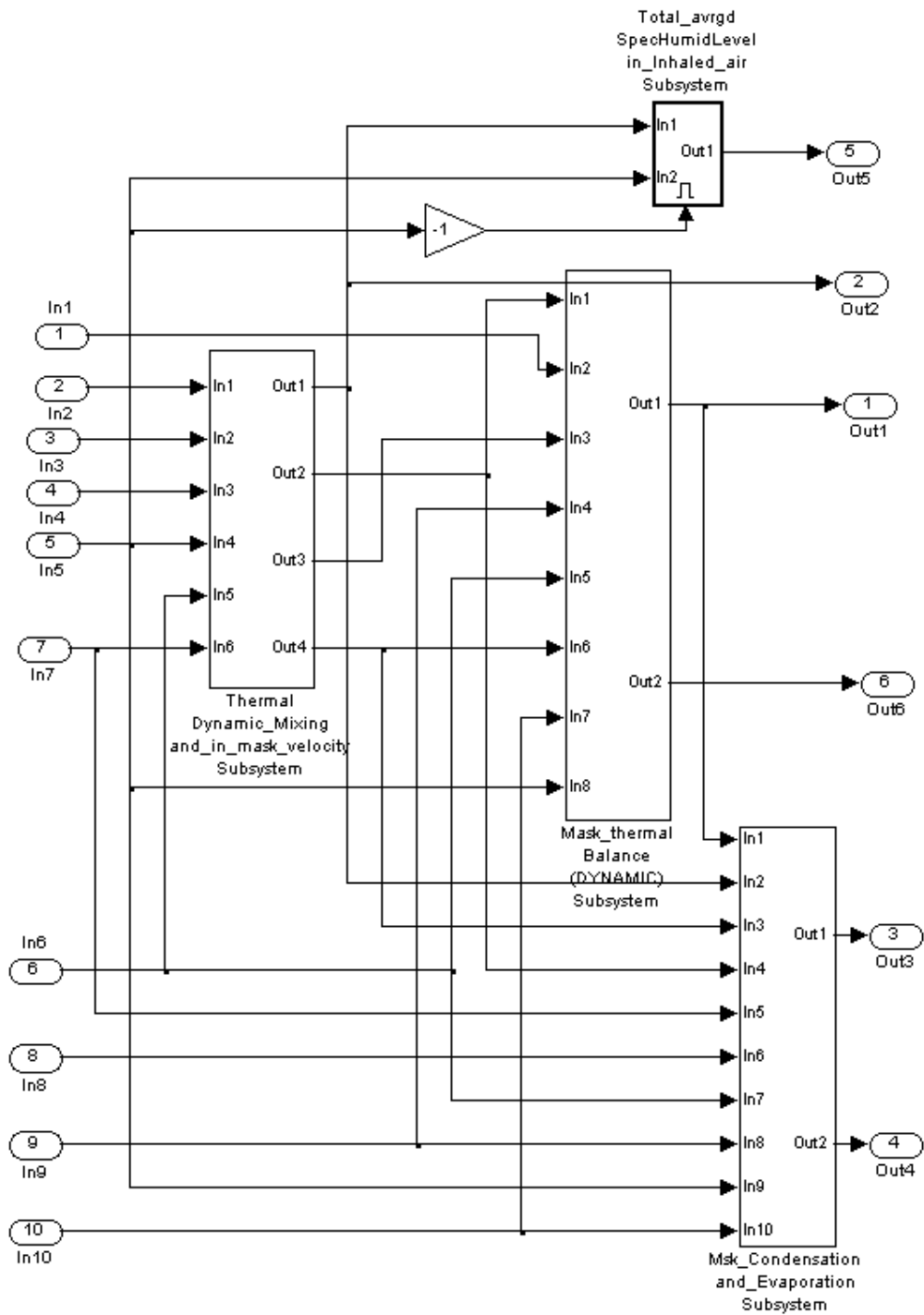
Figure 4.22 Mask air dynamic fluctuating thermal balance and condensation subsystem

The inputs are listed in Table 4.29 below.

Table 4.29 Inputs to the mask air dynamic fluctuating thermal balance and condensation subsystem

Input port number	Input	Unit
1	Mask capacity	m^3
2	Specific Humidity of airflow from HADT lump 30	In decimal
3	Ambient air specific humidity	In decimal

4	Temperature of airflow from HADT lump 30	°C
5	Breath load	g/s
6	Half width of the triangular plate inner surface	m
7	Mask inner height	m
8	Length of the rectangular plates inner surface	m
9	Length of the triangular plate inner surface	m
10	Temperature of mask wall with heat dissipation	°C

The outputs are listed in Table 4.30 below.

Table 4.30 Outputs from the mask air dynamic fluctuating thermal balance and condensation subsystem

Output port number	Output	Unit
1	Fluctuating air temperature in the mask	°C
2	Fluctuating specific humidity of air in the mask	In decimal
3	Net condensation/evaporation in a breath cycle	kg/s
4	Real time condensation/evaporation rate	kg/s
5	Average specific humidity in inhaled air	In decimal
6	Average temperature of inhaled air	°C

(See Appendix XII for details of these subsystems)

4.3.4 The auxiliary subsystems
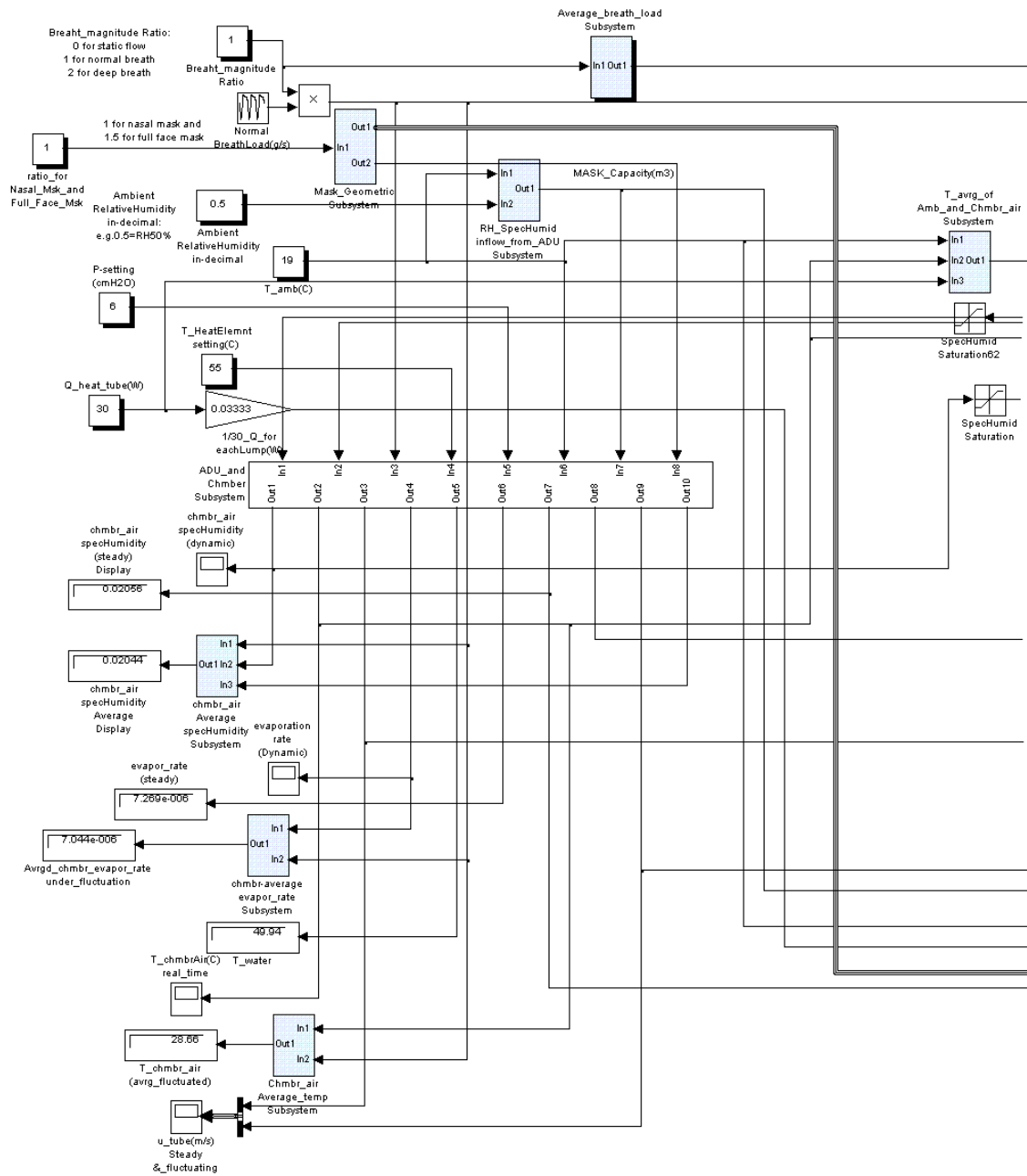
Figure 4.23 Auxiliary subsystems and their locations

There are several auxiliary small subsystems light-blue coloured in Figure 4.23.

They are listed below:

- Ambient relative humidity to specific humidity conversion subsystem
- Mask geometric parameter subsystem
- Breath load average subsystem
- Average of ambient temperature and chamber air temperature subsystem

- Average evaporation rate subsystem

- Chamber air average temperature subsystem

- Chamber air average specific humidity subsystem

(See Appendix XIII for details of these subsystems)

Chapter 5 Experimental Validation

5.1 Introduction

In this chapter, setups developed for the fluid and thermal experimental validations are described and explained. These include steady fluid, dynamic fluid, steady thermal and dynamic thermal validations. The dynamic experiments need a dynamically fluctuating breathing signal which is provided by a lung simulator. Outputs from models will be compared with experiment results.

5.2 Experimental validation of the fluid dynamic part

This section focuses on the fluid dynamic validation. There are two subsections, one under steady state flow and the other under patient breathing-added fluctuating flow.

5.2.1 Fluid dynamic model under steady flow

The outputs from this experiment include pressure drop along the HADT, airflow velocity in HADT and bias vent hole discharge coefficient. All these outputs were tested over the CPAP pressure setting range. The experimental setup consists of a HC600 CPAP unit, a HC365 chamber, a flowmeter (NDD Ultrasonic flow sensor) and a pressure transducer (Honeywell Precision Pressure Transducer PPT0001DWW2VA-A) as well as the softwares for the flow meter and pressure sensor which have been described in Chapter 2.

5.2.1.1 Pressure drop along HADT

Figure 5.1 is a schematic diagram of experiment setup for testing the pressure drop along the HADT. The mask is sealed so the air can only go away through the bias vent holes. A calibrated pressure sensor is used to measure the pressure drop. The thin tube of the pressure transducer for higher pressure (port P1) is inserted in the HADT near the chamber and another (port P2) is put right downstream of the HADT. An ultrasonic flowmeter is located between the downstream pressure measuring point and the short connecting tube. This connecting tube has the same cross sectional geometry as the

HADT and connects those upstream sections to the mask. Figure 5.2 shows the connection and location for the pressure transducer and the flowmetre.
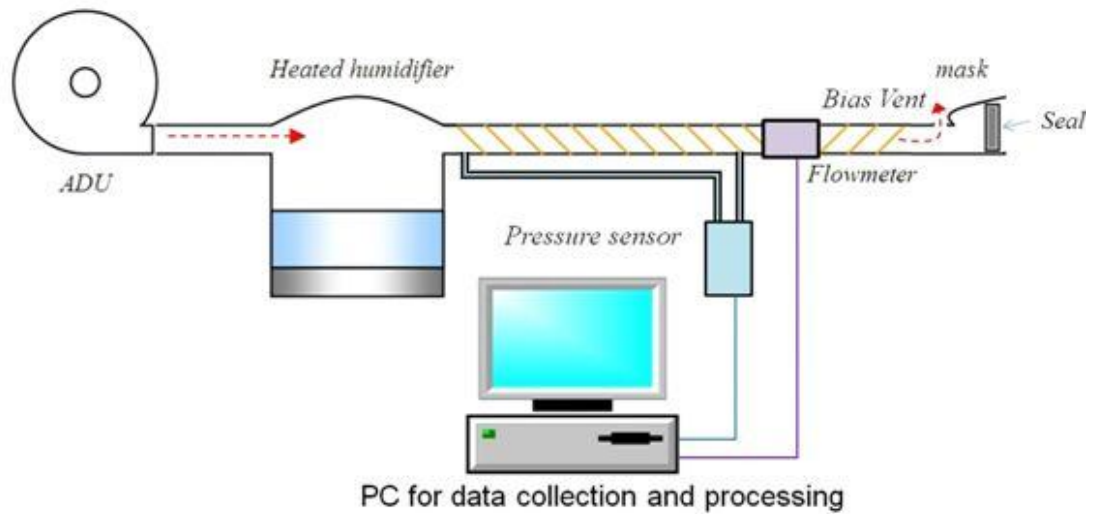
Figure 5.1 Experiment setup for pressure drop on HADT

The recording time of pressure is 40 seconds with 1000 readings (reading interval is 0.04 second). Averages of these readings were used as values of the pressure drop results at each measured setting. The pressure was converted from cmH_2O into Pascals. The experiment was carried out for two rounds at pressure settings with interval of $1cmH_2O$ over the CPAP pressure working range.
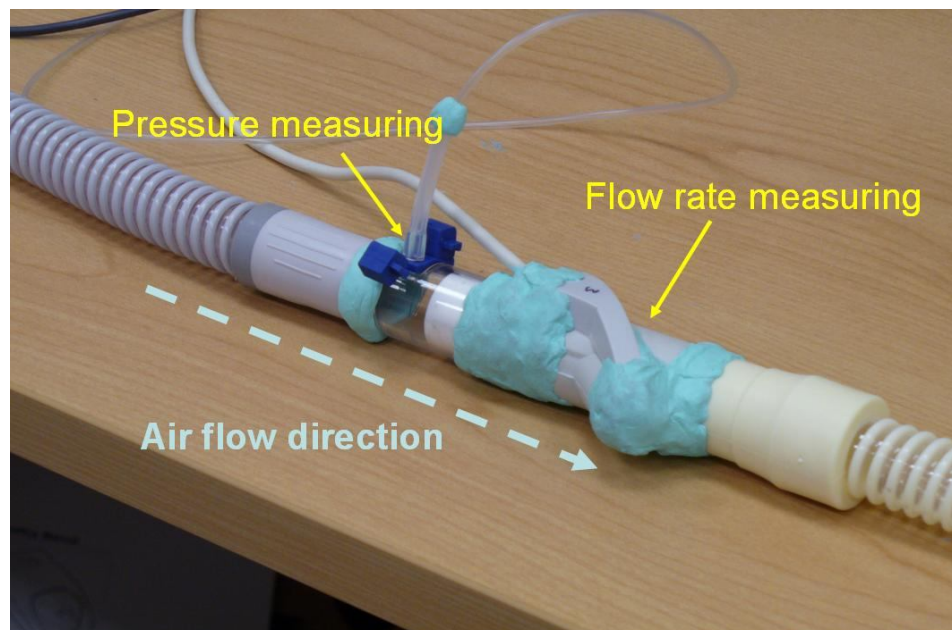
Figure 5.2 Connections for pressure measuring and flow rate measuring

The model outputs and experiment results comparison in this pressure drop are drawn in Figure 5.3. Overall the model gives very good prediction for the pressure drop.
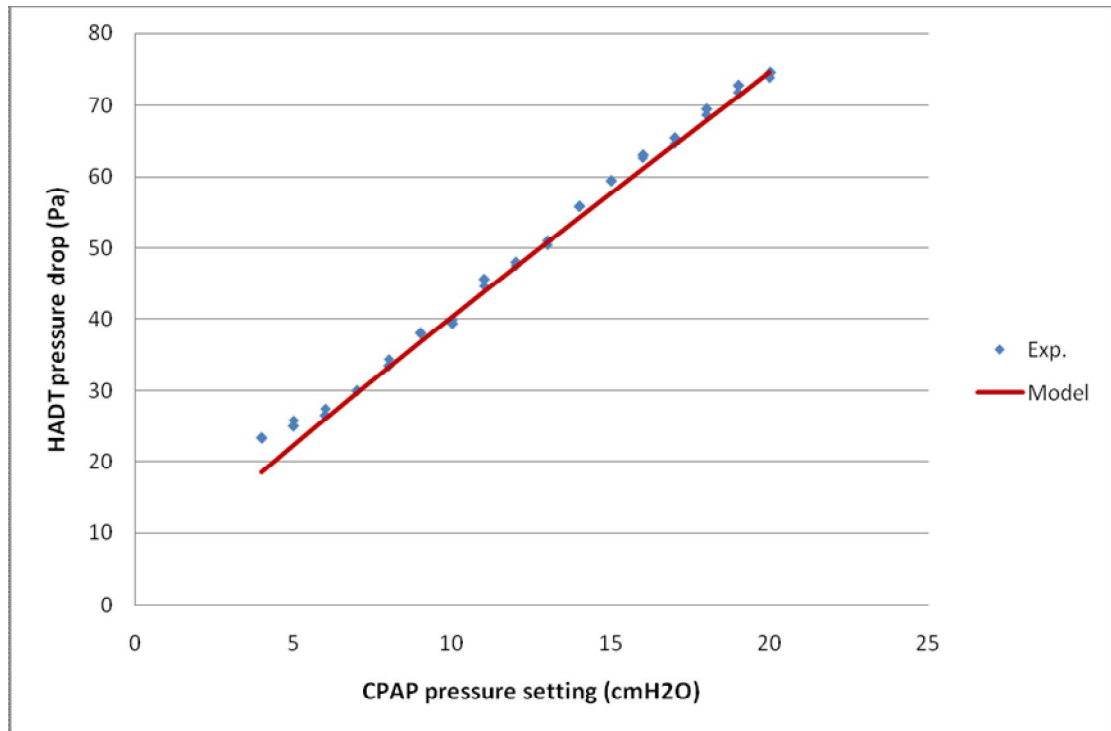
Figure 5.3 Pressure drop comparison between model output and experimental result

5.2.1.2   HADT airflow velocity

Figure 5.4 is a diagram of experiment setup for testing the airflow velocity in the HADT. The mask is also sealed and the flowmeter is also located after the HADT and before a short connecting tube.
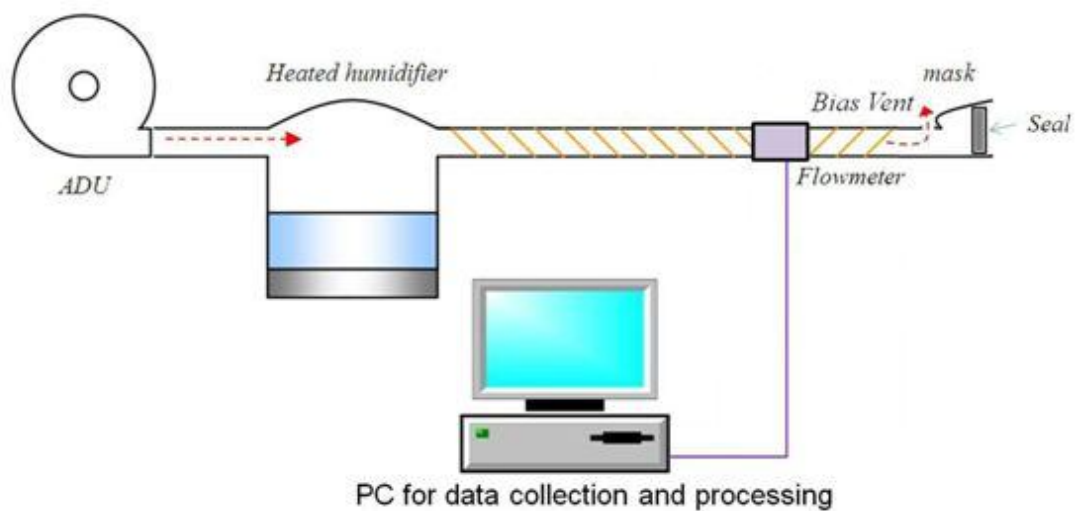
Figure 5.4 Experiment setup for air flow velocity in HADT

The experiment was also carried out for two rounds. The flow rates were converted into velocity. The experiment results and model outputs comparison are shown in Figure 5.5. The model also gives very close outputs to experiment results over the range.
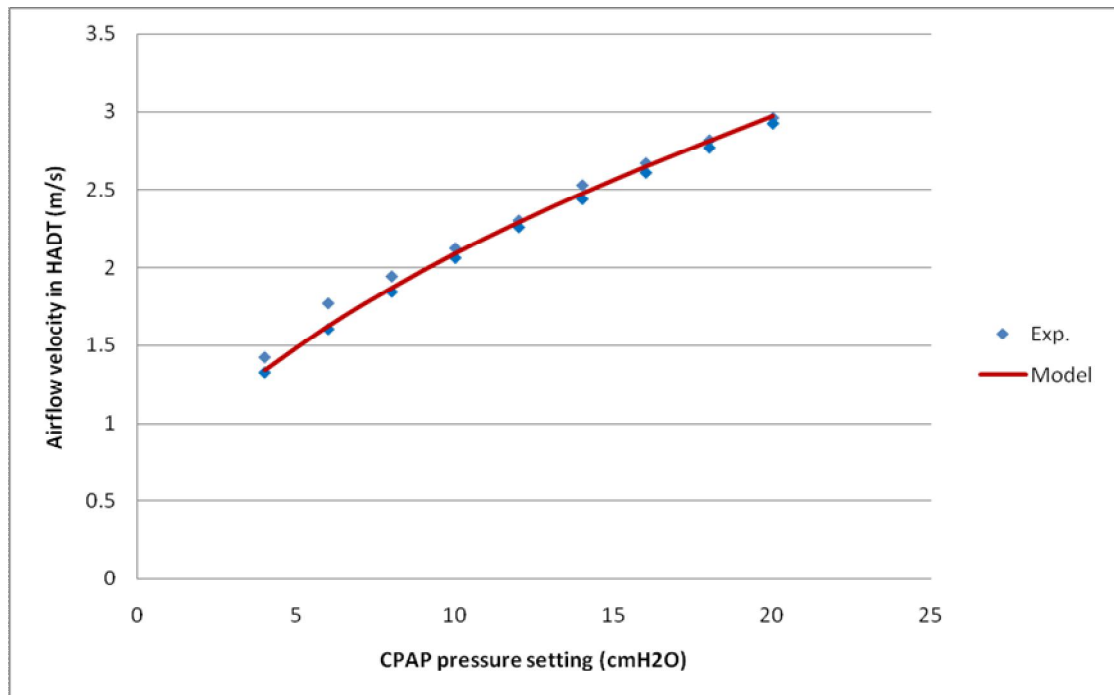
Figure 5.5 Comparison of airflow velocity in HADT between model output and experimental result

5.2.1.3   Pressure vs. Flow rate at bias vent

The bias vent holes are modelled as small Venturi tubes and an average discharge coefficient of 0.985 is used for them. The experimental setup for the coefficient validation is shown in Figure 5.6.
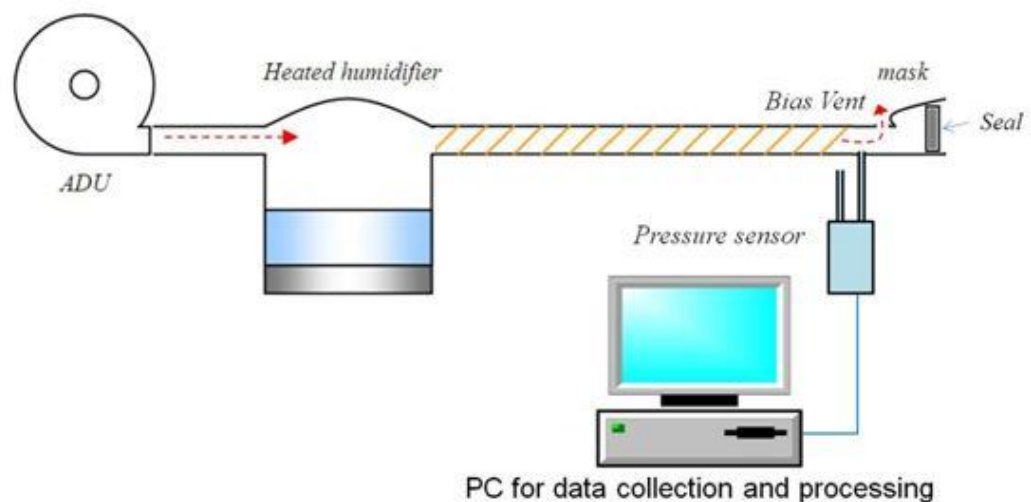
Figure 5.6 Experimental setup for bias vent hole discharge coefficient

115

The flow rate under each pressure setting is considered the same as in the tube airflow velocity test. The pressure sensor is located at the end of the HADT right before the elbow. Since the measured pressure here is static pressure, after the stagnant and static pressure gap compensation is added, the discharge coefficient can be calculated by converting Eq. (2.27) into:

$$C_d = \frac{\dot{m}_{BV}}{\sqrt{2\rho_{Ma}P_M}(A_{BH} \cdot n_{BH})}$$ (5.1)

ρ_{Ma} is chosen as 1.19 kg/m^3 as the temperature and relative humidity is about 22°C and 50% respectively when the experiment was conducted. $\dot{m}_{BV} = \dot{Q}_{BV} \cdot \rho_{Ma}$ and $\dot{Q}_{BV}$ is considered as the same as the airflow rate through the HADT.

The calculated discharge coefficient based on the experimental results are shown in Figure 5.7 with a line of 0.985 for reference. The average of the discharge coefficient over the pressure setting range is 0.9864 which is very close to the Venturi tube's discharge coefficient 0.985.
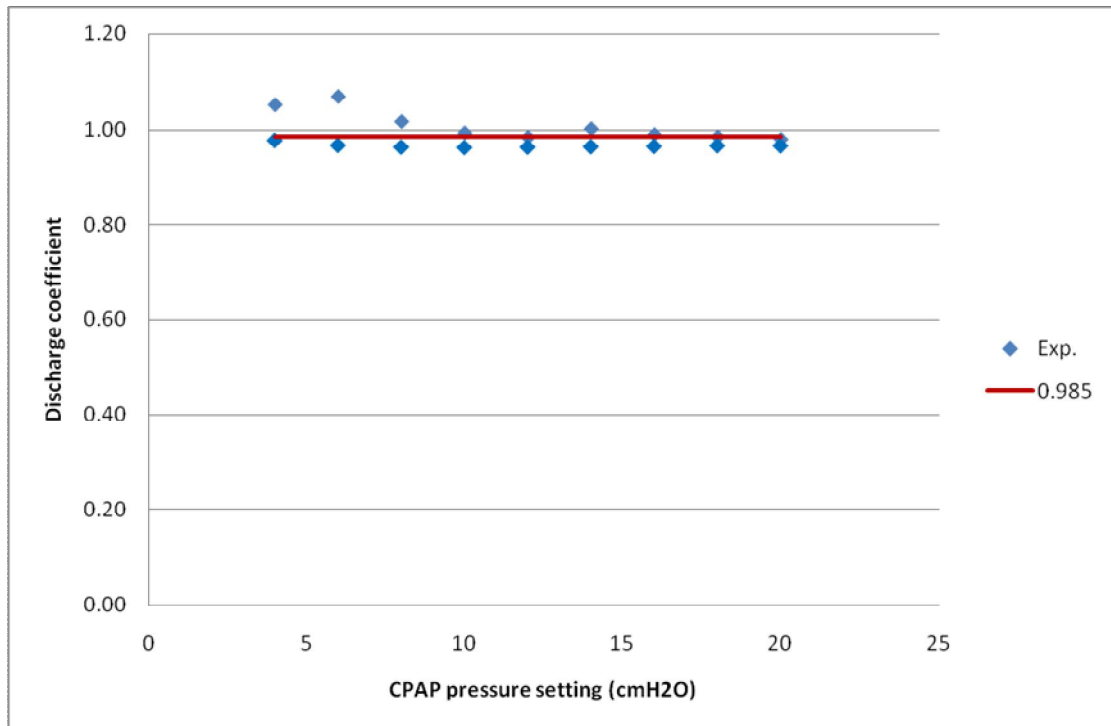
Figure 5.7 Bias vent holes discharge coefficient comparison between model output and experimental results

The values of the discharge coefficient at low settings are averagely higher than 0.985 is probably because the holes are on the outside curvature of the elbow. Therefore, when

116

air flowing through the elbow, a centrifugal force is created and increases the pressure at the outside radius of the elbow thus increases the bias flow and makes the discharge coefficient greater [45, 63]. On the other hand, when pressure setting becomes greater, the discharge coefficient decreases to 0.97. This is because when the pressure increases, the flow rate and flow velocity through the holes also increases. When the velocity is low, the Vena Contracta [45] may be close to the narrowest point of the holes near the shrinkage at the edge of the inner surface. However, when velocity increases, the higher velocity may make the Vena Contracta phenomenon gradually more significant (Figure 5.8). Overall the constant discharge coefficient 0.985 matches well with the experimental result over the CPAP working range.
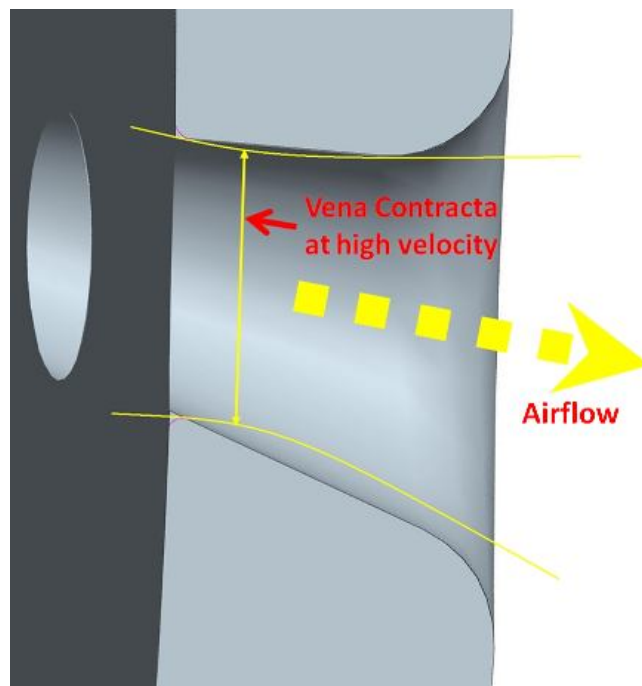
Figure 5.8 High velocity vena contracta phenomena at bias vent holes

5.2.2 Fluid dynamic model under breathing added fluctuating flow

The fluid dynamic outputs should include pressure fluctuation in the mask and the dynamic fluctuating airflow velocity in HADT. All these outputs should be tested over the CPAP pressure setting range. However, due to instruments availability, the validations have not been fully conducted. The setups for future validation are shown in Appendix XXI. The already conducted experiments are described and compared with the model outputs below.

5.2.2.1   Validation of dynamic fluctuating mask pressure

The setup for fluctuating mask pressure was shown in Figure 5.9.
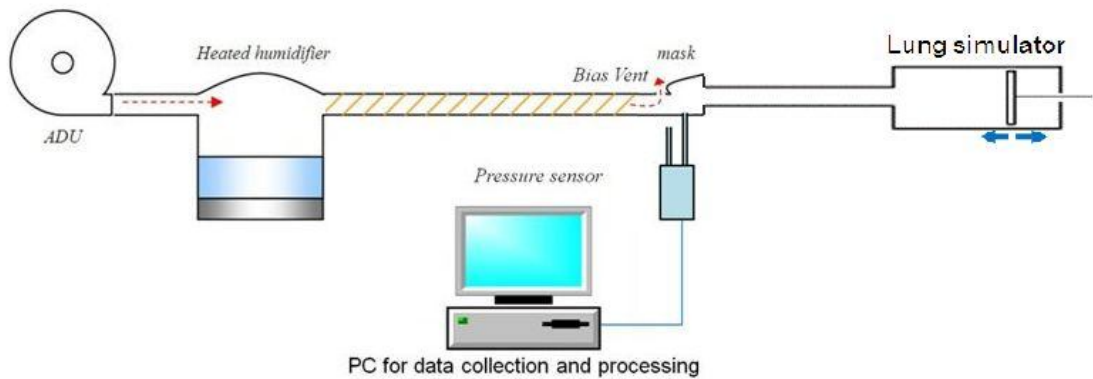
Figure 5.9 The setup for measuring the fluctuating mask pressure
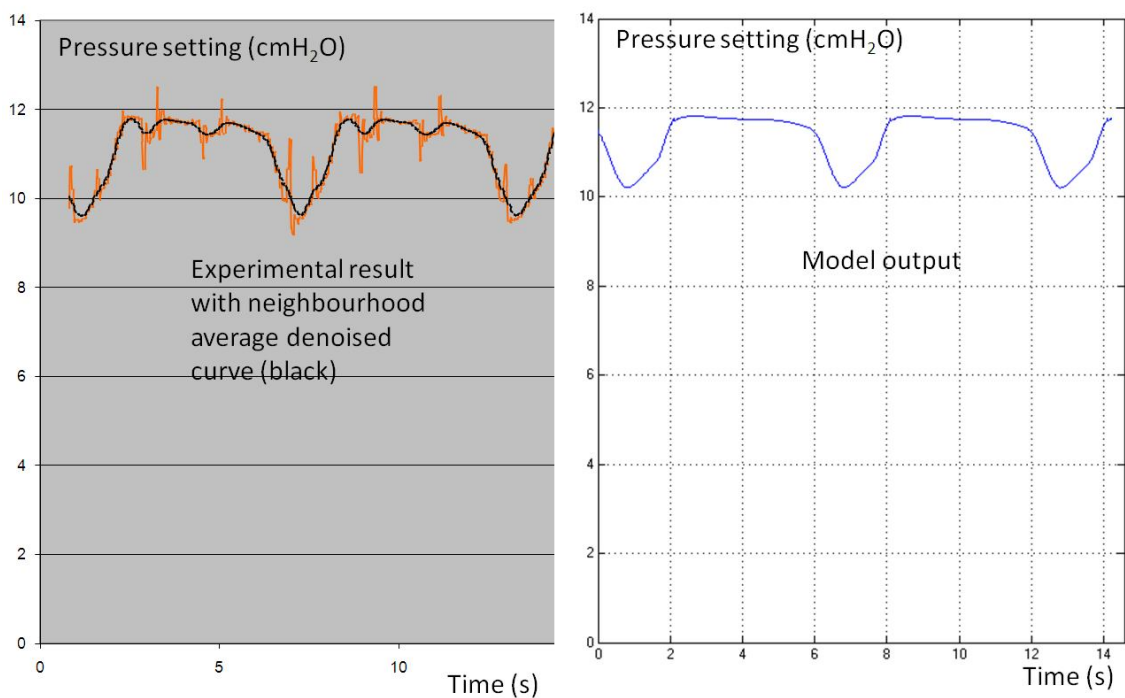
Figure 5.10 Comparison between experimental result and model output of dynamic pressure in mask (CPAP pressure setting at 12 cmH2O)

Figure 5.10 shows that the model predicts the mask pressure fluctuation very well except that the model gives a less pressure drop during inhalation (the model output is about 7.3% higher). This may be attributed to two reasons. Firstly, large centrifugal forces due to higher velocity during inhalation make the bias flow greater than the model's prediction which lowers the pressure in the mask. Secondly, the sudden

expansion from the elbow to the mask, which is not considered in the model, may induce minor head loss which further lowers the pressure in the mask. The breath load used in the experiment and the model is shown in Figure 5.11. The input to the lung simulator was the volumetric flow load which was converted from mass flow rate using air density of 1.19 kg/m^3.
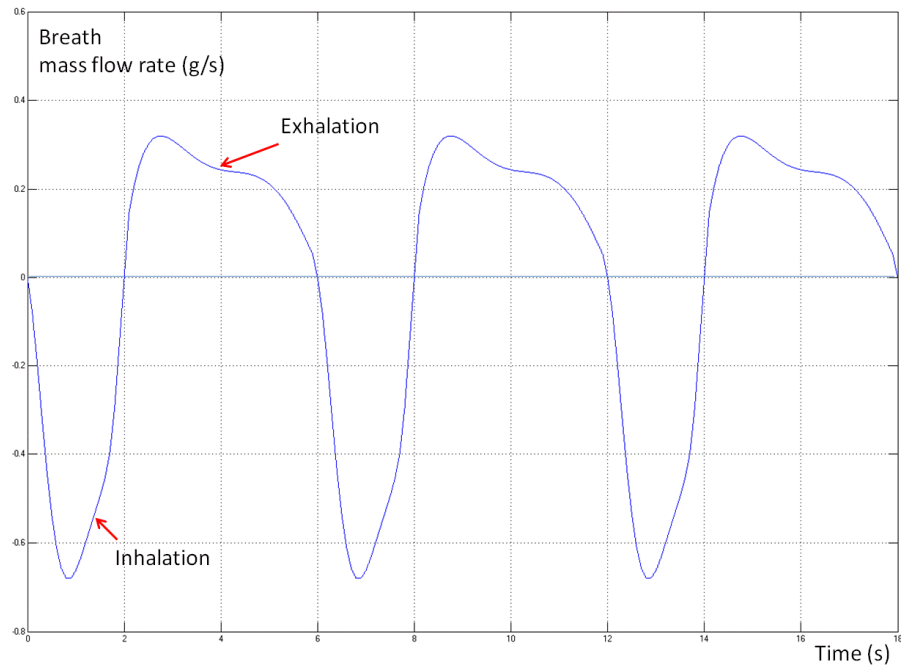
Figure 5.11 Normal breath load in mass flow rate (g/s)

5.2.2.2 Validation of CO_2 re-breathing

Erstich and Milivojevic from Fisher and Paykel Healthcare Co. Ltd. conducted experiments about CO_2 re-breathing [64] and the model outputs are discussed and compared with their results below.

They used FlexFit^{TM} 407 nasal mask with volunteers tested the CO_2 concentration in end tidal and in inhaled air. The volunteers breathed "restfully". By setting the pressure at a very low level and blocking some of the bias vent holes, they achieved very low flow rate. When flow rate was as low as 8.9 L/min. the inhaled air started to contain certain amount of measurable CO_2. The average respiratory rate of the volunteers was 11 times/min. when pressure setting was 3 cmH2O and flow rate was 8.9 L/min. the average CO_2 in inhaled air is 0.17% [64].

By adjusting the bias vent area, the model was set to provide very low flow rate under the pressure setting same as in the experiment. An average nose volume of 32 cm^3 [65, 66] is subtracted from the mask capacity since the nose volume is significant comparing with the capacity of a nasal mask. The breath load is adjusted to 500 ml for average "restful" breath. The CO_2 concentration in exhaled air is given as 5%. Based on these conditions, the model gives 0.252% of CO_2 in inhaled air. Comparing to the average experimental result 0.17%, the model prediction is reasonably close considering the small percentage, the sensitivity of the mask volume and the limited number of objects which does not represent a statistical average.

5.3 Experimental validation of the thermal dynamic part

This section focuses on the thermodynamic validation. There are two subsections; one is under steady flow and the other under patient breath-added fluctuating flow.

5.3.1 Thermal dynamic model under steady flow

This experimental investigation was conducted to quantify the steady flow situation and compare the results with the outputs from the thermal dynamic model. The results include evaporation rate, the chamber water temperature, in-chamber airflow temperature and airflow temperature at the end of the HADT near the elbow as well as observation of condensation in HADT. The experiment is conducted under combination of different ADU pressure settings, heater plate settings, tube heating settings and ambient conditions. The experiment was carried out under high ambient temperature, normal room temperature and low temperature to validate the model's applicability on a wide environmental variety. The high ambient temperature and low ambient temperature conditions were achieved by a big environmental control room (Figure 5.12). The high temperature is at about 33°C and low is at about 14°C.

Figure 5.12 Environmental control room for creating high temperature and low temperature conditions
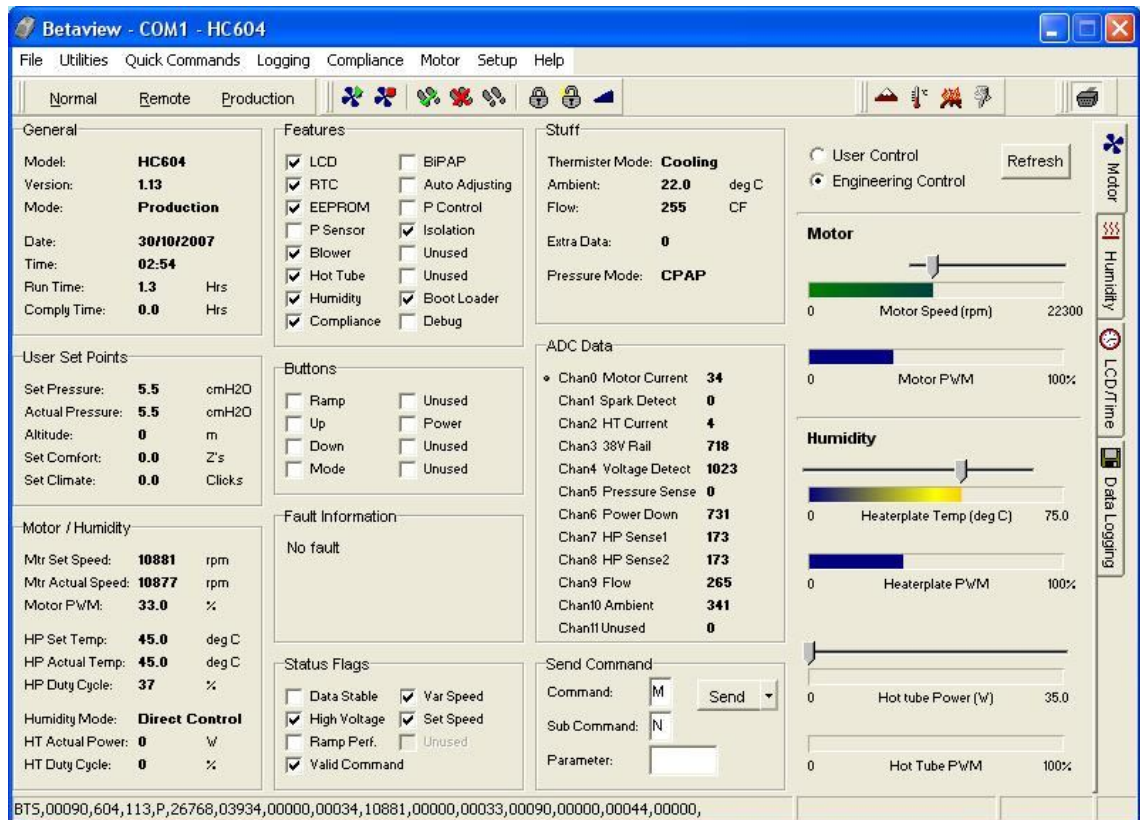
Figure 5.13 Betaview control window

The experiment setup consisted of a Betaview control software (Figure 5.13), an HC600 CPAP unit, an HC365 chamber. The meter used for measuring the ambient humidity was a "Humidity and temperature meter HM34C" with relative humidity measuring ranges of 0 ~ 100%. The meter measuring temperature was a "Fluke 51 II Thermometer" and a K-type thermal couple. A Sensirion CMOS temperature and humidity sensor was also used for reference and comparison (Figure 5.14).
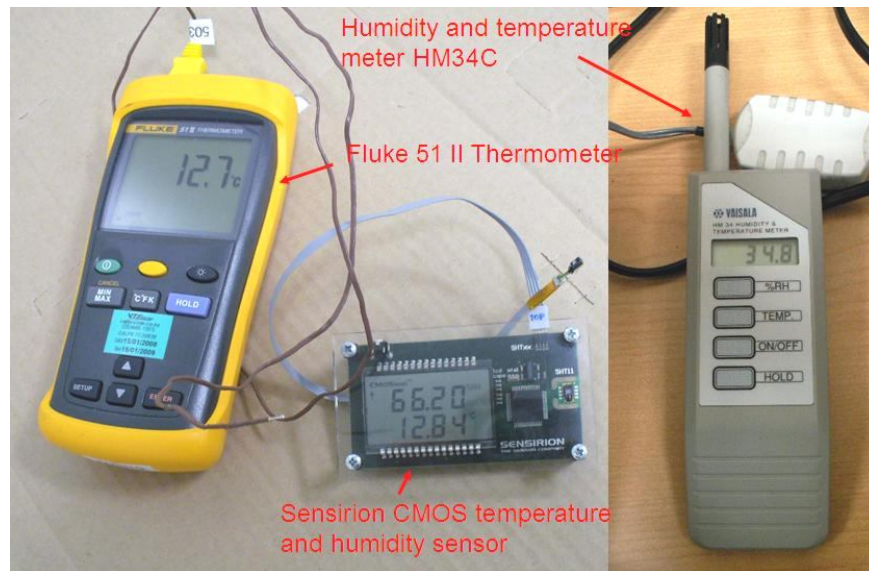
Figure 5.14 Meters used for measuring temperature and humidity

The Betaview control program is designed for bypassing the CPAP control system thus the machine can be controlled directly from the computer. In this experiment, the Betaview was used to control the heating element temperature and tube heating power supply.

All the experiment output recordings started after the CPAP machines had been running for 1 hour so the system reached steady state. During experiments, it is important to make sure that the condensation in HADT and the mask does not build up and significantly narrow the conduit or muffle the bias vent holes. The condensate can be drained away through the bias vent holes about every 10 minutes.

In real use, the tube heating of CPAP series 600 is coded as automatically controlled for preventing air flow being over heated which might harm patient's skin and damage upper airway. However, for validating the model, the tube heating was set to be 0 W, 15 W and 30 W.

Table 5.1 shows the combinations of conditions and settings under which the experiment was conducted:

Table 5.1 Combinations of conditions and settings for steady state thermal validation

T_{∞} (°C)	Pressure	Heating Element Setting	Tube Heating Setting
Low(about14°C)	4 cmH$_2$O	45°C	0 W
Normal(about22°C)	12 cmH$_2$O	55°C	15 W
High(about33°C)	20 cmH$_2$O	65°C	30 W

5.3.1.1 In-chamber water temperature

After the whole system reached steady state and the ambient conditions were stable (when using the big environmental control room for high and low ambient temperature), water temperature was then measured by putting the thermal couple junction of the Fluke 51 II Thermometer into the water (Figure 5.15). The temperature was measured again after about 2.5 hours. The average of the two measurements was considered the result of the water temperature and was used to compare with the model output. Meanwhile, the ambient temperature and relative humidity were also measured twice. One was measured at the beginning of the test and the other at the end of the test. The experimental results and model outputs are shown in Figure 5.16, Figure 5.17 and Figure 5.18 with corresponding discussions.
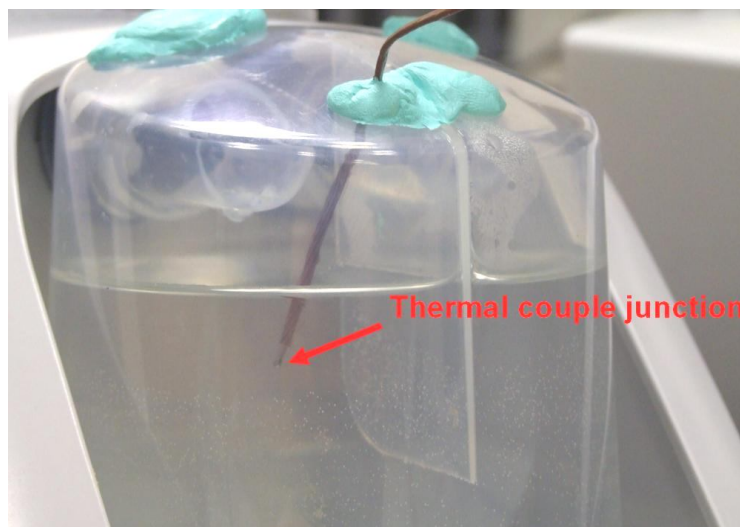
Figure 5.15 Measuring of airflow temperature at chamber outlet

5.3.1.1.1 Water temperature vs. heating element setting

Figure 5.16 shows the humidifier water temperature when the humidifier heating element temperature setting changes. It can be seen that when heating element temperature setting is high, the water temperature is also high.
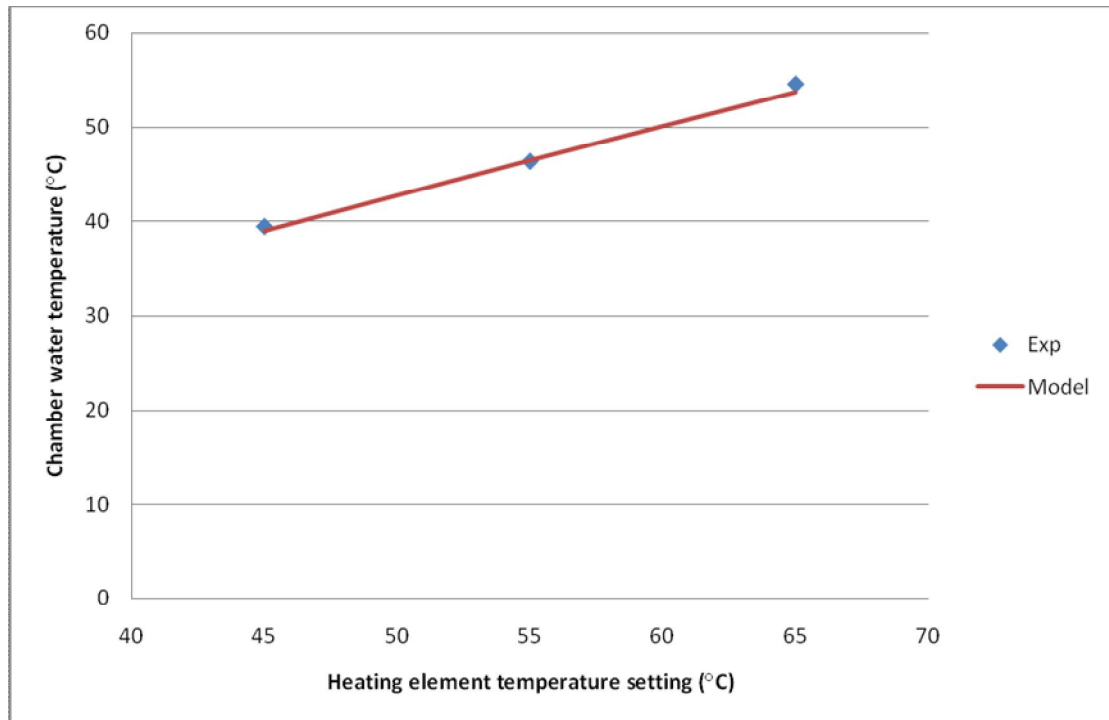
Figure 5.16 Comparison of model outputs and experimental results of humidifier water temperature vs. heating element temperature setting under normal ambient room temperature and pressure setting at 12cmH$_2$O

5.3.1.1.2 Water temperature vs. CPAP pressure setting

Figure 5.17 shows the water temperature under normal room temperature and humidifier heating element setting of 55°C. The tests were conducted on different days and the room temperature and relative humidity level were not exactly the same. However, still the trend is maintained. It can be seen that when pressure setting is high, the water temperature becomes lower. This is because the higher the pressure setting is, the higher the mass and heat convections and consequently the more heat energy is lost from the water to the air above it.
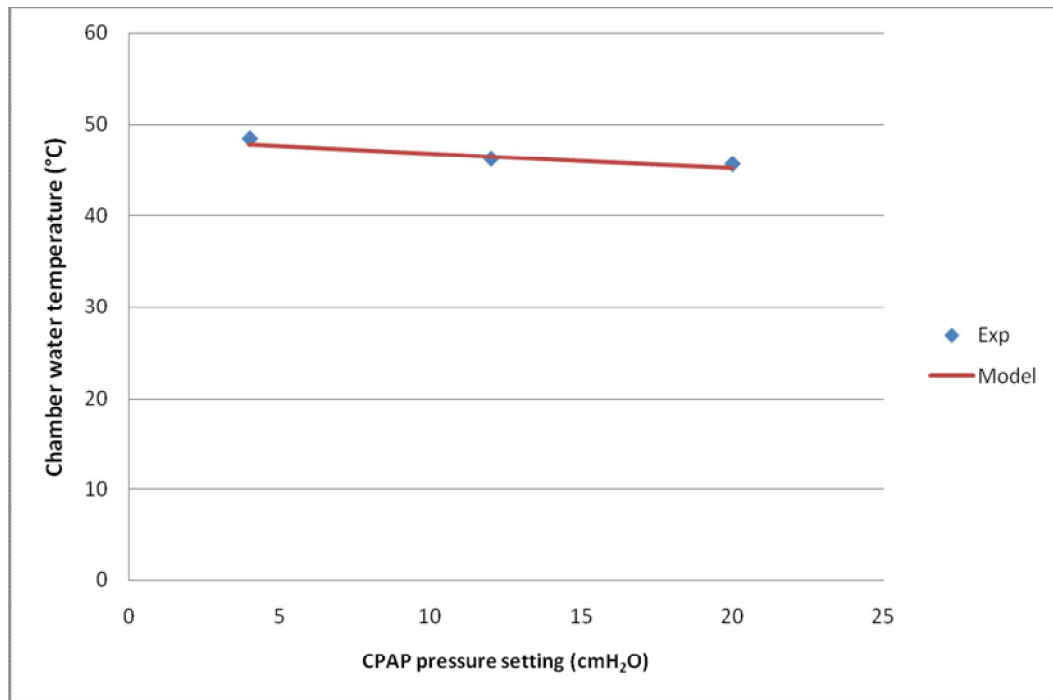
Figure 5.17 Comparison of model outputs and experimental results of humidifier water temperature vs. CPAP pressure setting under normal ambient temperature and heating element setting at 55°C

5.3.1.1.3 Water temperature vs. ambient temperature

Figure 5.18 shows the water temperature under CPAP pressure setting of 12 cmH$_2$O and humidifier heating element setting of 55°C under different ambient temperatures. It can be seen that when ambient temperature is high, the water temperature is slightly higher. This is because the higher the ambient temperature is, the higher the inlet temperature which lessen the heat convection from water to it. The higher ambient temperature also lessens the heat dissipation from water to the ambient through chamber wall.
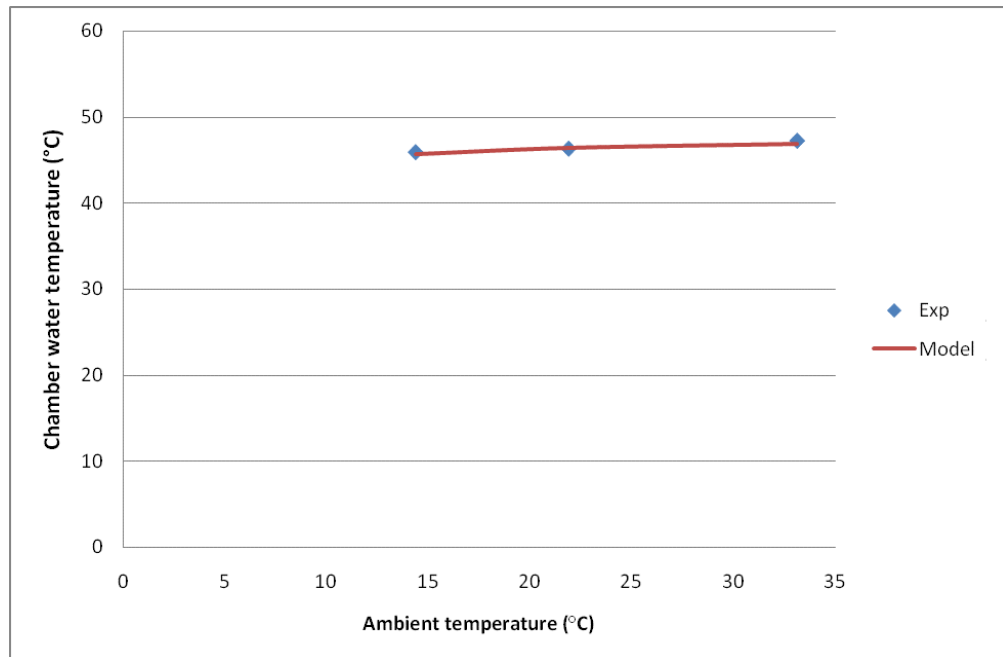
Figure 5.18 Comparison of model outputs and experimental results of humidifier water temperature vs. ambient temperature under heating element temperature setting at 55°C and pressure setting at 12cmH₂O

It can be seen that the most important factor influencing the water temperature is the heating element setting and the model predicts the water temperature very well.

5.3.1.2   In-chamber air temperature

The air temperature in the chamber varied from spot to spot. However the air temperature in the outlet extension tube was very stable and was within the varied range. Thus the air temperature in the outlet is used to represent the average temperature of the in-chamber air. The location for measuring it is shown in Figure 5.19.
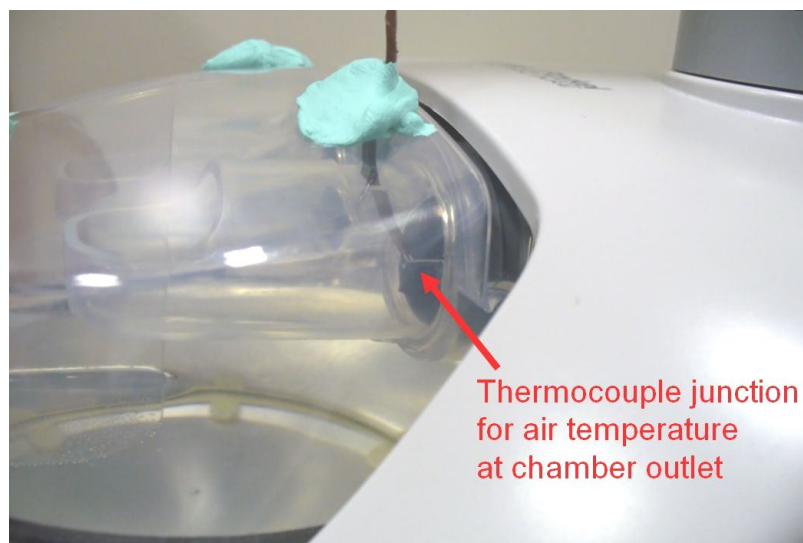
Figure 5.19 Measuring of airflow temperature at chamber outlet

126

The comparison of experimental results and model outputs vs. influencing factors are listed and discussed below.

5.3.1.2.1 In-chamber air temperature vs. heating element setting

Figure 5.20 shows a graph of air temperature in the chamber under ambient conditions $T_\infty = 21.9°C$, $RH_\infty = 64.0\%$ and CPAP pressure setting of 12 cmH$_2$O.

It can be seen that when heating element temperature setting is higher, the in-chamber air temperature is also higher. This is because the higher heating element temperature makes the in-chamber water temperature higher and consequently higher heat and mass convections from the water to the in-chamber air.
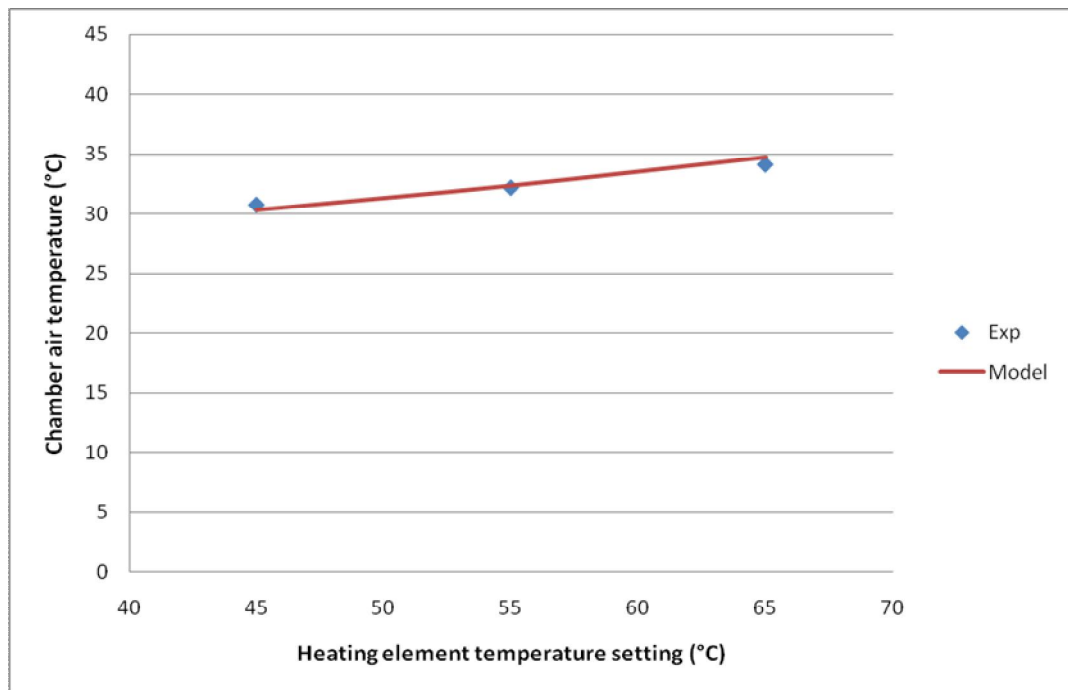
Figure 5.20 Comparison of model outputs and experimental results of in-chamber air temperature vs. heating element temperature setting under normal ambient room temperature and pressure setting at 12cmH$_2$O

5.3.1.2.2 In-chamber air temperature vs. CPAP pressure setting

Figure 5.21 shows the values of air temperature in the chamber under normal ambient room temperature and humidifier heating element setting of 55°C with different CPAP pressure settings. The tests were conducted on different days and the ambient temperature and relative humidity level were not exactly the same.
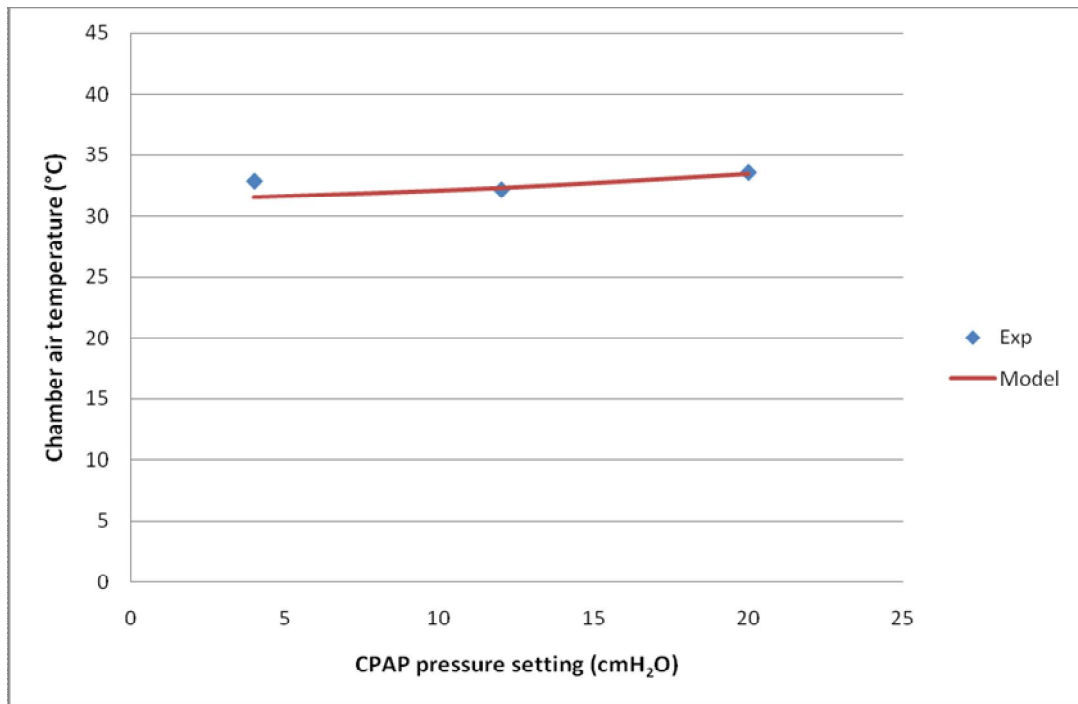
Figure 5.21 Comparison of model outputs and experimental results of in-chamber air temperature vs. CPAP pressure setting under normal ambient temperature and heating element setting at 55°C

It can be seen that when pressure setting is high, the in-chamber air temperature is also slightly high. This is because the higher the pressure setting is, the inlet air temperature is also higher due to the thermal enthalpy gain from the blower. On the other hand, although higher pressure setting makes higher flow rate thus higher heat and mass convection from the water to the air, the high flow rate makes per unit air receives less convected heat and vapour. These two phenomena work together make the in-chamber air temperature just slightly tilting up along with the pressure setting.

5.3.1.2.3 In-chamber air temperature vs. ambient temperature

Figure 5.22 shows the in-chamber air temperature under CPAP pressure setting at 12 cmH$_2$O and humidifier heating element setting of 55°C in different ambient temperatures. It can be seen when ambient temperature is higher, the in-chamber air temperature is also higher. This is because:

1. The higher the ambient temperature is, the higher the inlet temperature will be.
2. Higher ambient temperature also lessens the heat dissipation to the ambient through chamber walls (wall 2 and wall 3).
3. The water temperature is also a bit higher which can also contribute to the in-chamber air temperature.

128
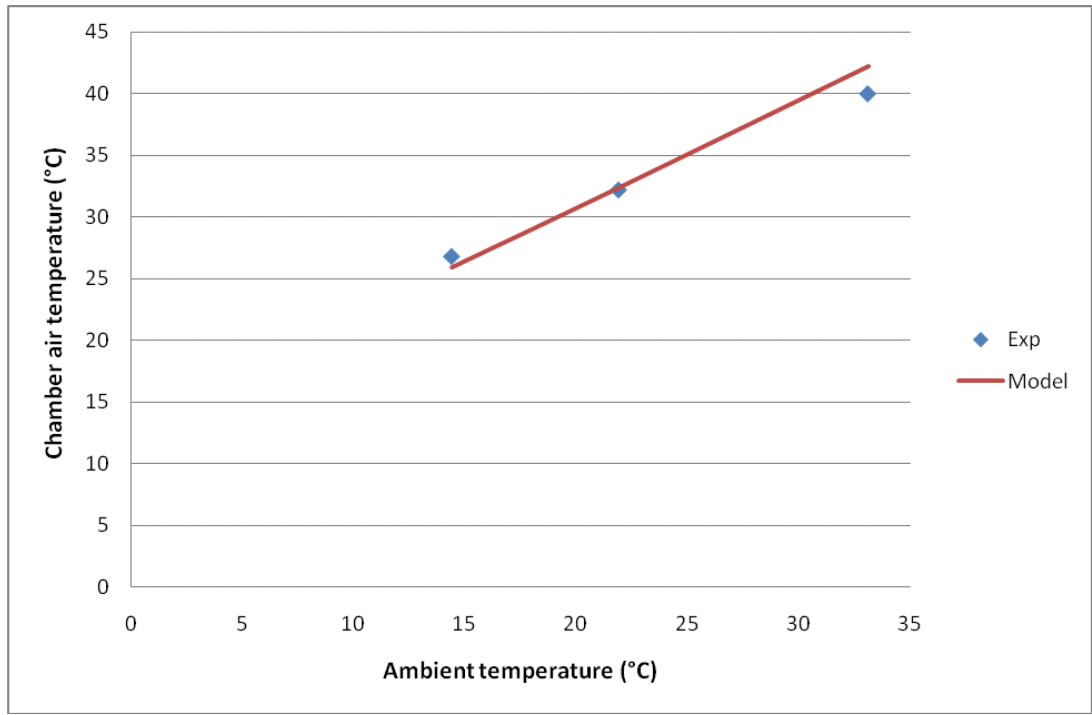
Figure 5.22 Comparison of model outputs and experimental results of in-chamber air temperature vs. ambient temperature under heating element temperature setting at 55°C and pressure setting at 12cmH$_2$O

The most important factor influencing in-chamber air temperature is the ambient temperature. The heating element temperature setting also has a significant influence. The in-chamber air temperature is very well predicted by the model.

5.3.1.3 Evaporation rate

Evaporation was measured by weighing the loss of water in the chamber. For each measurement, the first weighing was done after the CPAP ran for about one hour and the whole system became stable. The second weighing was done after continuing running for another two hours. The difference of the weights is considered as the amount of water being evaporated during the time. The error between experimental result and model output is defined as $\varepsilon = \dfrac{\dot{m}_{ev-Model} - \dot{m}_{ev-Exp}}{\dot{m}_{ev-Exp}} \times 100\%$.

5.3.1.3.1 Evaporation rate vs. heating element setting

Figure 5.23 shows the evaporation rates under ambient conditions, $T_\infty = 21.9°C$, $RH_\infty = 64.0\%$ and CPAP pressure setting of 12 cmH$_2$O.

129
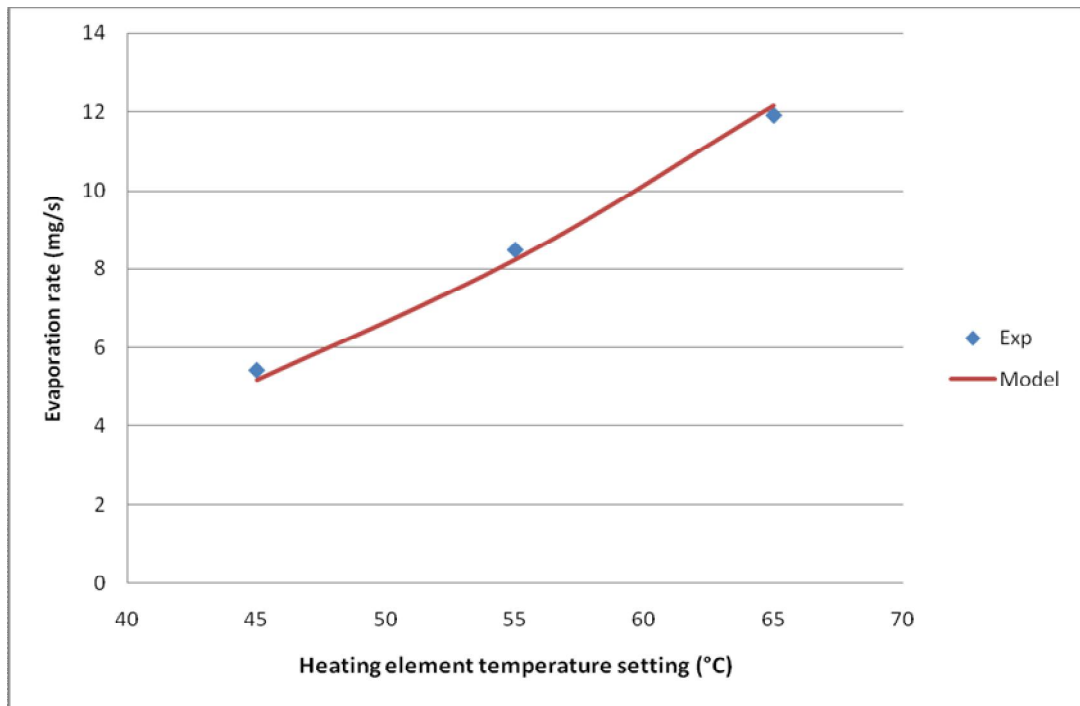
Figure 5.23 Comparison of model outputs and experimental results of evaporation rate vs. heating element temperature setting under normal ambient room temperature and pressure setting at 12cmH$_2$O

It can be clearly seen that when heating element temperature setting is high, the evaporation rate is also higher. This is because of higher water surface saturated absolute humidity as a result of higher temperature setting.

5.3.1.3.2 Evaporation rate vs. CPAP pressure setting

Figure 5.24 shows the values of evaporation rate under normal ambient room temperature and humidifier heating element setting of 55°C. The tests were conducted on different days and the room temperature and relative humidity were not exactly the same. However, the trend is maintained.
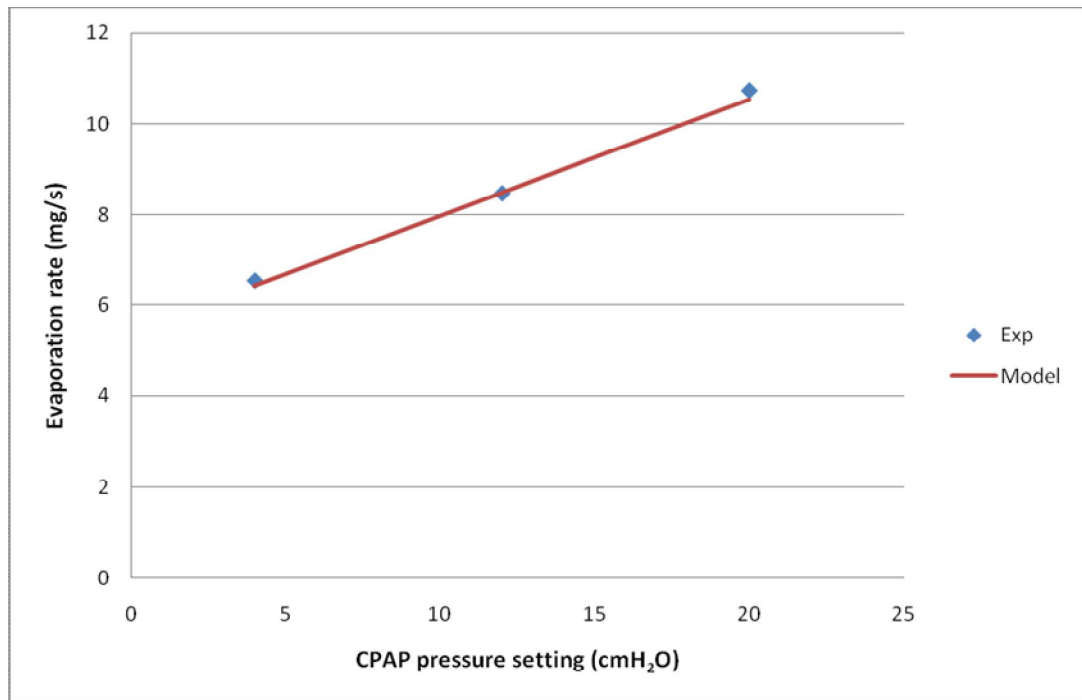
Figure 5.24 Comparison of model outputs and experimental results of evaporation rate vs. CPAP pressure setting under normal ambient temperature and heating element setting at 55°C

It can be seen that when CPAP pressure setting is high, the evaporation rate is also higher. This is because higher CPAP pressure setting thus higher airflow rate makes the forced mass convection rate higher.

5.3.1.3.3 Evaporation rate vs. ambient temperature

Figure 5.25 shows the evaporation rate under CPAP pressure setting of 12 cmH₂O and humidifier heating element setting of 55°C in different ambient temperatures.
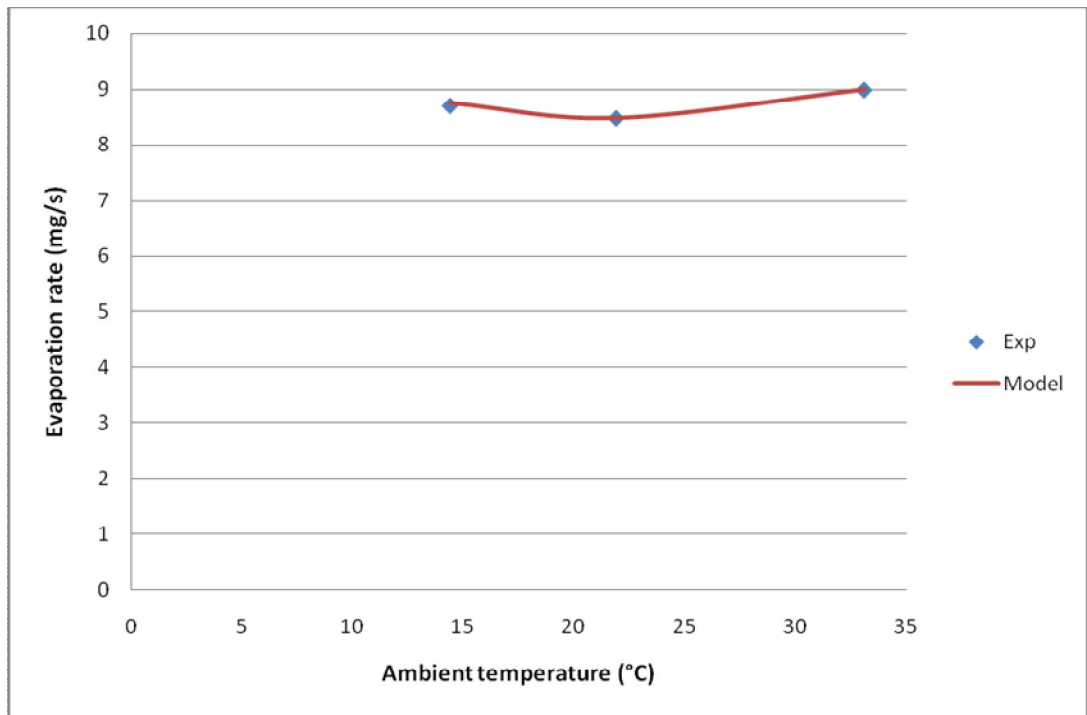
Figure 5.25 Comparison of model outputs and experimental results of evaporation rate vs. ambient temperature under heating element temperature setting at 55°C and pressure setting at 12cmH$_2$O

Both the model output and experimental result of evaporation rate have a curve-down at the normal room temperature in Figure 5.25. This is because the day was very humid when the normal room temperature test was carried out and the high specific humidity of inlet reduced the absolute humidity gap which lessened the evaporation rate in that test.

Inlet temperature may indirectly influence evaporation rate in the way that higher inlet temperature reduces the heat convection so makes the water to be kept at a slightly higher temperature. Also the higher ambient temperature can reduce the heat dissipation to the ambient thus can keep the water a little warmer so to increase the water surface saturated absolute humidity. However, the ambient temperature is not a significant factor influencing evaporation.

It can be seen that evaporation rate is significantly related to heating element temperature setting and CPAP pressure setting and the model predicts the evaporation rate very well.

5.3.1.4 Airflow temperature at the end of the HADT

Figure 5.26 Thermal junction couple inserted in elbow to test the temperature of the HADT outlet

As shown in Figure 5.26, the thermal couple junction was inserted into the end of the HADT to measure its outlet air temperature.

5.3.1.4.1 T_{Ta30} vs. heating element setting
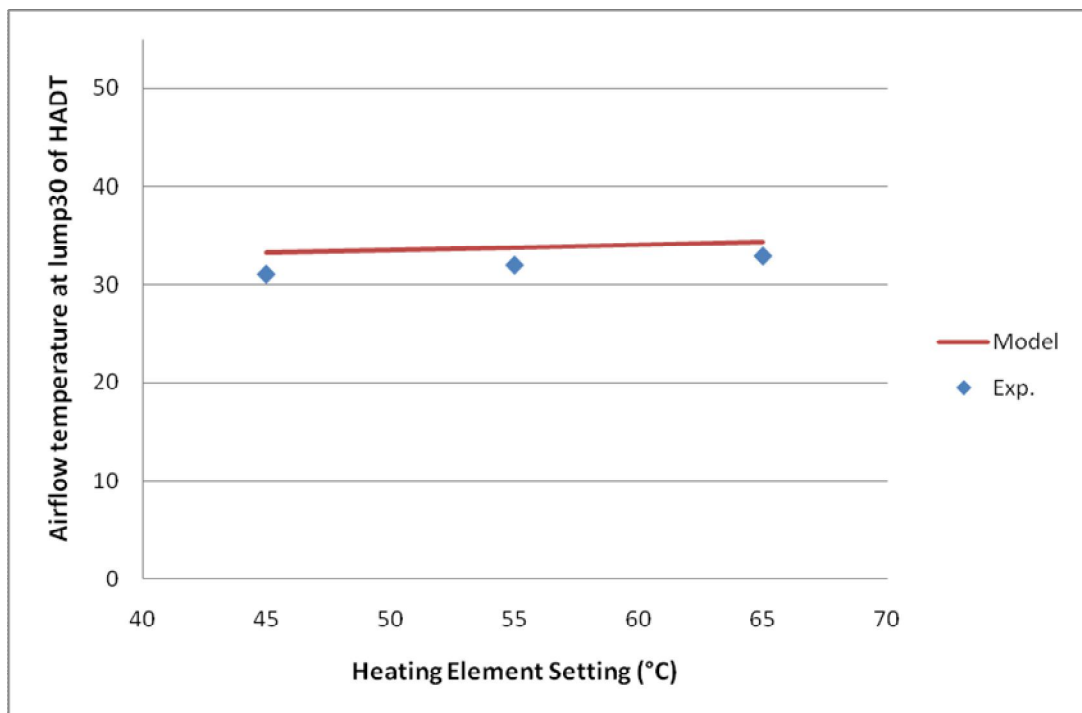
Figure 5.27 Comparison of model outputs and experimental results of Airflow temperature at HADT lump30 vs. heating element temperature setting under normal room temperature, pressure setting at 12cmH₂O and tube heating at 15W

Figure 5.27 shows the values of T_{Ta30} under ambient conditions T_∞ =21.9°C, $RH_\infty = 64.0\%$, CPAP pressure setting of 12 cmH$_2$O with 15 W tube heating but different heating element settings.

Higher heating element setting provides higher in-chamber air temperature. However the airflow temperature at the HADT outlet is only a bit higher. This is because the higher temperature airflow from the chamber gives away more heat to the HADT wall and the ambient. This makes the temperature at the HADT outlet not very different.

5.3.1.4.2 Airflow temperature at HADT lump30 vs. CPAP pressure setting

Figure 5.28 shows the values of T_{Ta30} under normal ambient room temperature and humidifier heating element setting of 55°C with 15 W tube heating but different CPAP pressure settings. The tests were conducted on different days and the room temperature and relative humidity were not exactly the same.
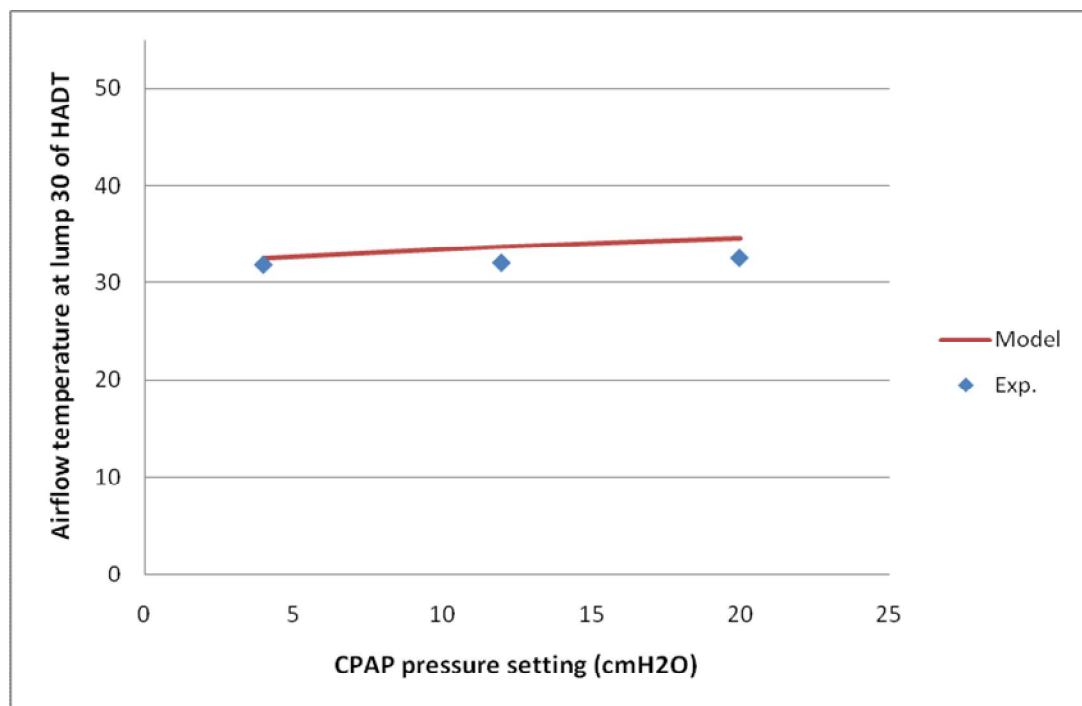
Figure 5.28 Comparison of model outputs and experimental results of Airflow temperature at HADT lump30 vs. CPAP pressure setting under normal room temperature and heating element setting at 55°C and tube heating at 15W

When the CPAP pressure setting was high and flow rate is also high, the in-chamber air temperature was also a little higher since the airflow gained more heat from the blower. After flowing through the HADT, this air temperature difference between high and low

flow rate had been even further increased because faster flow lessened air temperature change in the HADT.

5.3.1.4.3 Airflow temperature at HADT lump30 vs. ambient temperature

Figure 5.29 shows the values of T_{Ta30} in different ambient temperatures under CPAP pressure setting of 12 cmH$_2$O, humidifier heating element setting of 55°C with 15 W tube heating. It is clear that when ambient temperature was high the HADT outlet temperature was also high. The main reason here is the high ambient temperature keeps the HADT wall warmer.
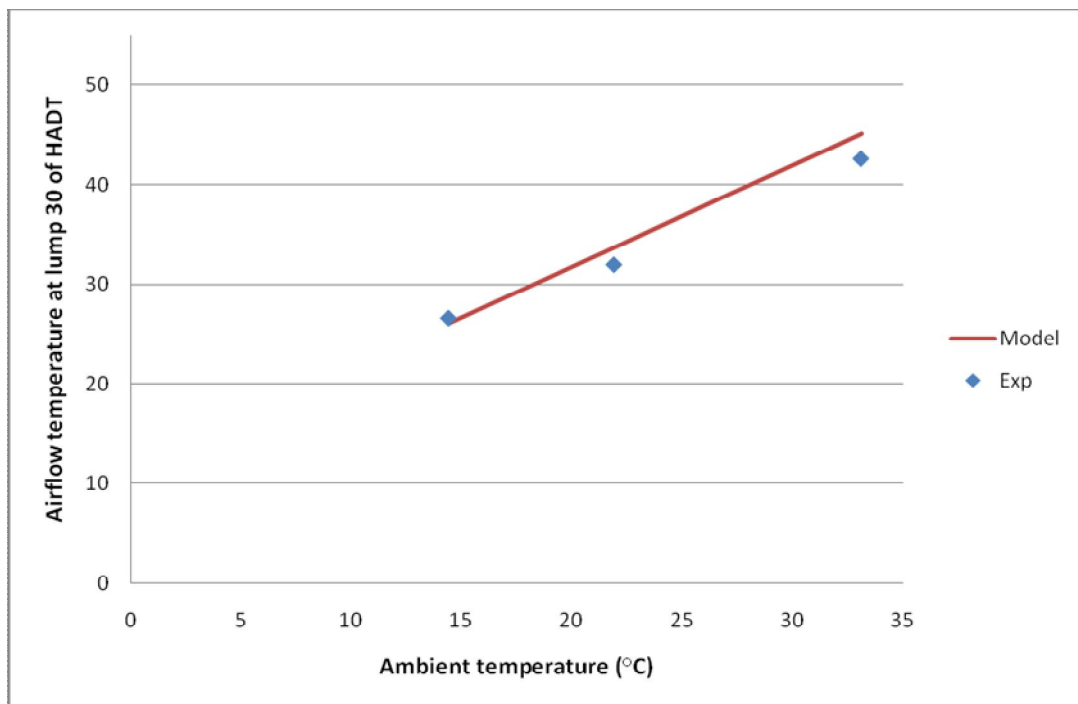
Figure 5.29 Comparison of model outputs and experimental results of airflow temperature at HADT lump30 vs. ambient temperature under heating element temperature setting at 55°C, pressure setting at 12cmH$_2$O and tube heating at 15W

5.3.1.4.4 Airflow temperature at HADT lump30 vs. tube heating

Figure 5.30 shows the values of T_{Ta30} under CPAP pressure setting of 12 cmH$_2$O, humidifier heating element setting of 55°C and normal room temperature. Obviously, higher tube heating, higher HADT outlet temperature.
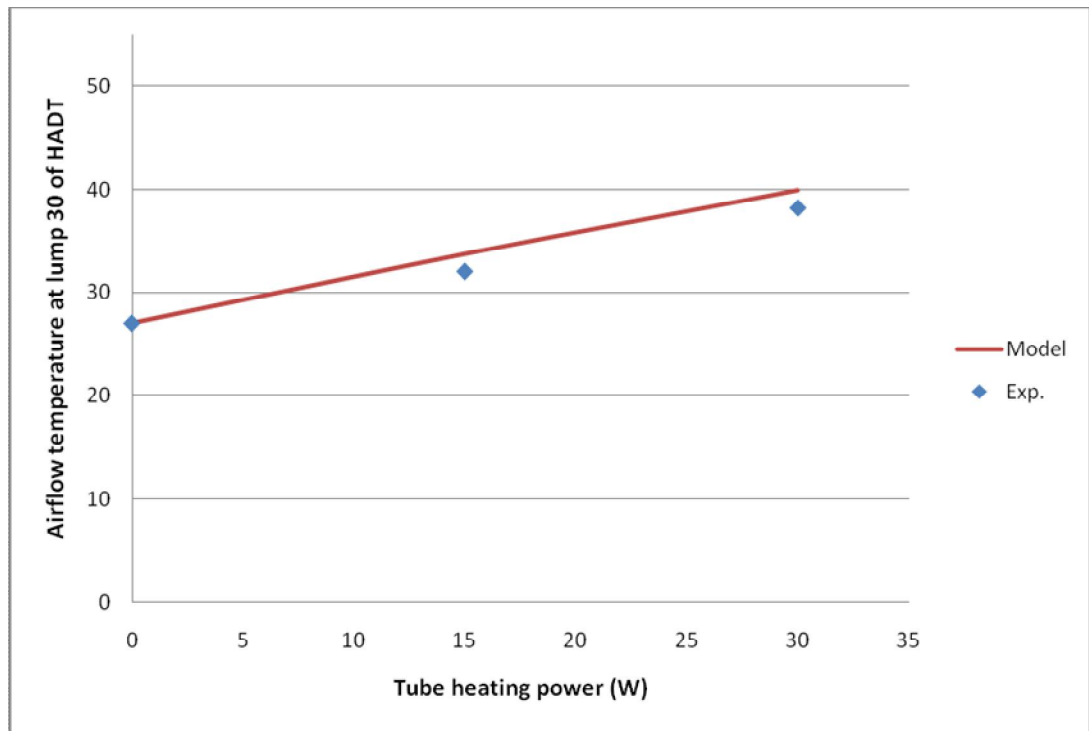
Figure 5.30 Comparison of model outputs and experimental results of Airflow temperature at HADT lump30 vs. setting of tube heating under heating element temperature setting at 55°C, pressure setting at 12cmH$_2$O and normal room temperature

From the data and graphs above, the ambient temperature and tube heating are the most important factors influencing the airflow temperature at the HADT outlet.

The model outputs match very well with the experimental results.

5.3.1.5   Condensation in the HADT

Condensation in the HADT was checked by observation. The photo below is used to define the terms describing the condensation severity (Figure 5.31).

136
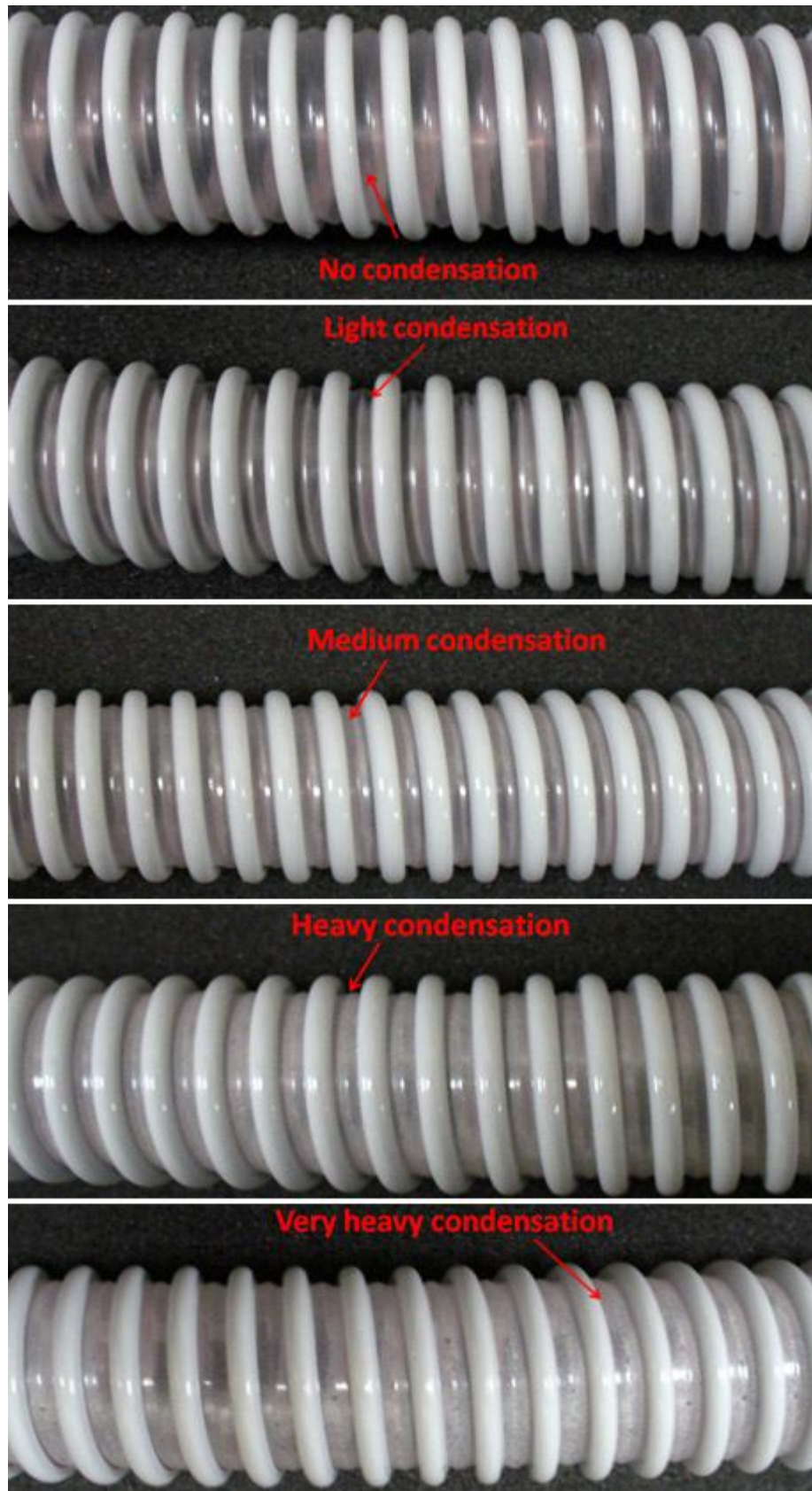
Figure 5.31 Comparison of condensation in HADT

5.3.1.5.1 Condensation vs. heating element setting

Table 5.2 shows the Condensation under ambient conditions T_∞ =21.9°C, $RH_\infty = 64.0\%$, CPAP pressure setting of 12 cmH$_2$O and no tube heating but with different heating element setting. It is shown that when humidifier heating element temperature setting is higher, the airflow humidity level is also higher and generates more condensate.

Table 5.2 Comparison of condensation between experimental results and model outputs vs. heating element temperature setting under normal room temperature, 12cmH2O CPAP pressure setting and no tube heating

Pressure Setting	Ambient Conditions	Tube heating	Heating Element Setting	Condensation (Exp.)	Condensation (Model)
12 cmH$_2$O	T_∞ =21.9°C $RH_\infty = 64.0\%$	0 W	45°C	Yes (Very light in grooves in second half of the HADT) (Lump 16)	No
			55°C	Yes After 28cm (Lump 5)	Yes Starts from lump 19
			65°C	Yes After 10cm (Lump 2)	Yes Starts from Lump 2

5.3.1.5.2 Condensation vs. CPAP pressure setting

Table 5.3 shows condensation under normal room temperature, humidifier heating element setting of 55°C and no tube heating but with different CPAP pressure settings. It is shown that when CPAP pressure setting is higher, the condensation becomes less.

Table 5.3 Comparison of condensation between experimental results and model outputs vs. CPAP pressure setting under normal room temperature, 55°C heating element setting and no tube heating

Tube heating	Heating Element Setting	Pressure Setting	Ambient Conditions	Condensation (Exp.)	Condensation (Model)
0 W	55°C	4 cmH$_2$O	$T_\infty = 21.6$°C $RH_\infty = 47.3\%$	Yes / After 16cm (Lump 3)	Yes / Starts from Lump 2
		12 cmH$_2$O	$T_\infty = 21.9$°C $RH_\infty = 64.0\%$	Yes / After 28cm (Lump 5)	Yes / Starts from lump 19
		20 cmH$_2$O	$T_\infty = 21.9$°C $RH_\infty = 39.5\%$	No	No

5.3.1.5.3 Condensation vs. ambient temperature

Table 5.4 shows Condensation under CPAP pressure setting of 12cmH$_2$O, humidifier heating element setting of 55°C with no tube heating. It is shown that when ambient temperature increases, the condensation decreases.

Table 5.4 Comparison and errors of Condensation between experimental results and model outputs vs. ambient temperature under CPAP pressure setting at 12cmH2O, heating element setting at 55°C and 15W tube heating

Pressure Setting	Tube heating	Heating Element Setting	Ambient Conditions	Condensation (Exp.)	Condensation (Model)
12 cmH$_2$O	0 W	55°C	$T_\infty = 14.4$°C $RH_\infty = 70.3\%$	Yes / After 8cm (Lump 2)	Yes / Starts from Lump 1
			$T_\infty = 21.9$°C $RH_\infty = 64.0\%$	Yes / After 28cm (Lump 5)	Yes / Starts from lump 19
			$T_\infty = 33.1$°C $RH_\infty = 23.6\%$	No	No

5.3.1.5.4 Condensation vs. tube heating

Table 5.5 shows the condensation under CPAP pressure setting of 12cmH$_2$O, humidifier heating element setting of 55°C and normal room temperature. It is shown that when tube heating power increases, the condensation decreases.

Table 5.5 Comparison of condensation between experimental results and model outputs vs. tube heating under CPAP pressure setting at 12cmH2O, heating element setting at 55°C and normal room temperature

Pressure Setting	Ambient Conditions	Heating Element Setting	Tube Heating	Condensation (Exp.)	Condensation (Model)
12 cmH$_2$O	$T_\infty = 21.9°C$ $RH_\infty = 64.0\%$	55°C	0 W	Yes	Yes
				Starts from Lump 5	Starts from Lump 19
			15 W	No	No
			30 W	No	No

From the experimental observation and model outputs, the higher humidifier heating element temperature setting generates more condensation. On the other hand, higher CPAP pressure setting, ambient temperature and tube heating decrease the condensation.

Overall, the condensation in HADT is determined by its wall temperature and the airflow humidity. The influences by factors are listed below:

Table 5.6 Factors influencing HADT condensation

Factor	Trends	condensation
Ambient temperature	Increase	Less
ambient humidity	Increase	More
CPAP pressure setting	Increase	Less
Humidifier heating	Increase	More
Tube heating	Increase	Less

Generally the model slightly under-predicts condensation in the HADT. This may be because:

1. There is a small in-room air movement which is not included in the model. The in-room air movement can increase thermal convection on the outer surface of the HADT thus decreases HADT wall temperature and increases condensation.
2. The model also generally gives a slightly lower evaporation rate which will also reduce the condensation in the HADT.

3. The corrugated grooves on the HADT inner surface may create partly-dead space (eddies). Such dead space reduces heat exchange between the internal airflow and the HADT wall and makes this part of the wall has a lower temperature (Figure 5.32). This may be the reason why sometimes condensation can only be seen in the grooves (Figure 5.33).
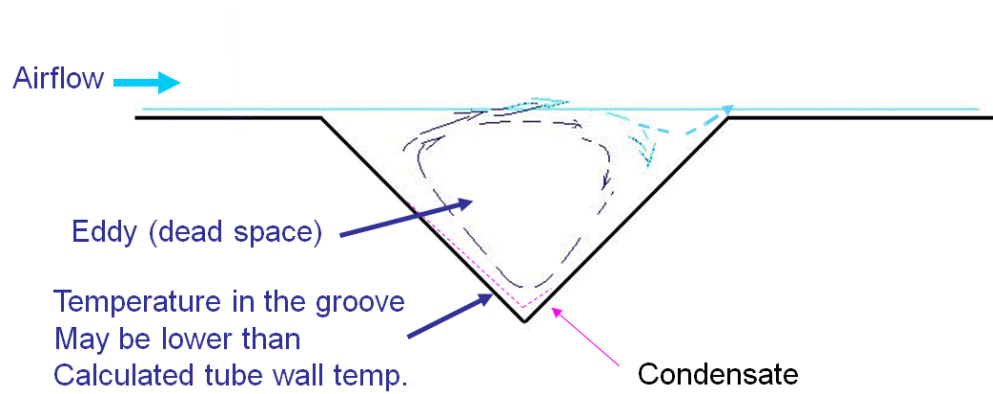
Figure 5.32 Temperature in grooves of the corrugated HADT may be lower
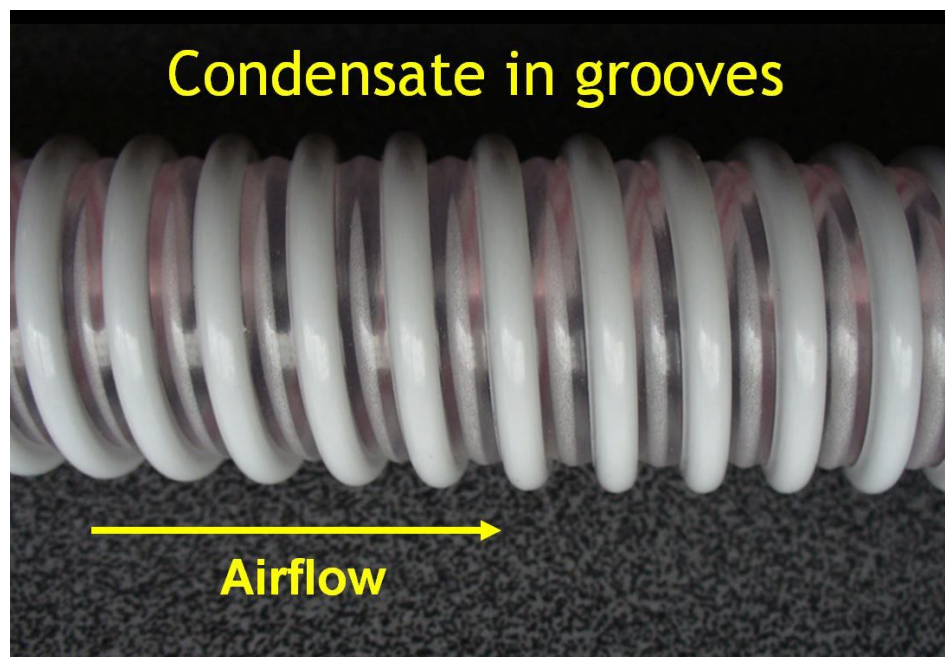
Figure 5.33 Condensate in grooves

On the other hand, it was observed in experiments that condensation started from lump 2 or lump 3 at several settings but the model predicts condensation starting from lump 1. This may be because the CPAP case was warm and a certain quantity of heat might conduct to the HADT. Since the model simplifies that there is no axial heat conduction

along the HADT wall and in the airflow, the actual temperature at the HADT inlet connecting to the CPAP case can be warmer than that the model calculated.

For steady state flow, the model also provides a condensation prediction by comparing the HADT lump wall temperature and the dew point of the airflow. Condensation occurs when HADT lump wall temperature is lower than the dew point. The dew point prediction is slightly closer to the experiment results than the condensation/evaporation calculation. This may be due to calculation errors such as in dew point regression.

The objective is to compare condensation between steady flow and breath-added fluctuating flows. When the ambient conditions and settings are the same, the under-prediction of condensation applies to both the steady flow and fluctuating flows. For this reason, the under-prediction may not have effect on the comparison.

Overall the model predicts the thermal performance very well except a slightly lower HADT condensation rate.

5.3.2 Thermal dynamic model under patient breath added fluctuating flow

For this project, the thermodynamic experiments should be able to get comparisons in evaporation rate and HADT condensation between steady state flow, normal breathing and deep breathing with reverse flow. Also due to instrument availability, the validations have not been fully conducted. The setups for future validation are shown in Appendix XXI. The already conducted experiments are described and compared with the model outputs below.

5.3.2.1 Validation of evaporation rate comparison between steady state and breath-added flows
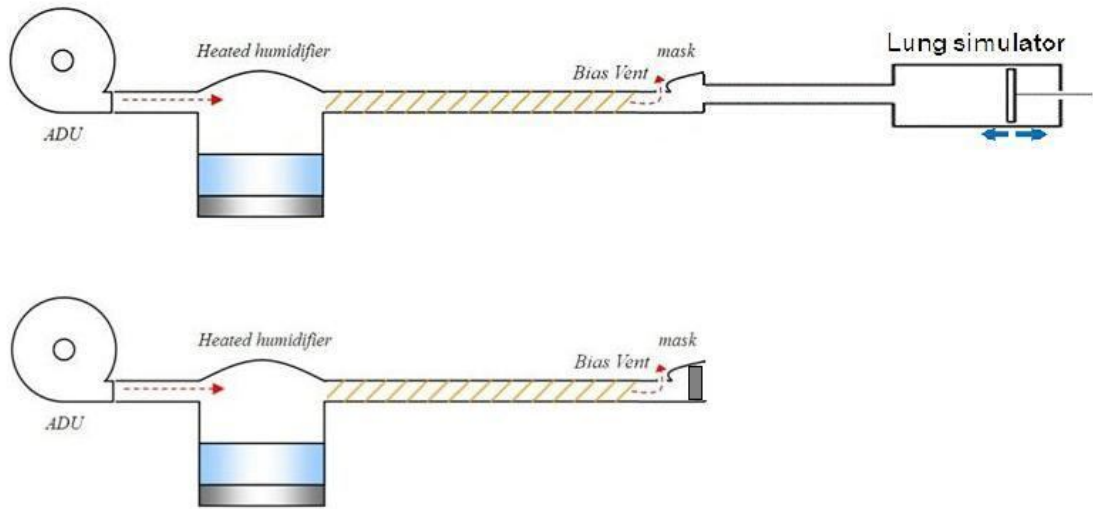
Figure 5.34 Experimental setup for evaporation rate comparison between steady flow and breath-added situation

The setup for comparing evaporation rate is as in Figure 5.34. The comparison experiment needs two CPAPs placed under the same ambient condition and same settings. One CPAP is connected to a lung simulator and another has mask sealed and bias orifice connected so to test its steady state evaporation rate. Such comparison experiment has been conducted by Sun from Fisher and Paykel Healthcare Co. Ltd. [67]. He set the CPAPs pressure setting at 10 cmH_2O under normal room condition for 4 hours. The lung simulator provided 500 ml normal breath load. The average evaporation rate in the lung simulator connected CPAP chamber was 9.74 mg/s and in the bias orifice connected CPAP chamber, it was 9.43 mg/s. The breath-added CPAP had a 3% higher evaporation rate. The author attributed it to minor leaks in the lung simulator connected system and concluded that there was no significant difference in average evaporation between steady state and breath-added situations.

For checking the model, the ambient condition inputs are the same as that of the experiment and the heating element setting is adjusted at 57°C. The model output steady state evaporation rate as 9.41 mg/s and the average of the dynamic fluctuating evaporation rate is 9.36 mg/s. The model gives 0.5% less evaporation rate for the breath-added situation. This matches well with Sun's experiment and supports his explanation.

143

5.3.2.2   Validation of HADT condensation comparison between steady state and breath-added situation

As for the experimental validation of the HADT condensation, a test with human deep breathing induced reverse flow was conducted. The conditions were as follow: The ambient temperature was 21.4°C and relative humidity was 55%, CPAP pressure setting was 4cmH2O and HADT tube heating was 5W. When the flow was steady there was no condensation in the HADT. When the deep breathing was added, condensation was seen in the last 30 cm of the HADT (Figure 5.35).
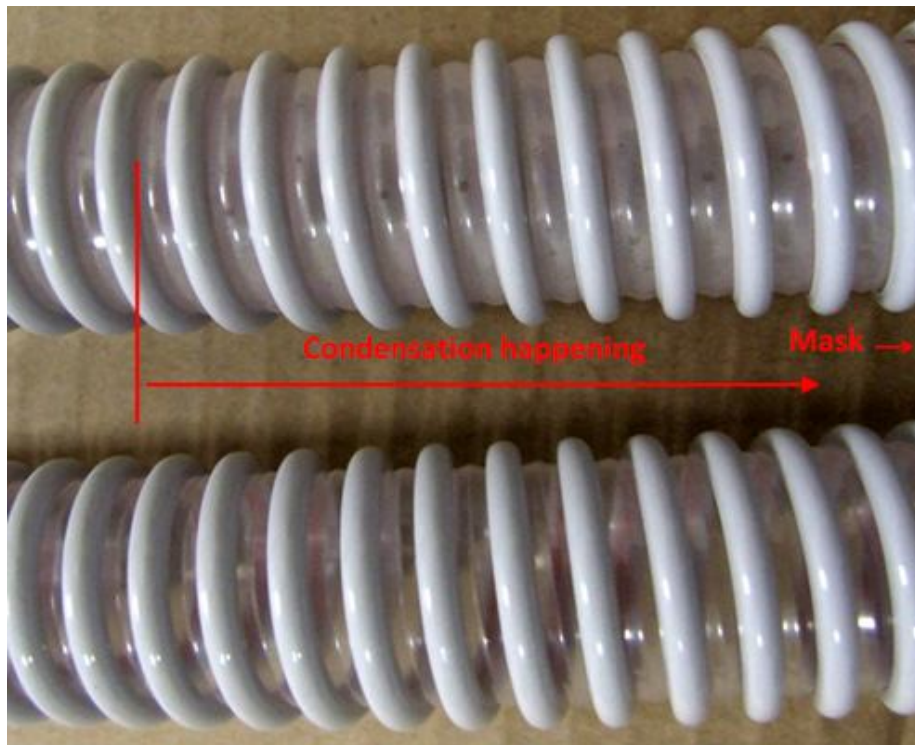
Figure 5.35 Comparison of in-HADT condensation between steady state and breath-added situation

As mentioned before, the model under-predicts HADT condensation. For comparing the observed experimental results with the model outputs, the model is given the same conditions as of the experiment except the tube heating is given as zero.

Under steady state, the model output condensation/evaporation rate at lump 30 is 1.72×10^{-3} mg/s which is considered as just no condensation. When deep breathing is added, the condensation/evaporation rates at lump 27 to lump 30 become negative. This means the model gives condensation in the last 23 cm of the HADT.

144

The experiment observation showed that deep breathing generated condensation in the near-mask section of the HADT when there was no condensation under steady flow. The model also predicted so. Thus the conclusion for the model dynamic validation can be drawn as: despite the under-prediction of condensation, the model can compare the results well between steady flow and breath-added situation.

Chapter 6 Discussion and Conclusions

6.1 Introduction

The outputs from the models validated in chapter 5 are discussed in this chapter. The discussion is focused on the conditions where reverse flow occurs and the consequent influence on exhaled air re-inhalation, condensation and humidity level in inhaled air. For better understanding of the situation, the related phenomena such as fluctuation amplitude, influences from ambient conditions and mask capacity are also discussed. The discussion is separated into two sections namely, fluid dynamics and thermodynamics. For simplification, the models do not include the influence of pressure setting on breath load. All models use a normal breath load with a 6 seconds breath cycle [37].

6.2 Fluid dynamics

Reverse flow and re-inhalation of exhaled air are discussed in this section.

6.2.1 Reverse flow

Three factors are considered in this section, the breath load, pressure setting and mask capacity.

6.2.1.1 Breath load and pressure setting

In general, under normal breathing, there is no reverse flow. However, when the breath load is increased by 1.5, 2 and 2.5 times of normal breathing under different CPAP pressure settings, the reverse flow outputs from the model are shown in Figure 6.1. It is indicated that there is almost no reverse flow at 1.5 times normal breathing. Reverse flow is cut off at 8 cmH$_2$O and 13 cmH$_2$O for 2 and 2.5 times respectively. Overall, when breathe load increases, reverse flow increases and when the pressure setting increases, the reverse flow drops.
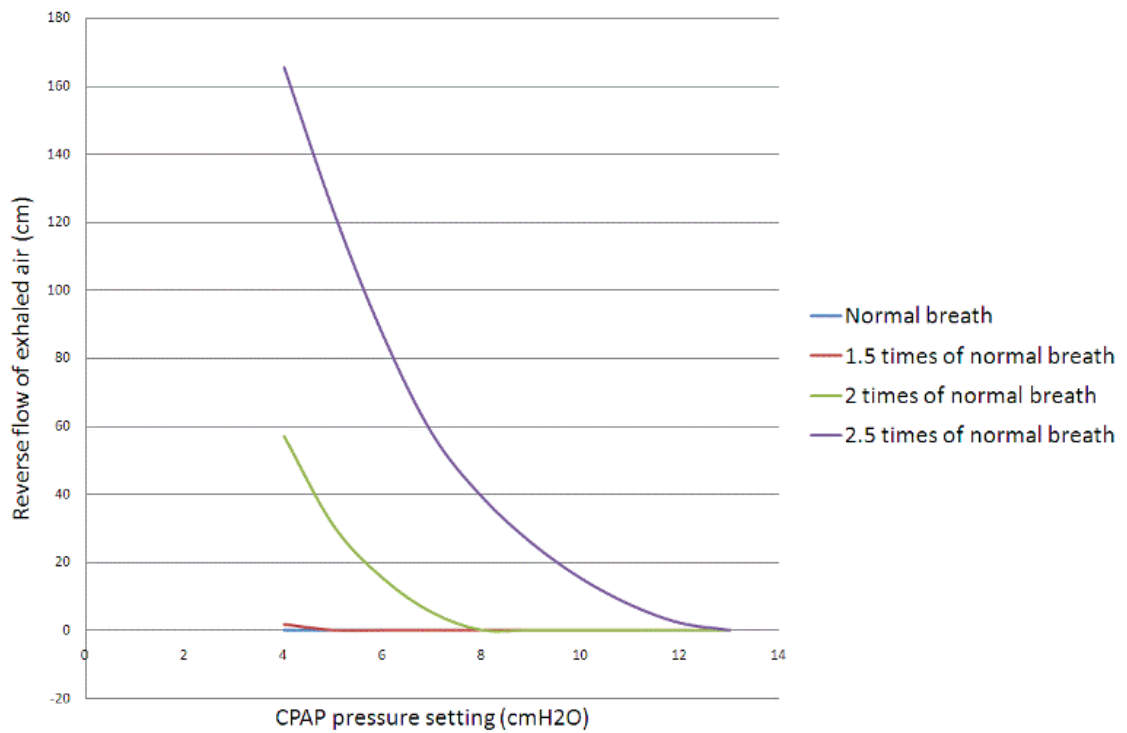
Figure 6.1 Reverse flow under different combinations of breath load and CPAP pressure setting

6.2.1.2   Mask capacity vs. reverse flow

The mask capacity in the model is adjustable. However, the model output shows that the distance of reverse flow is the same when mask capacity changes. This is because of the assumption of air incompressibility which means the distance of reverse flow is not influenced by the mask capacity.

6.2.2   Exhaled air re-inhalation

In this section, the breath load, pressure setting, the resulted reverse flow and mask capacity are discussed with respect to their influences on the exhaled air re-breathing.

6.2.2.1   Exhaled air re-inhalation vs. breath load and pressure setting

The percentage of exhaled air in inhalation vs. combination of breath load and pressure settings using the nasal mask is shown in Figure 6.2.
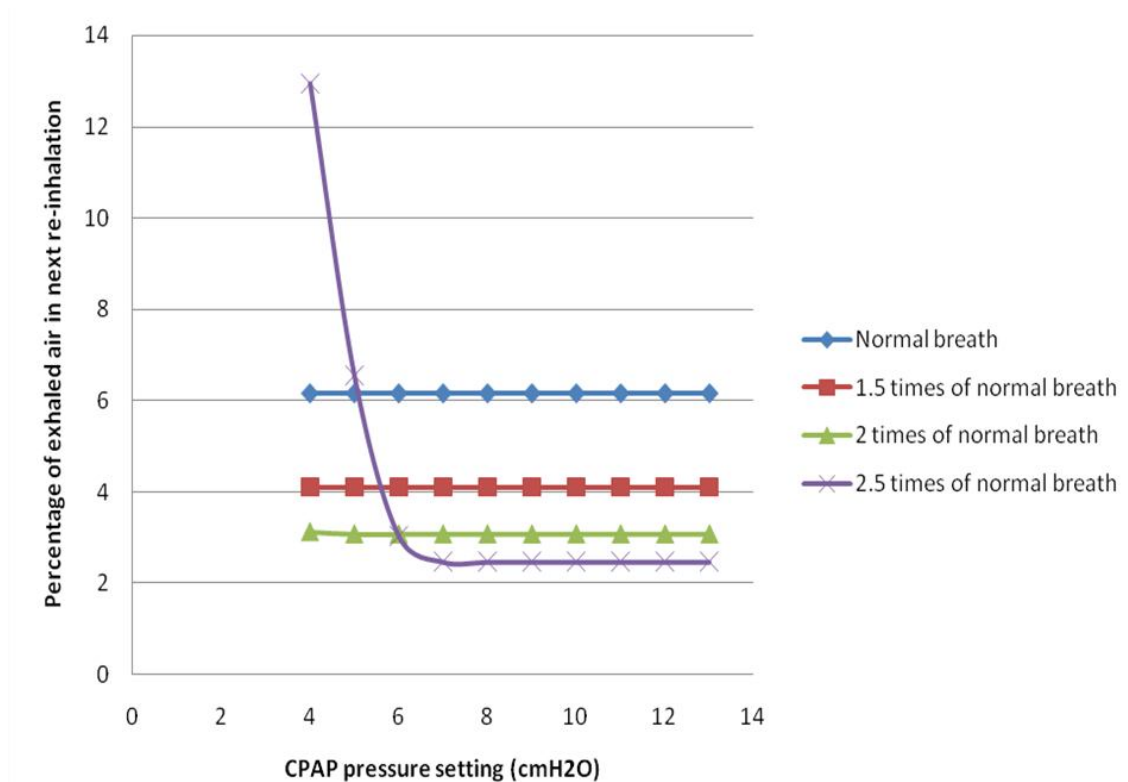
Figure 6.2 Percentage of exhaled air in inhalation under different combinations of breath load and CPAP pressure setting when using nasal mask

Comparing Figure 6.2 with Figure 6.1, indicates that reverse flow does not definitely increase exhaled air re-inhalation. When the breath load is 2 times normal breathing, reverse flow can occur until pressure setting of 7 cmH$_2$O however re-inhalation only increases slightly when the pressure setting is at the lowest 4 cmH$_2$O. When the breath load is 2.5 times normal breathing, reverse flow can occur when pressure is as high as 12 cmH$_2$O but the re-inhalation increase vanishes when pressure setting is above 6 cmH$_2$O. This is attributed to the fact that at the end of exhalation, the exhaling flow rate tapers to be smaller than the bias vent flow rate, and the air from CPAP resumes moving toward the mask before the inhalation phase starts. Since inhalation has not started yet, the airflow can only flow out from the bias vent holes. If the exhaled air in the HADT has already completely expelled before the patient starts the next inhalation, the airflow entering the mask will be fully fresh. However if the reverse flow is too far back into the HADT when the breath load is large and the pressure setting is low, a certain amount of the in-HADT exhaled air can re-enter the mask and adds to the re-inhalation.

The percentage of exhaled air in the next inhalation drops along with the increase of breath load. This is because the exhaled air in the mask is a fixed amount which is more diluted in a larger breath load.

It can also be seen in Figure 6.2 that when pressure setting is at 4 cmH$_2$O and the breath load is 2.5 times normal breathing which is 2023 ml for one inhalation, the exhaled air remaining in the mask consists of 2.07% of the next inhalation. When exhaled air from reverse flow is added in, it becomes 12.54% of the total volume of an inhalation. However, since the breath load rarely reaches 2000 ml [68], the reverse flow's influence on exhaled air re-inhalation is negligible.

6.2.2.2   Mask capacity vs. exhaled air inhalation

When there is no exhaled air added-in from reverse flow, the re-inhaled air is only that remaining in the mask. In this case the percentage of exhaled air in the next inhalation is proportional to mask capacity (Table 6.1).

Table 6.1 Ratio of percentage of exhaled air in inhalation between full-face mask and nasal mask

Breath load (times of normal breathing)	Exhaled air re-breath (% in inhalation)		Ratio of Full-face/Nasal Masks
	Nasal	Full-face	
normal	5.17	17.44	
1.5	3.45	11.63	3.375
2	2.58	8.72	
2.5	2.07	6.98	

From this table, if the mask capacity is that of the full-face mask FlexiFit$^{\text{TM}}$432 (236 ml) and breath load is normal, the percentage of exhaled air in inhalation can reach above 17% and the volumetric percentage of CO_2 can reach about 0.87% which is higher than the eight-hour-time limit but lower than the 15-minute average limit [26]. When reverse flow adds exhaled air to the inhalation, the full-face mask also gives a higher percentage of exhaled air to the inhalation (Figure 6.3). This means that the mask capacity is a significant factor influencing exhaled air re-breathing.
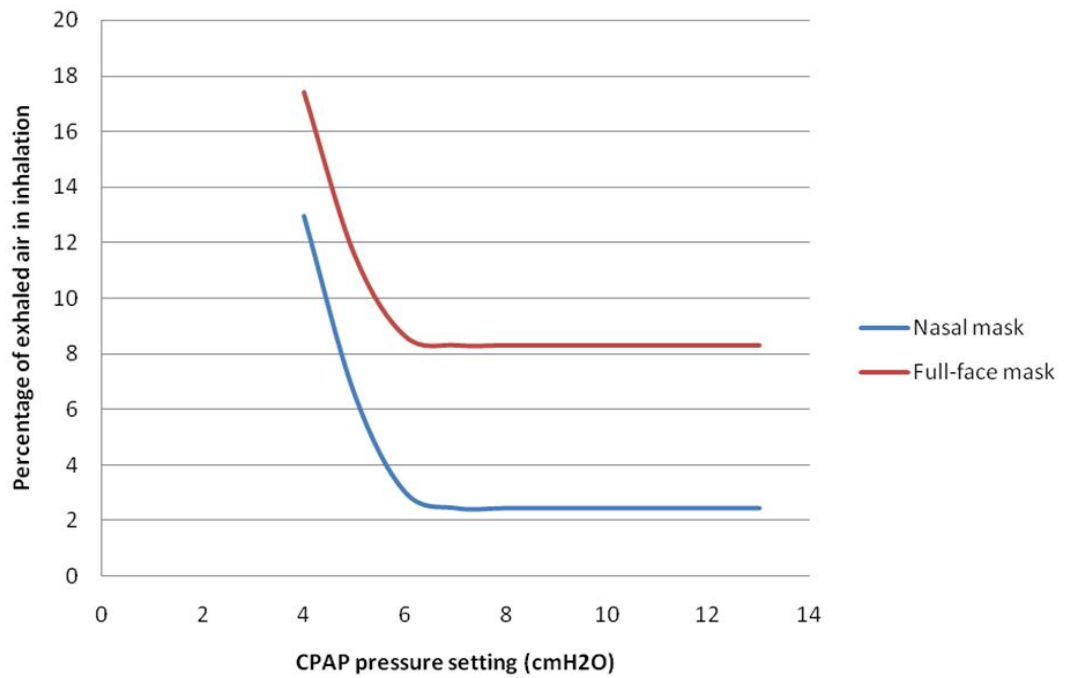
Figure 6.3 Comparison of exhaled air re-inhalation between nasal mask and full-face mask when there is reverse flow influence

6.3 Thermodynamics

Several terms need to be defined before the discussion. The average specific humidity, evaporation rate and condensation rate are all considered as the average value over a breath cycle's period. In the thermodynamic discussion, the comparison is limited only between normal breathing and 2 times normal breathing. The term deep breathing will be used to stand for the 2 times normal breathing.

As shown and validated in chapter 5, when airflow is steady, the evaporation is mainly influenced by the heating element temperature setting and CPAP pressure setting. The factors influencing the condensation in HADT are listed in Table 5.6. Beside these, when breathing is added in, the fluctuation introduces several other factors influencing the evaporation and condensation which are explained and defined below.

1. When the pressure drop along a conduit fluctuates, the average of the fluctuating flow velocity is smaller than the steady state flow velocity. This is because the flow velocity is proportional to the square root of the pressure drop which makes the pressure-velocity curve concave. This makes the total amount of the fluctuating flow within a breath cycle also smaller than that of the steady flow

150

within the same period. However, when reverse flow occurs, the total amount of flow, including the positive flow and the absolute value of the reverse flow, is greater than that of the steady state. This varying total amount of flow in a breath cycle certainly influences the convections in this period. This is defined as the absolute flow amount factor: the convections are influenced by the total absolute amount of flow within a breath cycle which varies due to fluctuation and reverse flow.

2. For the heat and mass convections in the chamber and the HADT, the Nusselt number and mass convection coefficient are proportional to Reynolds number to a power less than 1. When there is a fluctuation, the average convection rate is smaller than that of a steady flow at the medium velocity. The larger the fluctuation amplitude, the more significant is the difference. This is defined as the convection concavity factor which is depicted in Figure 6.4 below.
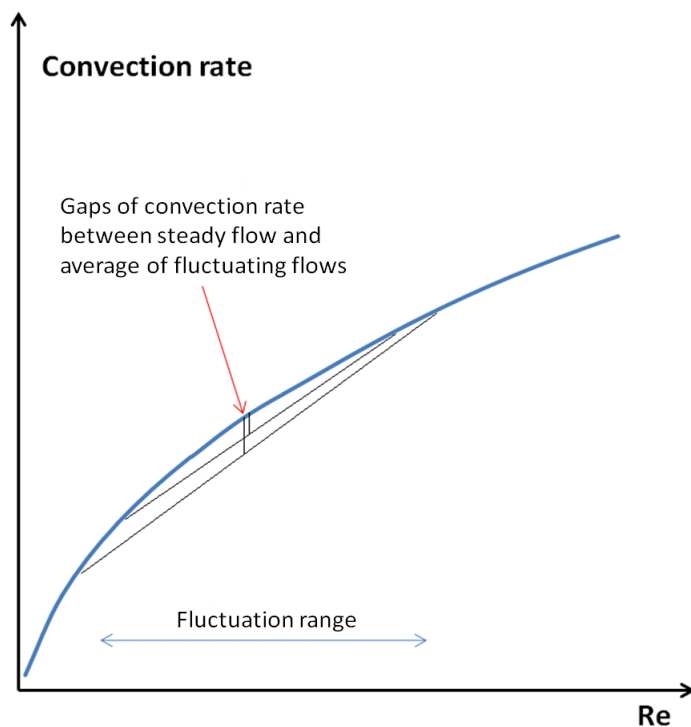
Figure 6.4 Explanation of comparison between steady flow convection rate and average convection rate of fluctuating flow (not to scale)

3. When the flow velocity is high, the mass and heat convections are also high. Therefore, in an HADT lump, when the airflow dew point is higher than the HADT wall inner surface temperature and coincides with a higher velocity, the condensation rate is also higher. On the other hand, when the dew point is lower than the inner surface temperature and coincides with a higher velocity, the

151

airflow will have a higher potentiality to vaporize water on the surface. This is defined as the velocity coincidence factor.

4. Since the specific humidity of airflow from the humidifier chamber is fluctuating, the dew point of the airflow can sometimes be higher than the inner surface temperature and sometimes lower. In this case the net condensation can be heavier than that of the steady flow even when the average humidity of the fluctuating flow is the same as that of the steady flow. This is attributed to the fact that the condensation rate is 1.2 times the evaporation rate (see Section 3.6). This can be defined as the condensation-to-evaporation coefficient factor.

These factors will be elaborated on below.

6.3.1 Influence of breathing induced flow rate fluctuation on the chamber evaporation
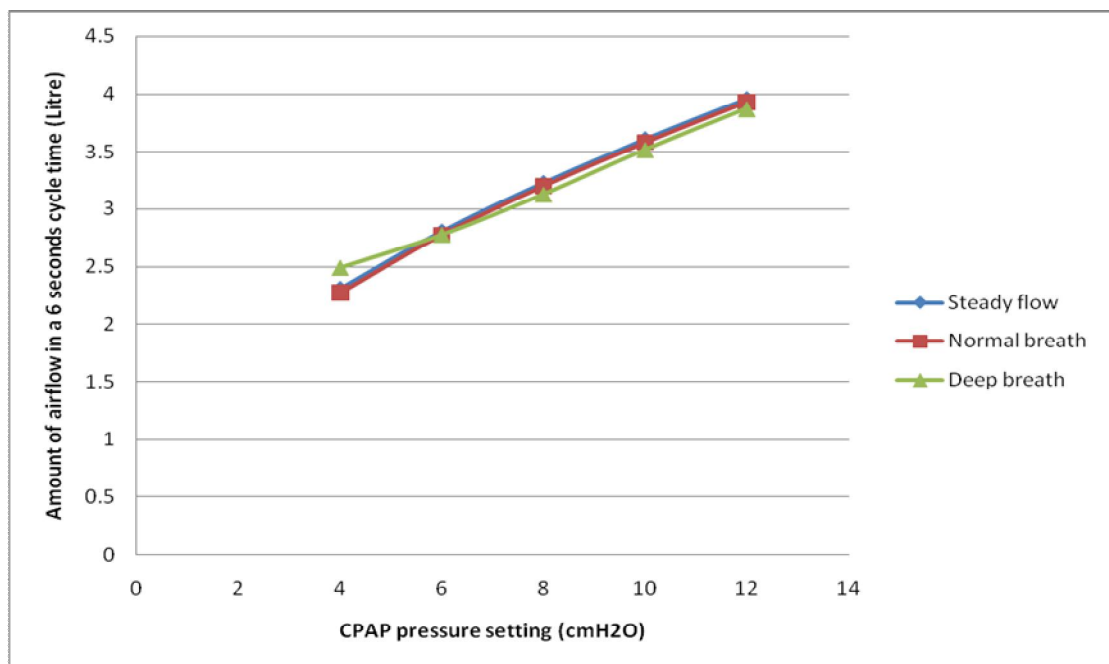
Figure 6.5 Comparison of total amount of air flowing through the system in a 6 seconds breathe cycle time between steady flow, normal and deep breathing added situations

Figure 6.5 shows the total amount of airflow in 6 seconds under steady flow, normal breathing and deep breathing added flows. It can be seen that the normal breathing flow amount is slightly smaller than steady flow. The amount is greater for deep breathing with reverse flow but even smaller when there is no reverse flow. This is because of the absolute flow amount factor.
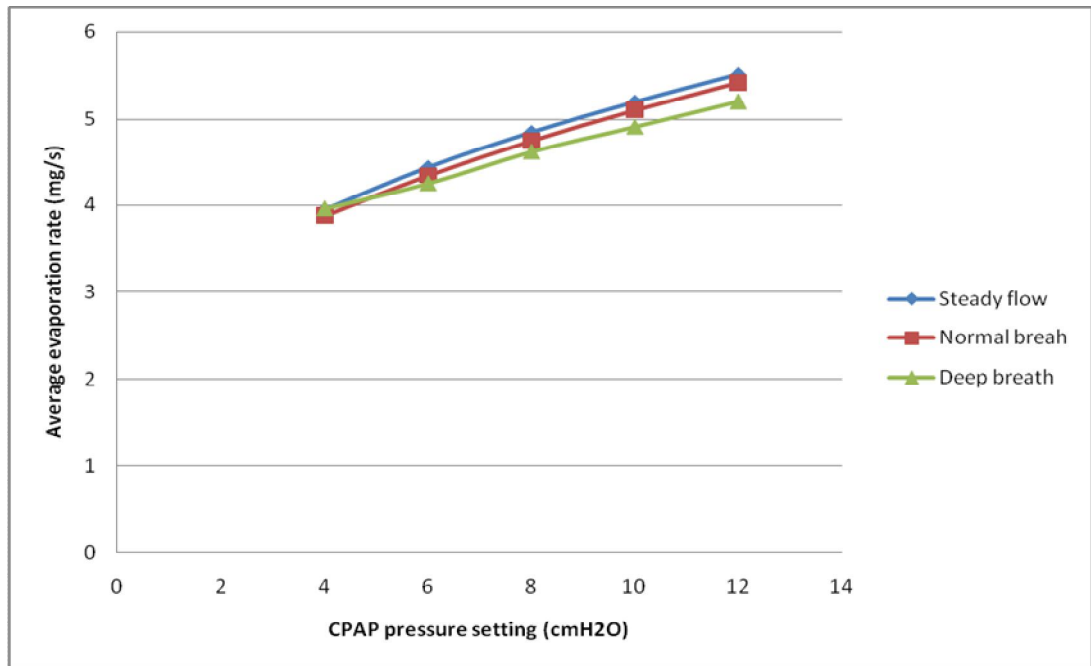
Figure 6.6 Comparison of evaporation rate averaged in a 6 seconds breathe cycle time between steady flow, normal and deep breathing added situations

Figure 6.6 shows the average evaporation rate comparison between steady state flow and breathing added fluctuating flows. Without reverse flow, the evaporation rate drops when breath load increases due to both the flow amount factor and the concavity factor. When the pressure setting is 4cmH$_2$O and breathing is deep, reverse flow occurs, and the average evaporation rate is almost the same as that of the steady flow. This is because the larger absolute amount of airflow offsets the concavity factor. Overall, deep breathing plus reverse flow do not significantly increase the average evaporation rate while deep breathing without reverse flow reduces the average evaporation rate.

6.3.2 Influence of breathing induced flow rate fluctuation on airflow temperature in HADT vs. different tube heating

Figure 6.7 shows the airflow average temperature along the HADT between the reverse flow and non-reverse-flow situations with different tube heating. When there is no tube heating, the temperature of the airflow from the chamber is, in most cases, lower than that of the reverse flow from the mask. Therefore, when there is reverse flow, the average air temperatures in the last few lumps are higher than when there is no reverse flow. However, when the HADT is heated and if the air from the humidifier chamber has a temperature similar to the exhaled air when reaching the last few lumps, the difference is of significance. The HADT wall temperature difference in these lumps is

153

even less significant. This means that the wall temperature is not significantly influenced by reverse flow.
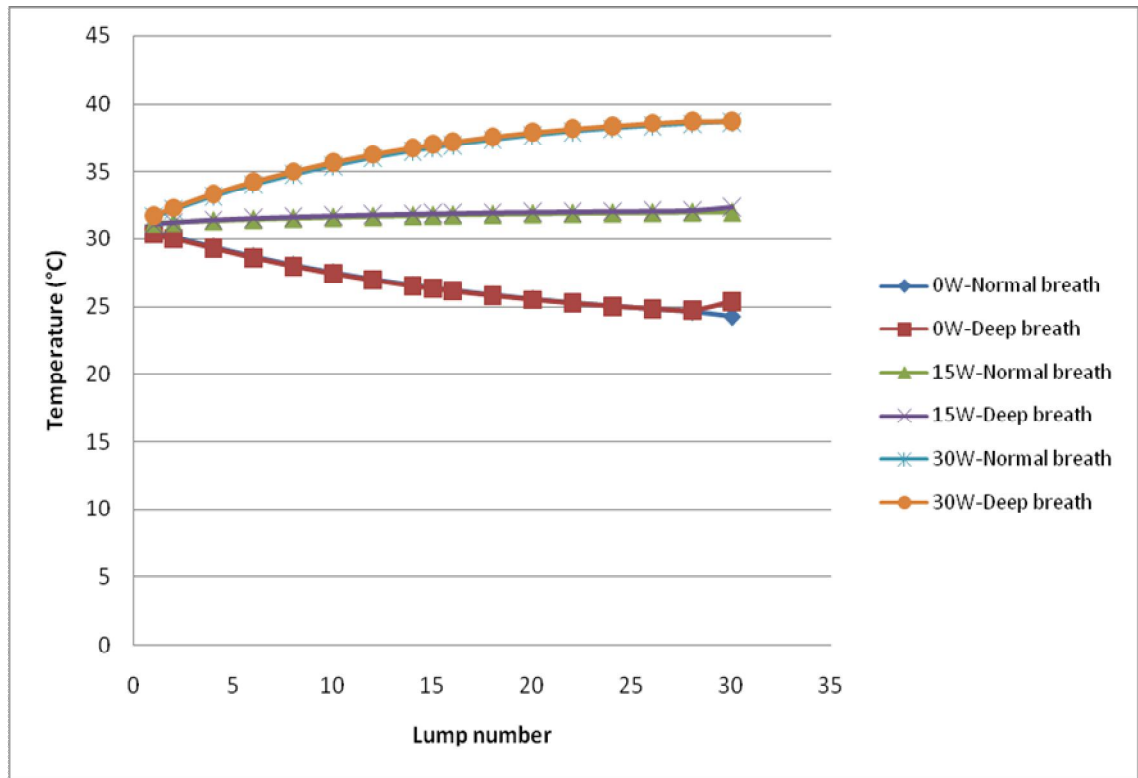
Figure 6.7 Comparison of average airflow temperature in HADT between normal breathing and deep breathing under different tube heating when pressure setting is 4cmH₂O, heating element is at 55°C, ambient temperature and relative humidity at 22°C and 50%

6.3.3   Influence of breathing induced flow fluctuation on condensation in HADT

When normal breathing is introduced, the velocity fluctuation causes the airflow humidity, temperature and Reynolds number to fluctuate as shown in Figure 6.8, Figure 6.9 and Figure 6.10 respectively. It can be seen that the transport of the fluctuating humidity is at a varying velocity.
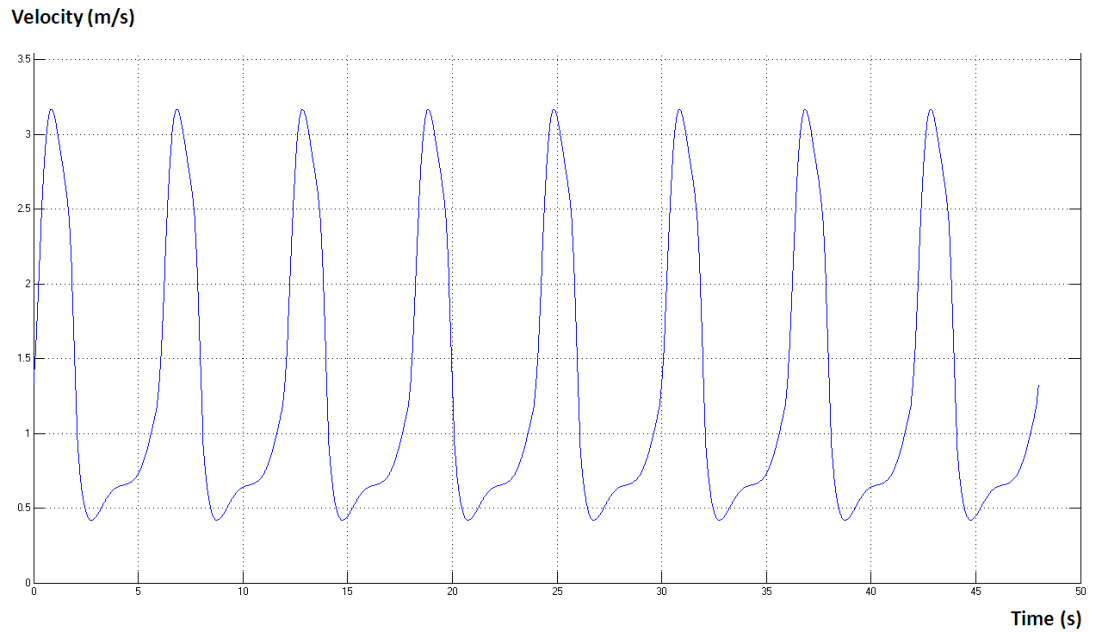
Figure 6.8 Airflow velocity in HADT under CPAP pressure setting at 4cmH₂O with normal breathing
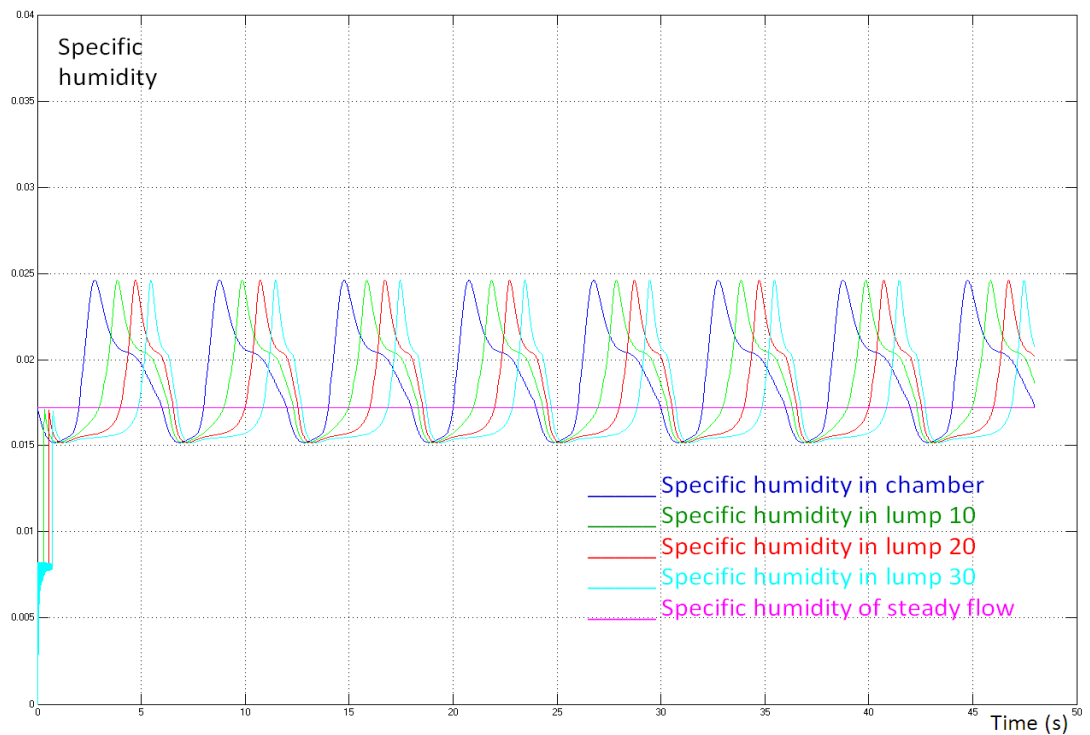
Figure 6.9 Fluctuation of airflow specific humidity in the chamber and at different locations in HADT under CPAP pressure setting at 4cmH₂O, Heating element 45°C with normal breathing without tube heating when ambient temperature is 22°C and relative humidity is 50% (the pink horizontal line is the specific humidity of steady flow for reference)

155
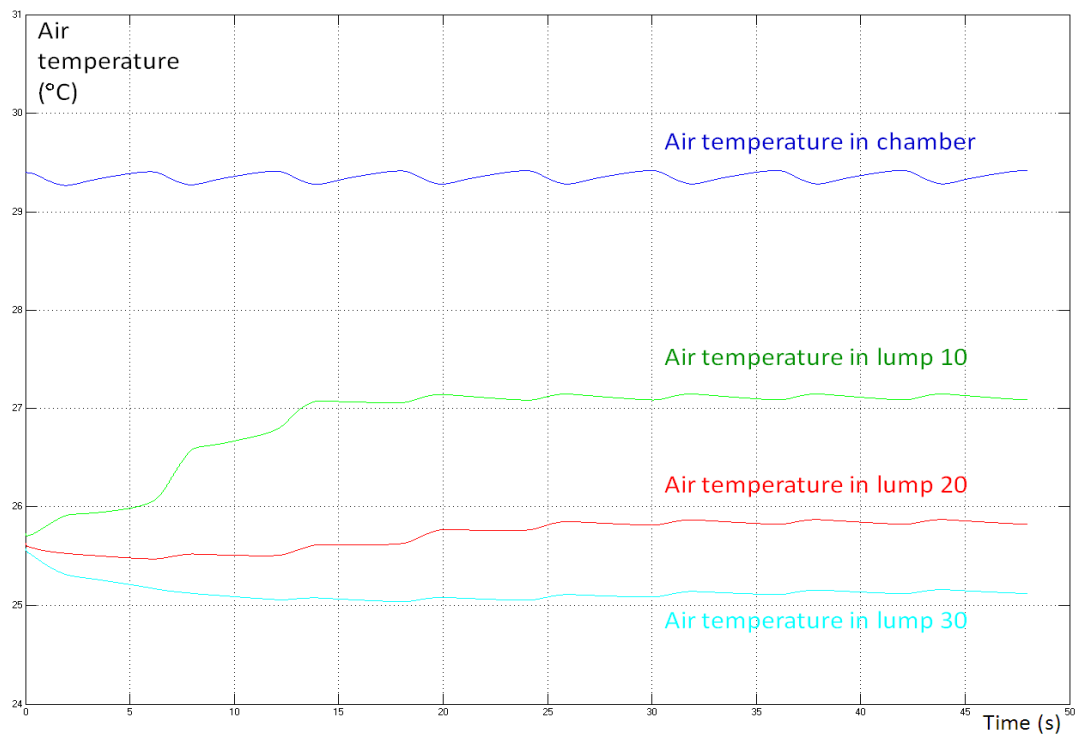
Figure 6.10 Fluctuation of airflow temperature in chamber and at different locations in HADT under CPAP pressure setting at 4cmH$_2$O, Heating element 45°C with normal breathing without tube heating when ambient temperature is 22°C and relative humidity is 50%

When breathing is deep the velocity of airflow in the HADT is sometimes negative which means reverse flow is occurring. The dynamic fluctuating velocity, humidity and temperature graphs are shown below (from Figure 6.11 to Figure 6.14).

156
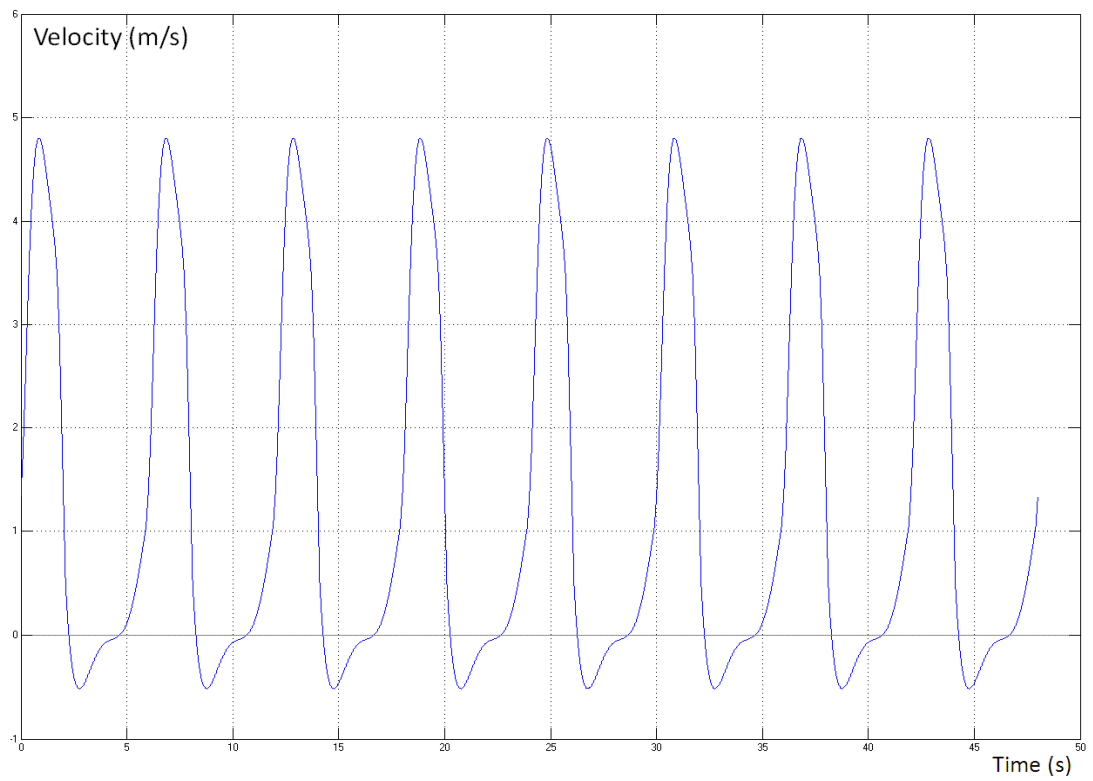
Figure 6.11 Airflow velocity in HADT under CPAP pressure setting at 4cmH₂O with deep breathing
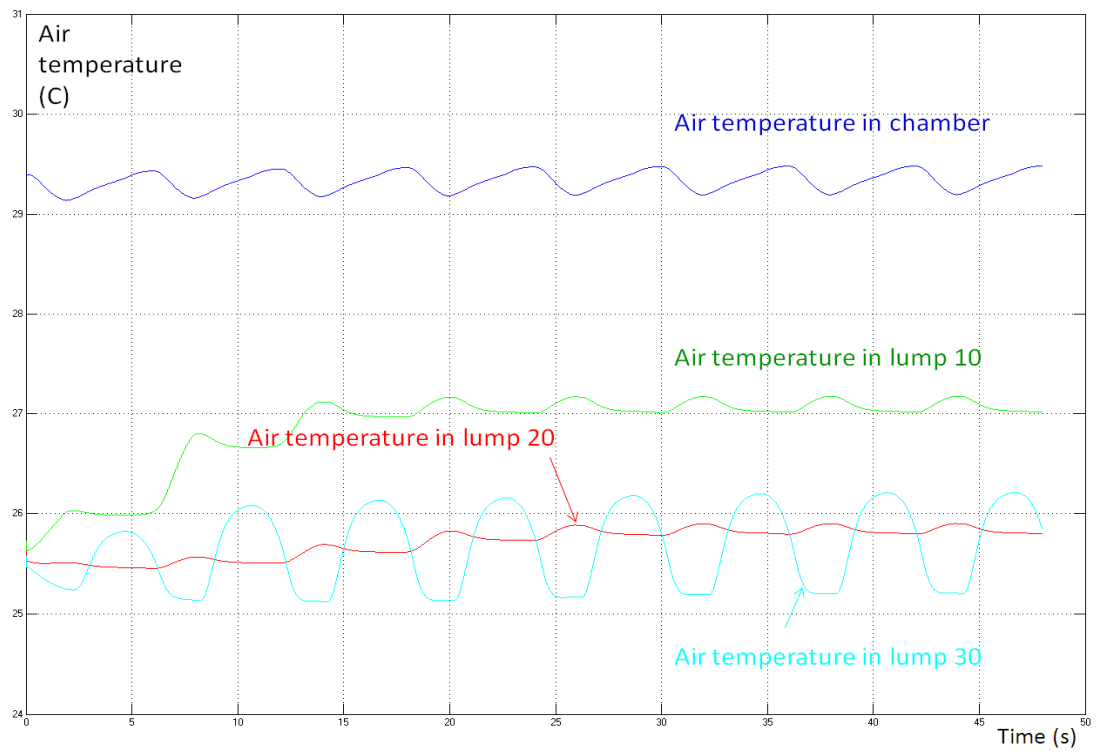
Figure 6.12 Fluctuation of airflow temperature in the chamber and at different locations in HADT under CPAP pressure setting at 4cmH₂O, Heating element 45°C with deep breathing without tube heating when ambient temperature is 22°C and relative humidity is 50%
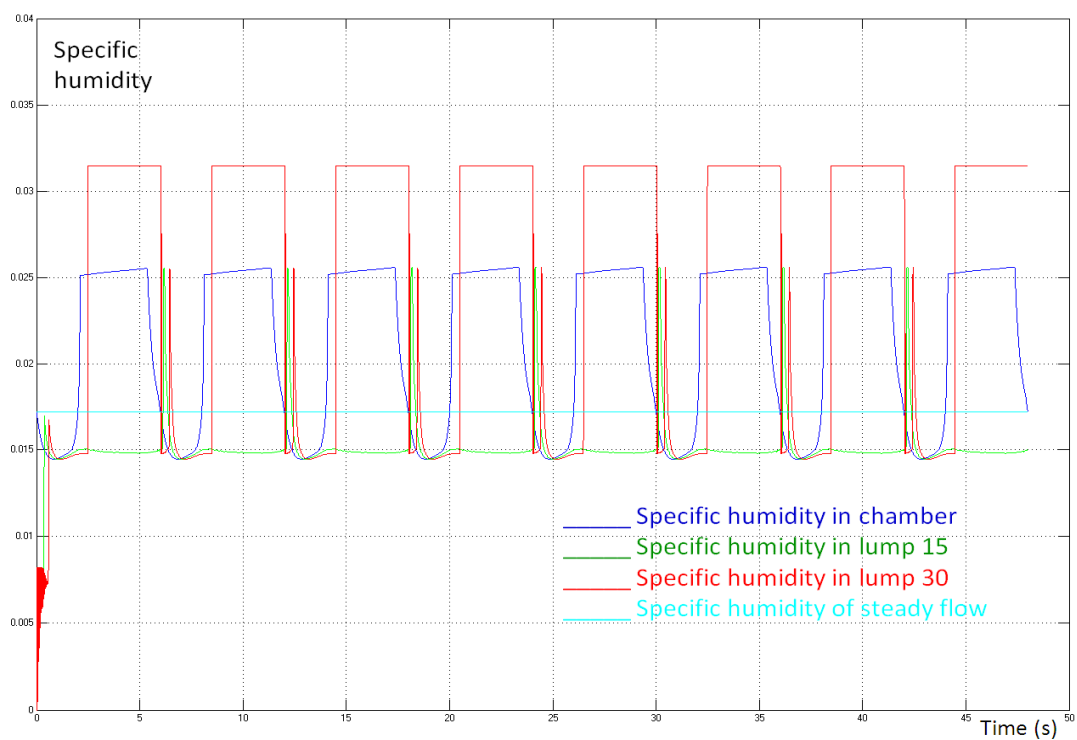
Figure 6.13 Fluctuation of airflow specific humidity in chamber and at different locations in HADT under CPAP pressure setting at 4cmH₂O, Heating element 45°C with deep breathing without tube heating when ambient temperature is 22°C and relative humidity is 50% (the light blue horizontal line is the specific humidity of steady flow for reference)
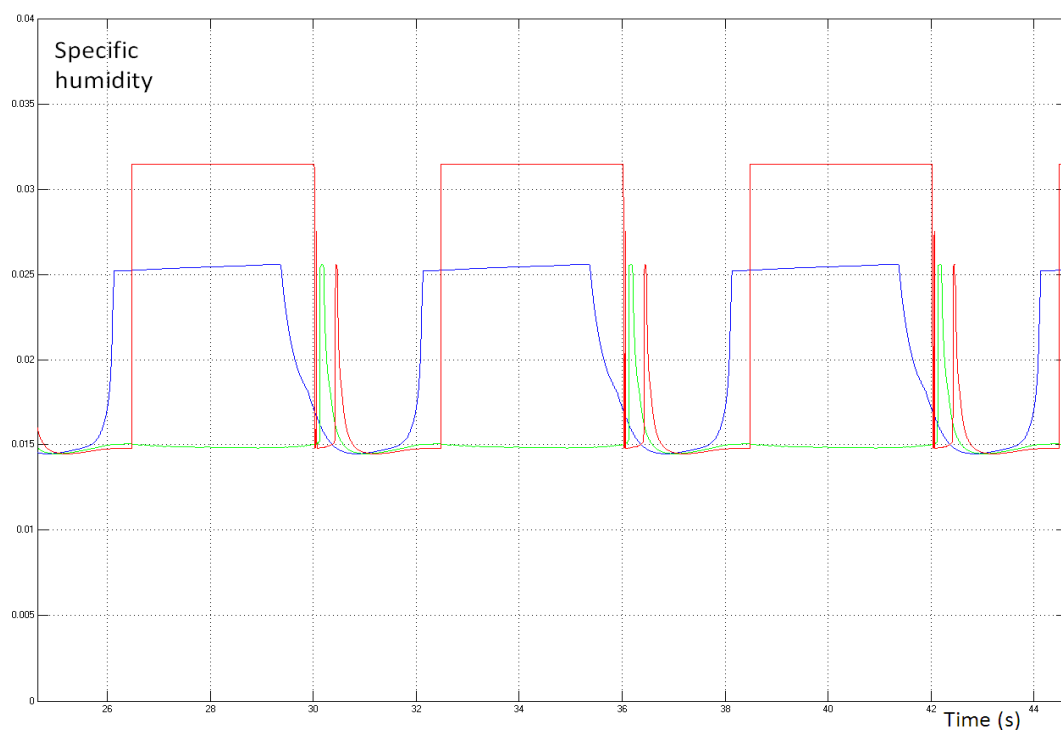
Figure 6.14 Enlarged from Figure 6.13 without specific humidity of steady flow

158

In Figure 6.14 the blue curve represents the humidity fluctuation in the chamber, the green curve in lump 15 and the red in lump 30. The plateau in the red curve is the specific humidity of exhaled air which is assumed saturated at 33°C. The plateau in the blue curve represents the specific humidity of the portion of air in the chamber when the air is saturated at the in-chamber air temperature. This saturation occurs about the reverse flow period when the air flows over the water surface three times. A high heating element temperature setting increases the chance of saturation. This plateau (the saturated portion) becomes very narrow peaks in the green curve (lump 15) and the red curve (lump 30) which means the plateau flows through these lumps at a much higher velocity.

For the condensation/evaporation graphs shown below, the values of condensation/evaporation rate are of net condensation/evaporation rate in a breath cycle for fluctuating flows and averaged to mg per second. When the curve is above 0, it means there is no condensate remaining over a breath cycle. This may mean that there is no condensation occurring at all. It may also be possible that there has been condensation occurring but the condensate can be taken away within a cycle's time by oncoming drier portion of the flow. When the curve is below 0, it means there is condensate remaining and building up.

6.3.3.1 Effect of airflow fluctuation amplitude on in-tube condensation

To analyse the influence of amplitude on condensation, the model is given the conditions as listed below. A comparison between normal and deep breathing is conducted under these conditions.

Conditions	Pressure setting	Tube heating	Ambient temperature	Ambient relative humidity	Heating element setting
1	9 cmH$_2$O	0 W	20°C	50%	45°C
2					65°C

When the pressure setting is at 9 cmH2O, there is no reverse flow even if the breathing is deep. The condensation rate graphs and related analysis are shown below.

159

6.3.3.1.1 Comparison when heating element setting is 45°C
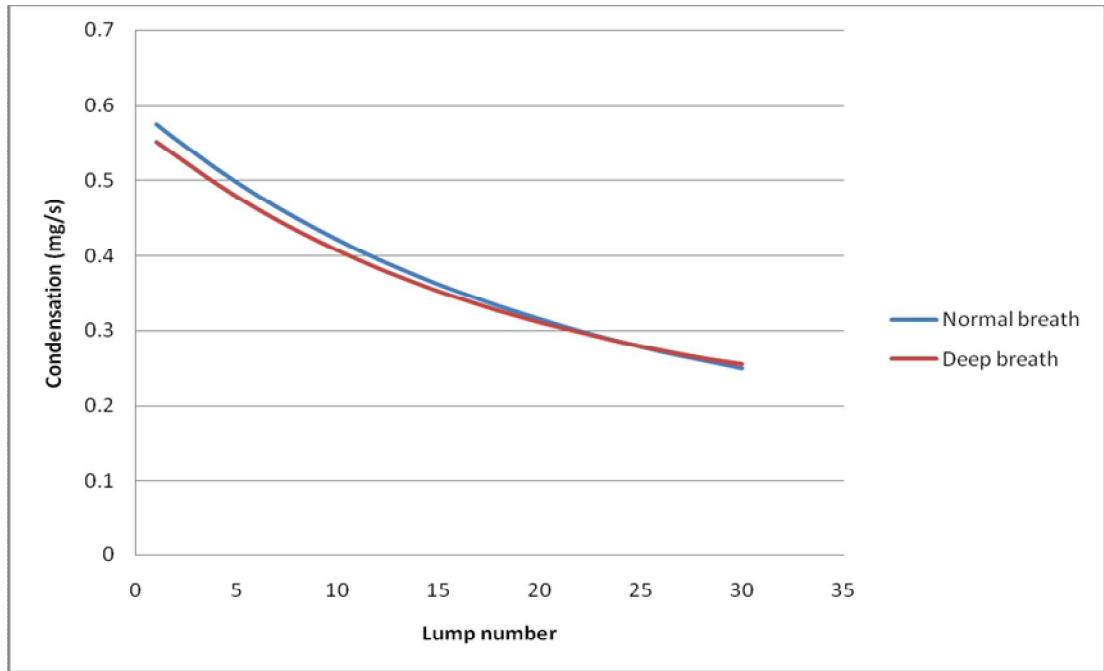
Figure 6.15 In-tube condensation with normal breathing and deep breathing added fluctuating flows under conditions of 9cmH₂O 45°C 0W 20°C&50%

It can be seen from Figure 6.15 that the deep breathing condensation rate curve stays close to the normal breath one. This maybe attributed to the following reasons:

1. When deep breathing makes the fluctuating amplitude larger, the average convection rate is even lower due to the concavity factor. This factor pulls the deep breathing curve towards the horizontal axis. Furthermore, when the breathing is deep, the velocity drops down to very low in the middle of exhalation phase which makes a certain portion of air have a much higher humidity than the average. This portion generates condensation when entering the HADT and the condensation-to-evaporation coefficient factor plays a role dragging the deep breathing curve downward further.

2. Drier air during inhalation phase coinciding with higher velocity creates a higher potentiality of vaporization which brings up the deep breathing curve.

A detailed explanation based on instantaneous condensation graphs is in Appendix XVII.

Figure 6.16 shows that when the humidifier chamber heating increases to 65°C, condensate builds up all over the HADT for both normal breathing and deep breathing. This time, the deep breathing curve stays all above the normal breathing curve. This is because the greater fluctuation pulls up the deep breathing curve towards the horizontal axis due to the concavity factor and the higher potentiality of vaporization (the coincidence factor) which also brings up the deep breathing curve.
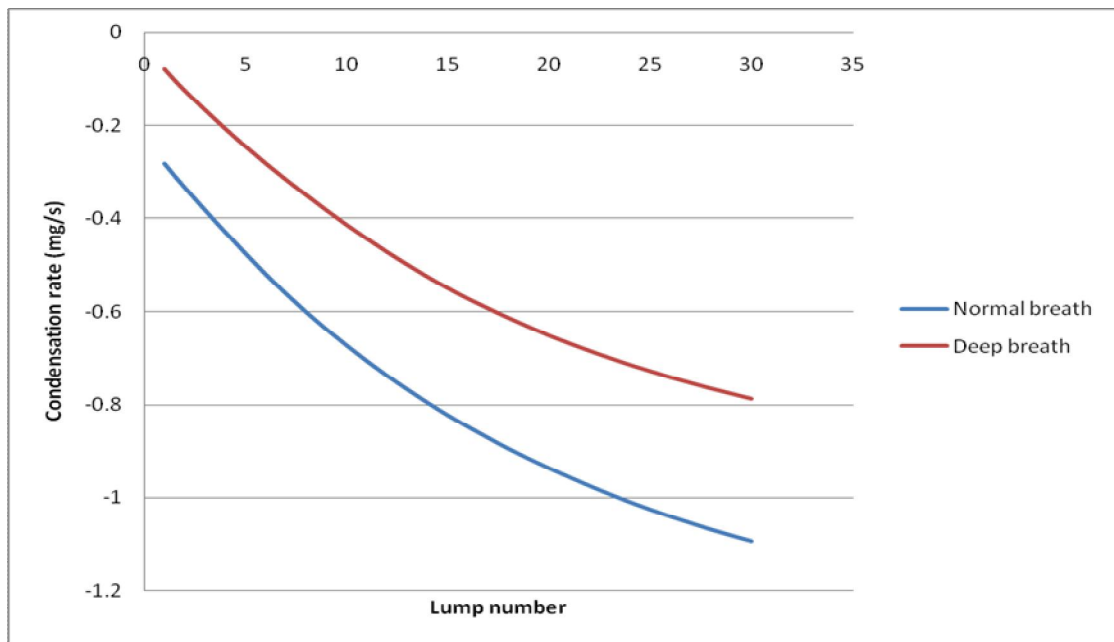
Figure 6.16 In-tube condensation of steady flow, breathing added fluctuating flows under conditions of 9cmH$_2$O 65°C 0W 20°C&50%

If condensation and evaporation occurs alternately, the condensation-to-evaporation coefficient factor plays a role and worsens the net condensation. The high velocity coincidence factor increases convections for both condensation and evaporation. The concavity factor reduces the average convection for both condensation and evaporation. The final result depends on their combined effect. Overall, without reverse flow, deep breathing at least does not worsen condensation.

6.3.3.2   Combined effect of fluctuation, reverse flow and humidity on the HADT
         condensation

To analyse the combined effect of fluctuation, reverse flow and airflow humidity on condensation, the model is set under conditions as listed below. The conditions are all

the same except the ambient relative humidity. This can almost keep all the other factors constant except the airflow humidity from the CPAP.

Conditions	Pressure setting	Tube heating	Ambient temperature	Ambient relative humidity	Heating element setting
1				20%	
2	4 cmH$_2$O	0 W	22°C	50%	55°C
3				80%	

6.3.3.2.1 Comparison when ambient relative humidity is 20%
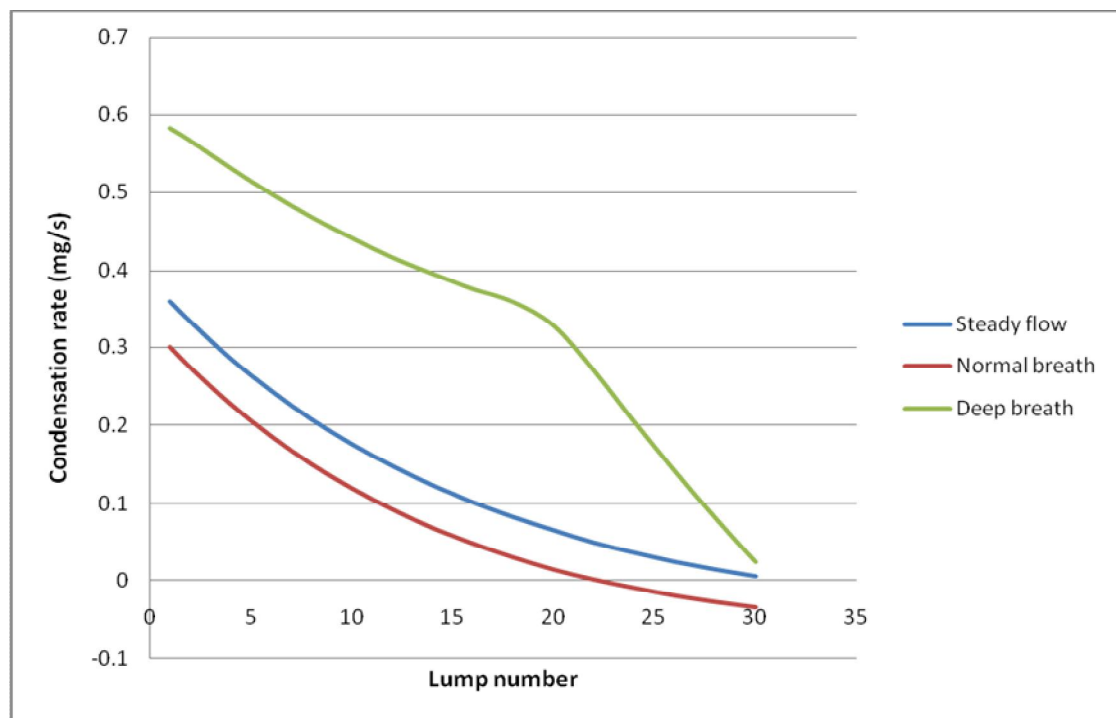
Figure 6.17 In-tube condensation of steady flow, breathing added fluctuating flows under conditions of 4cmH$_2$O, 55°C, 0W, 22°C&20% (condensation occurs when curve is below zero)

Figure 6.17 shows that the normal breathing condensation/evaporation curve is below that of the steady flow. The normal breathing induced fluctuation makes condensation starting in the last lumps of the HADT. This is due to firstly the concavity factor which drags the curve towards the X-axial, and secondly the condensation-to-evaporation coefficient factor, especially in the last few lumps. As for the deep breathing curve, the flow rate fluctuation amplitude becomes much larger. The portion of airflow travelling at much higher velocity through the chamber gains less humidity. Because of the high velocity, the dry portion coincides with high velocity in most of the lumps in this case.

162

This vaporization potentiality (coincidence factor) overcomes the condensation-to-evaporation coefficient factor. This can explain why the first section of the deep breathing curve is significantly above the normal breathing curve and the steady flow curve. The graph also shows that the second section of the deep breathing curve drops sharply. This is because the exhaled air with higher humidity reaches these lumps and flows through these lumps twice. This high humidity reverse flow offsets a large portion of the vaporization potentiality. A detailed explanation based on the instantaneous condensation/evaporation rate is in Appendix XVIII.

6.3.3.2.2 Comparison when ambient relative humidity is 50%
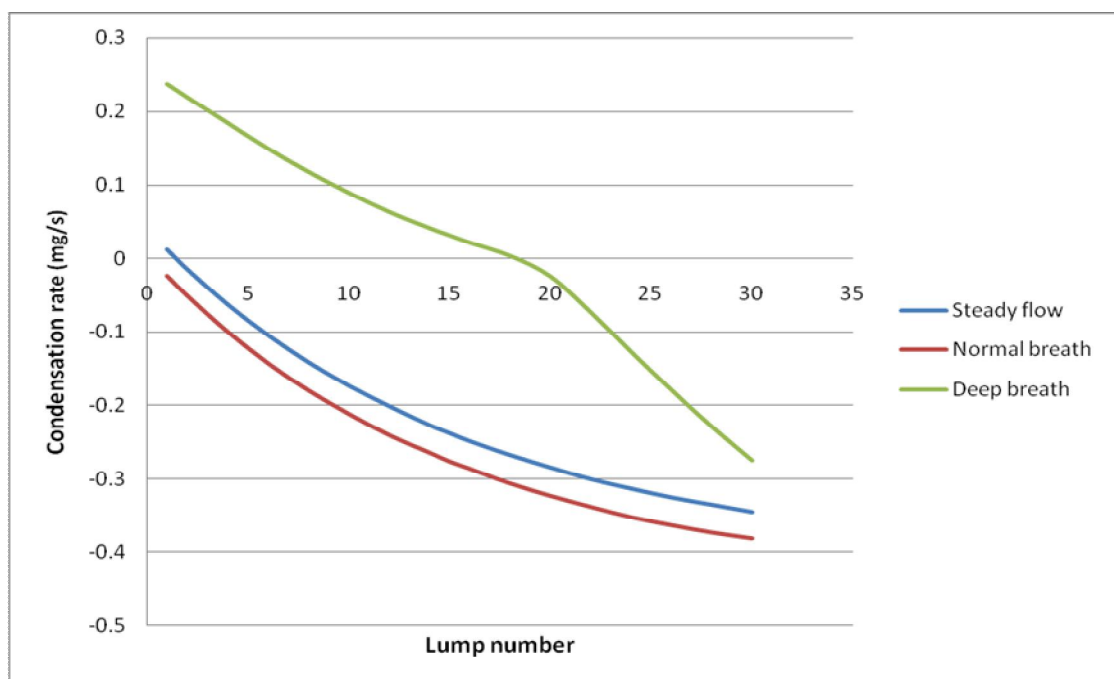
Figure 6.18 In-tube condensation of steady flow, breathing added fluctuating flows under conditions of 4cmH$_2$O, 55°C, 0W, 22°C&50%

Figure 6.18 shows that when the ambient relative humidity increases to 50%, the reverse flow induced curve drop is less sharp than that when relative humidity is 20%.

6.3.3.2.3 Comparison when ambient relative humidity is 80%

Figure 6.19 shows the condensation comparison when the ambient relative humidity continues to increase up to 80%. This time, the HADT wall temperature is always below the dew point which eliminates the vaporization potentiality. The reason for the former part of the deep breathing curve staying above the other two curves is that the highly humid portion coincides with low velocity while the low humid portion

163

coincides with high velocity which make the whole cycle averaged condensation lighter. It can also be seen that the reverse flow induced curve drop is even less sharp.
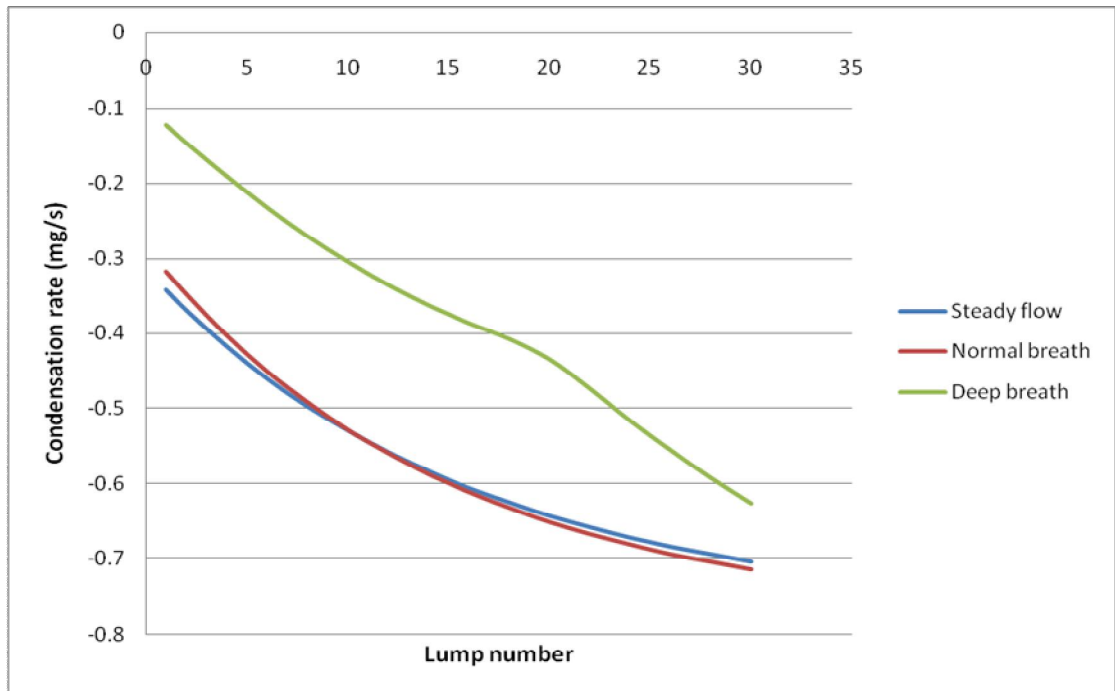
Figure 6.19 In-tube condensation of steady flow, breathing added fluctuating flows under conditions of 4cmH$_2$O, 55°C, 0W, 22°C&80%

From these figures above, it can be seen that the deep breathing still does not increase or worsen the condensation even if there is reverse flow.

Comparing these three graphs, a trend can be seen. The deep breathing curve turns down sharper when humidity difference between the airflow from humidifier chamber and the exhaled air increases (e.g. when the ambient RH is 20%). If, under some conditions, the exhaled air can drag the curve down enough to outdo the vaporization potentiality, then the deep breathing curve can drop below the normal breathing curve.

6.3.3.2.4   The conditions when reverse flow creates or worsen condensation

From Figure 6.20, it can be seen that when the heating element temperature setting is lowered to 45°C and the ambient temperature drops to 21°C, the second section of the deep breathing curve drops below the other two curves. It further drops below 0 in the last few lumps. This means that the condensation worsens and builds up in these lumps. The reason for it is that the condensation increased by the exhaled air outdoes the vaporization potentiality in these lumps.

164
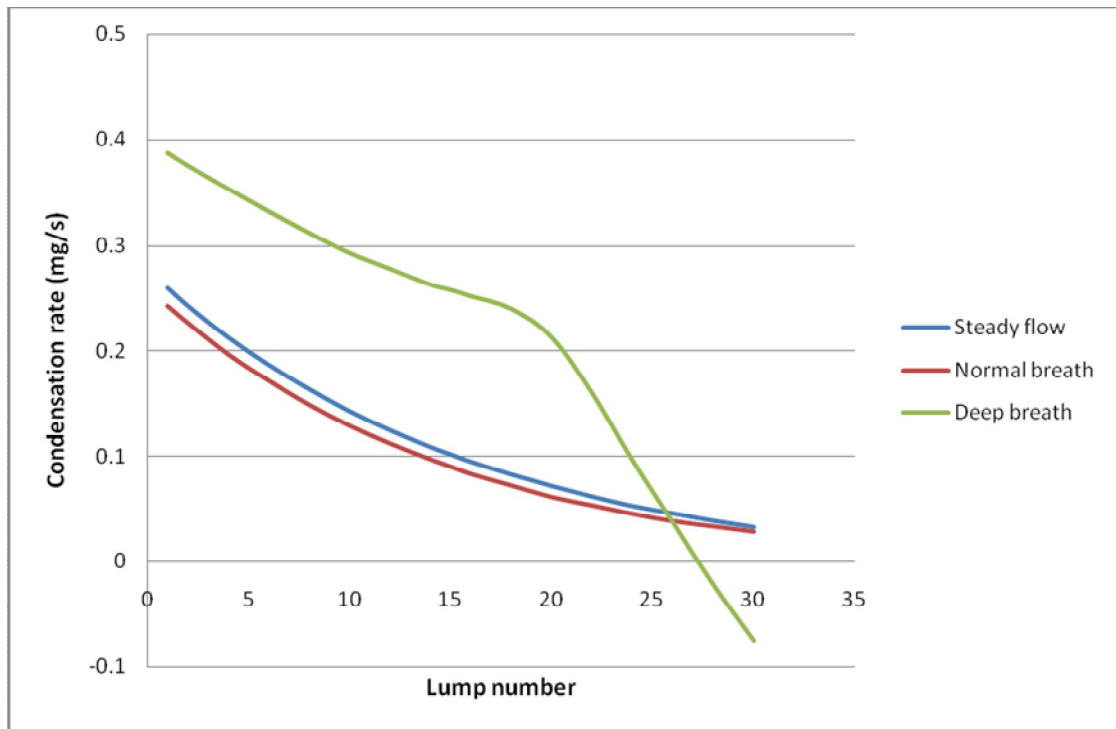
Figure 6.20 In-tube condensation of steady flow, breathing added fluctuating flows under conditions of 4cmH2O, 45°C, 0W, 21°C&50%

To summarize, due to the coincidence factor, reverse flow alleviates condensation in the HADT lumps where the exhaled air can not reach. Even for the last few lumps where the exhaled air can reach, reverse flow does not always create or worsen condensation. It creates or worsens condensation only when the humidity of the airflow from the CPAP is much lower than that of the exhaled air and the wall temperature in the last few lumps is low enough for condensation to occur and build up.

6.3.3.3 Combined effect of fluctuation and tube heating on in-tube condensation
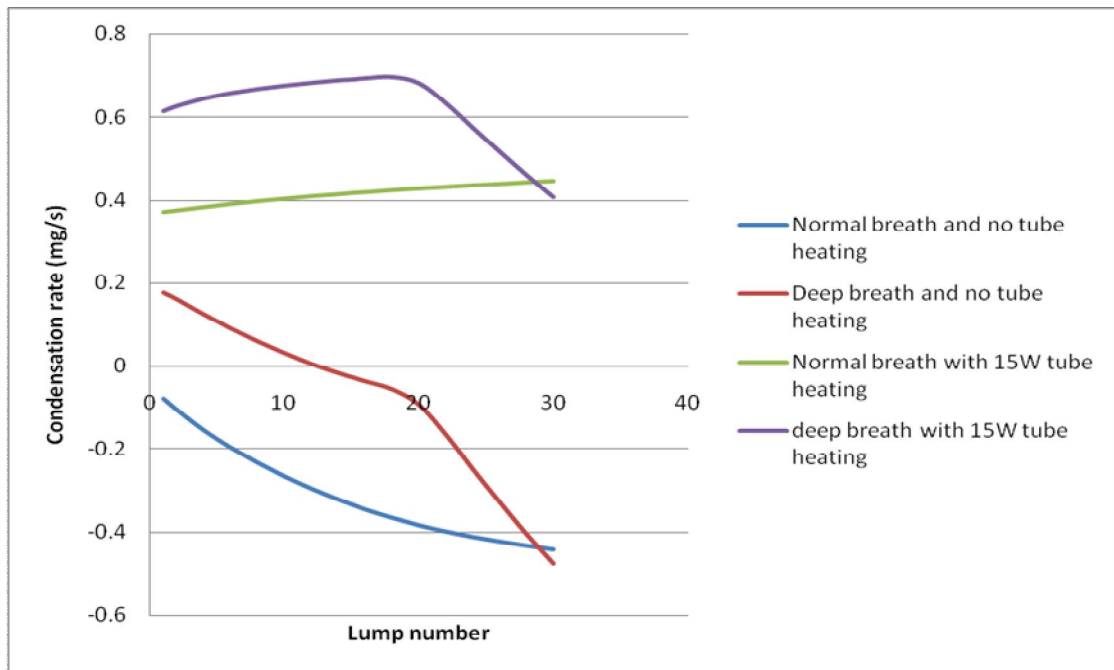
Figure 6.21 Tube heating influence on tube condensation under normal and deep breathing 4cmH$_2$O 55°C 22°C&50% (comparison of tube heating between 0W and 15W)

When condensation occurs in the HADT, tube heating can alleviate or eliminate condensation. However, the tube heating does not significantly change the relative position between the normal breathing and deep breathing curves (Figure 6.21).

6.3.3.4 Combined effect of fluctuation and mask capacity on in-tube condensation

To analyse the combined effect of fluctuation and humidity of airflow from the CPAP on the HADT condensation using different sized mask, the model is set under conditions as listed below. The conditions are all the same except the ambient temperature. To remove the influence of the ambient humidity, the ambient relative humidity is given as 0%.

Conditions	Pressure setting	Tube heating	Ambient temperature	Ambient relative humidity	Heating element setting
1			15°C		
2	4 cmH$_2$O	0 W	22°C	0%	55°C
3			29°C		

166

When using different sized masks, the air temperature and humidity in the mask may fluctuate with somewhat different amplitudes. With deep breathing, the air from the mask reverses into the HADT. However, the results from the model show there is no actual difference in HADT condensation (Table 6.2).

Table 6.2 Comparison of condensation/evaporation in the last lumps of HADT using different size of masks (cycle-wise net condensation/evaporation amount in mg/s)

Ambient temperature	15°C		22°C		29°C	
Mask type	Nasal	Full face	Nasal	Full face	Nasal	Full face
Lump 28	-0.294	-0.294	0.282	0.282	1.08	1.08
Lump 30	-0.362*	-0.361*	0.217	0.217	1.02	1.02

6.3.4 Influence of breathing induced flow rate fluctuation on air conditions in the mask and in the inhaled air

The effects of mask capacity, breath load, fluctuation amplitude and reverse flow on temperature and specific humidity of in-mask air and inhaled air are discussed in this section.

6.3.4.1 The effect of mask capacity and breath load on air temperature in the mask and in inhaled air

Table 6.3 and Table 6.4 show that the changes of breath load and mask capacity do not significantly influence the average temperatures of air in the mask and in inhalation.

Table 6.3 Comparison of average temperature in the mask using different sized masks with different breath load

	Normal breathing		Deep breathing	
Mask type	Nasal	Full face	Nasal	Full face
Average air temperature in the mask	29.15	28.61	29.27	29.12

Table 6.4 Comparison of average temperature in inhaled air using different sized masks with different breath load

	Normal breathing		Deep breathing	
Mask type	Nasal	Full face	Nasal	Full face
Average air temperature of inhaled air	29.10	28.58	29.10	29.09

6.3.4.2   The effect of airflow fluctuation amplitude on specific humidity in the mask
         and in inhaled air

Firstly, the model's CPAP pressure is set at 9 cmH$_2$O to consider the influence only from fluctuation amplitude. The conditions are the same as in sub-section 6.3.3.1. The average specific humidity in the mask under normal breathing and deep breathing are shown in Figure 6.22 in comparison.
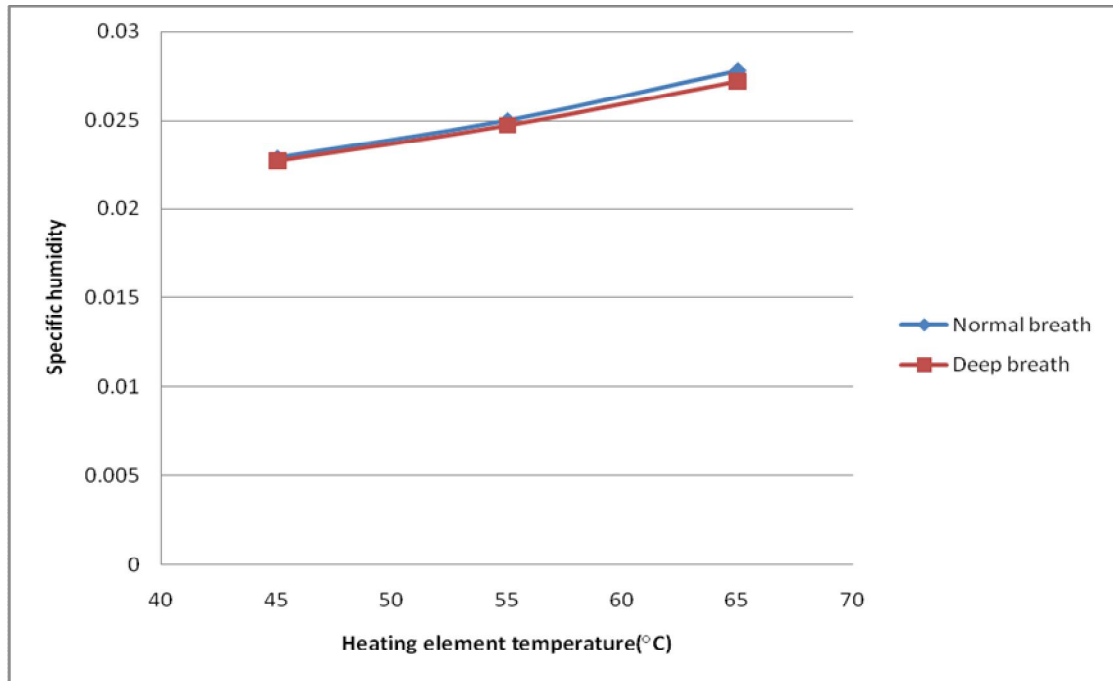
Figure 6.22 Average specific humidity in the mask under 9 cmH$_2$O pressure setting without reverse flow

The average specific humidity in the mask is slightly lower under deep breathing than normal breathing. This is because the airflow entering the mask from the HADT is mainly the portion flowing through the chamber at higher velocity thus with less humidity. During the inhalation phase of deep breathing, the velocity is much higher and the humidity is lower.

The average specific humidity in the mask includes the high specific humidity of exhaled air in the exhalation phase. This exhaled air will be mostly expelled before the next inhalation starts. So the average specific humidity within inhalation is lower than the average specific humidity in the mask. The average specific humidity within inhalation under normal breathing and deep breathing are shown in Figure 6.23 for comparison.

168
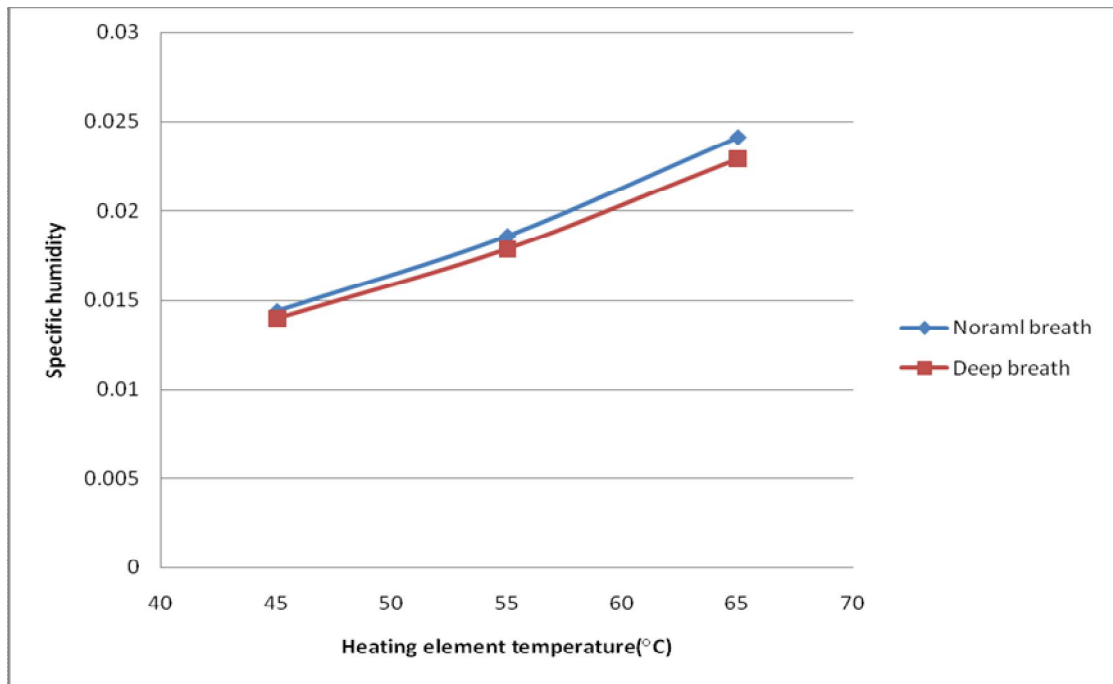
Figure 6.23 Average specific humidity in inhaled air under 9 cmH$_2$O pressure setting without reverse flow

The average specific humidity within an inhalation under deep breathing is about 95~97% of that of normal breathing also due to the lower humidity from the chamber during the deep breathing inhalation phase.

6.3.4.3 Specific humidity in the mask and in inhaled air when reverse flow occurs

To analyse the combined effect of reverse flow and humidity of airflow from the CPAP on the specific humidity in the mask and in the inhaled air, the model is set under conditions as listed below.

Conditions	Pressure setting	Tube heating	Ambient temperature	Ambient relative humidity	Heating element setting
1					45°C
2	4 cmH$_2$O	0 W	22°C	50%	55°C
3					65°C

The average specific humidity in the mask under normal breathing and under deep breathing with reverse flow are shown in Figure 6.24 in comparison.
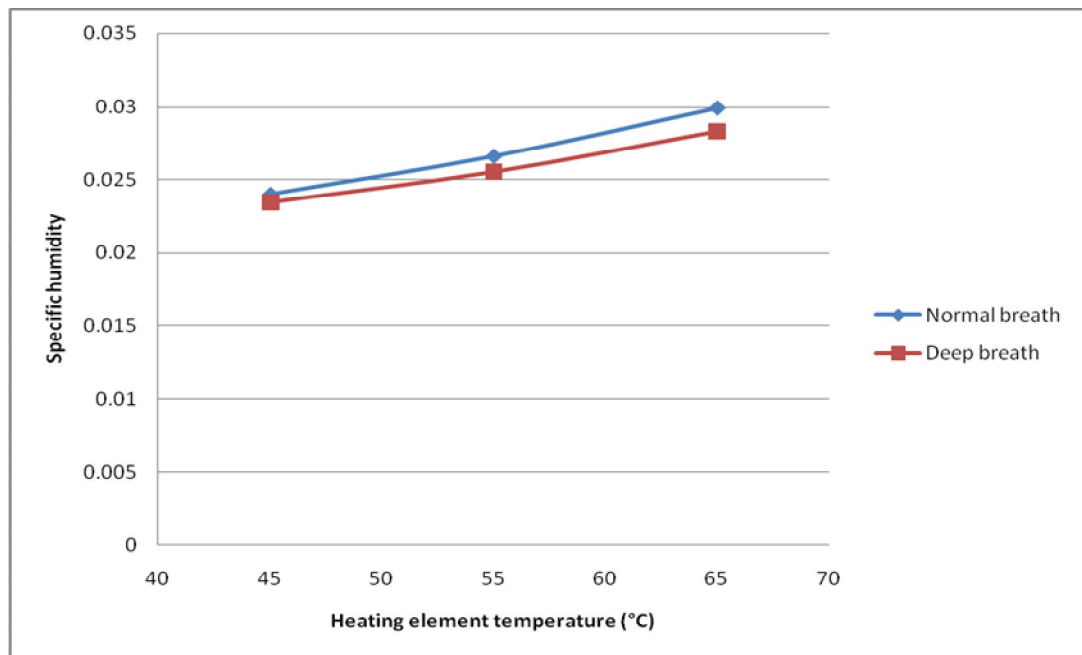
Figure 6.24 Average specific humidity in the mask under 4 cmH₂O pressure setting

The average specific humidity in the mask is also lower under deep breathing. This is because when the breath load is twice that of normal breathing, the exhaled air in reverse flow mostly expels through bias vent holes, and reverse flow does not actually contribute humidity to the air in the mask. Thus the lower specific humidity with deep breathing is also only because of the lower humidity airflow from the chamber.

The average specific humidity in the inhaled air under normal breathing and the average under deep breathing with pressure setting of 4 cmH₂O are shown in Figure 6.25.
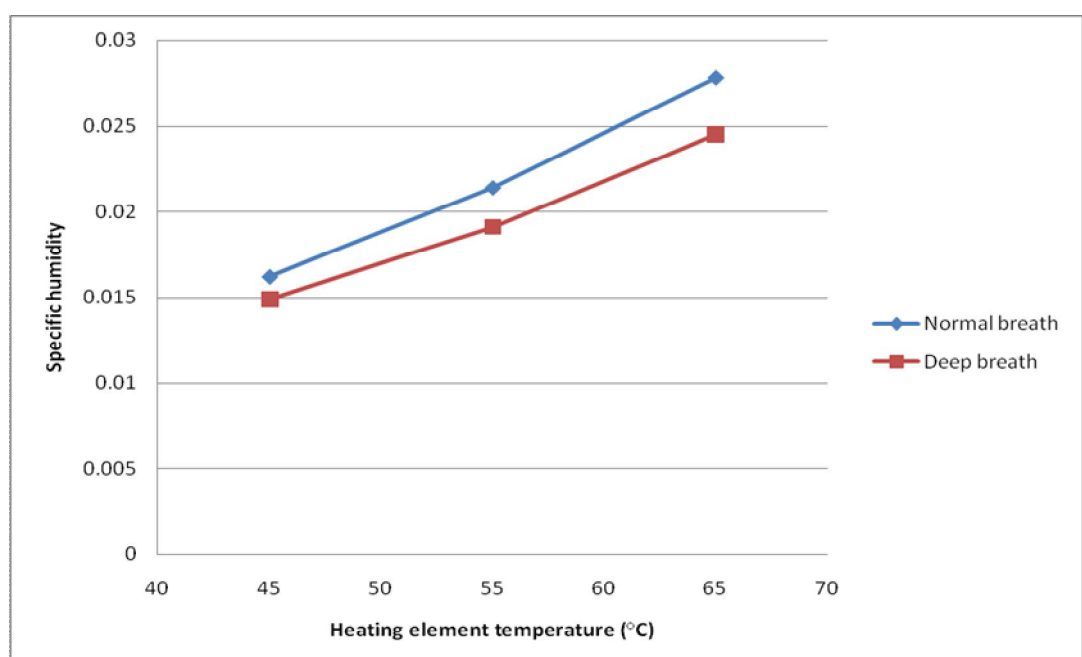
Figure 6.25 Average specific humidity in inhaled air under 4 cmH₂O pressure setting

The average specific humidity in an inhalation under deep breathing is about 90% of that of normal breathing. Comparing to the example under 9cmH$_2$O pressure setting, the humidity difference is greater here. This is because the pressure setting here is low and consequently the normal breathing inhalation phase flow velocity is also low. This allows the humid portion shifts more to coincide with the patient inhalation phase when reaching the mask (Figure 6.26). Thus under normal breathing, the inhaled air average specific humidity is even higher compared to that with deep breathing under the same conditions.
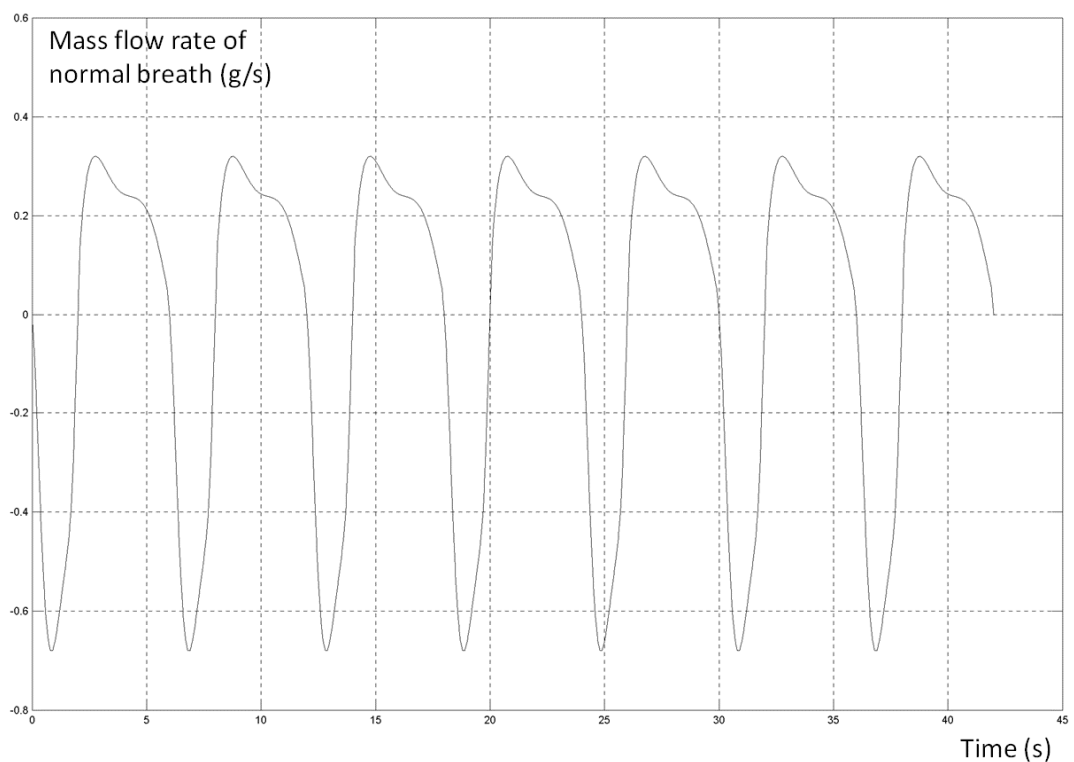
Figure 6.26 Mass flow rate of normal breathing under pressure setting of 4 cmH$_2$O
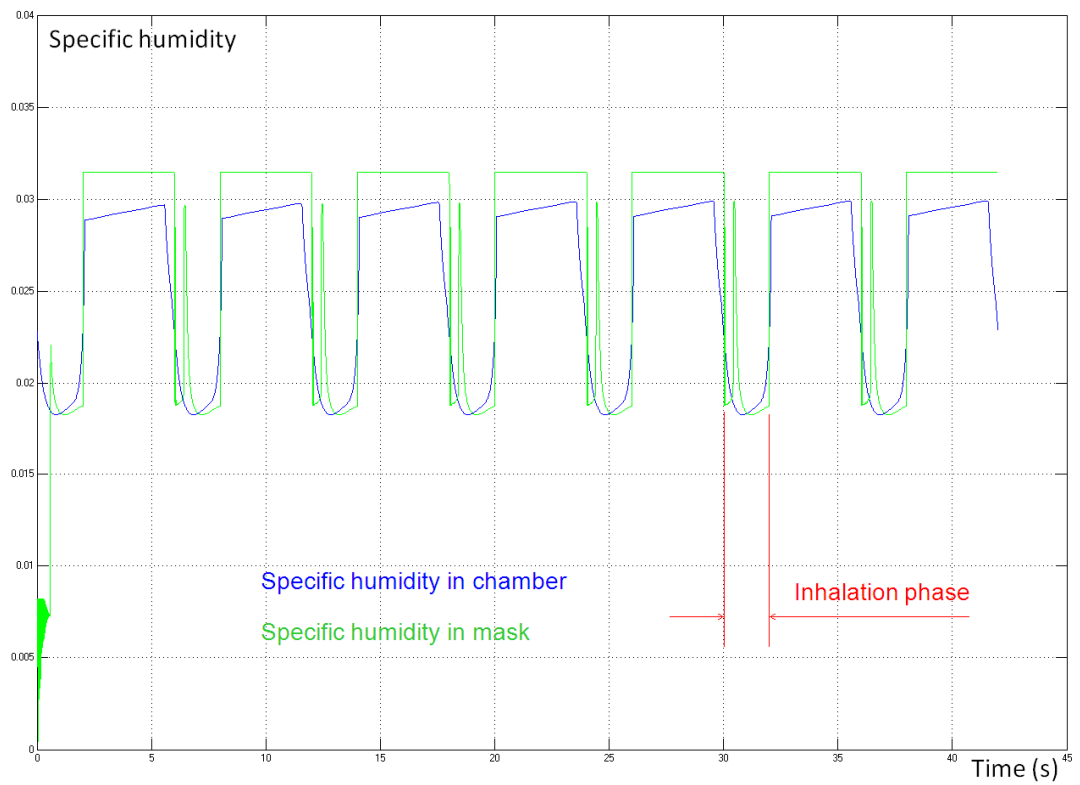
Figure 6.27 Comparison of specific humidity in the chamber and the mask under normal breathing and pressure setting at 4 cmH$_2$O

6.3.4.4 Effect of mask capacity on specific humidity in the mask and in inhaled air

The model is set under conditions as listed below. The conditions are all the same except the breath load and mask capacity.

Conditions	Pressure setting	Tube heating	Ambient temperature	Ambient relative humidity	Heating element setting
Value	4 cmH$_2$O	0 W	22°C	50%	55°C

Table 6.5 shows that the mask capacity does not have an influence on average specific humidity in the mask and in inhaled air.

Table 6.5 Comparison of average specific humidity in the mask and in inhaled air using different size of masks with normal breathing

	Normal breathing		Deep breathing	
Mask type	Nasal	Full face	Nasal	Full face
Average specific humidity in the mask	0.0266	0.0266	0.0255	0.0255
Average specific humidity in inhaled air	0.0214	0.0214	0.0191	0.0191

6.4 Conclusions

Based on the discussion above, conclusions are drawn and listed below for the fluid dynamic study and the thermodynamic study.

6.4.1 Conclusion for fluid dynamic study

1. Mask capacity does not influence reverse flow.

2. Reverse flow increases along with the breath load. Reverse flow also increases when the pressure setting decreases. Overall, the combination of the CPAP pressure setting and the breath load determines the reverse flow.

3. Reverse flow does not definitely add exhaled air to the next inhalation unless the reverse flow is too far back in the HADT. This may occur only when the pressure setting is at the lowest and the breath load is unusually large.

4. When there is no exhaled air added in from reverse flow, re-inhalation of exhaled air is proportional to mask capacity.

5. When there is no exhaled air added in from reverse flow, the percentage of exhaled air in inhalation drops along with the increase of breath load.

6.4.2 Conclusion for thermodynamic study

The conclusions drawn for the steady state flow are:

1. The main factor influencing the chamber water temperature is the heating element temperature.

2. The main factors influencing air temperature in the chamber are the heating element temperature and ambient temperature.

3. The main factors influencing evaporation rate in the existing chamber are the heating element temperature and CPAP pressure setting.

4. The main factors influencing the air temperature at the outlet of the HADT are the HADT heating and ambient temperature.

5. The main factors influencing the condensation in the HADT are all the five factors: the heating element temperature, CPAP pressure setting, the HADT heating, ambient temperature and humidity.

6. Different flow patterns influence heat and mass convections on the chamber water surface. The larger area the direct impact flow can cover, the larger the convection rates can be.

The conclusions drawn for the dynamic fluctuation situation are:

1. Deep breathing does not significantly change the breath-cycle-wise total evaporation in the chamber.

2. When breathing induced fluctuation is introduced, the change of condensation is a combined effect of several factors. Without reverse flow, the deep breathing induced greater fluctuation amplitude at least does not worsen condensation.

3. When reverse flow occurs, the condensation occurs or worsens in the HADT near the mask only when the humidity of the airflow from the CPAP is much lower than that of the exhaled air and the HADT wall temperature in these lumps is low enough for condensation to occur and build up. Thus, additional reverse flow induced condensation may occur when ambient air is dry and cool and the humidifier heating is also set low. Since deep breathing decreases the average humidity in inhaled air, it is not proper to reduce chamber outlet humidity for eliminating the reverse flow induced condensation in the HADT. Increasing tube heating may be the way to remove this extra condensation.

4. Tube heating can alleviate or eliminate condensation but does not significantly change condensation gap between normal breathing and deep breathing.

5. The overall specific humidity in inhaled air is lower under deep breathing.

6. The deep breathing and reverse flow do not significantly influence the average inhaled air temperature.

7. Mask capacity does not influence the thermal conditions in the HADT.

8. Mask capacity does not influence the inhaled air specific humidity and does not significantly influence its temperature.

6.5 Future work

Through the course of this project, further investigations in specific areas have been identified for future research and design. They are listed and briefly discussed below.

1. Full range experiment to validate the models' dynamic performance.

2. From chapter 1, by volume, the CO_2 limit in inhaled air is 0.325% [26] and the average CO_2 concentration in exhaled air is 3.7%, thus the exhaled air should not surpass 8.8% in the next inhalation. Based on the model, the nasal mask gives 6.16% of exhaled air being re-breathed when breathing is normal. Considering that the air stayed in the mask is the end of the last exhalation, it may contain a higher percentage of CO_2 than the average. Hence, the CO_2 concentration may be already close to the limit. Different location of bias vent holes may influence the mixing process in the mask. It may be good to re-consider the location of the bias vent holes in future design. A quantitative analysis of the location influence on mixing and exhaled air re-inhalation may be helpful for the design.

3. Further investigation in chamber evaporation. Firstly, as analysed in chapter 3, the direct impact of airflow onto the chamber water surface has much greater Nusselt number and mass convection coefficient than surface flow. Through a new design of the chamber, it may be possible to enlarge the water surface area covered by direct impact so to increase the evaporation rate without increasing the heating element setting and the water temperature. Secondly, although the project does not include the chamber water level change in the modelling, the airflow characteristic velocity in the chamber relates the velocity with the height of chamber air space. When the water level drops, the bigger air space makes the airflow velocity in the chamber lower and reduces the convections. A Computational Fluid Dynamics Analysis considering these factors for a more

accurate and real flow pattern analysis may be helpful for future design. I.e. a design which can also compensate for the influence of water level change on evaporation rate.

4. It will be helpful to develop a scheme which would be able to adjust the humidifier heating inputs so to compensate for the airflow humidity change due to the change of the pressure setting and the water level drop.

5. It will also be beneficial to develop a scheme which will be able to adjust the heating element setting to offset the breath load induced inhaled air humidity change.

6. A scheme may also be needed for the tube heating adjustment to alleviate the condensation induced by the above-mentioned humidifier heating adjustments and reverse flow. This means a higher humidifier heating and a higher tube heating to cooperatively provide an ideal humidity level without increasing condensation.

7. Usually, the inhaled air has a lower humidity than the average humidity of airflow from the chamber. This means the majority of the water evaporated is not utilized but may only increase the possibility of downstream condensation. It would be ideal to find a way to reduce the humidity fluctuation from the chamber which could increase the inhaled air humidity without increasing condensation.

Appendices

Appendix I Regression of the pressure at air delivery unit blower outlet

Appendix II Regression of the pressure drop on the connecting duct

Appendix III Regression of the air temperature increase after flowing through the blower

Appendix IV The corrugated HADT outer surface area

Appendix V Regression of dew point

Appendix VI Relationship regressions between relative humidity, specific humidity and absolute humidity

Appendix VII Details of the CPAP fluid dynamic section after ADU outlet

Appendix VIII Details of whole chamber steady state subsystem

Appendix IX Details of steady state HADT lump full thermal balance subsystem

Appendix X Details of HADT lump air dynamic fluctuating thermal balance and condensation subsystem

Appendix XI Details of steady state mask full thermal balance subsystem

Appendix XII Details of mask air dynamic fluctuating thermal balance and condensation subsystem

Appendix XIII Details of the auxiliary subsystems

Appendix XIV Steady state thermal-validation experiment result and model output comparison

Appendix XV Regression of temperature related water properties for Grashof number

Appendix I. Regression of the pressure at air delivery unit blower outlet

This appendix is to show the data process for the relationship of ADU outlet pressure with its pressure setting and volumetric flow rate.

The pressure readings were taken after the pressure sensor calibration. These data were corrected to produce stagnation pressure.

Two rounds of tests were done for at pressure settings of 4, 6, 8, 10, 12, 14, 16, 18 and 20 cmH$_2$O. For each setting the ADU outlet actual pressure is tested at different volumetric flow rate. Due to the flow rate was controlled by valve at the downstream tube end which was difficult to control the flow rate accurately so the flow rate was adjusted to approximately -30, -20, -10, 0, 15, 30, 45, 60, 75, 90 and 105 L/min.

Because the pressure sensing orifice is located at the ADU outlet and the air flows normal to it, a compensation of the gap of static and stagnant pressure was calculated as [69]:

$$P_{stag} = P_{static} + \frac{1}{2}[(1+\frac{4}{Re})\rho u^2]$$

After this compensation and averaging of regressed expression of each setting in each round, the relationship of outlet pressure vs. flow rate may be regressed as:

$$P_{Ao} = au_D{}^3 + bu_D{}^2 + cu_D + d$$

When pressure setting is at 4cmH2O, the relationship of ADU outlet pressure vs. volumetric flow rate are measured and recorded below. (Airflow velocity converted from volumetric flow rate is also included)

First round:

Table I. 1 First round of ADU outlet pressure

Q(L/min)	V(m/s)	P_Measured (static) (Pa)	P Compensate (Pa)	P_stag(Pa)
-29.28	-1.69	451.03	1.64	452.67
-20.35	-1.17	435.54	0.79	436.33
-9.55	-0.55	419.21	0.17	419.38

0.08	0	407.32	0	407.32
15.81	0.91	408.9	0.48	409.38
31.22	1.8	409.33	1.86	411.19
45.44	2.62	395.43	3.94	399.37
60.67	3.49	369.65	7.02	376.67
74.81	4.31	335.84	10.67	346.51
89.77	5.17	291.29	15.36	306.65
97.75	5.63	264.59	18.22	282.81

Table I. 2 Second round of ADU outlet pressure

Q(L/min)	V(m/s)	P_Measured (static) (Pa)	P Compensate (Pa)	P_stag(Pa)
-30.77	-1.77	450	1.81	451.81
-21.36	-1.23	435.82	0.88	436.7
-9.87	-0.57	421.75	0.19	421.94
0.06	0	406.5	0	406.5
14.44	0.83	408.84	0.4	409.24
29.5	1.7	411.44	1.66	413.1
44.74	2.58	394.71	3.82	398.53
59.57	3.43	371.94	6.77	378.71
74.56	4.29	337.22	10.6	347.82
88.36	5.09	296.6	14.88	311.48
97.26	5.6	267.33	18.04	285.37

By using curve fitting and averaging of the two rounds, the relationship of ADU outlet pressure vs. airflow velocity in the duct can be expressed as:

$$P_{Ao} = -1.1387u_D^3 + 3.2879u_D^2 - 10.0609u_D + 415.40$$

The tested results and the regressed curve is shown in figure below:
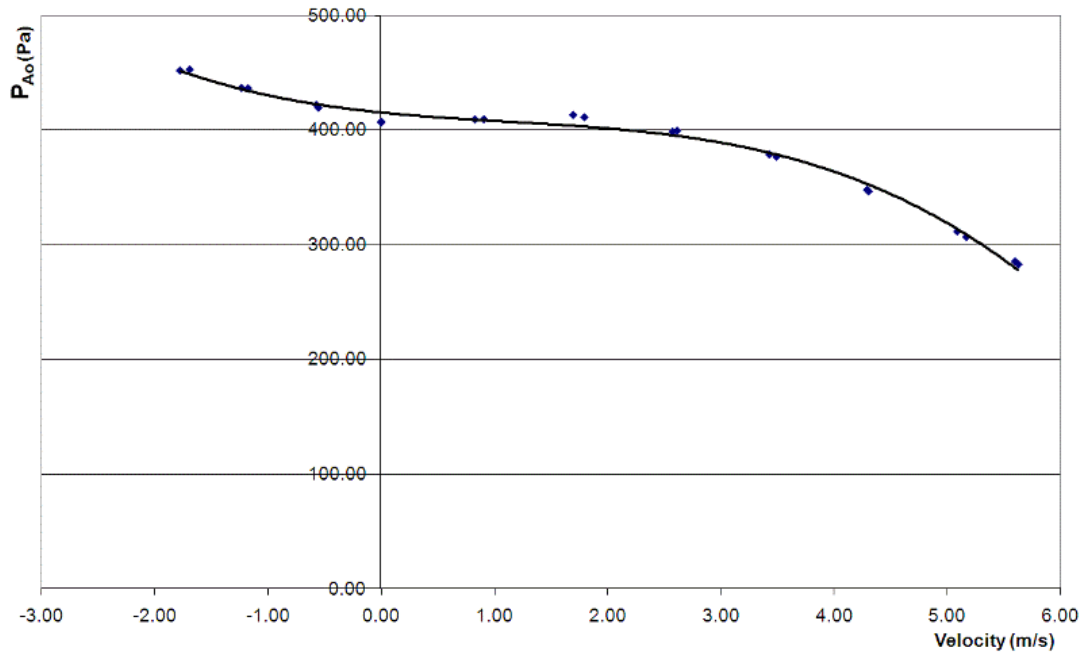
Figure I. 1 Tested results and the regressed curve for ADU outlet pressure when pressure setting is 4cmH2O

By using the same method, such a 3-ordered expression can be obtained for each of the tested pressure settings. The coefficients for each pressure setting are listed below:

P_{Ao}	a	b	c	d
4cmH2O	-1.1387	3.2879	-10.0609	415.40
6cmH2O	-1.1219	3.8749	-9.4252	611.44
8cmH2O	-1.3316	5.8853	-10.4933	807.36
10cmH2O	-1.4676	7.2633	-9.4144	1001.50
12cmH2O	-1.6729	9.3706	-11.9589	1187.60
14cmH2O	-1.8456	10.7920	-10.7130	1378.05
16cmH2O	-2.1916	14.0150	-14.9430	1563.70
18cmH2O	-2.4434	15.5360	-9.6832	1748.35
20cmH2O	-2.5066	16.9690	-12.4421	1957.05

It is convenient for dynamic simulation modelling to unify them by regressing the coefficients again as:

$$a_i = -0.0961 P_{set} - 0.5932$$

$$b_i = 0.9124 P_{set} - 1.2827$$

$$c_i = -0.1791 P_{set} - 8.9763$$

$$d_i = 95.555 P_{set} + 38.95$$

Where P_{set} is in cmH2O for easy user-input.

So the global expression for the ADU outlet pressure may result in:

$$P_{Ao} = (-0.0961 P_{set} - 0.5932) v_D{}^3 + (0.9124 P_{set} - 1.2827) v_D{}^2$$
$$+ (-0.1791 P_{set} - 8.9763) v_D + (95.555 P_{set} + 38.95)$$

The tested results and the regressed curves are shown in Figure 2.11.

Appendix II.   Regression of the pressure drop on the connecting duct

This appendix is to show the data process for the pressure drop on the connecting duct.

The relationship of connecting duct flow velocity and pressure drop has been shown by Eq. (2.13). Choosing friction factor form as:

$$f = \frac{k_f}{Re^a}$$

After a compensation of the gap of static and stagnant pressure, data from experiment were used to determine the relationship of duct flow velocity and overall pressure drop from the outlet of the blower to the chamber.

Table II. 1 Test result of airflow velocity and pressure drop in the connecting duct

Test Round A		Test Round B	
u_D (m/s)	$(P_{Ao} - P_C)$(pa)	u_D (m/s)	$(P_{Ao} - P_C)$(pa)
0.9064	2.8911	0.9179	2.9369
1.7402	7.9231	1.7528	7.8076
2.5523	16.5899	2.6246	17.4839
3.4541	29.8144	3.5022	30.6139
4.3338	46.9712	4.3251	46.0076
5.1804	66.7598	5.1966	65.9512
6.0851	91.5251	6.3109	93.1875

Regressing the data gave $a = 0.1679$ and $k_f = 0.4226$. The data from experiment and the fitted curve has been shown in Figure 2.14. So the relationship of velocity and pressure drop on the connecting duct can be expressed as Eq. (2.15).

Appendix III.   Regression of the air temperature increase after flowing through the blower

This appendix is to explain the data process of obtaining the relationship between enthalpy increase and CPAP pressure setting and the corresponding data process.

Repeating the tests under three different ambient conditions as listed below:

- Temperature 10°C and relative humidity 50% for cold and dry condition
- Temperature 20°C and relative humidity 70% for most common room condition
- Temperature 35°C and relative humidity 90% for hot and humid condition

The thermal enthalpy increase is calculated by Eq. (3.2). When under temperature 10°C and relative humidity 50%, the specific humidity level is $d = 0.003761$ (kg/kg) and the result is shown below：

Table III. 1 Airflow temperature and enthalpy increases after flowing through ADU when ambient temperature is 10°C and relative humidity is 50%

P-set(cmH2O)	$T_{Ao}(°C)$	$\Delta T_{Ao}(°C)$	$\Delta H(J/kg)$
4	12.29	2.29	2311.15
6	13.12	3.12	3141.45
8	13.87	3.87	3905.57
10	14.56	4.56	4601.74
12	15.29	5.29	5332.23
14	15.95	5.95	6000.24
16	16.47	6.47	6525.47
18	16.63	6.63	6680.55
20	17.10	7.10	7160.88

When under temperature 20°C and relative humidity 70%, the specific humidity level is $d = 0.0101$ (kg/kg) and the result is shown below：

Table III. 2 Airflow temperature and enthalpy increases after flowing through ADU when ambient temperature is 20°C and relative humidity is 70%

P-set(cmH2O)	$T_{Ao}(°C)$	$\Delta T_{Ao}(°C)$	$\Delta H(J/kg)$
4	22.89	2.89	2928.67
6	22.93	2.93	2969.04
8	23.20	3.20	3239.90
10	23.73	3.73	3780.83
12	24.40	4.40	4460.65
14	25.19	5.19	5262.07
16	25.92	5.92	6002.51
18	26.66	6.66	6746.34
20	27.03	7.03	7129.71

When under temperature 35°C and relative humidity 90%, the specific humidity level is d = 0.03167 (kg/kg) and the result is shown below:

Table III. 3 Airflow temperature and enthalpy increases after flowing through ADU when ambient temperature is 35°C and relative humidity is 90%

P-set(cmH2O)	$T_{Ao}(°C)$	$\Delta T_{Ao}(°C)$	$\Delta H(J/kg)$
4	37.89	2.89	2978.92
6	38.46	3.46	3568.89
8	39.01	4.01	4140.59
10	39.58	4.58	4727.30
12	40.15	5.15	5310.94
14	40.66	5.66	5836.77
16	41.00	6.00	6197.36
18	41.37	6.37	6578.09
20	41.44	6.44	6642.78

The average gained enthalpy is listed below:

P-set(cmH2O)	$\Delta H(J/kg)$			
	$T_\infty = 10°C$ $RH_\infty = 50\%$	$T_\infty = 20°C$ $RH_\infty = 70\%$	$T_\infty = 35°C$ $RH_\infty = 90\%$	Averaged
4	2311.15	2928.67	2978.92	2739.58
6	3141.45	2969.04	3568.89	3226.46
8	3905.57	3239.90	4140.59	3762.02
10	4601.74	3780.83	4727.30	4369.96
12	5332.23	4460.65	5310.94	5034.61
14	6000.24	5262.07	5836.77	5699.70
16	6525.47	6002.51	6197.36	6241.78
18	6680.55	6746.34	6578.09	6668.33
20	7160.88	7129.71	6642.78	6977.79

The averaged enthalpy gains have been shown in Figure 3.4. Thus the resulting curve fitting may be expressed by Eq. (3.4). The correlation of R^2=0.999 shows excellent fit. Therefore the temperature of chamber inlet from ADU can be expressed by Eq. (3.6).

Appendix IV.   The corrugated HADT outer surface area

The geometric shape of the corrugation is shown in figure below.
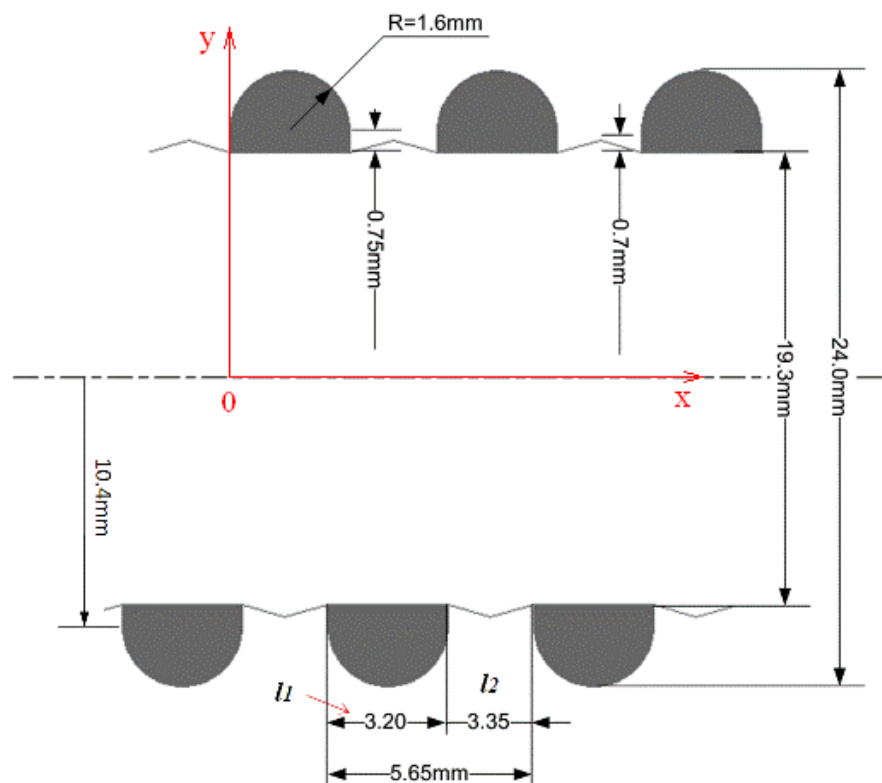
Figure IV 1 HADT corrugated outer surface
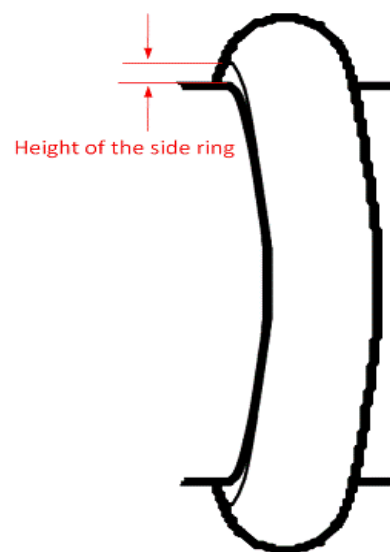
Figure IV 2 the height of the side ring of the bead

The geometric parameters are listed below:

symbol	parameter	(mm)
l	Pitch length	5.65
l_1	Bead width	3.2
l_2	Width of the film part	3.35
r	Radius of the bead (1/2 of l1)	1.6
h	Height of the side ring of the bead	0.75
H	Height from HADT centre axis to the top of the side ring of the bead	10.4

When the origin of the co-ordinators is as in the figure above, the expression of the semi-circle is:

$$y = \sqrt{r^2 - (x-r)^2} + H = \sqrt{1.6^2 - (x-1.6)^2} + 10.4 = \sqrt{3.2x - x^2} + 10.4$$

So the semi-circular revolved surface area is [70]:

$$A_{cb} = 2\pi \int_0^{3.2} y\sqrt{1+(y')^2}\, dx$$

Where $y' = [(3.2x - x^2)^{1/2}]' = \dfrac{1.6 - x}{\sqrt{3.2x - x^2}}$ and $\sqrt{1+(y')^2} = \sqrt{\dfrac{2.56}{3.2x - x^2}}$.

Thus $A_{cb} = 2\pi \int_0^{3.2} y\sqrt{1+(y')^2}\, dx = 2\pi\sqrt{2.56} \int_0^{3.2} [\dfrac{\sqrt{3.2x - x^2} + 10.4}{\sqrt{3.2x - x^2}}] dx = 360.63$ (mm^2)

The area of the two flat rings (see Figure IV 3):

$$A_r = 2 \times (\pi H^2 - \pi R_2^2) = 2 \times \pi(10.4^2 - 9.65^2) = 94.48 \ (\text{mm}^2)$$

The two parts of the film are like two frusta of cones (see Figure IV. 1) and the area can be calculated as:

$$A_f = 2 \times [\pi(R_1 + R_2)\sqrt{(\dfrac{l_2}{2})^2 + (R_1 - R_2)^2}] = 2 \times [\pi(10.35 + 9.65)\sqrt{(\dfrac{2.95}{2})^2 + (10.35 - 9.65)^2}]$$

$= 205.17$ (mm^2)

The total area of the complicated corrugated surface is:

$$A_{Total} = A_{cb} + A_r + A_f = 360.63 + 94.48 + 205.17 = 660.28(mm^2) = 660.28 \text{ (mm}^2)$$

The area of the base cylinder is:

$$A_{Base-cylinder} = \pi Dl = 19.3 \times 5.65\pi = 342.58 \text{ (mm}^2)$$

Thus the ratio of the corrugated surface area to the base cylindrical surface area is:

Ratio=660.28/342.58=195%

Appendix V.   Regression of dew point

According to the definition in this thesis, the specific humidity is:

$$d = \frac{m_v}{m_v + m_d} = \frac{m_v / m_d}{m_v / m_d + 1} = \frac{AbsoluteHumidity}{1 + AbsoluteHumidity}$$

Based on The relationship between temperature and Humidity ratio at Saturation [71], the corresponding specific humidity at saturation is calculated and listed below along with the temperature and the saturated humidity ratio:

Table V. 1 Saturated humidity ratio, specific humidity vs. temperature

Temperature	Humidity Ratio at Saturation	Specific Humidity at Saturation
(°C)	(kg of vapour/kg of dry air)	(kg of vapour/kg of moist air)
5	0.0054	0.005371
10	0.0077	0.007641
15	0.011	0.01088
20	0.015	0.014778
25	0.02	0.019608
30	0.027	0.02629
35	0.037	0.03568
40	0.049	0.046711
45	0.065	0.061033
50	0.087	0.080037
55	0.12	0.107143
60	0.15	0.130435
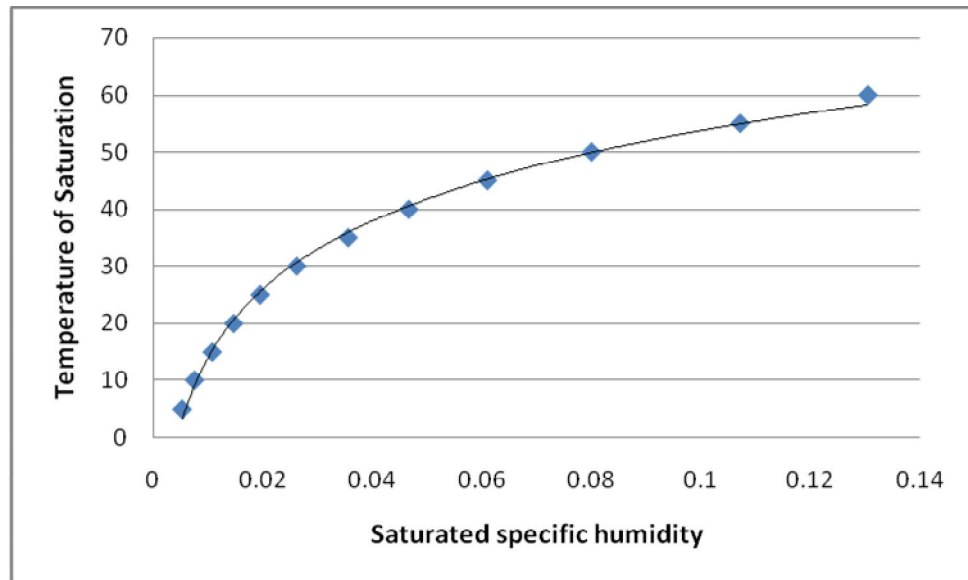
Figure V. 1 Regression of saturated specific humidity vs. temperature

Regress the saturation temperature from 5 to 60°C against specific humidity gives dew point temperature as expressed by Eq. (3.82) with R² = 0.9974.

Appendix VI.   Relationship regressions between relative humidity, specific humidity and absolute humidity

This appendix is for explanations of the conversions between relative humidity, specific humidity and absolute humidity.

VI.1   Conversion of relative humidity into specific humidity

The ratio between partial pressure of any air component to the total pressure is proportional to the component mole fraction [72]. For saturated moist air, its partial pressure of vapour can be expressed as:

$$P_{Satu} = \frac{m_v / 18.01}{m_v / 18.01 + m_d / 28.966} P_{Total}$$

Where m_v is mass of vapour in the moist air, m_d is the mass of dry air in the moist air, P_{Total} is total pressure, 18.01 and 28.966 are molar weight of water vapour and dry air respectively.

The ratio of saturated vapour partial pressure to the total pressure vs. temperature is given below [49]:

Temperature $(°C)$	P_{Satu} / P_{Total}
5	0.008721
10	0.012276
15	0.017051
20	0.02339
25	0.03169
30	0.04246
35	0.05628
40	0.07384
45	0.09593
50	0.1235
55	0.1576
60	0.1994

This ratio can be regressed against temperature as:

$$P_{Satu} / P_{Total} = 8.63 \times 10^{-7} T^3 - 1.344 \times 10^{-5} T^2 + 8.784 \times 10^{-4} T + 4.268 \times 10^{-3}$$

with $R^2 = 0.9999$.

Since specific humidity is defined as:

$$d = \frac{m_v}{m_d + m_v} = \frac{18.01 P_{Vapor}}{28.966 P_{DryAir} + 18.01 P_{Vapor}}$$

Where $P_{Vapor} = P_{Satu} \cdot RH$, RH is relative humidity in decimal and:

$$P_{DryAir} = 28.966(P_{Total} - P_{Satu} \cdot RH)$$

Thus specific humidity can be expressed by relative humidity as:

$$d = \frac{18.01(8.63 \times 10^{-7} T^3 - 1.344 \times 10^{-5} T^2 + 8.784 \times 10^{-4} T + 4.268 \times 10^{-3}) \cdot RH}{28.966 - 10.956(8.63 \times 10^{-7} T^3 - 1.344 \times 10^{-5} T^2 + 8.784 \times 10^{-4} T + 4.268 \times 10^{-3}) \cdot RH}$$

VI.2 Conversion of specific humidity into relative humidity

Since: $RH = \frac{m_v}{m_{vs}} = (m_v / m_d) \div (m_{vs} / m_d)$ and m_{vs} / m_d is the humidity ratio of saturated

air and can be acquired from table 1 and regressed as below:

$$m_{vs} / m_d = 1.00 \times 10^{-6} T^3 - 3.55 \times 10^{-5} T^2 + 1.03 \times 10^{-3} T + 5.47 \times 10^{-4}$$

On the other hand, Since:

$$\frac{m_v}{m_d} = \frac{m_v / (m_v + m_d)}{\dfrac{(m_v + m_d) - m_v}{m_v + m_d}} = \frac{m_v / (m_v + m_d)}{1 - \dfrac{m_v}{m_v + m_d}} = \frac{d}{1-d}$$

Thus

$$RH = \frac{d / (1-d)}{1.00 \times 10^{-6} T^3 - 3.55 \times 10^{-5} T^2 + 1.03 \times 10^{-3} T + 5.47 \times 10^{-4}}$$

VI.3 Conversion of specific humidity into absolute humidity

Absolute humidity is defined as vapour mass in a certain volume which can be expressed as:

$$C_v = \frac{m_v}{V}$$

For 1 mole of moist air:

$$V = 8.31T / P$$

Thus:

$$C_v = \frac{m_v P}{8.31T} = \frac{(m_v + m_d)d \cdot P}{8.31T} = \frac{[18.01d + 28.966(1-d)]d \cdot P}{8.31T}$$

The unit for C_v can be g/L or kg/m^3 and the latter kg/m^3 is used in this project.

Appendix VII. Details of the CPAP fluid dynamic section after ADU outlet

The CPAP fluid dynamic section after ADU outlet subsystem has been shown in Figure 4.5, section 4.2.1.2 and its details are shown below.

VII.1 The connecting duct airflow velocity subsystem

Figure VII. 1 shows the connecting duct airflow velocity subsystem which is created from Eq. (2.21). The model chooses average chamber air temperature and average chamber air density for fluid dynamic section to simplify the modelling as mentioned in chapter two. Chamber air capacity is given as the amount of 206ml as is filled at highest water level.

Input port number	Input	Unit
1	Pressure in chamber	Pascal
2	Airflow velocity in HADT	m/s

Its output is connecting duct airflow velocity in m/s.
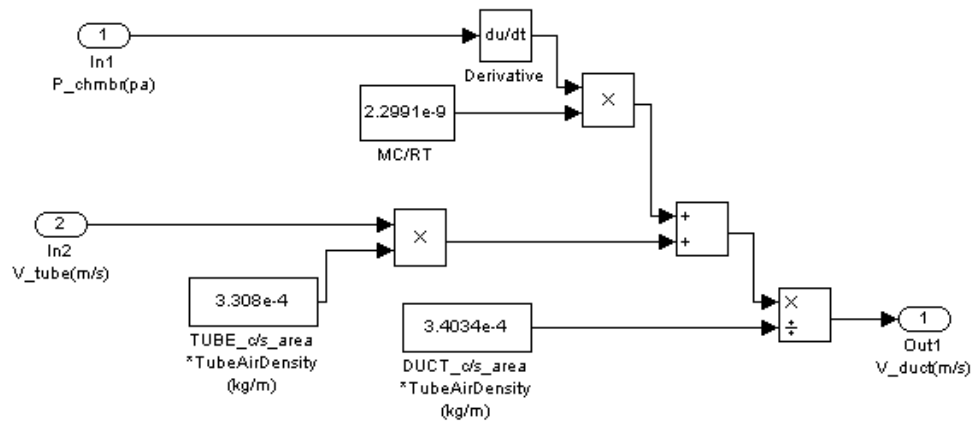
Figure VII. 1 Connecting duct Airflow Velocity Subsystem

VII.2 The chamber pressure subsystem

The chamber pressure subsystem is shown in Figure VII. 2. It is created from Eq. (2.16) . Value of 13.36 in block "Duct P/V-coef" is calculated from $\dfrac{0.8451}{D_D(\dfrac{D_D\rho_{Da}}{\eta_{Da}})^{0.1679}}$.

Inputs to this subsystem are listed below.

Input port number	Input	Unit
1	Pressure at ADU outlet	Pascal
2	Airflow velocity in connecting duct	m/s

Its output is dynamic chamber pressure in Pascal.
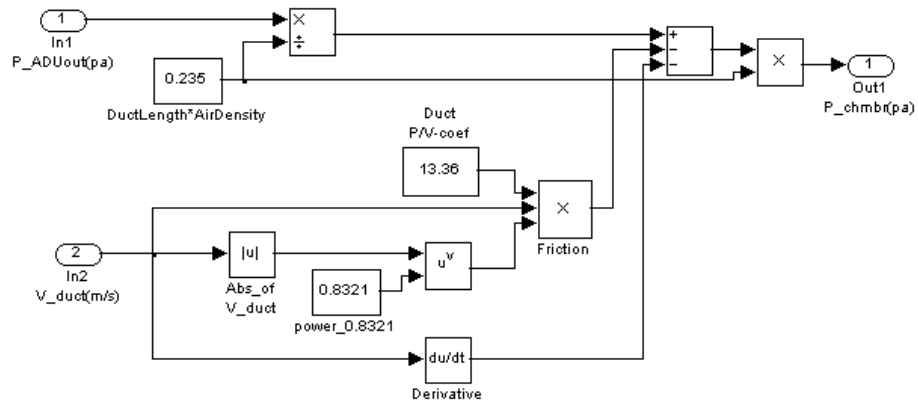
Figure VII. 2 Chamber Pressure Subsystem

VII.3   The HADT airflow velocity subsystem

Figure VII. 3 shows the HADT airflow velocity subsystem created from Eq. (2.28). Again, air temperature and density in the mask are simplified as fixed average values. Inputs are listed below.

Input port number	Input	Unit
1	Pressure in the mask	Pascal
2	Patient's breath load	kg/s
3	Mask capacity	m^3

Its output is HADT airflow velocity in m/s.

Figure VII. 3 HADT Airflow Velocity Subsystem

VII.4 The mask pressure subsystem

Figure VII. 4 shows the mask pressure subsystem created from Eq. (2.24). Value of 5.63 in block "Tube P/V-coef" is calculated from $\dfrac{0.6328}{D_{Ti}(\dfrac{D_{Ti}\rho_{Ta}}{\eta_{Ta}})^{0.25}}$. Inputs are listed below.

Input port number	Input	Unit
1	Pressure in chamber	Pascal
2	Airflow velocity in HADT	m/s

The output is mask pressure in Pascal.

Figure VII. 4 Mask Pressure Subsystem

Appendix VIII.   Details of whole chamber steady state subsystem

The whole chamber steady state subsystem has been shown in Figure 4.15, section 4.3.1.1 and its details are shown below.

VIII.1   The CPAP chamber inlet temperature subsystem

Figure VIII. 1 is the subsystem calculating the chamber inlet temperature. It is based on Eq. (3.5) and Eq. (3.6). Inputs to this subsystem are listed below.

Input port number	Input	Unit
1	Ambient air temperature	°C
2	CPAP pressure setting	cmH2O
3	Ambient air specific humidity	In decimal

The output is the chamber inlet temperature from ADU.
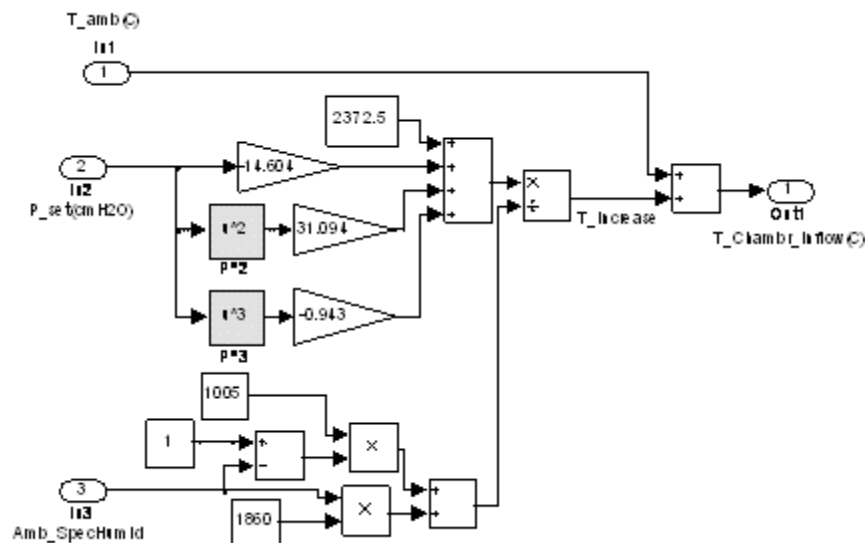
Figure VIII. 1 CPAP chamber inlet temperature subsystem

VIII.2   The CPAP chamber-water thermal balance subsystem

The subsystem is created based on Eq. (3.49). The water thermal balance subsystem is mainly for producing steady state water temperature with the simplification that the water temperature does not change along with breath-induced flow fluctuation as long as all the settings stay unchanged. Another output is evaporation rate under such steady state which can be used in comparison with breath-induced fluctuating evaporation rate.

Inputs to this water-centred subsystem are listed below.

Input port number	Input	Unit
1	Heat element temperature setting	°C
2	Ambient air specific humidity	In decimal
3	Pressure in chamber	Pascal
4	Average of fluctuating airflow velocities in HADT and the connecting duct	m/s
5	Ambient air temperature	°C
6	Portion of direct impact area to total water surface area	In decimal
7	Temperature of inlet to the chamber from ADU	°C
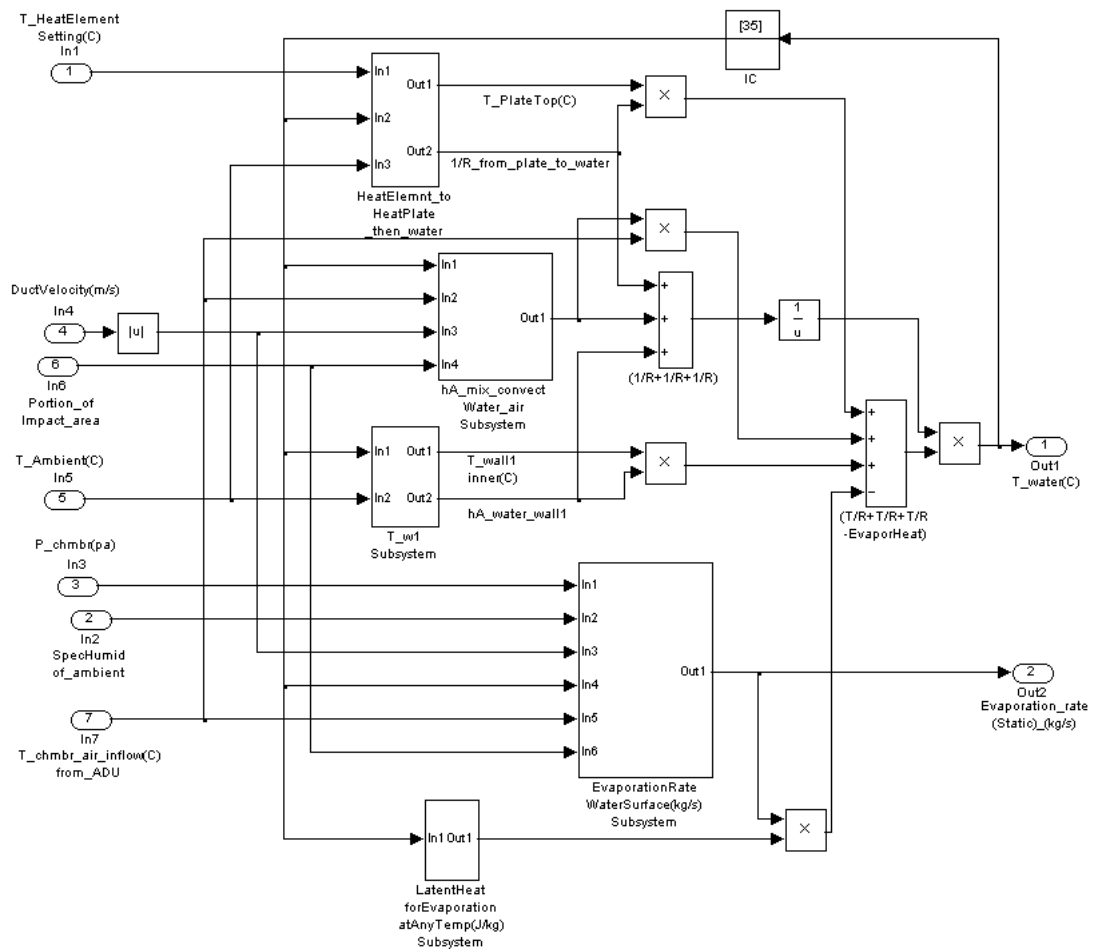
Figure VIII. 2 CPAP chamber-water thermal balance subsystem

The outputs from this subsystem are:

Output port number	Output	Unit
1	Water temperature	°C
2	Steady state evaporation rate	kg/s

This water-centred subsystem contains 5 subsystems which are listed below and described in sub-sections below.

- Heat element to water bottom second-level subsystem

- Water surface heat transfer second-level subsystem

- Water surface mass transfer (evaporation) subsystem

- Water surface evaporation latent heat calculation subsystem

- Lower chamber wall (wall 1) heat transfer subsystem

VIII.2.1   Heat element to water bottom subsystem

This subsystem is to produce heat-plate-top temperature and the reciprocal of total thermal resistance from heat plate to the bottom of water. It is based on Eq. (3.26).
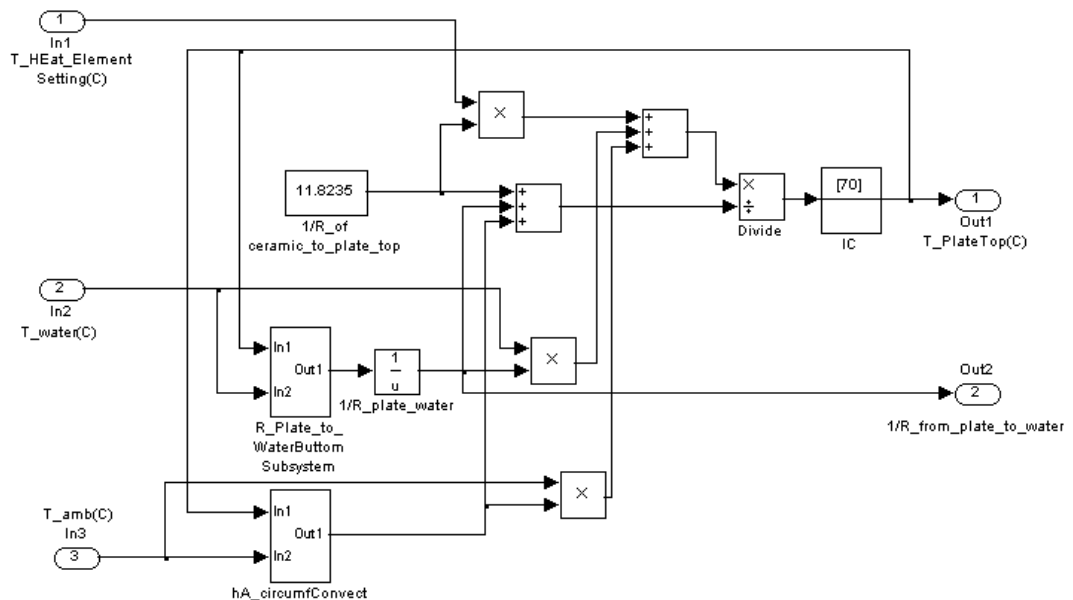
Figure VIII. 3 Heat element to water bottom thermal balance subsystem

Inputs to this subsystem are listed below:

Input port number	Input	Unit
1	Heat element temperature setting	°C
2	Water temperature	°C
3	Ambient air temperature	°C

The outputs from this subsystem are:

Output port number	Output	Unit
1	Heating plate top temperature	°C
2	Reciprocal of thermal resistance from heating plate top to water bottom	$(°C /W)^{-1}$

Both of the outputs will be used for calculating water temperature.

This subsystem contains several sub-subsystems in it. They are for calculating reciprocals of thermal resistances on the heat plate outer surface and the chamber base rim surface and total thermal resistance from heat plate to the bottom of the water. They are shown and explained below.

VIII.2.1.1 Total thermal resistance from heat plate to water bottom

This sub-subsystem is based on Eq. (3.17). Inputs to this subsystem are listed below.

Input port number	Input	Unit
1	Temperature on chamber base top	°C
2	Water temperature	°C

The output is the total resistance from heat plate top to water.
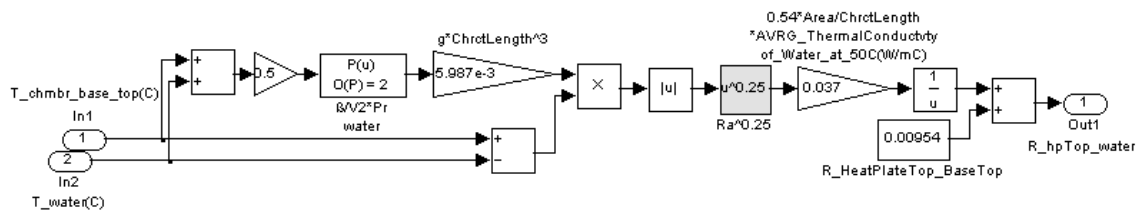
Figure VIII. 4 Total thermal resistance from heat plate to water bottom subsystem

There is a polynomial for calculating the coefficient combination $\dfrac{\beta \cdot \mathrm{Pr}}{v^2}$ of water. It is a function of chamber base to water interface temperature (see Appendix XV).

VIII.2.1.2 Subsystem of reciprocal of thermal resistances on heat plate circumferential outer surface

This subsystem is based on Eq. (3.24). Inputs to this subsystem are listed below:

Input port number	Input	Unit
1	Temperature on heat plate top	°C
2	Ambient air temperature	°C

The output is the reciprocal of the thermal resistances on heat plate circumferential outer surface.
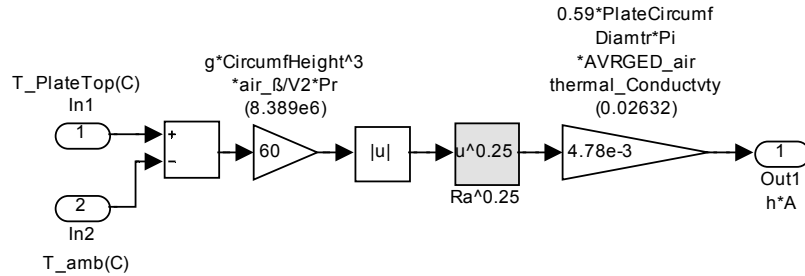
Figure VIII. 5 Heat plate circumferential outer surface subsystem

VIII.2.2   Water surface heat transfer subsystem

The water surface heat transfer subsystem is based on Eq. (3.39) but output is the reciprocal of the resistance. The total mixed Nusselt number is calculated by Eq. (3.38). Inputs to this subsystem are listed below.

Input port number	Input	Unit
1	Water temperature	°C
2	Temperature of inlet to the chamber from ADU	°C
3	Velocity of inlet to the chamber	m/s
4	Portion of impact area to total water surface area	Decimal

For the water thermal balance subsystem, it only considers the steady status so to calculate the stable water temperature as discussed in Chapter 3. The inlet uses the steady flow from ADU and inlet temperature is also of that. The input 3 is actually the average velocity of airflow at the outlet of the connecting duct and in the HADT and

input 4 is the portion of impact area to the total water-air interface area (50%). There is a polynomial for calculating air kinetic viscosity as a function of the interface film temperature (see Appendix XVI).
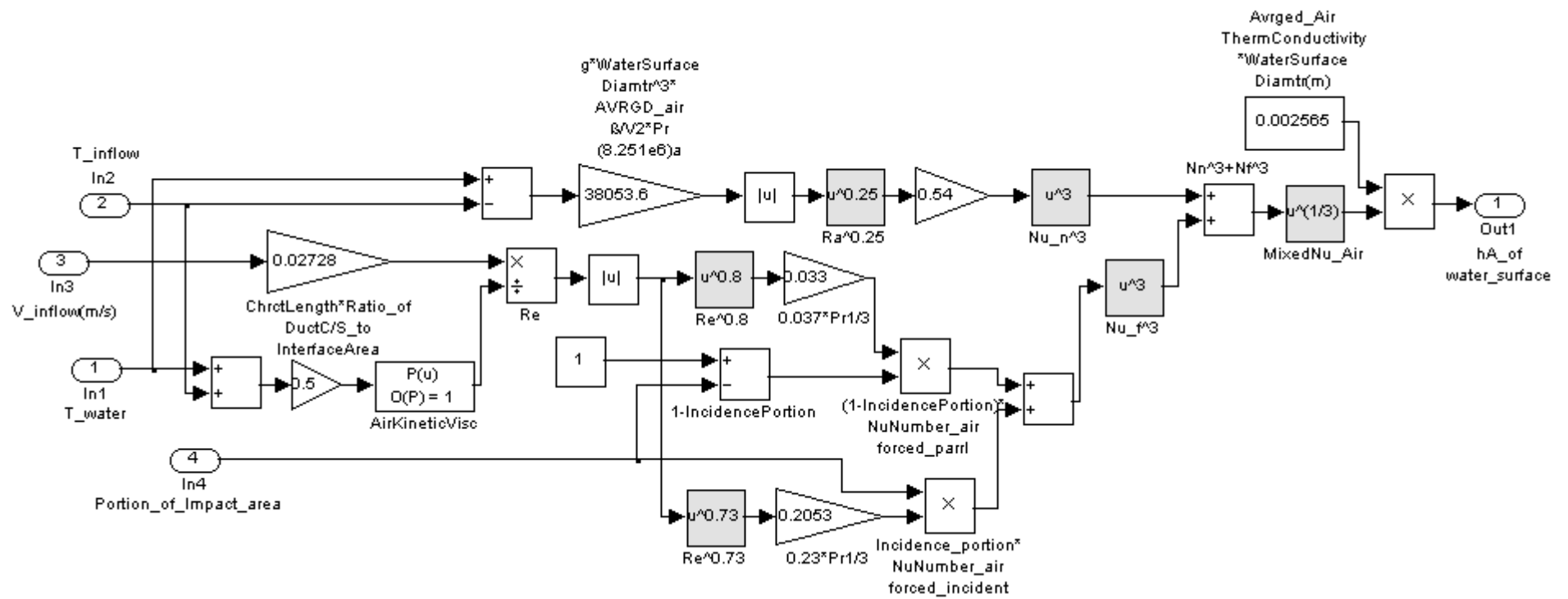
Figure VIII. 6 Water surface heat transfer subsystem

VIII.2.3   Water surface mass transfer (evaporation) subsystem

This water surface mass transfer (evaporation) subsystem is created based on Eq. (3.40). The mixed mass convection (evaporation) coefficient is calculated based on Eq. (3.44), Eq. (3.45) and Eq. (3.48).

Inputs to this subsystem are listed below.

Input port number	Input	Unit
1	Relative pressure in the chamber	Pascal
2	Ambient air specific humidity	In decimal
3	Velocity of air flowing into the chamber	m/s
4	Water temperature	°C
5	Temperature of inlet to the chamber from ADU	°C
6	Portion of impact area to total water surface area	In decimal

The output of this subsystem is steady state evaporation rate which is required for calculating the water temperature and can also be used in comparison with dynamic state evaporation rate obtained from dynamic chamber-air thermal balance subsystem.
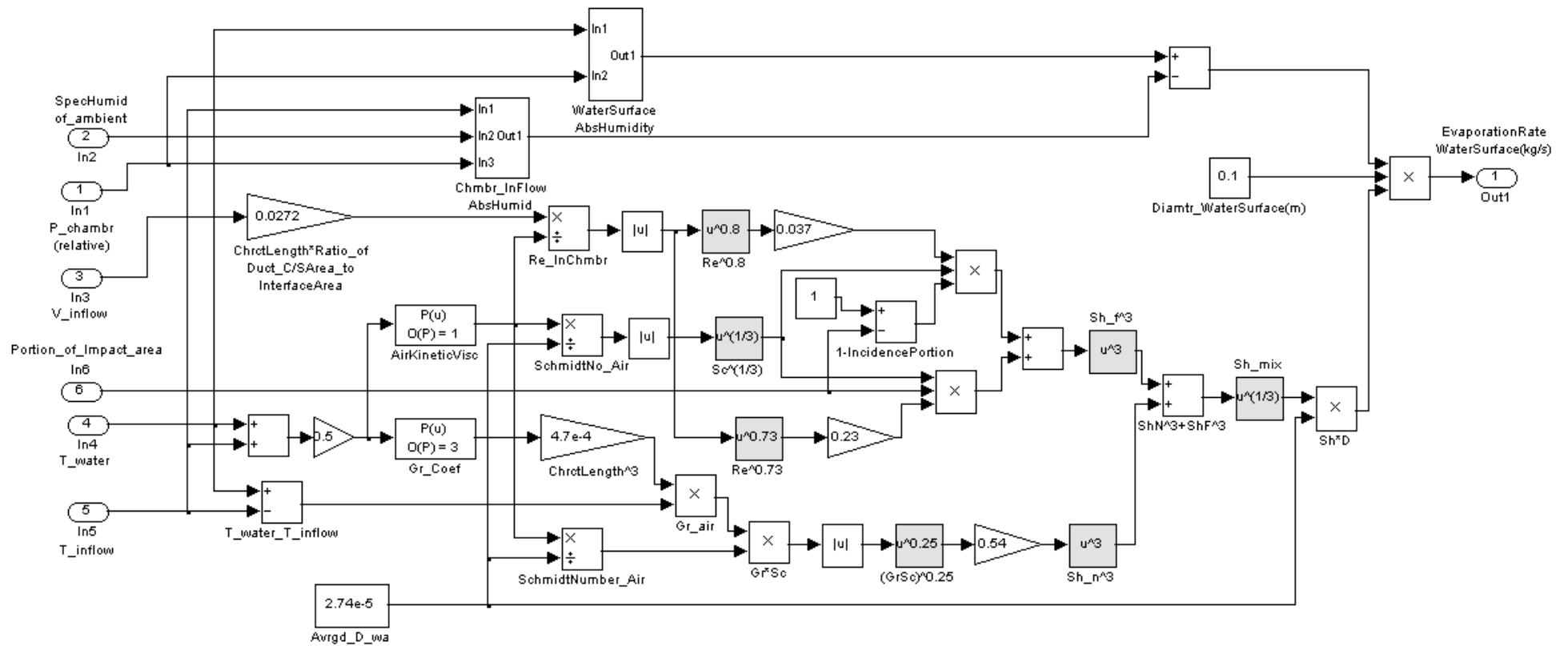
Figure VIII. 7 Water surface mass transfer (evaporation) subsystem

This subsystem also contains two subsystems:

- Inlet absolute humidity sub-subsystem
- Water surface saturated absolute humidity sub-subsystem

They are shown and explained below.

VIII.2.3.1 Chamber inlet absolute humidity sub-subsystem

The inlet absolute humidity sub-subsystem is based on Eq. (3.41). The pressure in this calculation is in kPa and *T* is temperature of inlet to the chamber in K. The conversion from specific humidity to absolute humidity is calculated and explained in Appendix VI.

Inputs to this subsystem are listed below.

Input port number	Input	Unit
1	Temperature of inlet to the chamber from ADU	°C
2	Ambient air specific humidity	In decimal
3	Relative pressure in chamber	Pascal
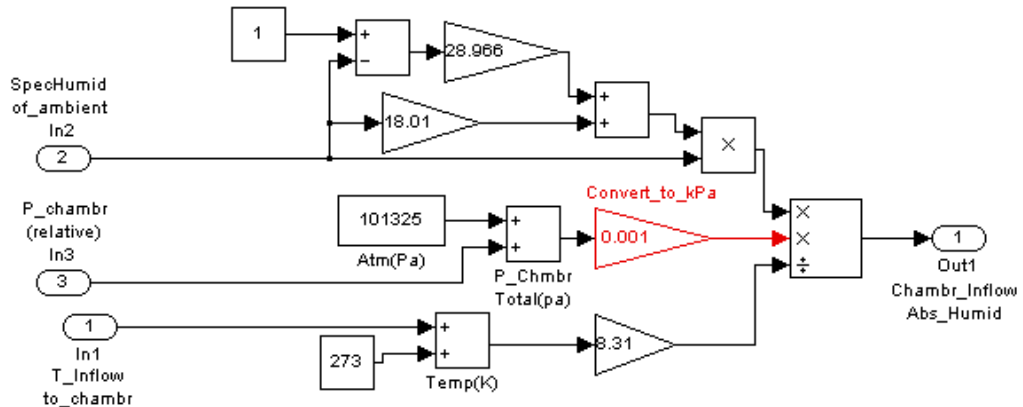
Figure VIII. 8 Chamber inlet absolute humidity subsystem

VIII.2.3.2 Chamber water surface saturated absolute humidity sub-subsystem

The chamber water surface saturated absolute humidity subsystem is based on the same Eq. (3.41). The differences are water temperature instead of airflow temperature and humidity is the saturated humidity at water temperature. The "RH_SpecHumid

Subsystem" is the same as the one described in section above but with the relative humidity input always as constant 1. The calculation is explained in Appendix VI.

Inputs to this subsystem are listed below:

Input port number	Input	Unit
1	Water temperature	°C
2	Relative pressure in the chamber	Pascal
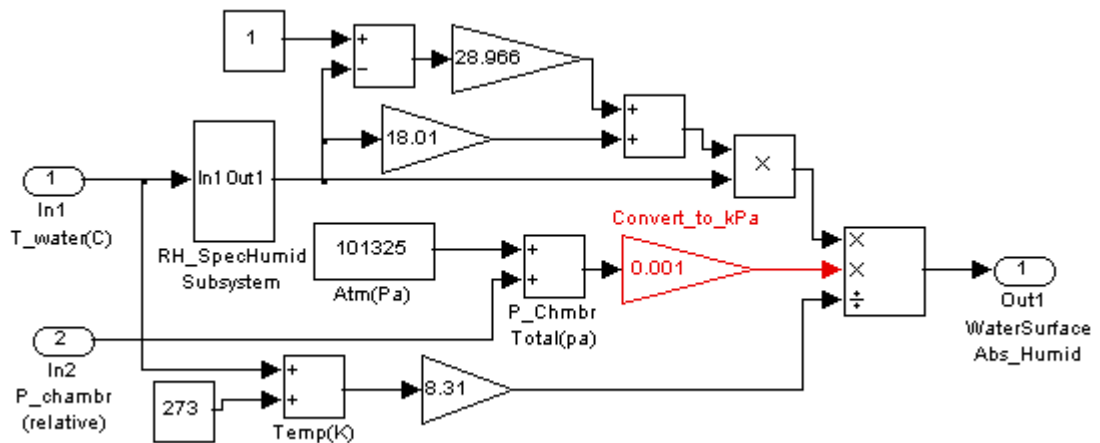
Figure VIII. 9 Chamber water surface saturated absolute humidity subsystem

VIII.2.4   Water surface evaporation latent heat calculation subsystem

The evaporation latent heat subsystem is created based on Eq. (3.43). Input to the subsystem is the water temperature.
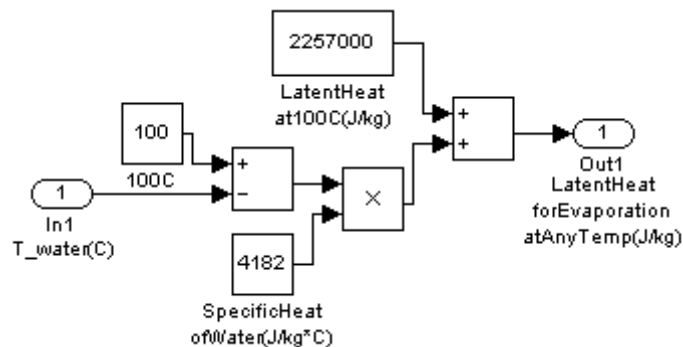
Figure VIII. 10 Water surface evaporation latent heat calculation subsystem

VIII.2.5   Chamber wall 1 heat transfer subsystem

This wall 1 heat balance and heat transfer subsystem is created based on Eq. (3.31).
Inputs to this subsystem are listed below:

Input port number	Input	Unit
1	Water temperature	°C
2	Ambient air temperature	°C
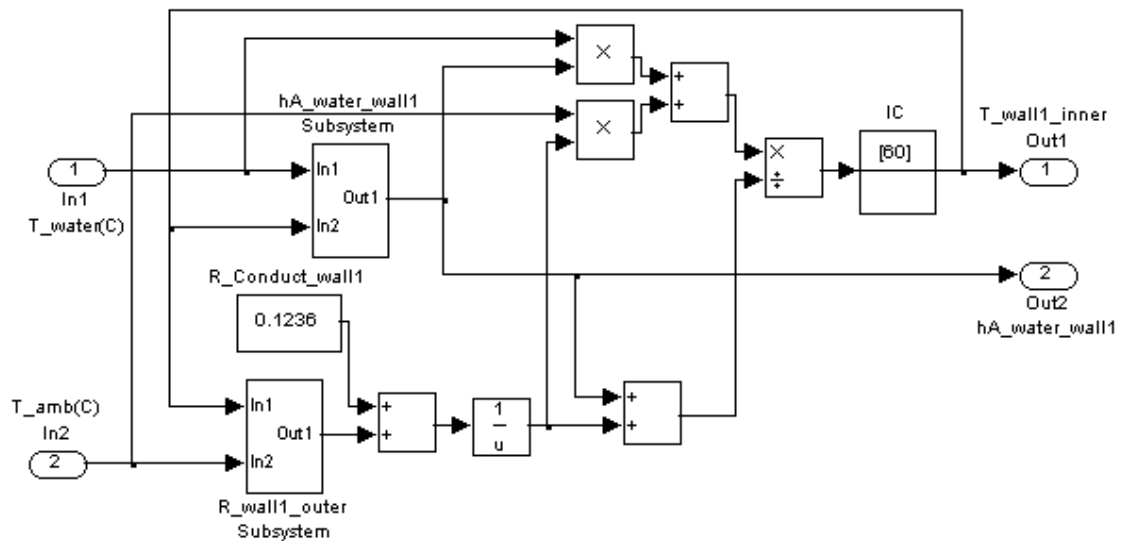
Figure VIII. 11 Chamber wall 1 heat transfer subsystem

The outputs from this subsystem are:

Output port number	Output	Unit
1	wall 1 inner surface temperature	°C
2	Reciprocal of natural convectional thermal resistance on wall 1 inner surface	$(°C /W)^{-1}$

These two outputs are used in the calculation of the water temperature. Wall 1 inner
surface temperature is used replacing outer surface temperature for calculating outer
surface resistances.

This subsystem also contains two sub-subsystems. The wall 1 inner surface natural
convectional thermal resistance subsystem and the outer surface heat dissipation
subsystem. They are shown below.

VIII.2.5.1 Wall 1 inner surface natural convectional thermal resistance subsystem

This subsystem actually gives out the reciprocal of the Wall 1 inner surface natural convectional thermal resistance.

Inputs to this subsystem are listed below.

Input port number	Input	Unit
1	Water temperature	°C
2	Wall 1 temperature	°C
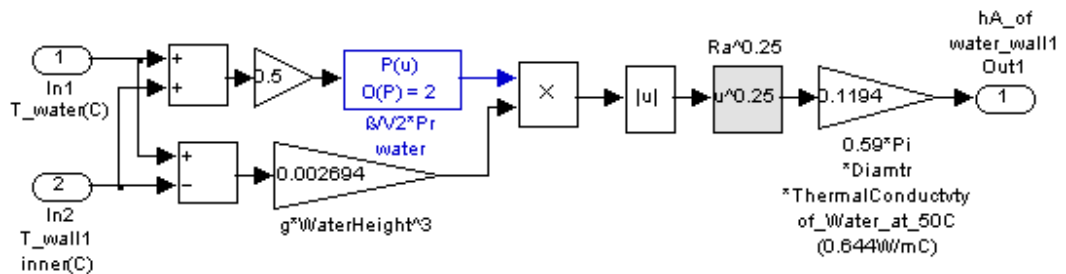
Figure VIII. 12 Wall 1 inner surface natural convectional thermal resistance subsystem

VIII.2.5.2 Wall 1 outer surface natural convectional and radiation thermal resistances subsystem

The subsystem is built based on natural convection calculation. Inputs to this subsystem are listed below.

Input port number	Input	Unit
1	Wall 1 temperature	°C
2	Ambient air temperature	°C
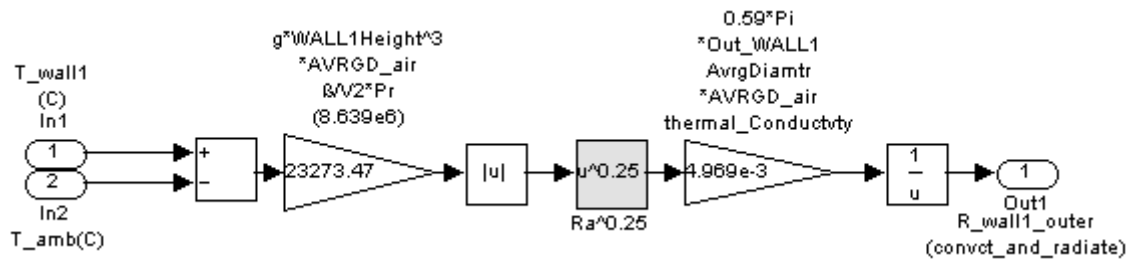
Figure VIII. 13 Wall 1 outer surface natural convectional and radiation thermal

VIII.3 The CPAP chamber-air thermal balance subsystem (steady state)

This steady state chamber-air thermal balance subsystem is to provide steady state in-chamber air temperature and temperature of wall 2 and wall 3 inner surfaces. The steady state in-chamber air temperature is used as properties of airflow going into HADT used in calculating of HADT lump 1 wall temperature. This subsystem is created based on Eq. (3.64).

Inputs to this subsystem are listed below.

Input port number	Input	Unit
1	In-chamber air specific humidity	In decimal
2	Ambient air temperature	°C
3	Ambient air specific humidity	In decimal
4	Pressure in the chamber	Pascal
5	Temperature of airflow entering the chamber	°C
6	Water temperature	°C
7	Velocity of air flowing into the chamber	m/s
8	Portion of impact area to total water surface area	In decimal
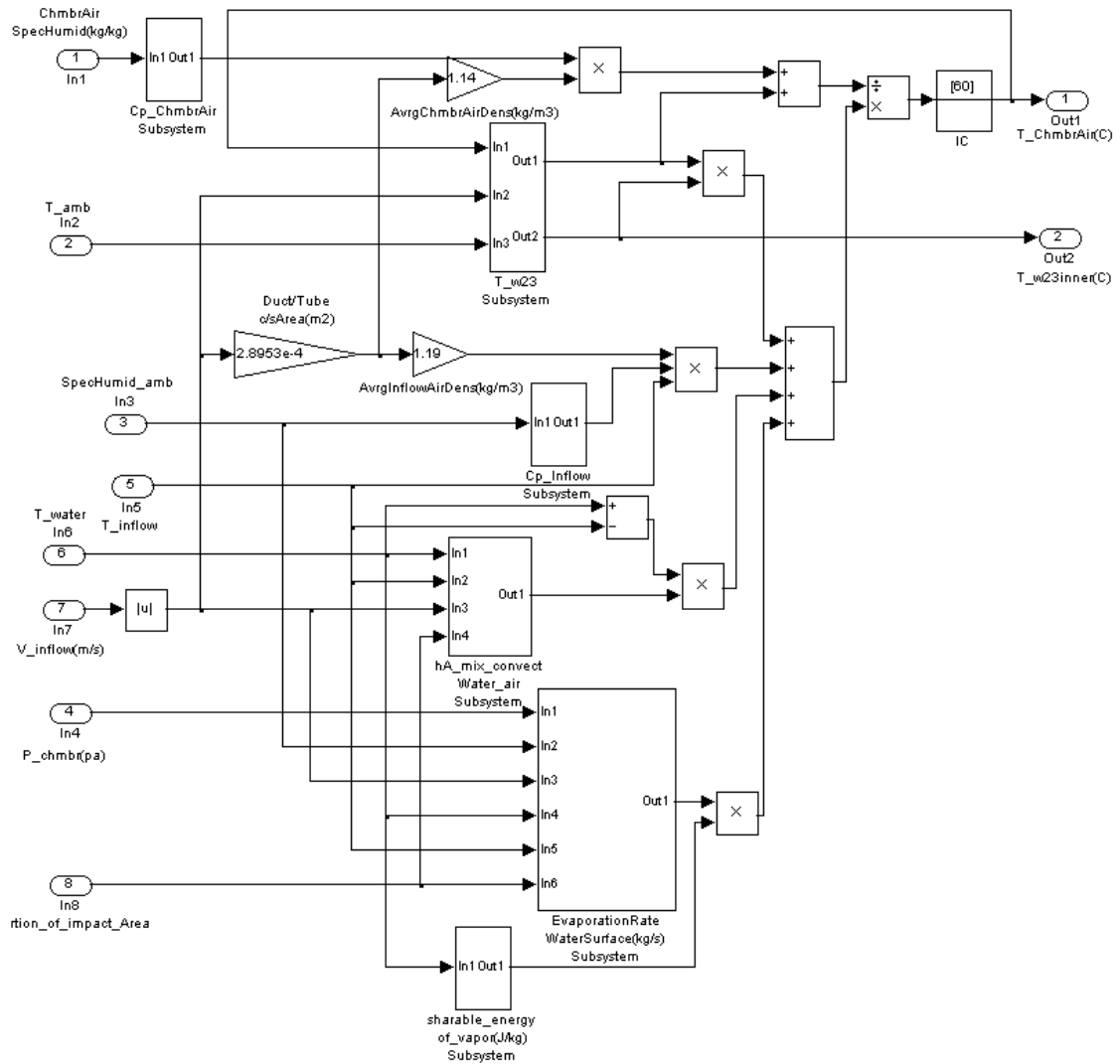
Figure VIII. 14 CPAP chamber-air steady state thermal balance subsystem

The outputs from this subsystem are:

Output port number	Output	Unit
1	Steady state chamber air temperature	°C
2	Wall 2 and 3 temperature	°C

This subsystem contains 6 subsystems which are listed below and will be described in following sub-sections.

- In-chamber air specific thermal capacity subsystem
- Chamber inlet specific thermal capacity subsystem
- Water surface convectional thermal resistance subsystem
- Evaporation rate subsystem
- Sharable energy from evaporated water molecules subsystem

- Wall 2 and 3 inner surface temperature subsystem

VIII.3.1   Water surface heat transfer subsystem

This subsystem is exactly the same as the one in section VIII.2.2 with the same name. However, the subsystem here is for calculating the heat the chamber air acquired from water through surface convection while the subsystem in section VIII.2.2 is for calculating the convectional heat loss from water to the chamber air through the same surface.

VIII.3.2   Water surface mass transfer (evaporation) subsystem

This subsystem is also exactly the same as the one in section VIII.2.3 with the same name. However, the subsystem here is for calculating amount of vapour gained from water while the subsystem used in section VIII.2.3 is for calculating the amount of water lost to chamber air through the same surface.

VIII.3.3   Sharable energy from vapour calculation subsystem

This simple subsystem provides the amount of energy stored in the evaporated water molecules which is sharable when the water vapour is mixing with air. Input to this subsystem is water temperature which is also the temperature of vapour molecules when escaping from the water.
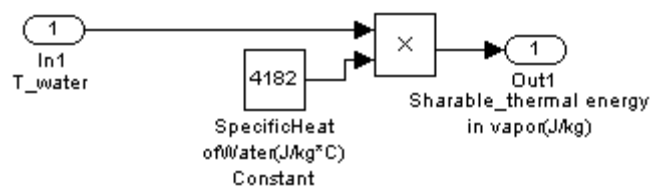
Figure VIII. 15 Sharable thermal energy from vapour calculation subsystem

VIII.3.4   In-chamber air specific thermal capacity subsystem

This subsystem is created based on Eq. (3.2). Input is specific humidity of air in the chamber. Output is specific thermal capacity of air in the chamber.
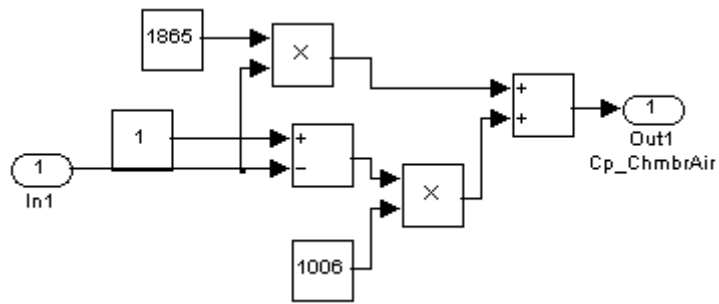
Figure VIII. 16 In-chamber air specific thermal capacity subsystem

VIII.3.5   Chamber inlet specific thermal capacity subsystem

This subsystem is the same as in section above. The only difference is that its input is specific humidity of inlet to the chamber.

VIII.3.6   Wall 2 and 3 inner surface temperature subsystem

This subsystem is created based on Eq. (3.59). Inputs to this subsystem are listed below.

Input port number	Input	Unit
1	In-chamber air temperature	°C
2	Velocity of air flowing into the chamber	m/s
3	Ambient air temperature	°C

Outputs from this subsystem are listed below.

Output port number	output	Unit
1	Reciprocal of mixed convectional thermal resistance on wall 2 and 3 inner surface	$(°C /W)^{-1}$
2	Wall 2 and 3 temperature	°C

Output 2 is temperature of the walls with simplifications as wall 2 and wall 3 have the same temperature and inner surface temperature replacing the wall temperature.
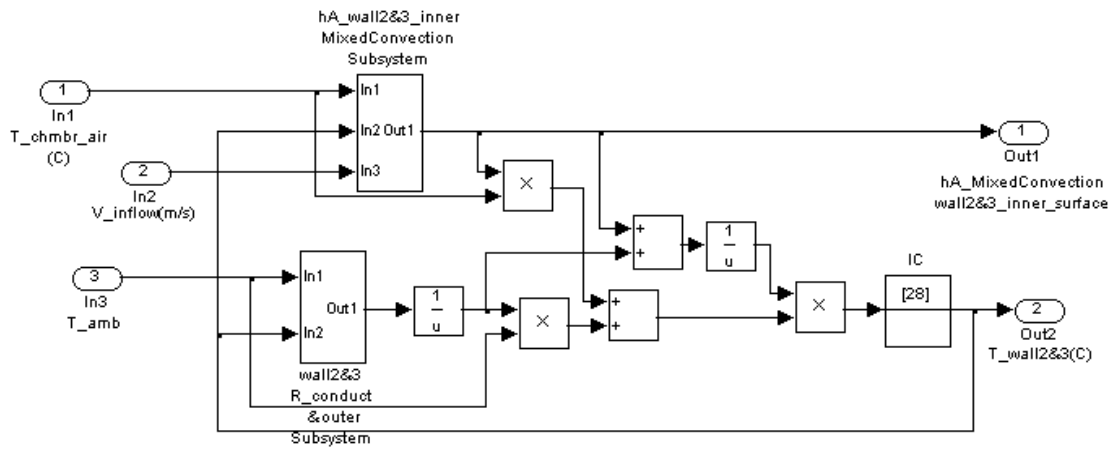
Figure VIII. 17 Chamber wall 2 and 3 inner surface temperature subsystem

This subsystem contains two sub-subsystems. They are shown and explained below.

VIII.3.6.1   Wall 2 and 3 inner surface thermal resistance subsystem

This subsystem is created based on Eq. (3.61). The output is the reciprocal of the resistance.
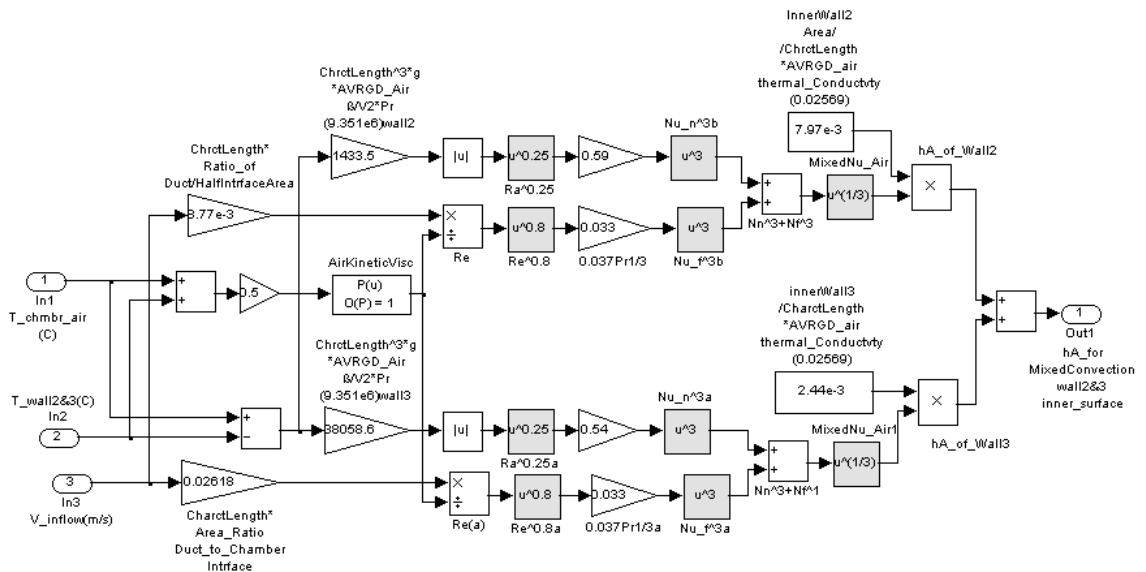
Figure VIII. 18 Chamber wall 2 and 3 inner surface thermal resistance subsystem

VIII.3.6.2   Wall 2 and 3 conductive and outer surface resistance subsystem

This subsystem is created for calculating the thermal resistance from wall 2 and 3 inner surface to ambient air. It is actually based on Eq. (3.62) and Eq. (3.63). Since thermal conductivity of the chamber wall material Polyethylene is considered constant within

the working temperature range thus Eq. (3.62) is simplified as a constant value of 0.2205°C /W for the conductive thermal resistance R_{C23}.
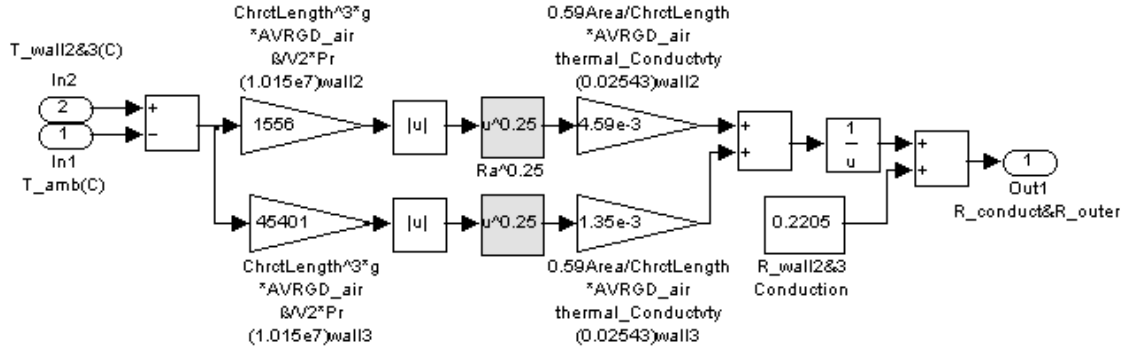
Figure VIII. 19 Chamber wall 2 and 3 conductive and outer surface resistance subsystem

VIII.4 In-chamber air specific humidity calculation subsystem

This subsystem is created for calculating the specific humidity of air in the chamber. It is actually a calculation of the mixing of the inlet and the evaporated water vapour. It is based on Eq. (3.66) i.e. $d_{Ca} = \dfrac{d_{\infty} \cdot \dot{m}_C + \dot{m}_{ev}}{\dot{m}_C}$. However, when the flow rate is near zero, the calculated specific humidity level from Eq. (3.66) is extraordinarily high. This makes the result unreal and the model stuck. In fact the change of total vapour amount in the chamber is far from so significant as the calculated result since the extremity occurs only when flow rate is very small. To get rid of the influence of such unreal calculated result, a saturation-control subsystem is placed after this subsystem to curb the result no more than saturation level. Thus this subsystem contains two subsystems. One is for calculating the specific humidity of in-chamber air after such mixing and another following this is the humidity-level curbing subsystem using saturation controlling. They are shown below.
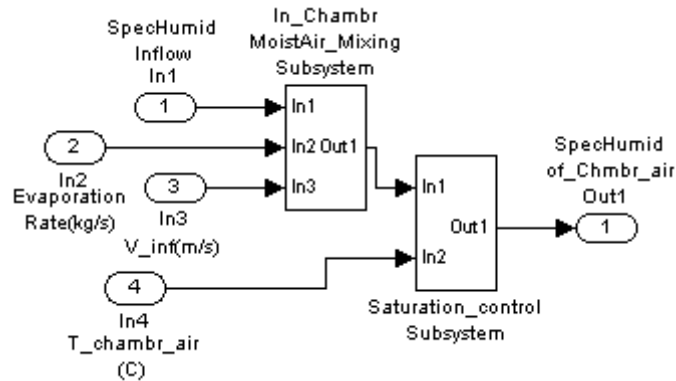
Figure VIII. 20 In-chamber air specific humidity calculation subsystem

216

Inputs to this subsystem are listed below.

Input port number	Input	Unit
1	Specific humidity of chamber inlet	In decimal
2	Dynamic evaporation rate	kg/s
3	Velocity of air flowing into the chamber	m/s
4	In-chamber air temperature	°C

VIII.4.1   In-chamber air mixing for specific humidity subsystem

This sub-subsystem is based on Eq. (3.66).
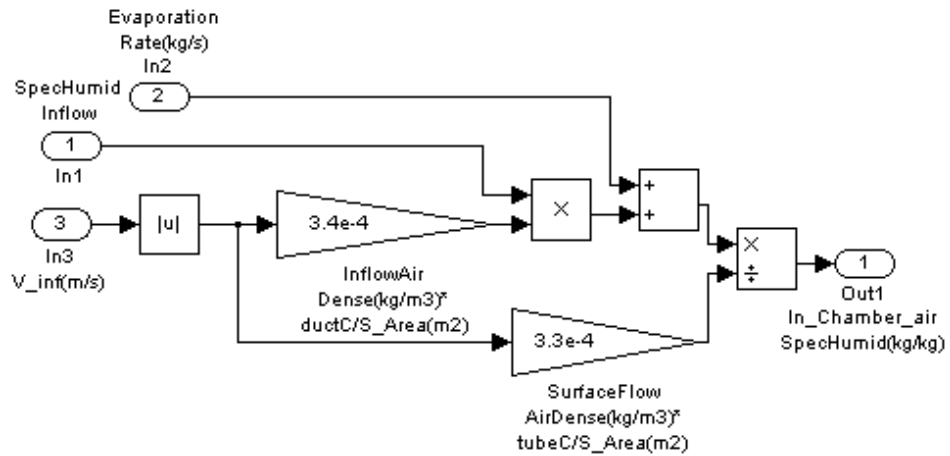
Figure VIII. 21 In-chamber air mixing for specific humidity subsystem

VIII.4.2   In-chamber air specific humidity curbing subsystem

This subsystem is for curbing the unreal high specific humidity level from calculation when air flow velocity is near zero (see Appendix VI for calculation details). Output from this subsystem is the in-chamber air specific humidity curbed by the chamber air temperature.
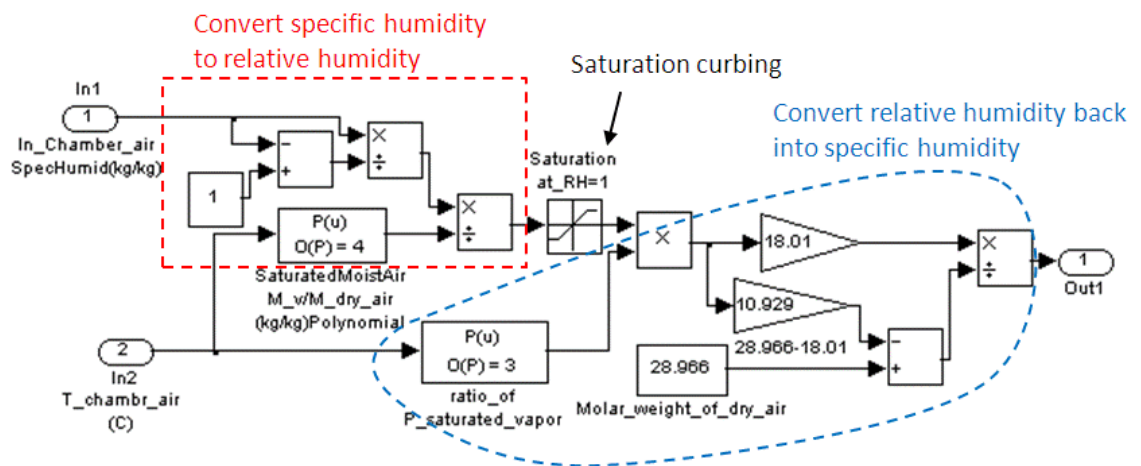
Figure VIII. 22 In-chamber air specific humidity curbing subsystem

Appendix IX. Details of steady state HADT lump full thermal balance subsystem

The steady state HADT lump full thermal balance subsystem has been shown in Figure 4.18, section 4.3.2.1 and its details are shown below.

IX.1 The HADT lump wall temperature subsystem

This subsystem is created for calculating the HADT wall temperature at the inspected lump. It is based on Eq. (3.80).
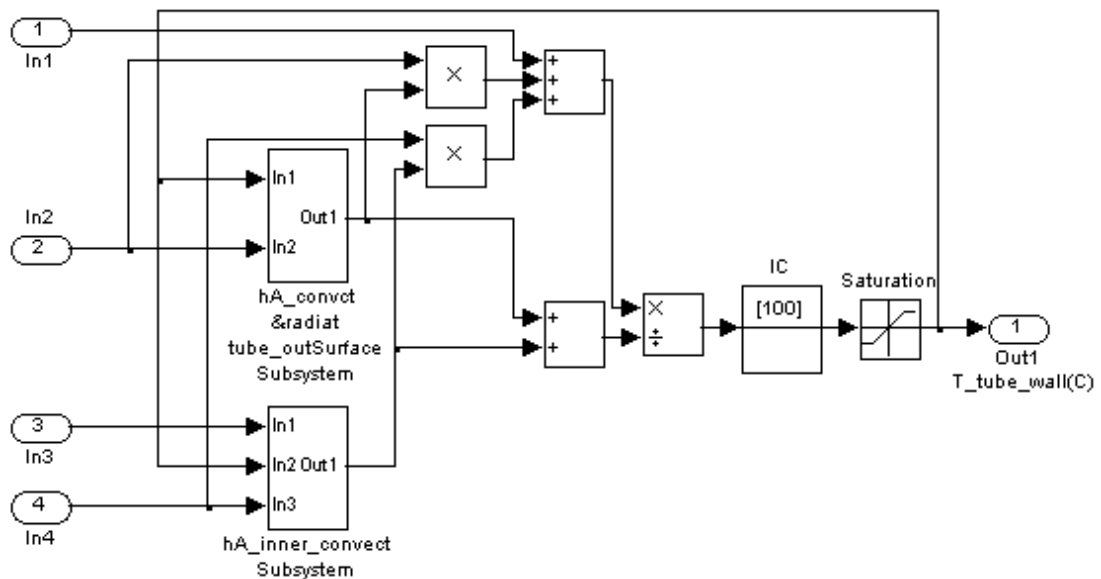
Figure IX. 1 The HADT lump wall temperature subsystem

Inputs to this subsystem are listed below:

Input port number	Input	Unit
1	Tube heating power to each lump (1/30 of the total)	W
2	Ambient air temperature	°C
3	Steady state airflow velocity in HADT	m/s
4	Steady state temperature of air in the lump	°C

This subsystem contains two subsystems. Details of them are shown below.

IX.1.1   The HADT lump wall inner surface thermal resistance subsystem
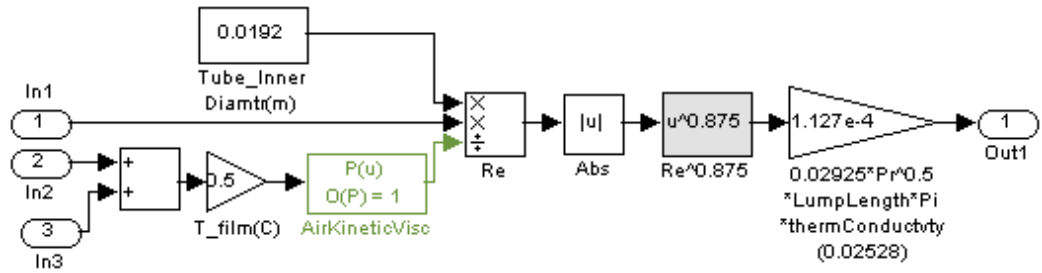
Figure IX. 2 The HADT lump wall inner surface thermal resistance subsystem

This sub-subsystem is created based on Eq. (3.73).

Inputs to this subsystem are listed below:

Input port number	Input	Unit
1	Steady state airflow velocity in HADT	m/s
2	HADT wall temperature at the lump	°C
3	Steady state temperature of air in the lump	°C

IX.1.2   The HADT lump wall outer surface thermal resistance subsystem

This subsystem is created based on Eq. (3.77).

Inputs to this subsystem are listed below:

Input port number	Input	Unit
1	HADT wall temperature at the lump	°C
2	Ambient air temperature	°C
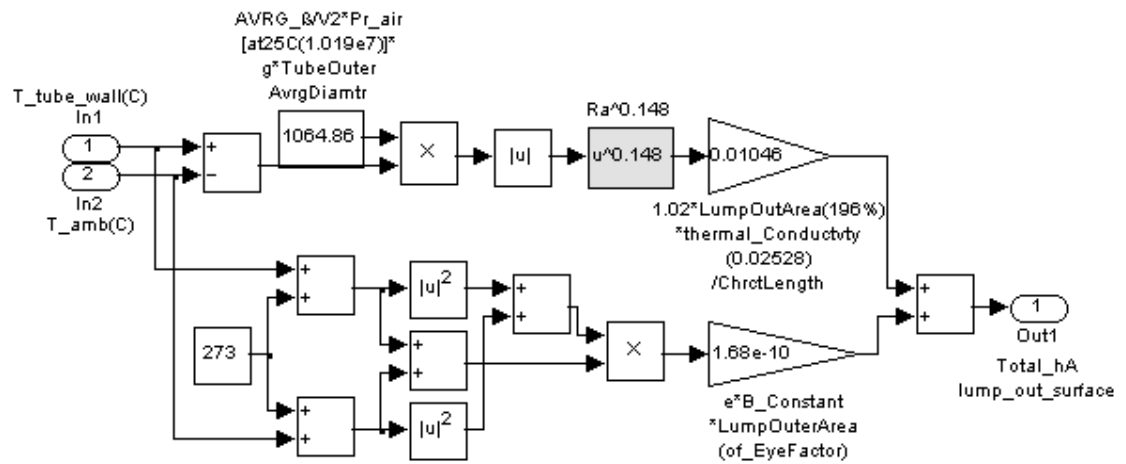
Figure IX. 3 The HADT lump wall outer surface thermal resistance subsystem

IX.2 The steady state lump air temperature subsystem

This subsystem is created for calculating the air temperature in the inspected lump. It is based on Eq. (3.79). Inputs to this subsystem are listed below:

Input port number	Input	Unit
1	Temperature of inlet to the lump	°C
2	Steady state airflow velocity in HADT	m/s
3	HADT wall temperature at the lump	°C
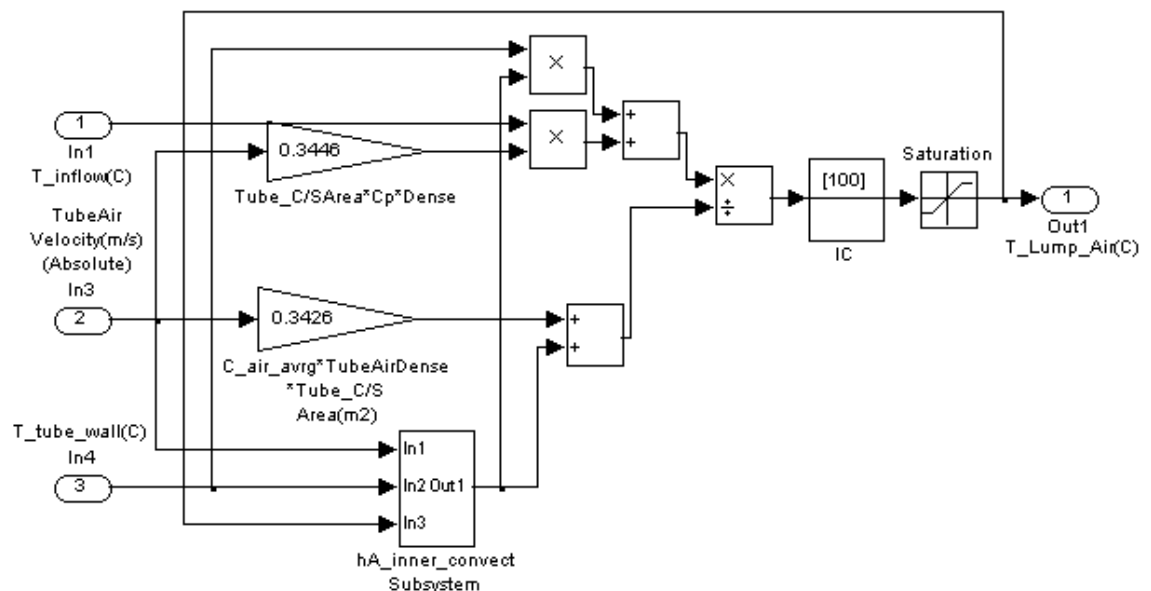
Figure IX. 4 Steady state lump air temperature subsystem

There is a subsystem in it for calculating the HADT lump wall inner surface thermal resistance which is the same as the one in the HADT lump wall temperature subsystem above.

IX.3   Flow dew point and HADT lump wall temperature gap subsystem

The dew point and HADT wall temperature comparison subsystem is used for determine condensation under steady state. The dew point calculation is based on Eq. (3.82).

Inputs to this subsystem are listed below:

Input port number	Input	Unit
1	HADT wall temperature at the lump	°C
2	Specific humidity of HADT steady state airflow	In decimal
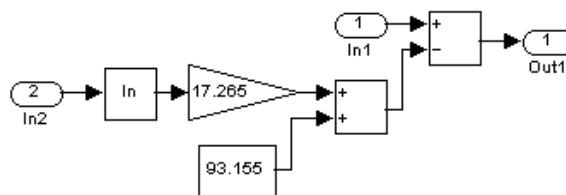
Figure IX. 5 Flow dew point and HADT lump wall temperature gap subsystem

Appendix X. Details of HADT lump air dynamic fluctuating thermal balance and condensation subsystem

The HADT lump air dynamic fluctuating thermal balance and condensation subsystem has been shown in Figure 4.19, section 4.3.2.2 and its details are shown below.

X.1 Dynamic fluctuating lump air thermal balance subsystem

The subsystem contains a one-lump delay subsystem for temperature signal transportation, two half-lump delay subsystems for specific humidity signal transportation and a dynamic fluctuating lump air temperature subsystem for calculating the fluctuating air temperature in the lump.
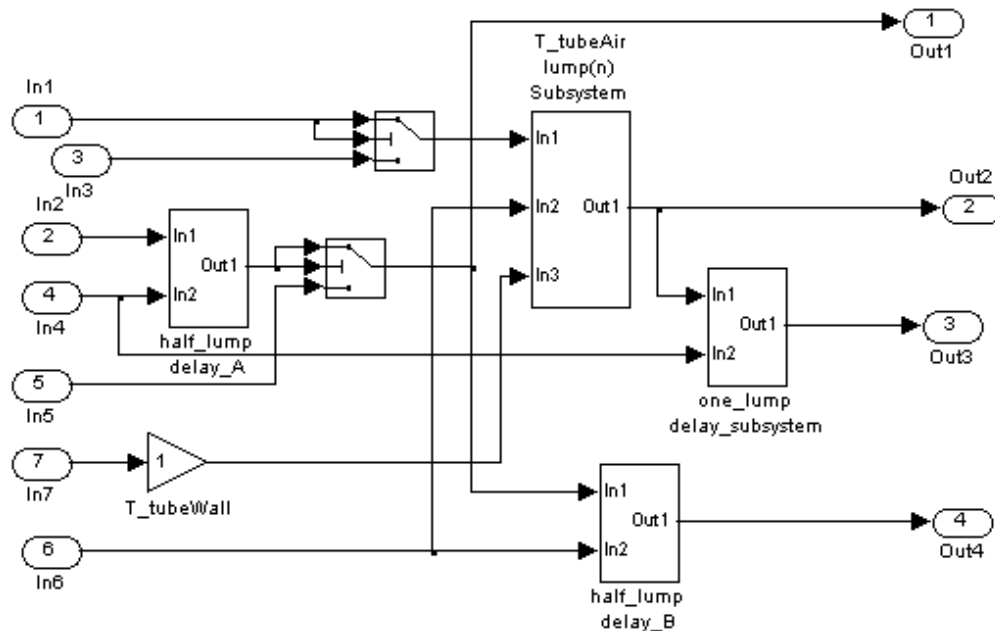
Figure X. 1 Dynamic fluctuating lump air thermal balance subsystem

Inputs to this subsystem are listed below:

Input port number	Inputs	Unit
1	Temperature of air flowing into the lump	°C
2	Specific humidity of air flowing into the lump	In decimal
3	Initial in-tube air temperature	°C
4	Fluctuating airflow velocity in HADT	m/s
5	Ambient air specific humidity	In decimal

6	Fluctuating airflow absolute velocity in HADT	m/s
7	HADT wall temperature at the lump	°C

The outputs are listed in table below.

output port number	output	Unit
1	Specific humidity of air in the lump	In decimal
2	Fluctuating temperature of air in the lump	°C
3	Air temperature of outlet from the lump	°C
4	Specific humidity of outlet from the lump	In decimal

The included dynamic fluctuating lump air temperature subsystem is shown below:
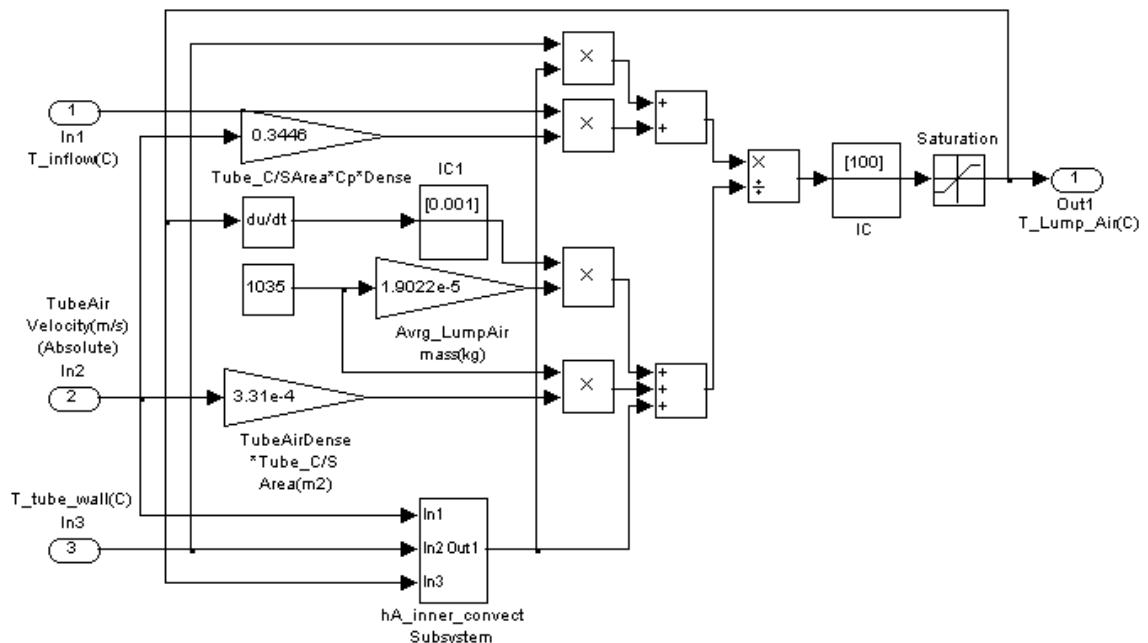
Figure X. 2 Dynamic fluctuating lump air temperature subsystem

This subsystem is created for calculating the dynamic fluctuating air temperature in the inspected lump. It is based on Eq. (3.79).

Inputs to this subsystem are listed below:

Input port number	Input	Unit
1	Temperature of inlet to the lump	°C

2	Absolute value of airflow velocity in HADT	m/s
3	HADT wall temperature at the lump	°C

This subsystem contains a sub-subsystem for calculating reciprocal of convectional thermal resistance on the inner surface of the HADT lump which is the same as the one in the HADT lump wall temperature subsystem above.

X.2 Dynamic fluctuating HADT lump condensation/evaporation Subsystem

This subsystem is for calculating the dynamic fluctuating HADT lump condensation/evaporation and the breath-cycle-wise net condensation/evaporation. The dynamic fluctuating HADT lump condensation/evaporation is calculated based on Eq. (3.83).
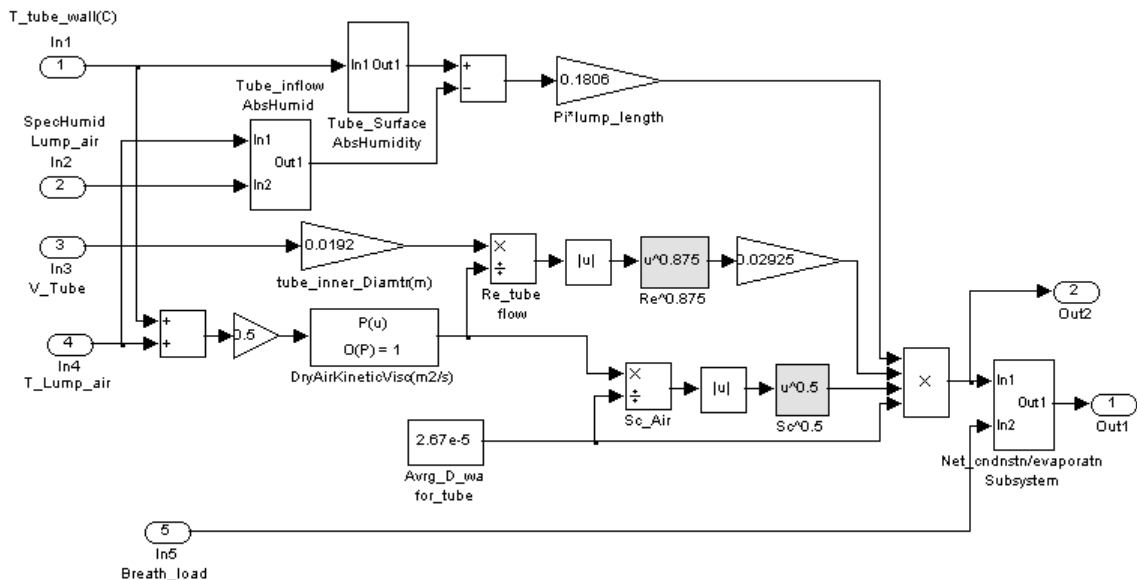
Figure X. 3 Dynamic fluctuating HADT lump condensation or evaporation Subsystem

Inputs to this subsystem are listed below:

Input port number	Input	Unit
1	HADT wall temperature at the lump	°C
2	Specific Humidity of air in the lump	In decimal
3	Airflow velocity in HADT	m/s
4	Air temperature in the lump	°C
5	Breath load (for integration control)	g/s

The outputs are listed in table below.

output port number	output	Unit
1	Net condensation/evaporation rate (over a breath cycle)	kg/s
2	Fluctuating condensation/evaporation rate	kg/s

The details of the two subsystems are shown below.

X.2.1   HADT inner surface absolute humidity subsystem

This subsystem is for determine the saturated absolute humidity at the temperature of the HADT lump wall inner surface. The details for the saturated absolute humidity calculation is in Appendix VI. The input is the wall temperature at the lump.
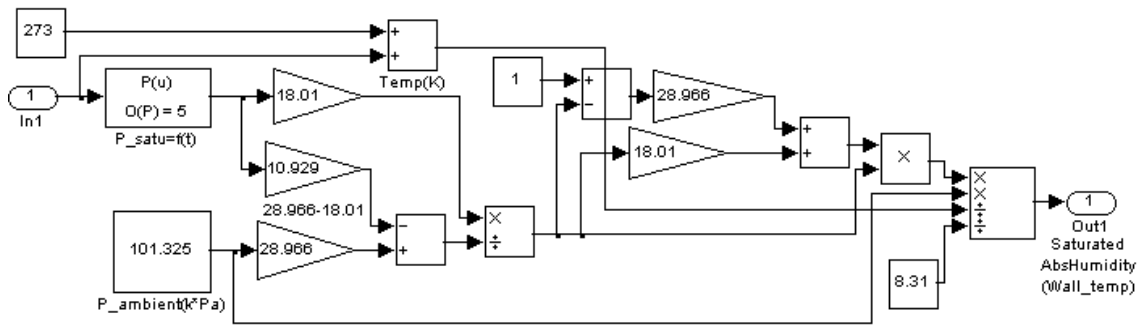
Figure X. 4 HADT inner surface absolute humidity subsystem

X.2.2   HADT lump inlet absolute humidity subsystem

This subsystem is to convert specific humidity to absolute humidity for the airflow in the lump. The details for the absolute humidity calculation is in Appendix VI.

Inputs to this subsystem are listed below:

Input port number	Input	Unit
1	Air temperature in the lump	°C
2	Specific Humidity of air in the lump	In decimal
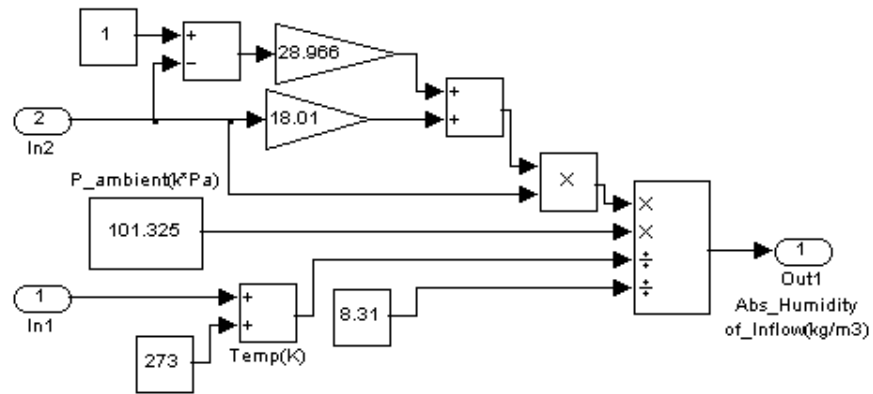
Figure X. 5 HADT lump inlet absolute humidity subsystem

X.2.3   Integration for breath-cycle-wise net condensation/evaporation subsystem

This subsystem is for calculating the breath-cycle-wise net condensation/evaporation.

It is created based on Eq. (3.87) and Eq. (3.88).

Inputs to this subsystem are listed below.

Input port number	Input	Unit
1	Fluctuating condensation/evaporation rate	kg/s
2	Breath load (for integration control)	g/s

The output from it is a sum of two integrals within a breath cycle which means the net condensation/evaporation within the same period.
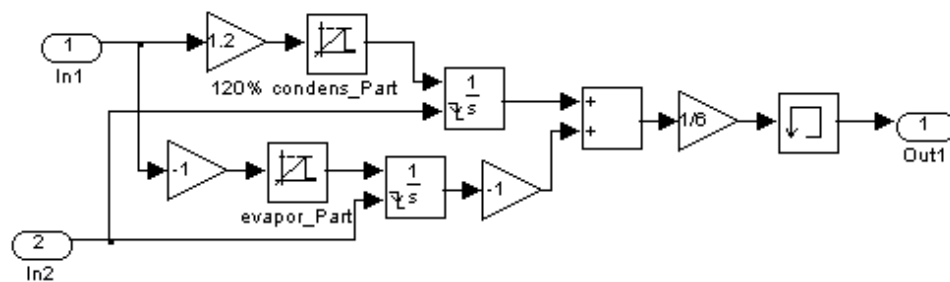
Figure X. 6 Integration for breath-cycle-wise net condensation/evaporation subsystem

Appendix XI. Details of steady state mask full thermal balance subsystem

The Steady state mask full thermal balance subsystem has been shown in Figure 4.21, section 4.3.3.1 and its details are shown below.

XI.1 Average inlet temperature subsystem

This simple subsystem is to obtain the average mask inlet temperature for steady state heat balance calculation so the mask wall temperature under breathing-added scenario. The input is the airflow temperature from HADT lump 30.
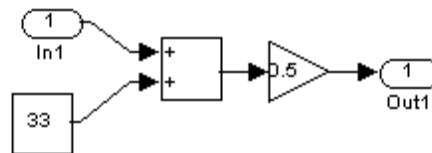
Figure XI. 1 Average mask inlet temperature subsystem

XI.2 Steady state mask mixing and in-mask velocity subsystem

The "Steady state mask mixing and in-mask velocity subsystem" is to obtain the averaged absolute values of in-mask volumetric flow rate and characteristic velocity under breathing-added scenario. The in-mask characteristic velocity is based on Eq.(3.90).

Inputs of the subsystem are listed below.

Input port number	Input	Unit
1	Half of Plate 1 inner width	m
2	Mask inner height	m
3	Average mass flow rate in the mask (absolute value)	g/s

Outputs of the subsystem are listed below:

output port number	output	Unit
1	Average volumetric flow rate in the mask(absolute value)	m^3/s
2	Average velocity in the mask(absolute value)	m/s
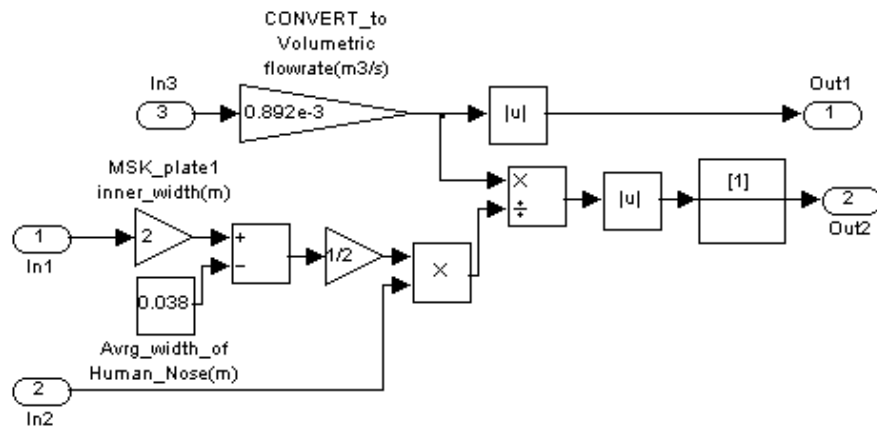
Figure XI. 2 Steady state mask mixing and in-mask velocity subsystem

XI.3 Steady state mask thermal balance subsystem

This subsystem contains an in-mask steady state air temperature subsystem and a mask wall temperature subsystem.

The inputs are listed in table below.

Input port number	Input	Unit
1	Average mask inlet temperature	°C
2	Average volumetric flow rate in the mask(absolute value)	m³/s
3	Length of the triangular plate inner surface	m
4	Half width of the triangular plate inner surface	m
5	Average velocity in the mask(absolute value)	m/s
6	Length of the triangular plate outer surface	m
7	Half width of the triangular plate outer surface	m
8	Ambient air temperature	°C
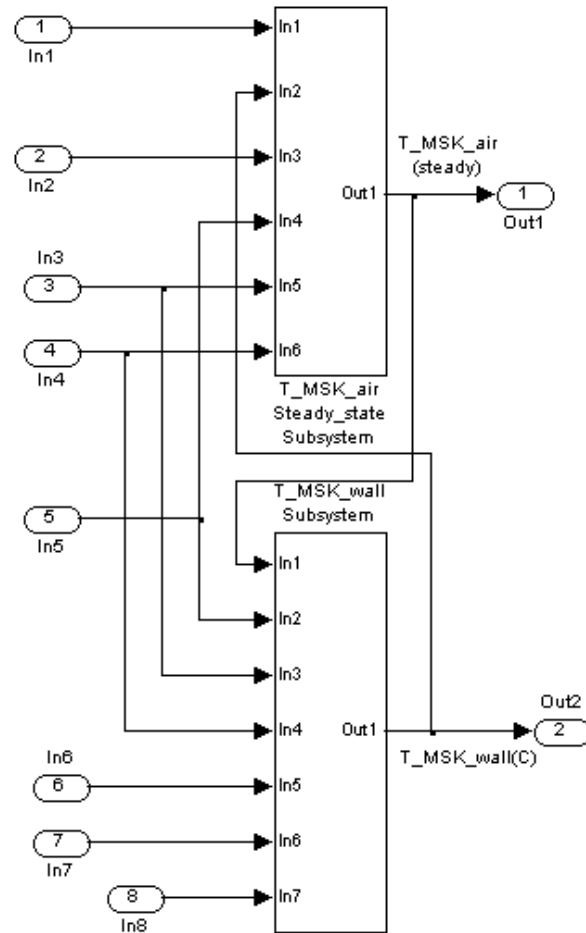
Figure XI. 3 Whole mask steady state thermal balance subsystem

The outputs are listed in table below.

output port number	output	Unit
1	Steady air temperature in the mask (for reference)	°C
2	Temperature of mask wall with heat dissipation	°C

Details of the contained "Mask wall temperature subsystem" and "Steady state mask air temperature subsystem" are shown below.

XI.3.1   Steady state mask wall temperature subsystem

This subsystem is to obtain the mask wall temperature. It is created based on Eq. (3.94).
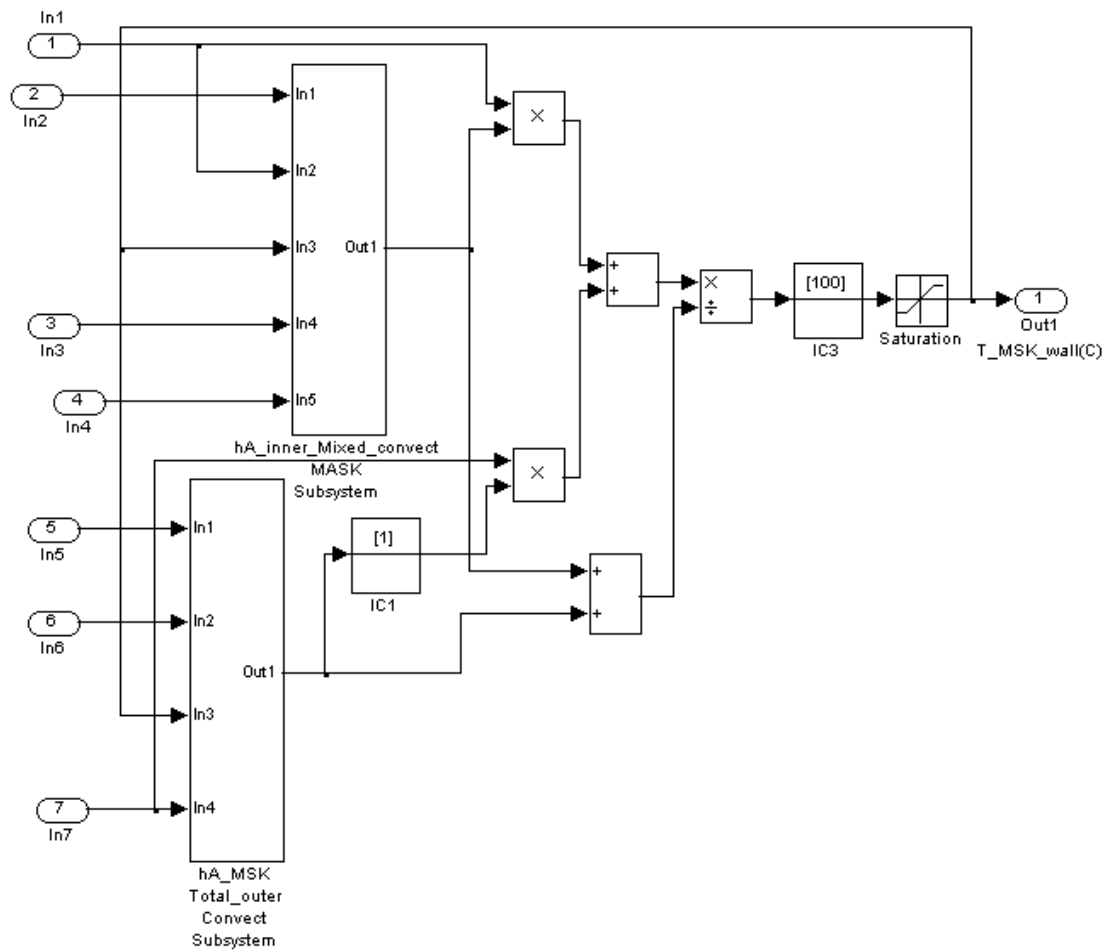
Figure XI. 4 Steady state mask wall temperature subsystem

The inputs are listed in table below.

Input port number	Input	Unit
1	Steady air temperature in the mask (for reference)	°C
2	Average velocity in the mask(absolute value)	m/s
3	Length of the triangular plate inner surface	m
4	Half width of the triangular plate inner surface	m
5	Length of the triangular plate outer surface	m
6	Half width of the triangular plate outer surface	m
7	Ambient air temperature	°C

The contained subsystems are shown and explained below.

XI.3.1.1 Mask outer surface thermal resistance subsystem

The subsystem for outer surface natural convection is shown in Figure XV 1. As discussed in chapter 3, the outer surface convection is considered as only exists on the triangular wall since the rectangular side walls are silicon seal and foam insulated.

The inputs are listed in table below.

Input port number	Input	Unit
1	Length of the triangular plate outer surface	m
2	Half width of the triangular plate outer surface	m
3	Temperature of mask wall with heat dissipation	°C
4	Ambient air temperature	°C
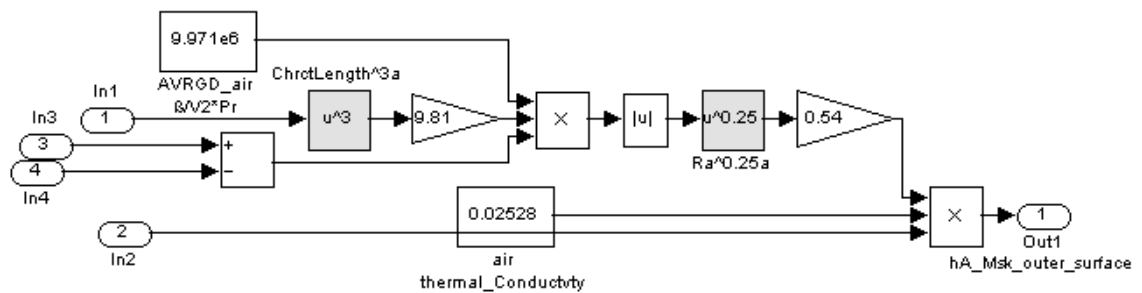
Figure XI. 5 Mask outer surface thermal resistance subsystem

XI.3.1.2 Mask inner surface thermal resistance subsystem

The subsystem for outer surface natural convection is shown above. Again the inner surface convection is also considered as only exists on the triangular wall.
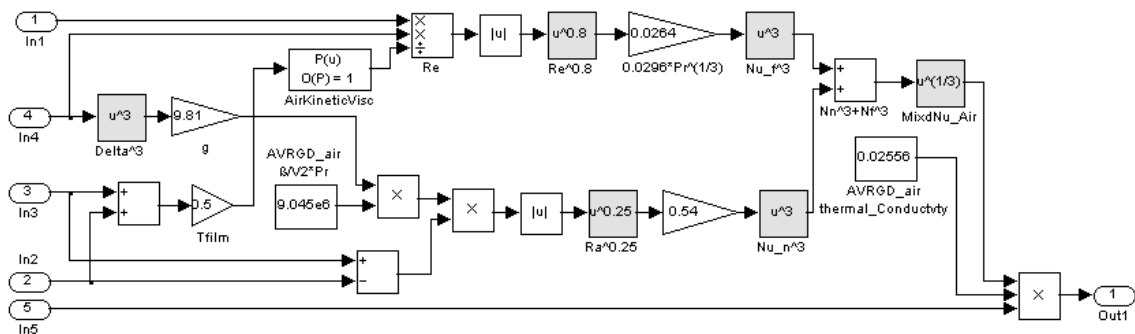
Figure XI. 6 Mask inner surface thermal resistance subsystem

The inputs are listed in table below.

Input port number	Input	Unit
1	Average velocity in the mask(absolute value)	m/s
2	Steady air temperature in the mask (for reference)	°C
3	Temperature of mask wall with heat dissipation	°C
4	Length of the triangular plate inner surface	m
5	Half width of the triangular plate inner surface	m

XI.3.2 Steady state mask air temperature subsystem

This subsystem is for calculating the steady state air temperature in the mask. It is based on Eq. (3.93).

The inputs are listed in table below.

Input port number	Input	Unit
1	Average mask inlet temperature	°C
2	Temperature of mask wall with heat dissipation	°C
3	Average volumetric flow rate in the mask(absolute value)	m^3/s
4	Average velocity in the mask(absolute value)	m/s
5	Length of the triangular plate inner surface	m
6	Half width of the triangular plate inner surface	m

The subsystem in it is the same as the one in section XI.3.1.2 above.
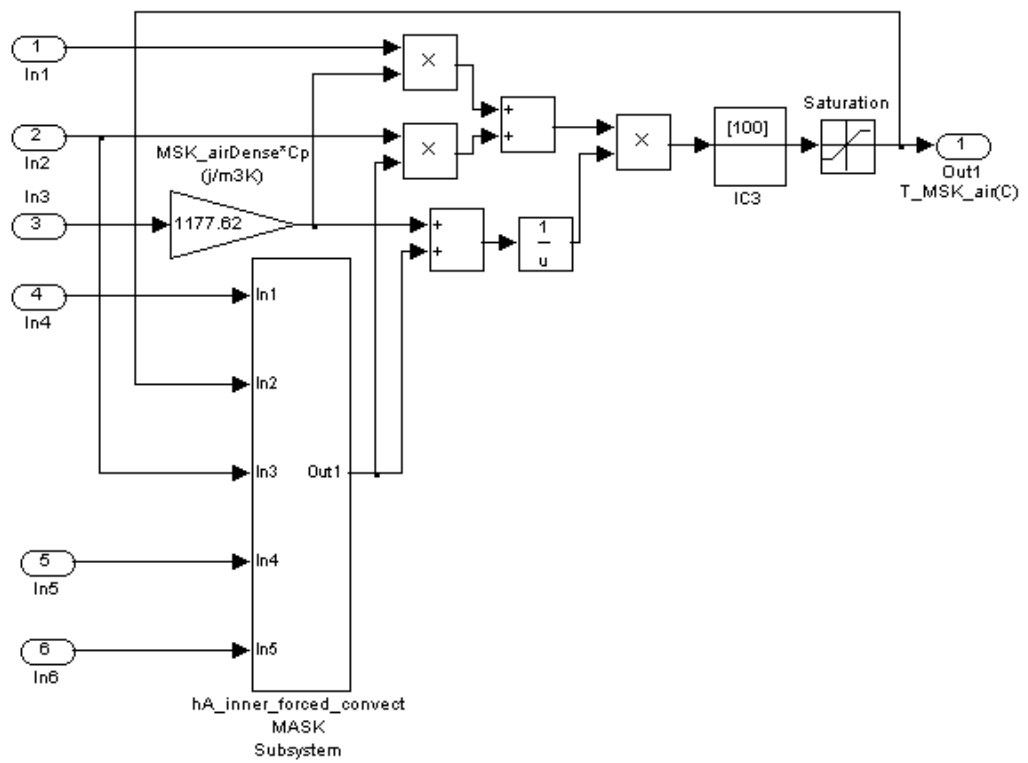
Figure XI. 7 Steady state mask air temperature subsystem

Appendix XII. Details of mask air dynamic fluctuating thermal balance and condensation subsystem

The mask air dynamic fluctuating thermal balance and condensation subsystem has been shown in Figure 4.22, section 4.3.3.2 and its details are shown below.

XII.1 Dynamic mixing and in-mask characteristic velocity subsystem

The "Dynamic mixing and in-mask characteristic velocity subsystem" is to obtain the dynamic fluctuating inlet related parameters: the mask inlet specific humidity, inlet temperature and the in-mask airflow characteristic velocity.

Inputs of the subsystem are listed below:

Input port number	Input	Unit
1	Specific Humidity of airflow from HADT lump 30	In decimal
2	Ambient air specific humidity	In decimal
3	Temperature of airflow from HADT lump 30	°C
4	Breath load	g/s
5	Half width of the triangular plate inner surface	m
6	Mask inner height	m
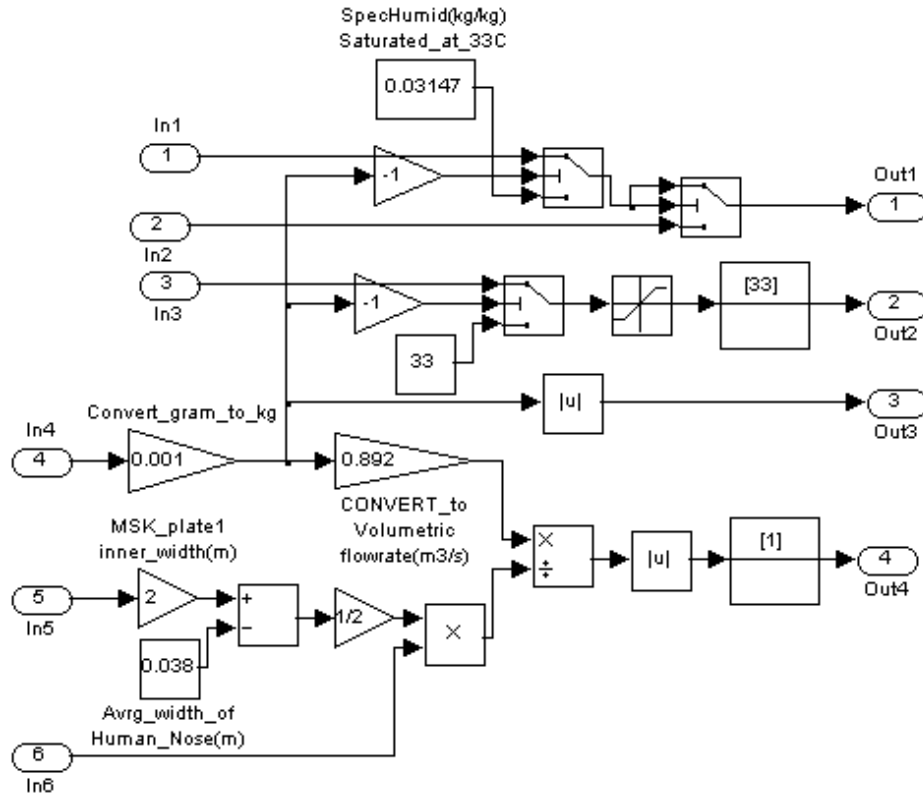
Figure XII. 1 Dynamic mixing and in-mask characteristic velocity subsystem

Outputs of the subsystem are listed below:

output port number	output	Unit
1	Specific humidity of airflow into the mask	In decimal
2	Temperature of airflow into the mask	°C
3	Absolute value of patient's breath mass flow rate	kg/s
4	Characteristic flow velocity on mask inner surfaces	m/s

XII.2 Dynamic fluctuating mask air thermal balance subsystem

This subsystem is for calculating the dynamically fluctuating air temperature in the mask and the average temperature of inhaled air. It is based on Eq. (3.93). The inputs are listed in table below.

Input port number	Input	Unit
1	Temperature of airflow into the mask	°C
2	Mask capacity	m^3
3	Absolute value of patient's breath mass flow rate	kg/s

236

4	Length of the triangular plate inner surface	m
5	Half width of the triangular plate inner surface	m
6	Characteristic flow velocity on mask inner surfaces	m/s
7	Temperature of mask wall with heat dissipation	°C
8	Breath load	g/s
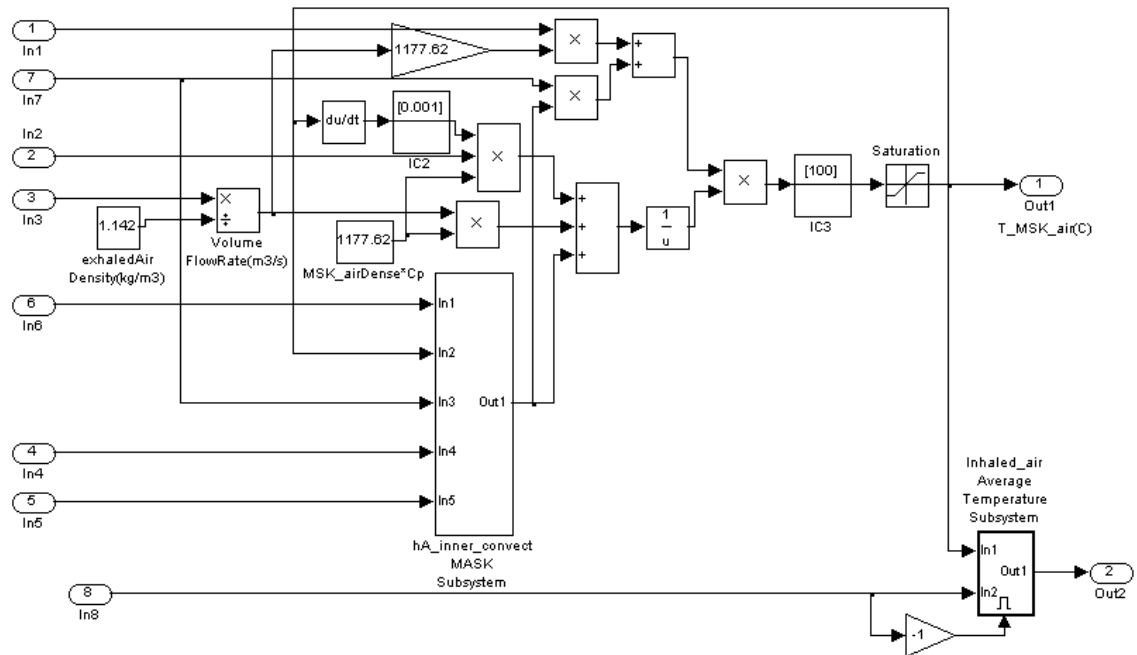
Figure XII. 2 Dynamic fluctuating mask air thermal balance subsystem

Outputs of the subsystem are listed below:

output port number	output	Unit
1	Fluctuating air temperature in the mask	°C
2	Average temperature of inhaled air	°C

The mask inner surface convection resistance subsystem is the same as the one in section XI.3.1.2. The "Inhaled air average temperature subsystem" is shown and explained below.

The included inhaled air average temperature subsystem is shown below:
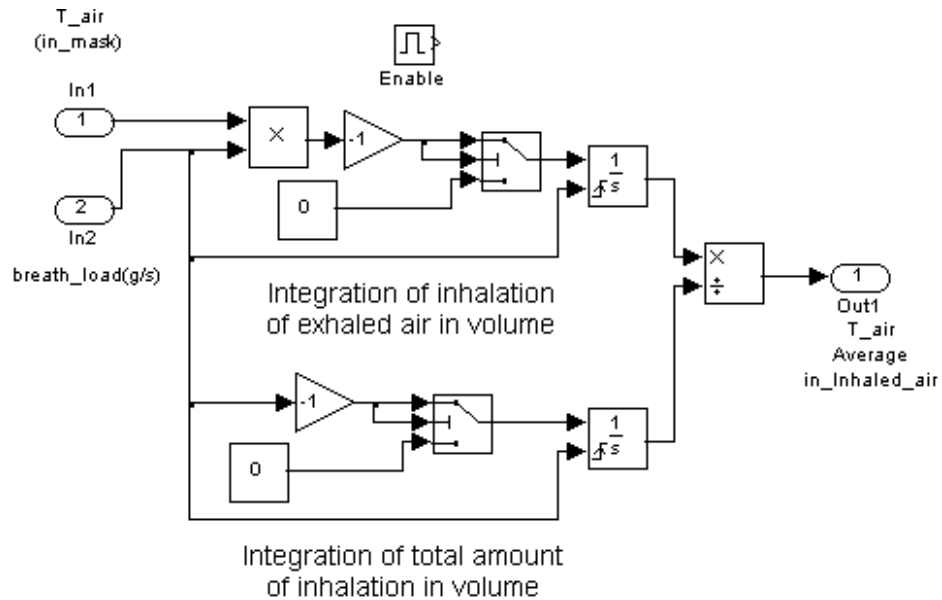
Figure XII. 3 Inhaled air average temperature subsystem

This subsystem is based on Eq. (3.99). The integration is controlled only over the inhalation phase.

The inputs are listed in table below.

Input port number	Input	Unit
1	Fluctuating air temperature in the mask	°C
2	Breath load	g/s

XII.3   Dynamic fluctuating mask condensation/evaporation subsystem

All the subsystems in it are the same as the ones for HADT lumps. For the foam-seal part, the input temperature is the air temperature (assumed isolated) and for the triangular plate, it is the wall temperature. The inputs are listed in table below.

Input port number	Input	Unit
1	Temperature of airflow into the mask	°C
2	Specific humidity of airflow into the mask	In decimal
3	Characteristic flow velocity on mask inner surfaces	m/s
4	Temperature of airflow into the mask	°C
5	Mask inner height	m
6	Length of the rectangular plates inner surface	m
7	Half width of the triangular plate inner surface	m

238

8	Length of the triangular plate inner surface	m
9	Breath load	g/s
10	Temperature of mask wall with heat dissipation	°C
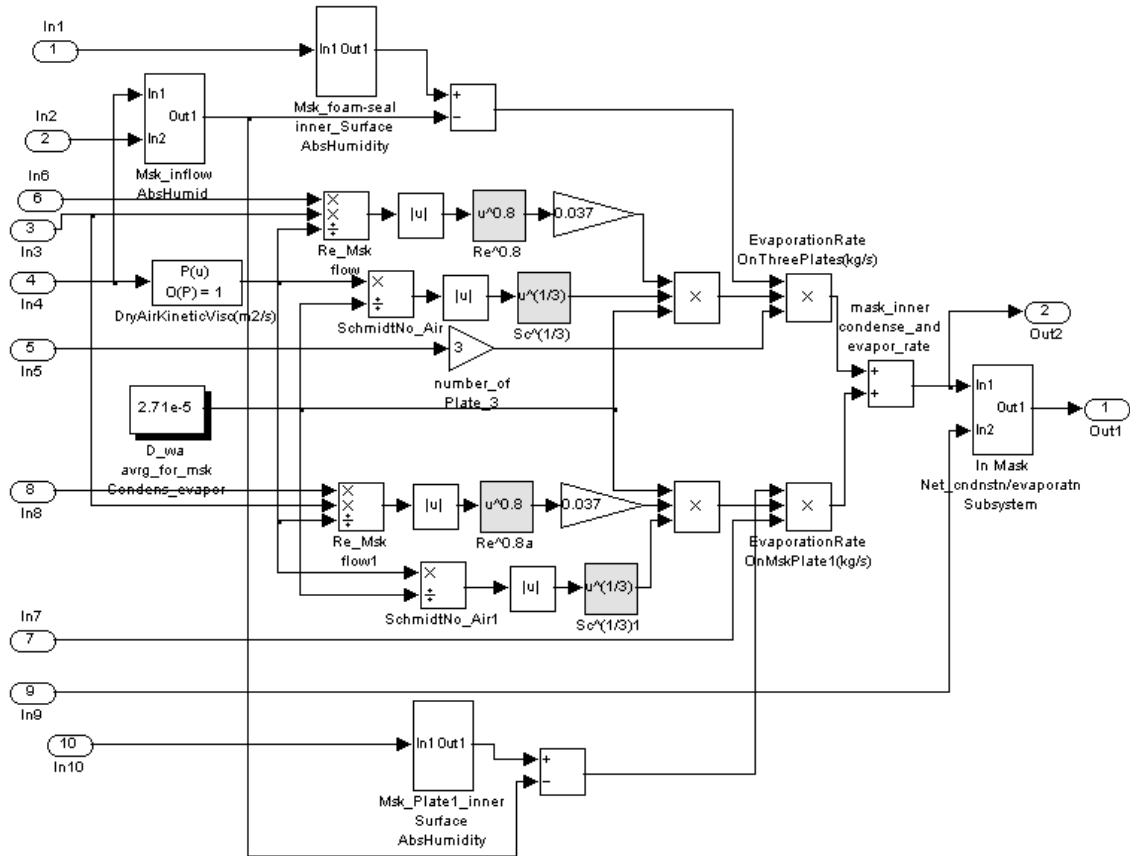
Figure XII. 4 Dynamic fluctuating mask condensation/evaporation subsystem

The outputs are listed in table below.

output port number	output	Unit
1	Net condensation/evaporation in a breath cycle	kg/s
2	Real time condensation/evaporation rate	kg/s

XII.4 Average specific humidity in inhaled air

This subsystem is based on Eq. (3.100). The integration is controlled only over the inhalation phase.

The inputs are listed in table below.

Input port number	Input	Unit
1	Specific humidity of air in the mask	In decimal
2	Breath load	g/s
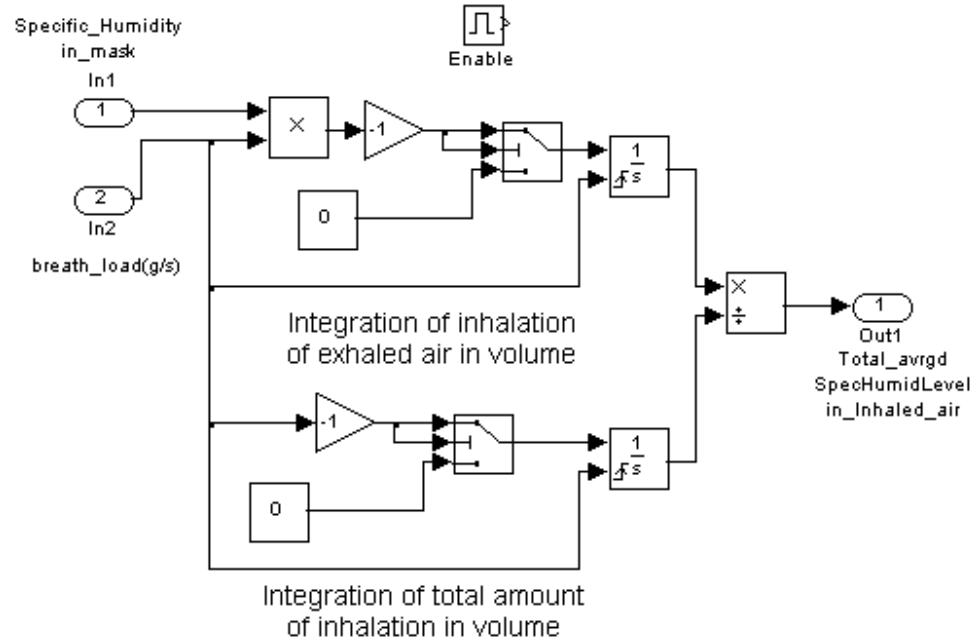
Figure XII. 5 Average specific humidity in inhaled air

Appendix XIII. Details of the auxiliary subsystems
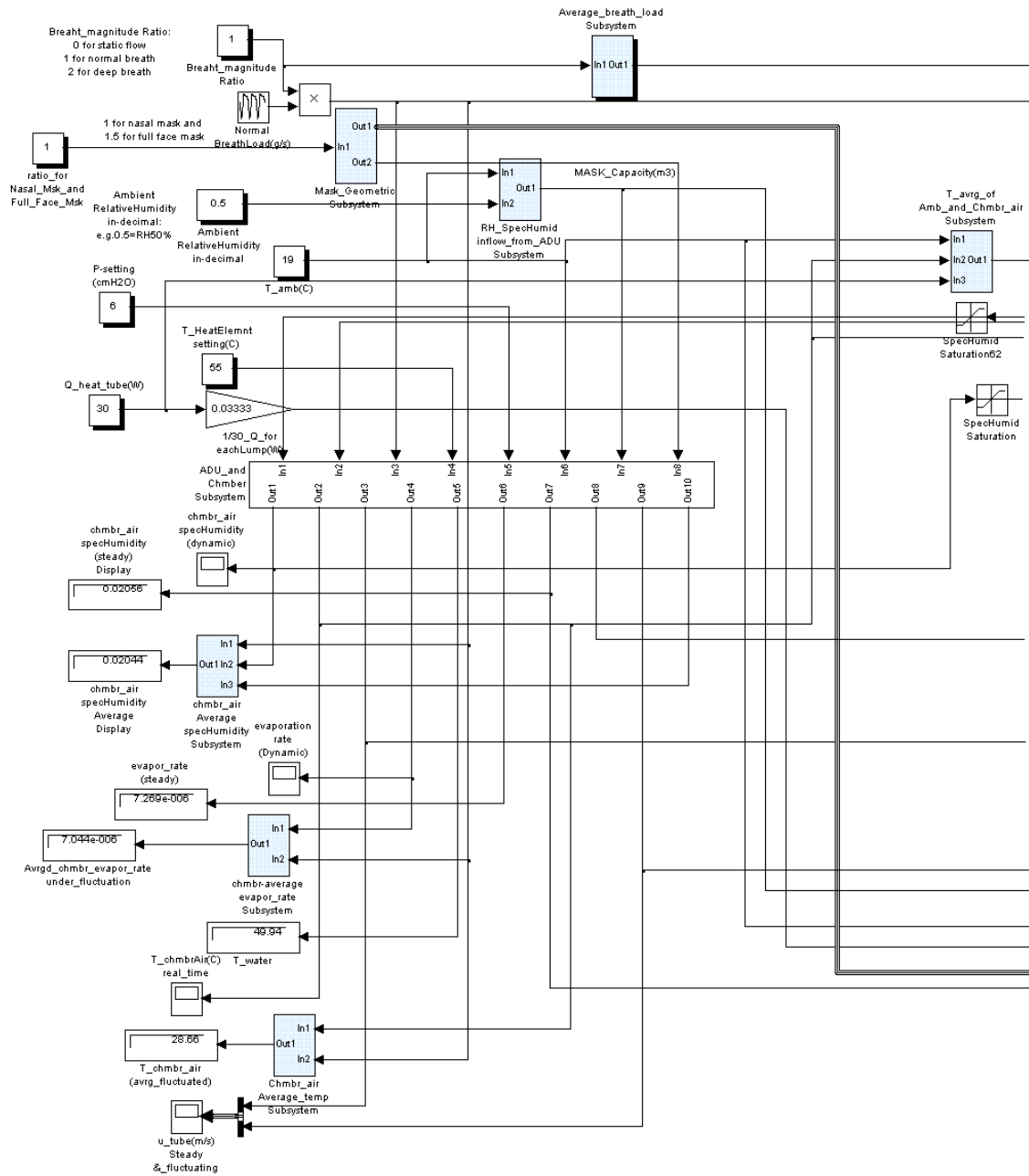
Figure XIII. 1 Auxiliary subsystems and their locations

There are several auxiliary small subsystems light-blue coloured in figure above and listed below:

- Ambient relative humidity to specific humidity conversion subsystem
- Mask geometric parameter subsystem
- Breath load average subsystem
- Average of ambient temperature and chamber air temperature subsystem
- Average evaporation rate subsystem

- Chamber air average temperature subsystem
- Chamber air average specific humidity subsystem

Their functions are explained below.

XIII.1   Ambient relative humidity to specific humidity conversion subsystem

The calculation of the conversion is explained in Appendix VI. The inputs to this subsystem are listed below.

Input port number	Input	Unit
1	Ambient temperature	°C
2	Ambient relative humidity	In decimal
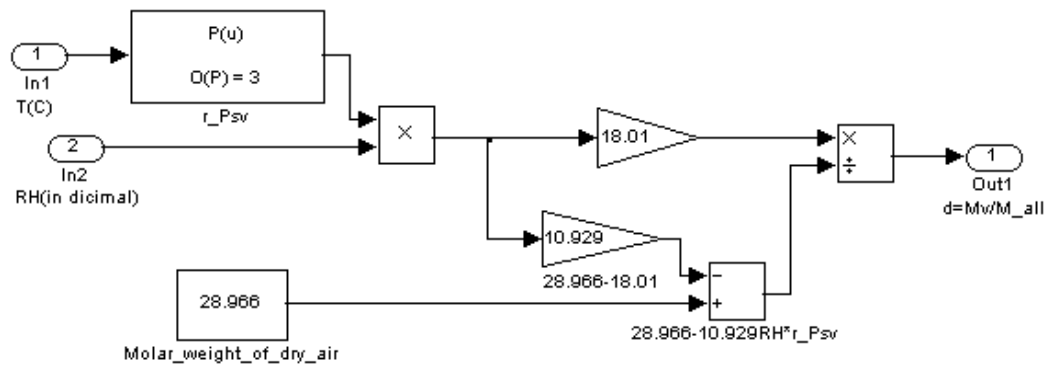
Figure XIII. 2 Ambient relative humidity to specific humidity conversion subsystem

XIII.2   Mask geometric parameter subsystem

This subsystem is for providing the mask geometric parameters to the mask subsystem. The input to this subsystem is the ratio of mask type. The ratio is 1 for nasal mask and 1.5 for full face mask. The output 1 is a multiplex output to the mask. The output 2 is the mask capacity to the fluid dynamic subsystems in the chamber main subsystem.
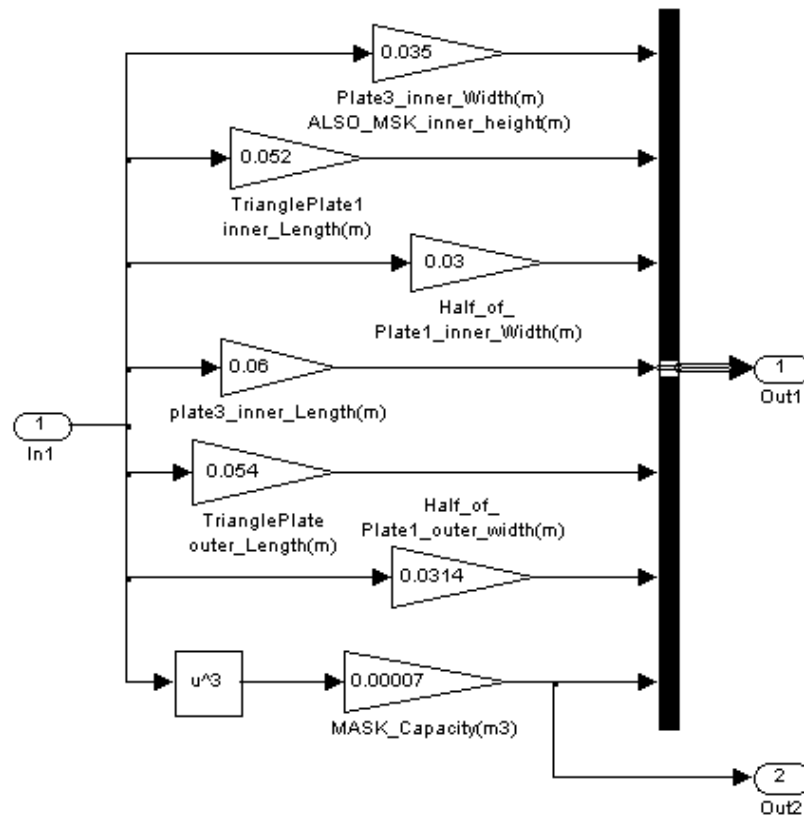
Figure XIII. 3 Mask geometric parameter subsystem

XIII.3 Breath load average subsystem

This subsystem is to provide the average breath load to the steady state mask thermal balance subsystem. The input is the breath load ratio. The ratio is 1 for normal breathing and 2 for deep breathing.
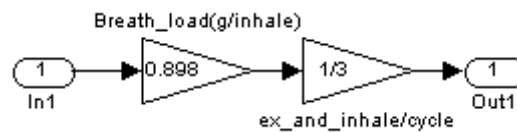
Figure XIII. 4 Breath load average subsystem

XIII.4 Average of ambient temperature and chamber air temperature subsystem

This subsystem is to provide an initial temperature for air in each of the HADT lump. The initial temperature should be somewhere between the stabilized air temperature in lump 1 and lump 30 over all the condition ranges thus to reduce the temperature ramping time.

The inputs are listed in table below.

Input port number	Input	Unit
1	Ambient temperature	°C
2	Steady state in-chamber air temperature	°C
3	Total tube heating power	W
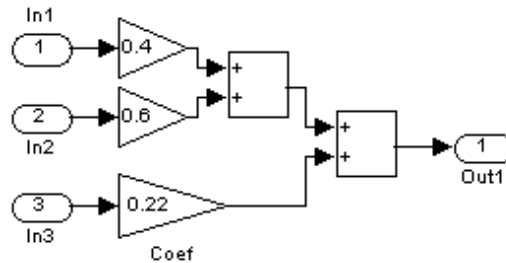
Figure XIII. 5 Average of ambient temperature and chamber air temperature subsystem

XIII.5   Average evaporation rate subsystem

This subsystem is to provide the average evaporation rate over a breath cycle by integrating the real time evaporation rate and being divided by the breath cycle time.

The inputs are listed in table below.

Input port number	Input	Unit
1	Fluctuating evaporation rate	kg/s
2	Breath load (for control purpose)	g/s

The output is the averaged evaporation rate in kg/s.
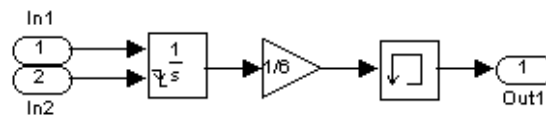
Figure XIII. 6 Average evaporation rate subsystem

XIII.6   Chamber air average temperature subsystem

This subsystem is to provide the chamber air average temperature over a breath cycle. It can be seen that it is the same as the subsystem above. The only difference is the input 1 is the real time chamber air temperature.
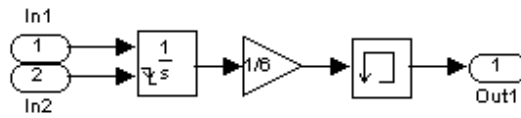
Figure XIII. 7 Average evaporation rate subsystem

XIII.7 Chamber air average specific humidity subsystem

This subsystem is to provide a weighed chamber air average specific humidity over a breath cycle. It can be used for comparison with the specific humidity under the steady state for analysis. It is based on the weighed integration: $d_{avrg} = \dfrac{\int d \cdot \dot{q}_P dt}{\int \dot{q}_P dt}$.

The inputs are listed in table below.

Input port number	Input	Unit
1	Breath load	g/s
2	Fluctuating specific humidity in the chamber	In decimal
3	Average of fluctuating airflow velocities in HADT and the connecting duct	m/s
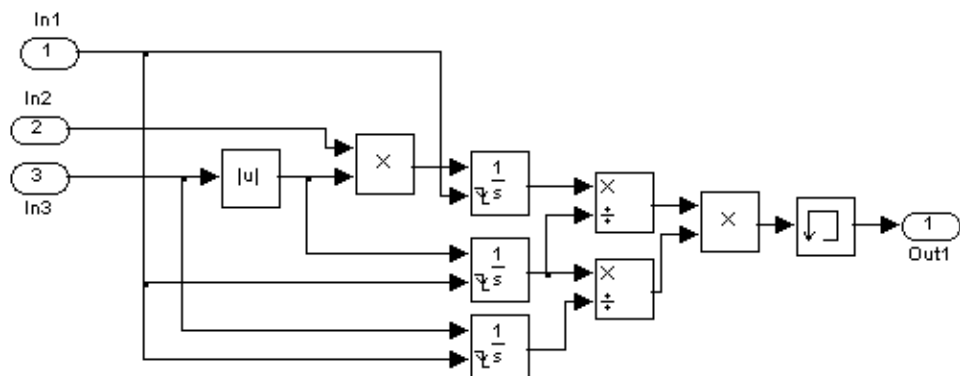
Figure XIII. 8 Chamber air average specific humidity subsystem

Appendix XIV.   Steady state thermal-validation experiment result and model output comparison

The table below shows the combinations of conditions and settings under which the experiments were conducted:

Table XIV. 1 Conditions for steady state thermal-validation experiment

$T_\infty(°C)$	P_{set}	Heating Element Setting	Tube Heating Setting
Low(about 14 $°C$)	4cmH2O	45 $°C$	0 W
Normal(about 22 $°C$)	12cmH2O	55 $°C$	15 W
High(about 33 $°C$)	20cmH2O	65 $°C$	30 W

The experiments were conducted under normal room temperature, low temperature and high temperature. The low and high temperatures were achieved in a big environmental control room. The actual temperature in the room was about 14°C for low temperature and about 33°C for high temperature. The error between experimental result and model output is defined as: $\varepsilon = \dfrac{T_{Model} - T_{Exp}}{T_{Exp}} \times 100\%$. It gives how much the model outputs are deviating from the experimental results.

XIV.1   In-chamber water temperature

XIV.1.1   Under low ambient temperature

Pressure Setting	Ambient Conditions	Heating Element Setting	T_Water (Exp.)	T_Water (Model)	ε (error)
4cmH2O	$T_\infty = 14.2\,°C$	45 $°C$	39.5 $°C$	39.33 $°C$	-0.43%
		55 $°C$	46.1 $°C$	47.29 $°C$	2.58%
	$RH_\infty = 71.7\%$	65 $°C$	54.1 $°C$	55.01 $°C$	1.68%
12cmH2O	$T_\infty = 14.4\,°C$	45 $°C$	38.5 $°C$	38.13 $°C$	-0.96%
		55 $°C$	45.9 $°C$	45.67 $°C$	-0.50%
	$RH_\infty = 70.3\%$	65 $°C$	53.3 $°C$	52.94 $°C$	-0.68%
20cmH2O	$T_\infty = 14.4\,°C$	45 $°C$	37.6 $°C$	37.45 $°C$	-0.40%
		55 $°C$	44.7 $°C$	44.73 $°C$	0.07%
	$RH_\infty = 70.7\%$	65 $°C$	52.8 $°C$	51.74 $°C$	-2.01%

XIV.1.2   Under normal ambient temperature

Pressure Setting	Ambient Conditions	Heating Element Setting	T_Water (Exp.)	T_Water (Model)	ε (error)
4cmH2O	$T_\infty = 21.6\,°C$	$45\,°C$	$39.7\,°C$	$39.87\,°C$	0.43%
		$55\,°C$	$48.5\,°C$	$47.80\,°C$	-1.44%
	$RH_\infty = 47.3\%$	$65\,°C$	$56.5\,°C$	$55.51\,°C$	-1.75%
12cmH2O	$T_\infty = 21.9\,°C$	$45\,°C$	$39.4\,°C$	$38.98\,°C$	-1.07%
		$55\,°C$	$46.3\,°C$	$46.44\,°C$	0.30%
	$RH_\infty = 64.0\%$	$65\,°C$	$54.5\,°C$	$53.67\,°C$	-1.52%
20cmH2O	$T_\infty = 21.9\,°C$	$45\,°C$	$38.7\,°C$	$37.92\,°C$	-2.02%
		$55\,°C$	$45.7\,°C$	$45.18\,°C$	-1.14%
	$RH_\infty = 39.5\%$	$65\,°C$	$53.4\,°C$	$52.18\,°C$	-2.28%

XIV.1.3   Under high ambient temperature

Pressure Setting	Ambient Conditions	Heating Element Setting	T_Water (Exp.)	T_Water (Model)	ε (error)
4cmH2O	$T_\infty = 33.0\,°C$	$45\,°C$	$40.8\,°C$	$40.74\,°C$	-0.15%
		$55\,°C$	$48.4\,°C$	$48.65\,°C$	0.52%
	$RH_\infty = 30.2\%$	$65\,°C$	$56.6\,°C$	$56.33\,°C$	-0.48%
12cmH2O	$T_\infty = 33.1\,°C$	$45\,°C$	$39.8\,°C$	$39.45\,°C$	-0.88%
		$55\,°C$	$47.2\,°C$	$46.93\,°C$	-0.57%
	$RH_\infty = 23.6\%$	$65\,°C$	$54.7\,°C$	$54.16\,°C$	-0.99%
20cmH2O	$T_\infty = 32.9\,°C$	$45\,°C$	$39.9\,°C$	$38.96\,°C$	-2.36%
		$55\,°C$	$46.8\,°C$	$46.16\,°C$	-1.37%
	$RH_\infty = 29.4\%$	$65\,°C$	$53.5\,°C$	$53.10\,°C$	-0.75%

XIV.2 Chamber outlet air temperature

The air temperature at the outlet is used to represent the average temperature of in-chamber air.

XIV.2.1 Under low ambient temperature

Pressure Setting	Ambient Conditions	Heating Element Setting	T_Ca (Exp.)	T_Ca (Model)	ε (error)
4cmH2O	$T_\infty = 14.2\,°C$	$45\,°C$	$21.5\,°C$	$22.84\,°C$	6.23%
		$55\,°C$	$24.4\,°C$	$25.45\,°C$	4.30%
	$RH_\infty = 71.7\%$	$65\,°C$	$26.8\,°C$	$28.57\,°C$	6.60%
12cmH2O	$T_\infty = 14.4\,°C$	$45\,°C$	$24.8\,°C$	$23.86\,°C$	-3.79%
		$55\,°C$	$26.8\,°C$	$25.92\,°C$	-3.28%
	$RH_\infty = 70.3\%$	$65\,°C$	$28.7\,°C$	$28.31\,°C$	-1.36%
20cmH2O	$T_\infty = 14.4\,°C$	$45\,°C$	$25.9\,°C$	$25.04\,°C$	-3.32%
		$55\,°C$	$28.4\,°C$	$26.88\,°C$	-5.35%
	$RH_\infty = 70.7\%$	$65\,°C$	$31.0\,°C$	$28.98\,°C$	-6.52%

XIV.2.2 Under normal ambient temperature

Pressure Setting	Ambient Conditions	Heating Element Setting	T_Ca (Exp.)	T_Ca (Model)	ε (error)
4cmH2O	$T_\infty = 21.6\,°C$	$45\,°C$	$30.5\,°C$	$29.06\,°C$	-4.72%
		$55\,°C$	$32.9\,°C$	$31.63\,°C$	-3.86%
	$RH_\infty = 47.3\%$	$65\,°C$	$35.9\,°C$	$34.68\,°C$	-3.40%
12cmH2O	$T_\infty = 21.9\,°C$	$45\,°C$	$30.8\,°C$	$30.33\,°C$	-1.53%
		$55\,°C$	$32.2\,°C$	$32.37\,°C$	0.53%
	$RH_\infty = 64.0\%$	$65\,°C$	$34.1\,°C$	$34.73\,°C$	1.85%
20cmH2O	$T_\infty = 21.9\,°C$	$45\,°C$	$32.5\,°C$	$31.63\,°C$	-2.68%
		$55\,°C$	$33.6\,°C$	$33.47\,°C$	-0.39%
	$RH_\infty = 39.5\%$	$65\,°C$	$34.9\,°C$	$35.58\,°C$	1.95%

XIV.2.3 Under high ambient temperature

Pressure Setting	Ambient Conditions	Heating Element Setting	T_Ca (Exp.)	T_Ca (Model)	ε (error)
4cmH2O	$T_\infty = 33.0\,°C$	$45\,°C$	$35.8\,°C$	$38.67\,°C$	8.02%
		$55\,°C$	$38.0\,°C$	$41.23\,°C$	8.50%
	$RH_\infty = 30.2\%$	$65\,°C$	$40.3\,°C$	$44.28\,°C$	9.88%
12cmH2O	$T_\infty = 33.1\,°C$	$45\,°C$	$39.1\,°C$	$40.12\,°C$	2.61%
		$55\,°C$	$40.0\,°C$	$42.18\,°C$	5.45%
	$RH_\infty = 23.6\%$	$65\,°C$	$41.1\,°C$	$44.57\,°C$	8.44%
20cmH2O	$T_\infty = 32.9\,°C$	$45\,°C$	$40.1\,°C$	$41.34\,°C$	3.09%
		$55\,°C$	$41.9\,°C$	$43.16\,°C$	3.01%
	$RH_\infty = 29.4\%$	$65\,°C$	$42.7\,°C$	$45.26\,°C$	6.00%

The model outputs of in-chamber air temperature match very well with the experimental results all over the range.

XIV.3 Airflow temperature at the end of the HADT (when tube heating=0W)

XIV.3.1 Under low ambient temperature

Pressure Setting	Ambient Conditions	Heating Element Setting	T_{Ta30} (Exp.)	T_{Ta30} (Model)	ε (error)
4cmH2O	$T_\infty = 14.2\,°C$	$45\,°C$	$16.9\,°C$	$16.87\,°C$	-0.18%
		$55\,°C$	$18.4\,°C$	$17.28\,°C$	-6.09%
	$RH_\infty = 71.7\%$	$65\,°C$	$19.6\,°C$	$17.77\,°C$	-9.34%
12cmH2O	$T_\infty = 14.4\,°C$	$45\,°C$	$19.8\,°C$	$18.71\,°C$	-5.51%
		$55\,°C$	$21.3\,°C$	$19.27\,°C$	-9.53%
	$RH_\infty = 70.3\%$	$65\,°C$	$21.8\,°C$	$19.93\,°C$	-8.58%
20cmH2O	$T_\infty = 14.4\,°C$	$45\,°C$	$20.0\,°C$	$19.99\,°C$	-0.05%
		$55\,°C$	$22.1\,°C$	$20.63\,°C$	-6.65%
	$RH_\infty = 70.7\%$	$65\,°C$	$23.2\,°C$	$21.35\,°C$	-7.97%

XIV.3.2   Under normal ambient temperature

Pressure Setting	Ambient Conditions	Heating Element Setting	T_{Ta30} (Exp.)	T_{Ta30} (Model)	ε (error)
4cmH2O	$T_\infty = 21.6\,°C$	$45\,°C$	$24.0\,°C$	$24.67\,°C$	2.79%
		$55\,°C$	$25.5\,°C$	$25.08\,°C$	-1.65%
	$RH_\infty = 47.3\%$	$65\,°C$	$26.8\,°C$	$25.56\,°C$	-4.63%
12cmH2O	$T_\infty = 21.9\,°C$	$45\,°C$	$25.1\,°C$	$26.63\,°C$	6.10%
		$55\,°C$	$27.0\,°C$	$27.19\,°C$	0.70%
	$RH_\infty = 64.0\%$	$65\,°C$	$27.9\,°C$	$27.84\,°C$	-0.22%
20cmH2O	$T_\infty = 21.9\,°C$	$45\,°C$	$26.1\,°C$	$27.94\,°C$	7.05%
		$55\,°C$	$27.2\,°C$	$28.58\,°C$	5.07%
	$RH_\infty = 39.5\%$	$65\,°C$	$29.3\,°C$	$29.30\,°C$	0.00%

XIV.3.3   Under high ambient temperature

Pressure Setting	Ambient Conditions	Heating Element Setting	T_{Ta30} (Exp.)	T_{Ta30} (Model)	ε (error)
4cmH2O	$T_\infty = 33.0\,°C$	$45\,°C$	$33.8\,°C$	$36.68\,°C$	8.52%
		$55\,°C$	$34.3\,°C$	$37.10\,°C$	8.16%
	$RH_\infty = 30.2\%$	$65\,°C$	$34.9\,°C$	$37.59\,°C$	7.71%
12cmH2O	$T_\infty = 33.1\,°C$	$45\,°C$	$35.4\,°C$	$38.50\,°C$	8.76%
		$55\,°C$	$36.0\,°C$	$39.07\,°C$	8.53%
	$RH_\infty = 23.6\%$	$65\,°C$	$36.5\,°C$	$39.72\,°C$	8.82%
20cmH2O	$T_\infty = 32.9\,°C$	$45\,°C$	$37.3\,°C$	$39.61\,°C$	6.19%
		$55\,°C$	$37.8\,°C$	$40.24\,°C$	6.46%
	$RH_\infty = 29.4\%$	$65\,°C$	$38.4\,°C$	$40.96\,°C$	6.67%

XIV.4 Airflow temperature at the end of the HADT (when tube heating=15W)

XIV.4.1   Under low ambient temperature

Pressure Setting	Ambient Conditions	Heating Element Setting	T_{Ta30} (Exp.)	T_{Ta30} (Model)	ε (error)
4cmH2O	$T_\infty = 14.2\,°C$	45 °C	24.5 °C	24.61 °C	0.45%
		55 °C	26.1 °C	24.97 °C	-4.33%
	$RH_\infty = 71.7\%$	65 °C	27.7 °C	25.40 °C	-8.30%
12cmH2O	$T_\infty = 14.4\,°C$	45 °C	24.4 °C	25.47 °C	4.39%
		55 °C	26.6 °C	25.98 °C	-2.33%
	$RH_\infty = 70.3\%$	65 °C	28.5 °C	26.58 °C	-6.74%
20cmH2O	$T_\infty = 14.4\,°C$	45 °C	27.6 °C	26.14 °C	-5.29%
		55 °C	28.5 °C	26.74 °C	-6.18%
	$RH_\infty = 70.7\%$	65 °C	29.8 °C	27.41 °C	-8.02%

XIV.4.2   Under normal ambient temperature

Pressure Setting	Ambient Conditions	Heating Element Setting	T_{Ta30} (Exp.)	T_{Ta30} (Model)	ε (error)
4cmH2O	$T_\infty = 21.6\,°C$	45 °C	31.2 °C	32.24 °C	3.33%
		55 °C	31.8 °C	32.60 °C	2.52%
	$RH_\infty = 47.3\%$	65 °C	33.0 °C	33.03 °C	0.09%
12cmH2O	$T_\infty = 21.9\,°C$	45 °C	31.1 °C	33.25 °C	6.91%
		55 °C	32.0 °C	33.77 °C	5.53%
	$RH_\infty = 64.0\%$	65 °C	32.9 °C	34.36 °C	4.44%
20cmH2O	$T_\infty = 21.9\,°C$	45 °C	31.5 °C	33.98 °C	7.87%
		55 °C	32.5 °C	34.57 °C	6.37%
	$RH_\infty = 39.5\%$	65 °C	33.2 °C	35.25 °C	6.17%

XIV.4.3 Under high ambient temperature

Pressure Setting	Ambient Conditions	Heating Element Setting	T_{Ta30} (Exp.)	T_{Ta30} (Model)	ε (error)
4cmH2O	$T_\infty = 33.0\,°C$	$45\,°C$	$40.2\,°C$	$44.00\,°C$	9.45%
		$55\,°C$	$41.3\,°C$	$44.36\,°C$	7.41%
	$RH_\infty = 30.2\%$	$65\,°C$	$41.9\,°C$	$44.80\,°C$	6.92%
12cmH2O	$T_\infty = 33.1\,°C$	$45\,°C$	$41.3\,°C$	$44.91\,°C$	8.74%
		$55\,°C$	$42.6\,°C$	$45.44\,°C$	6.67%
	$RH_\infty = 23.6\%$	$65\,°C$	$42.8\,°C$	$46.04\,°C$	7.57%
20cmH2O	$T_\infty = 32.9\,°C$	$45\,°C$	$42.5\,°C$	$45.48\,°C$	7.01%
		$55\,°C$	$43.1\,°C$	$46.06\,°C$	6.87%
	$RH_\infty = 29.4\%$	$65\,°C$	$44.3\,°C$	$46.74\,°C$	5.51%

XIV.5 Airflow temperature at the end of the HADT (when tube heating=30W)

XIV.5.1 Under low ambient temperature

Pressure Setting	Ambient Conditions	Heating Element Setting	T_{Ta30} (Exp.)	T_{Ta30} (Model)	ε (error)
4cmH2O	$T_\infty = 14.2\,°C$	$45\,°C$	$29.2\,°C$	$31.62\,°C$	8.29%
		$55\,°C$	$31.0\,°C$	$31.96\,°C$	3.10%
	$RH_\infty = 71.7\%$	$65\,°C$	$31.2\,°C$	$32.36\,°C$	3.72%
12cmH2O	$T_\infty = 14.4\,°C$	$45\,°C$	$29.6\,°C$	$31.76\,°C$	7.30%
		$55\,°C$	$31.8\,°C$	$32.26\,°C$	1.45%
	$RH_\infty = 70.3\%$	$65\,°C$	$33.4\,°C$	$32.82\,°C$	-1.74%
20cmH2O	$T_\infty = 14.4\,°C$	$45\,°C$	$30.2\,°C$	$31.96\,°C$	5.83%
		$55\,°C$	$31.5\,°C$	$32.53\,°C$	3.27%
	$RH_\infty = 70.7\%$	$65\,°C$	$32.6\,°C$	$33.18\,°C$	1.78%

XIV.5.2 Under normal ambient temperature

Pressure Setting	Ambient Conditions	Heating Element Setting	T_{Ta30} (Exp.)	T_{Ta30} (Model)	ε (error)
4cmH2O	$T_\infty = 21.6\,°C$ $RH_\infty = 47.3\%$	$45\,°C$	$38.0\,°C$	$39.11\,°C$	2.92%
		$55\,°C$	$38.7\,°C$	$39.45\,°C$	1.94%
		$65\,°C$	$39.5\,°C$	$39.85\,°C$	0.89%
12cmH2O	$T_\infty = 21.9\,°C$ $RH_\infty = 64.0\%$	$45\,°C$	$37.4\,°C$	$39.43\,°C$	5.43%
		$55\,°C$	$38.2\,°C$	$39.92\,°C$	4.50%
		$65\,°C$	$38.5\,°C$	$40.48\,°C$	5.14%
20cmH2O	$T_\infty = 21.9\,°C$ $RH_\infty = 39.5\%$	$45\,°C$	$36.6\,°C$	$39.69\,°C$	8.44%
		$55\,°C$	$37.0\,°C$	$40.26\,°C$	8.81%
		$65\,°C$	$37.7\,°C$	$40.91\,°C$	8.51%

XIV.5.3 Under high ambient temperature

Pressure Setting	Ambient Conditions	Heating Element Setting	T_{Ta30} (Exp.)	T_{Ta30} (Model)	ε (error)
4cmH2O	$T_\infty = 33.0\,°C$ $RH_\infty = 30.2\%$	$45\,°C$	$47.0\,°C$	$50.65\,°C$	7.77%
		$55\,°C$	$48.4\,°C$	$51.00\,°C$	5.37%
		$65\,°C$	$48.5\,°C$	$51.41\,°C$	6.00%
12cmH2O	$T_\infty = 33.1\,°C$ $RH_\infty = 23.6\%$	$45\,°C$	$47.5\,°C$	$50.91\,°C$	7.18%
		$55\,°C$	$48.0\,°C$	$51.40\,°C$	7.08%
		$65\,°C$	$48.3\,°C$	$51.98\,°C$	7.62%
20cmH2O	$T_\infty = 32.9\,°C$ $RH_\infty = 29.4\%$	$45\,°C$	$46.6\,°C$	$51.03\,°C$	9.51%
		$55\,°C$	$47.9\,°C$	$51.59\,°C$	7.70%
		$65\,°C$	$48.4\,°C$	$52.24\,°C$	7.93%

XIV.6 Evaporation rate

The error of evaporation rate between experimental result and model output is defined

as: $\varepsilon = \dfrac{\dot{m}_{ev-Model} - \dot{m}_{ev-Exp}}{\dot{m}_{ev-Exp}} \times 100\%$. It gives how much the model outputs are deviating

from the experimental results.

XIV.6.1 Under low ambient temperature

Pressure Setting	Ambient Conditions	Heating Element Setting	$\dot{m}_{ev}$ (mg/s) (Exp.)	$\dot{m}_{ev}$ (mg/s) (Model)	ε (error)
4cmH2O	$T_\infty = 14.2\,°C$	$45\,°C$	3.80	3.98	4.74%
		$55\,°C$	6.05	6.32	4.46%
	$RH_\infty = 71.7\%$	$65\,°C$	8.29	9.38	13.15%
12cmH2O	$T_\infty = 14.4\,°C$	$45\,°C$	5.87	5.42	-7.67%
		$55\,°C$	8.70	8.45	-2.87%
	$RH_\infty = 70.3\%$	$65\,°C$	12.49	12.32	-1.36%
20cmH2O	$T_\infty = 14.4\,°C$	$45\,°C$	6.95	6.31	-9.21%
		$55\,°C$	10.10	9.74	-3.56%
	$RH_\infty = 70.7\%$	$65\,°C$	14.29	14.09	-1.40%

XIV.6.2 Under normal ambient temperature

Pressure Setting	Ambient Conditions	Heating Element Setting	$\dot{m}_{ev}$ (mg/s) (Exp.)	$\dot{m}_{ev}$ (mg/s) (Model)	ε (error)
4cmH2O	$T_\infty = 21.6\,°C$	$45\,°C$	4.08	4.04	-0.98%
		$55\,°C$	6.54	6.4	-2.14%
	$RH_\infty = 47.3\%$	$65\,°C$	9.08	9.47	4.30%
12cmH2O	$T_\infty = 21.9\,°C$	$45\,°C$	5.41	5.17	-4.44%
		$55\,°C$	8.47	8.23	-2.83%
	$RH_\infty = 64.0\%$	$65\,°C$	11.90	12.15	2.10%
20cmH2O	$T_\infty = 21.9\,°C$	$45\,°C$	7.08	6.65	-6.07%
		$55\,°C$	10.73	10.1	-5.87%
	$RH_\infty = 39.5\%$	$65\,°C$	14.55	14.47	-0.55%

XIV.6.3   Under high ambient temperature

Pressure Setting	Ambient Conditions	Heating Element Setting	$\dot{m}_{ev}$ (mg/s) (Exp.)	$\dot{m}_{ev}$ (mg/s) (Model)	ε (error)
4cmH2O	$T_\infty = 33.0\,°C$	$45\,°C$	4.52	3.99	-11.73%
		$55\,°C$	6.69	6.37	-4.78%
	$RH_\infty = 30.2\%$	$65\,°C$	9.9	9.45	-4.55%
12cmH2O	$T_\infty = 33.1\,°C$	$45\,°C$	6.11	5.77	-5.56%
		$55\,°C$	8.99	8.86	-1.45%
	$RH_\infty = 23.6\%$	$65\,°C$	12.30	12.78	3.90%
20cmH2O	$T_\infty = 32.9\,°C$	$45\,°C$	7.15	6.53	-8.67%
		$55\,°C$	10.71	10.04	-6.26%
	$RH_\infty = 29.4\%$	$65\,°C$	14.79	14.46	-2.23%

Appendix XV. Regression of temperature related water properties for Grashof number

The table and figure below show the relevant data for calculating the combined parameter $\beta \mathrm{Pr} / \left(v^2 \right)$ for Grashof number of water[49].

T (°C)	ß (1/°C)	Pr	v (kg/(ms)	P (kg/m³)	ßPr/v² [s²/(m⁴·°C)]
10	0.000073	9.45	0.001307	999.7	403592305.4
20	0.000195	7.01	0.001002	998	1356058012
30	0.000294	5.42	0.000798	996	2482329972
40	0.000377	4.32	0.000653	992.1	3759322930
50	0.000451	3.55	0.000547	988	5223289912
60	0.000517	2.99	0.000467	983.3	6853304818
70	0.000578	2.55	0.000404	977.5	8628569882
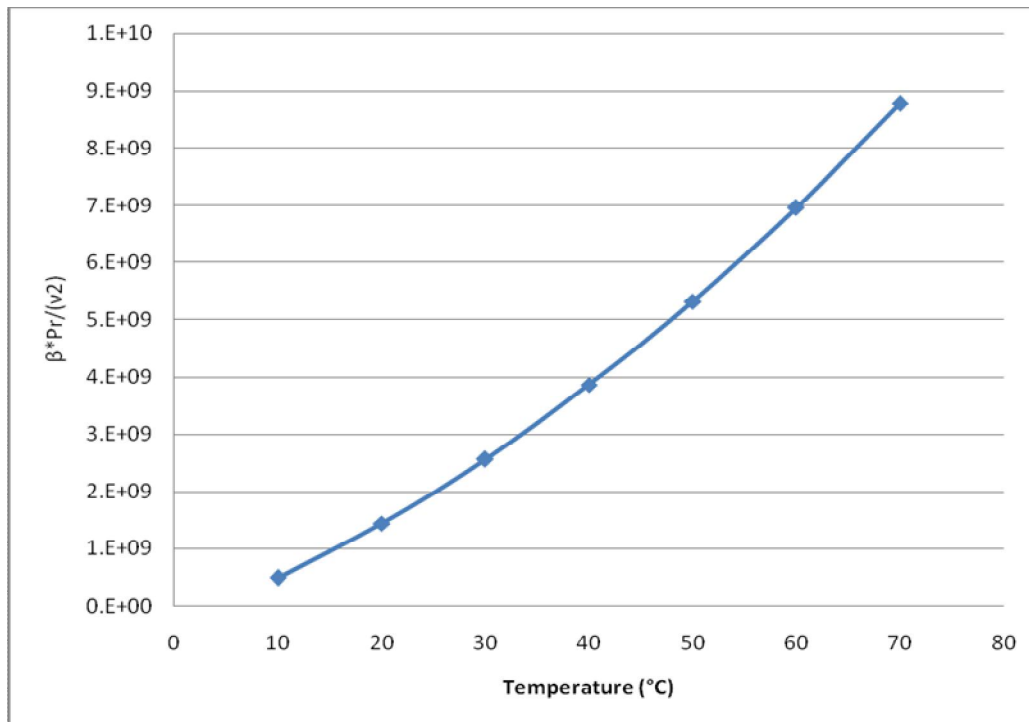
Regression gives expression for this combined coefficient of water Grashof number against temperature as:

$$\frac{\beta \, \mathrm{Pr}}{v^2} = 8.643 \times 10^5 T^2 + 6.895 \times 10^7 T - 2.847 \times 10^8 \qquad \text{with R}^2 = 1.0.$$

Appendix XVI.   Regression of kinetic viscosity of air

The kinetic viscosity of air against temperature from 0 to 60°C are listed and shown below [49].

Temperature (°C)	Kinematic viscosity (m²/s)
0	1.338×10^{-5}
10	1.426×10^{-5}
20	1.516×10^{-5}
30	1.608×10^{-5}
40	1.702×10^{-5}
50	1.798×10^{-5}
60	1.896×10^{-5}
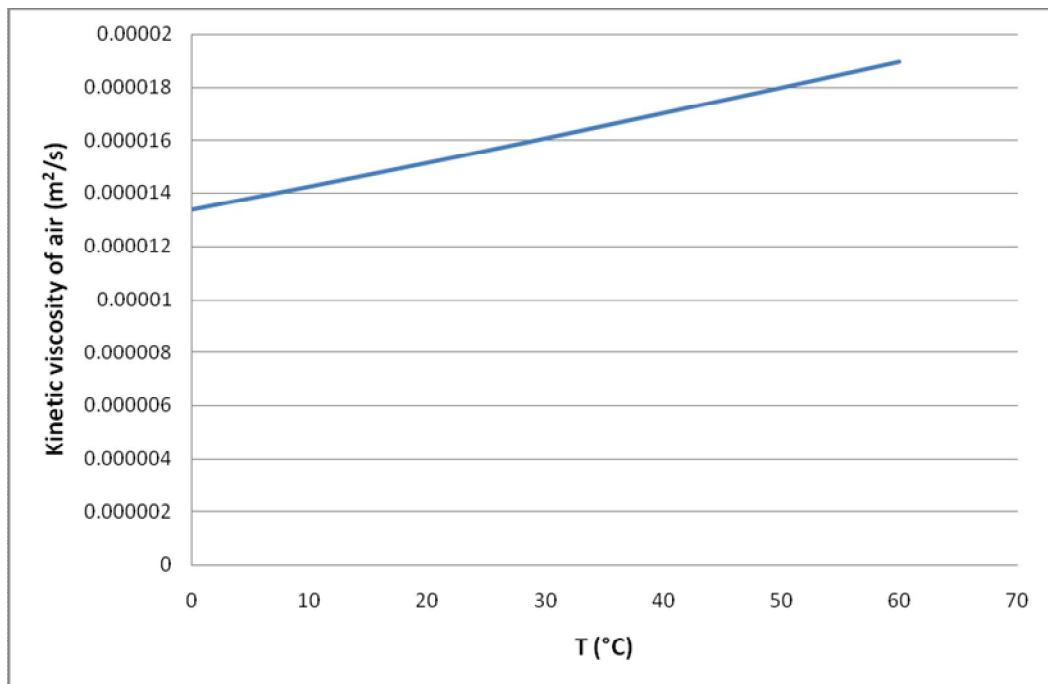
The regressed expression of air kinetic viscosity against temperature is:

$$v = 9.33 \times 10^{-8} T + 1.33 \times 10^{-5} \qquad \text{With R}^2 = 1.0.$$

Appendix XVII. In-tube condensation with normal breathing and deep breathing induced fluctuation under conditions of 9cmH$_2$O without reverse flow
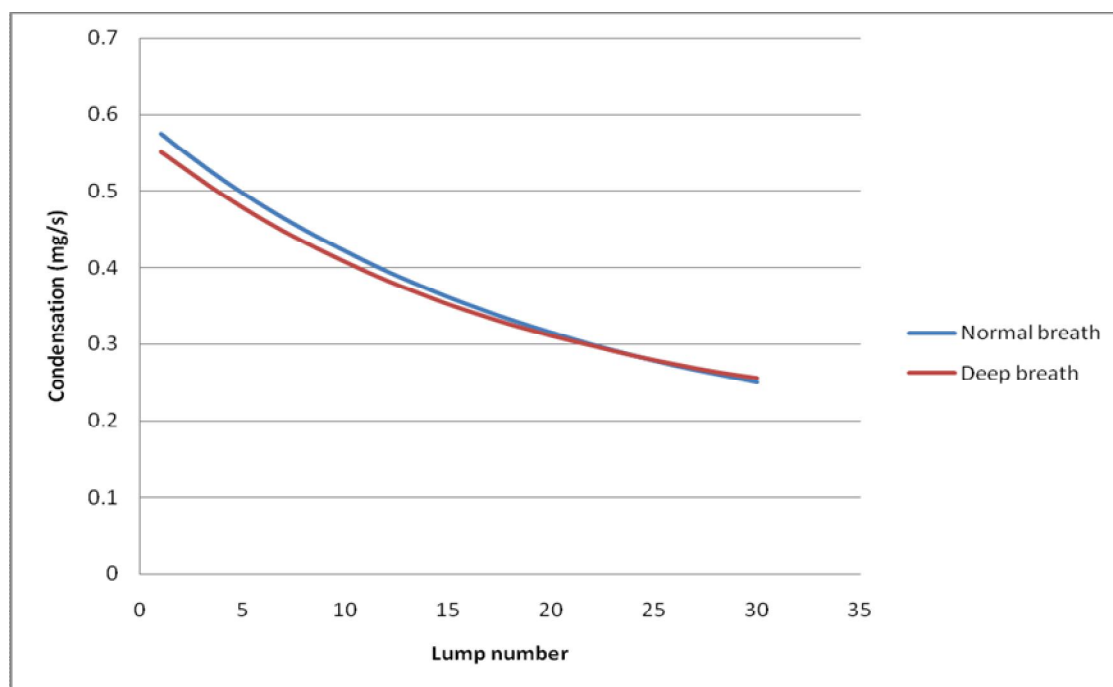
Figure XVII. 1 In-tube condensation with normal breathing and deep breathing added fluctuating flows under conditions of 9cmH$_2$O 45°C 0W 20°C&50%

Figure XVII. 1 shows the average condensation rates under normal breathing fluctuating flow and deep breathing fluctuating flow. It can be seen that basically the deep breathing curve stays close to the normal breathing one. The explanation based on instantaneous condensation/evaporation is as follow:

The graphs below show the condensation/evaporation rates of normal breathing and deep breathing and support the explanation above. In these graphs, when the curve is below X-axial, it means there is condensation occurring. If the curve is above X-axial, it means the airflow has a vaporization potentiality. The algebraic sum of the negative and positive areas between the curve and the X-axial over a breath cycle is the net amount of condensation/evaporation occurred in the time span. This sum of area is defined as the net area. It can be seen from the deep breathing condensation/evaporation graph that the condensation/evaporation rate fluctuates widely. However the net area is almost the same as that of the normal breathing. This explains why the two curves are close to each other.

Figure XVII. 2 Condensation/evaporation rate in lump 1 under conditions of normal breathing, 9cmH$_2$O pressure setting, 45°C heating element setting, ambient temperature and relative humidity of 20°C&50%, and no tube heating

Figure XVII. 3 Condensation/evaporation rate in lump 1 under conditions of deep breathing, 9cmH$_2$O pressure setting, 45°C heating element setting, ambient temperature and relative humidity of 20°C&50% and no tube heating

259

Appendix XVIII. In-tube condensation with normal breathing and deep breathing induced fluctuation under conditions of 4cmH₂O with reverse flow
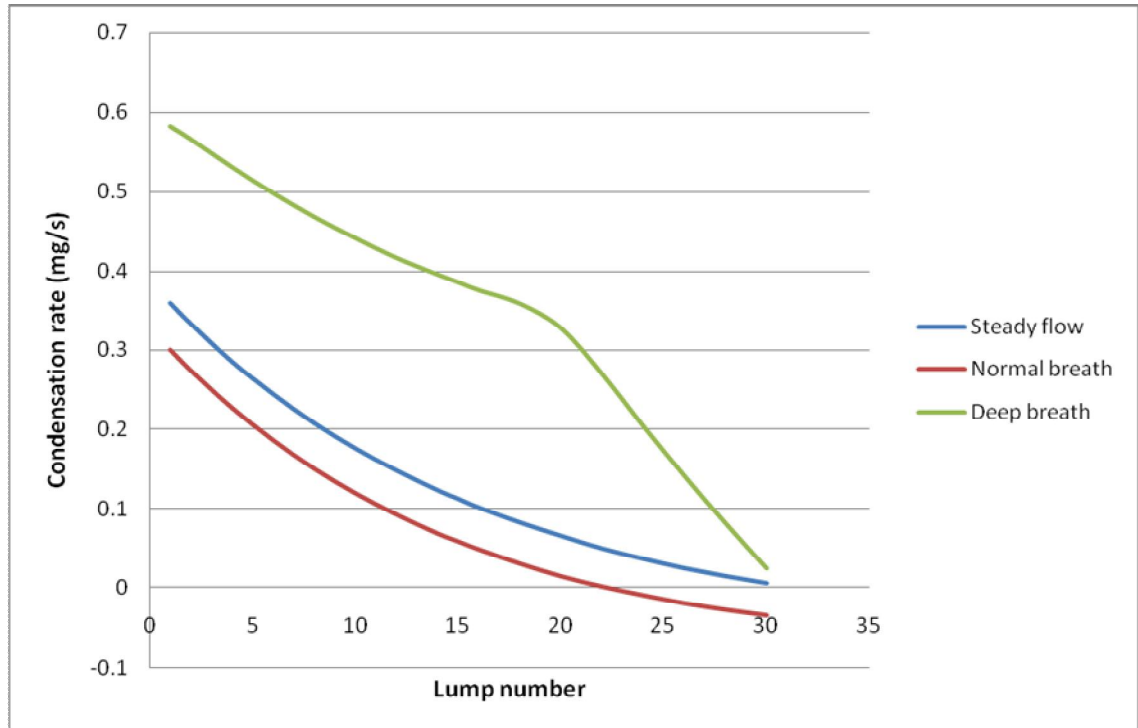
Figure XVIII. 1 In-tube condensation of steady flow, breathing added fluctuating flows under conditions of 4cmH₂O, 55°C, 0W, 22°C&20% (condensation occurs when curve is below zero)

Figure XVIII. 1 shows that the normal breathing condensation/evaporation curve is below that of the steady flow. The normal breathing induced fluctuation makes the condensation start to occur in the last lumps of the HADT. This is firstly because of the concavity factor which drags the curve towards the X-axial, secondly because of the condensation-to-evaporation coefficient factor, especially in the larger numbered lumps. Figure XVIII. 2 and Figure XVIII. 3 support the explanation. In these graphs, it can be seen that for normal breathing, the condensation and evaporation are alternatively occurring thus the condensation-to-evaporation coefficient plays a role.

Figure XVIII. 2 Condensation/evaporation rate in lump 1 under conditions of normal breathing, 4cmH₂O pressure setting, 55°C heating element setting, ambient temperature and relative humidity of 22°C&20% and no tube heating
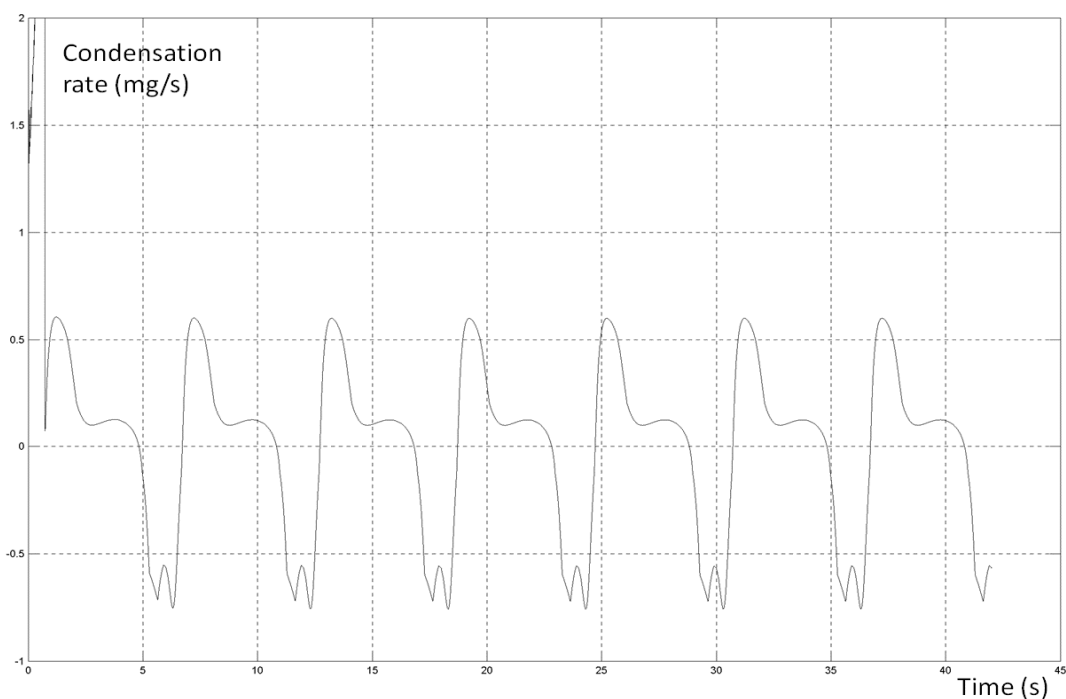
Figure XVIII. 3 Condensation/evaporation rate in lump 30 under conditions of normal breathing, 4cmH₂O pressure setting, 55°C heating element setting, ambient temperature and relative humidity of 22°C&20% and no tube heating

When under deep breathing, the flow rate fluctuation amplitude becomes much greater. The portion of airflow travelling at much higher velocity through the chamber gains less

261

humidity. Because of the high velocity, the dry portion coincides with high velocity in most of the lumps in this case. This vaporization potentiality (coincidence factor) overcomes the condensation-to-evaporation coefficient factor. This can explain why the first section of the deep breathing condensation/evaporation curve is significantly above the normal breathing curve and the steady flow curve. The graph also shows that the second section of the deep breathing curve drops sharply. This is because the exhaled air with higher humidity reaches these lumps and flows through these lumps twice. This high humidity reverse flow crosses off some of the vaporization potentiality. More details about the real-time condensation are explained below.
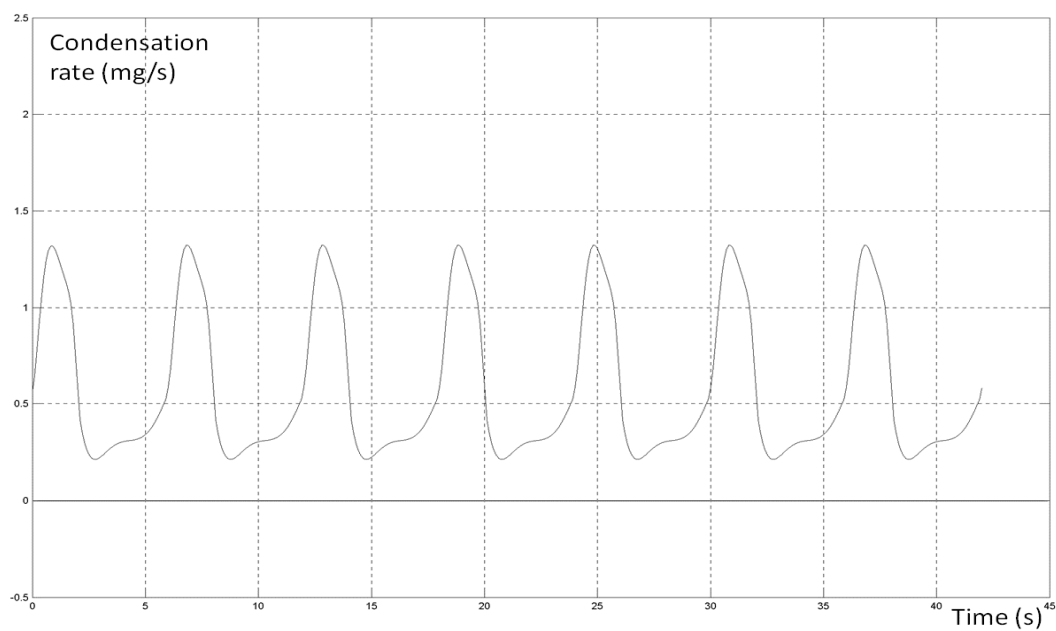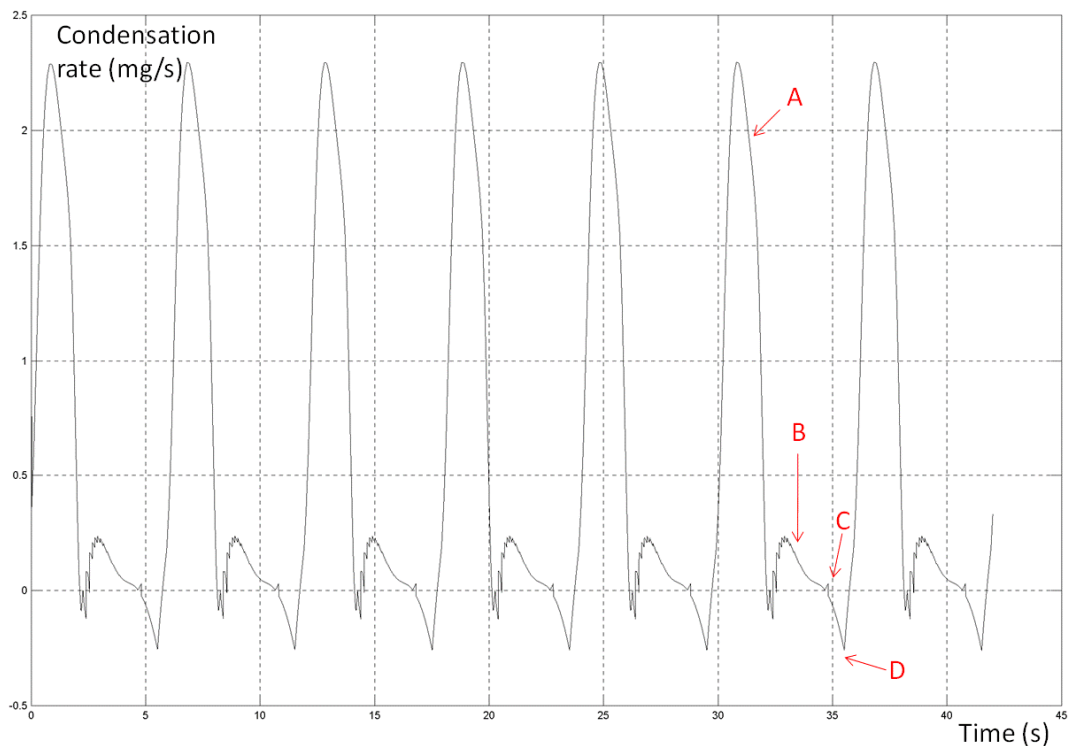

Figure XVIII. 4 Condensation/evaporation rate in lump 1 under conditions of deep breathing, 4cmH$_2$O pressure setting, 55°C heating element setting, ambient temperature and relative humidity of 22°C&20% and no tube heating

The real-time situation related to condensation is more complicated when there is reverse flow. Figure XVIII. 4 shows the condensation rate in lump 1. During inhalation, the high velocity coincides with the dry portion of air provides a very high peak of vaporization potentiality (point A in the graph). Around point B, certain amount of the air just flew through (some of the portion of A) flows back from bigger-numbered lumps because of reverse flow. The reverse flow is at a comparatively much lower velocity thus low convection rate therefore the B point is much lower than point A. When the reverse flow stops and positive flow resumes, the very short portion of air between the chamber and lump 1 flows through lump 1 again and forms the small peak

at point C. Right after that, here comes the very highly humidified portion of air which has flown over the water surface for three times because of the reverse flow. This portion flows on with a very high humidity but at a quite low velocity and forms the trough D (means condensation). Following this highly humid portion is the air the first time entering the chamber from the blower and ambient. This portion is drier and makes the curve returns back to above zero again. Then the next inhalation starts and the high velocity along with dry air makes a high peak of vaporization potentiality again (replica of point A). From the graph, it is clear that the overwhelming factor is the vaporization potentiality created by the coincidence of dry air and high velocity. This can explain why the first section of the deep breathing condensation/evaporation curve is significantly above the normal breathing curve and the steady curve.
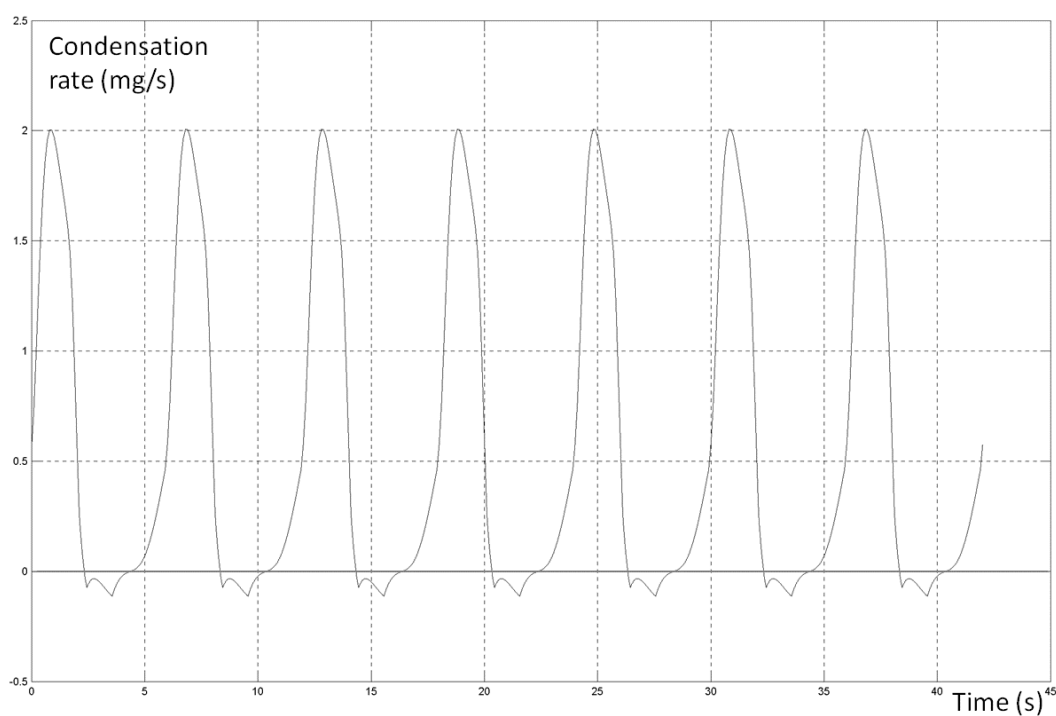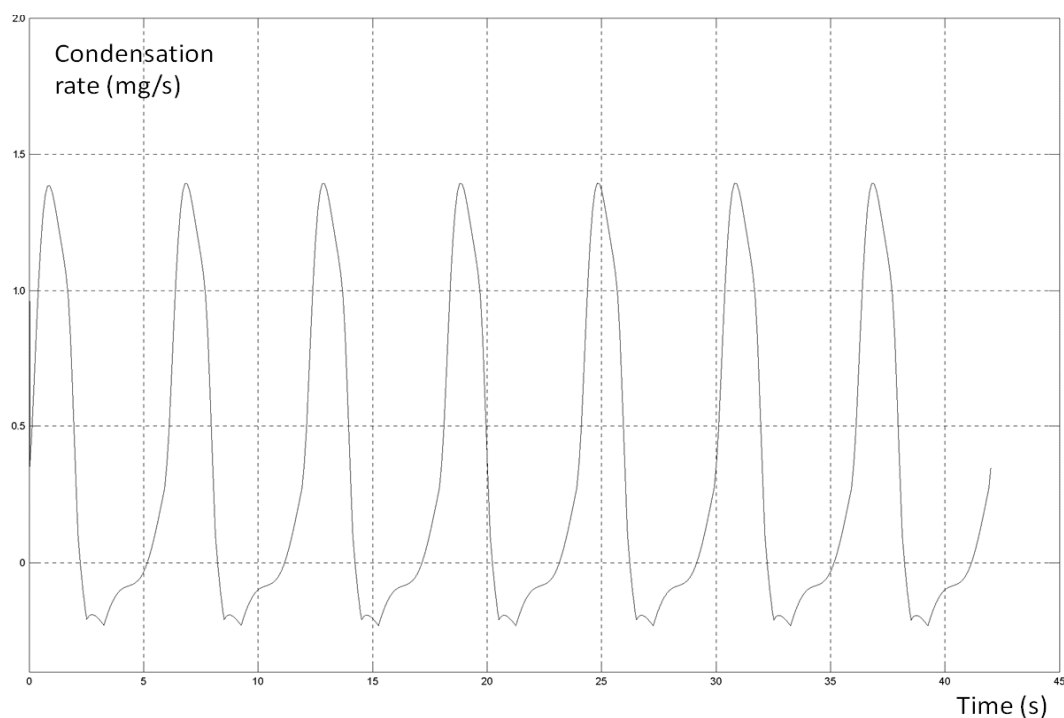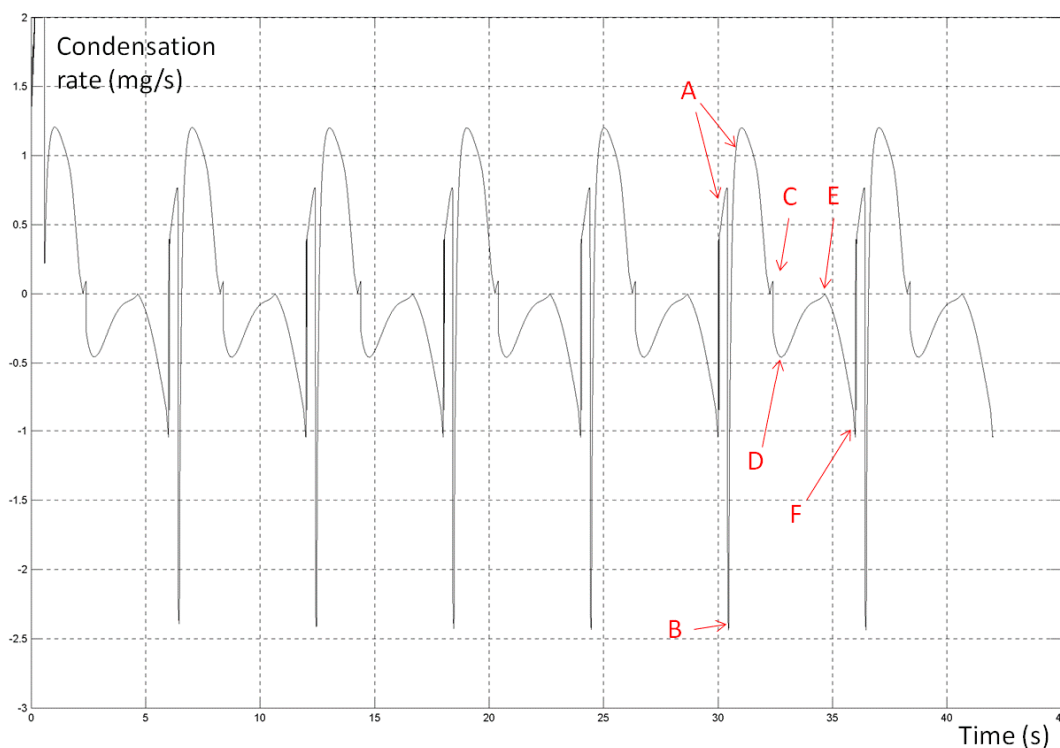

Figure XVIII. 5 Condensation/evaporation rate in lump 30 under conditions of deep breathing, 4cmH$_2$O pressure setting, 55°C heating element setting, ambient temperature and relative humidity of 22°C&20% and no tube heating

Figure XVIII. 5 shows the condensation rate in lump 30. At the beginning of a breath cycle, inhalation drags the drier portion of air flowing through very fast and makes a high peak of vaporization potentiality. Within this peak, there is a steep gorge (point B) which represents the very humid three-times-over-water portion travelling through this lump at a very high velocity. Reverse flow starts right before point C, the small peak of point C represents the fresh air stayed in the mask now being pushed back into the HADT. After this "maskful" of fresh air comes the exhaled air with very high humidity

which makes the trough D. the reverse flow stops at point E. After this, the positive flow resumes, the exhaled air in the HADT flows through lump 30 again now at a higher positive velocity creates a deeper trough around point F. After the exhaled air has passed, drier fresh air stayed in the upstream lumps during reverse flow phase now creates the first part of vaporization potentiality before the steep gorge of the new three-times-over-water portion. This is another cycle's start. From the graph, it is can be seen that condensation is mainly because of the exhaled air (Points D and F). However, the high vaporization potentiality (point A) offsets a significant amount of the condensation and makes the overall net condensation/evaporation within a breath cycle not very different from that of normal breathing.

Appendix XIX. Coefficient and parameter values for natural convection Nusselt number

The natural convection Nusselt number in this thesis has the form of [47]:

$$Nu = C \cdot Ra^n$$

The values for C and n for different situations are listed in table below:

Situation	C	n
Horizontal surface with hotter surface facing up or cooler surface facing down [47]	0.54	1/4
Vertical surface [47]	0.59	1/4
Horizontal cylinder outer surface [55]	1.02	0.148

Appendix XX.   Modelling parameters and constants

Geometric parameters		
Blower outlet diameter	19.2 mm	
Connecting duct central line length	200 mm	
Chamber average inner diameter	100 mm	Lower part
Chamber average inner diameter	98.5 mm	Upper part
Chamber wall thickness	1.2 mm	
Water level	65 mm	Fully filled
Water volume	600 ml	Fully filled
Chamber air volume	206 ml	Fully filled
Water surface diameter	99 mm	Fully filled
Water-chamber base contact surface diameter	107 mm	
Chamber top (wall 3) diameter	98 mm	
Chamber air part wall height	25 mm	
HADT length	1.725 m (1725 mm)	
HADT inner diameter	19.2 mm	
HADT film outside diameter	19.3 mm	
HADT lump wall mass	6.41 g	
Nasal mask capacity*	70 ml	
Nasal mask inner height	3.5 mm	Also width of rectangular plates
Width of nasal mask inner triangular plate	6 mm	Length of inner rectangular side plates
Mask wall thickness	1.2 mm	
Total bias vent area	1.5264×10^{-5} m^2 (15.264 mm^2)	
Nasal mask capacity	70 ml	
Full-face mask capacity	236.25 ml	
Average nose width	38 mm	
Average nose volume	32 cm^3	

Fluid properties		
Average water thermal conductivity	0.644 W/m·K	At 50°C
Specific heat of water	4186 J/kg·K	
Average molar mass of air in CPAP system	28.61 g/mole	
Average air thermal conductivity	0.02575 W/m·K	At 30°C
Average specific heat of dry air	1006 J/kg·K	
Average specific heat of vapour	1865 J/kg·K	
Average specific heat of moist air for this thesis	1035 J/kg·K	
Average air density in the connecting duct	1.176 kg/m^3	
Average air density in the chamber	1.14 kg/m^3	
Average air density in HADT	1.143 kg/m^3	
Average air density in the mask	1.14 kg/m^3	
Average dynamic viscosity of air	1.87×10^{-5} kg/m·s	
Average mass diffusivity of water molecules in air	2.71×10^{-5} m^2/s	
Prandtl number of air	0.711	
Average β·Pr/ν2 for chamber outer surface	8.639×10^6 (s^2/m^4·K)	Combined coefficient β·Pr/ν2 for Grashof number of air
Average β·Pr/ν2 for in-chamber air	8.251×10^6 (s^2/m^4·K)	
Average β·Pr/ν2 for HADT outer surface	9.998×10^6 (s^2/m^4·K)	
Average β·Pr/ν2 for mask outer surface	9.971×10^6 (s^2/m^4·K)	
Average β·Pr/ν2 for in-mask air	9.045×10^6 (s^2/m^4·K)	
Average air mass in the chamber	2.348×10^{-4} kg	
Average air mass in one HADT lump	1.902×10^{-5} kg	

Other parameters and constants		
Gravity acceleration	9.81 m/s^2	
Stefan-Boltzmann constant	5.67×10^{-8} W/m^2·K^4	
Emissivity of high density Polyethylene	0.85	
Thermal conductivity of high density Polyethylene	0.48 W/m·K	

* For full-face mask, the one-dimensional size is simplified as 1.5 times of nasal mask and the capacity is 3.375 times of nasal mask.

Appendix XXI. Fluid dynamic and thermal dynamic experiments setup for future validation

XXI.1 Validation of dynamic fluctuating airflow velocity and reverse flow in HADT

The setup for airflow velocity and reverse flow in HADT can be as below:
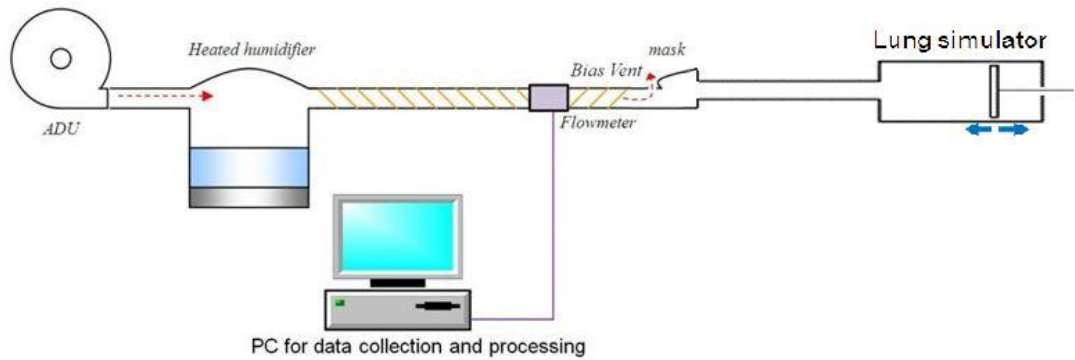
Figure XXI. 1 The setup for measuring the fluctuating airflow velocity and reverse flow in HADT

The measurement can start after the "breath load" from the lung simulator is adjusted. The two sections of tube between the chamber and the mask should be the same length of a single HADT. The NDD Ultrasonic Flow Sensor's fluctuating reading will be compared with the model output. When the reading is negative, it means there is reverse flow. The sum of these negative reading multiplied by the reading interval will be the experimental result of how far the reverse flow can go. This will be compared with the output from model.

XXI.2 Validation of CO2 re-breathing

Since CO_2 is colourless, transparent and odourless, it is difficult to measure or observe the re-breath of CO_2 or exhaled air. Smoke can be used to measure the re-breath. The setup is shown in Figure XXI. 2 below.
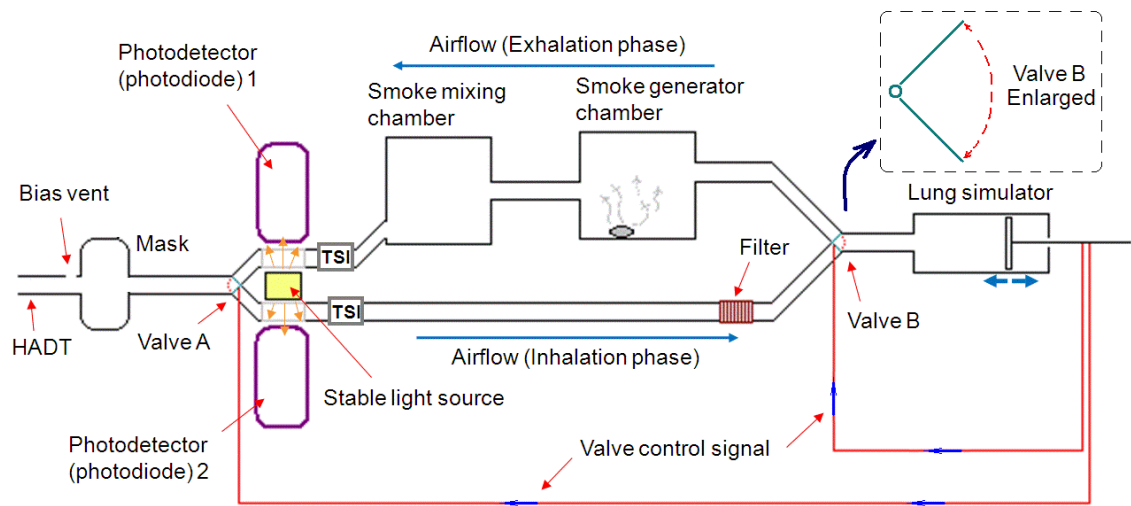
Figure XXI. 2 Experimental setup for CO2 re-breathing validation

There are two separate channels for exhalation phase flow and inhalation phase flow to guarantee the "exhaled" air has a consistent concentration of smoke. Besides the lung simulator, the CPAP and the mask, the components of the setup and their functions are listed below.

Table XXI. 1 Components in CO_2 re-breathing validation experimental setup and their functions

Component	Function
Two flipper valves	To direct the flow to the proper channel
Smoke generating chamber	To provide smoke
Smoke mixing chamber	To even smoke concentration
Flow meters	To check the breath load before measurement
Stable light source	To provide light to the photo-detectors
Two photo-detectors	To continuously record the smoke concentration in airflow
Smoke filter	For providing a stable smoke thickness for next breath cycle and for protecting the lung simulator cylinder

The flow meters are used to check the breath load before the measurement is conducted. Since the exhalation phase channel is different from the inhalation channel, the inhalation phase breath load and the exhalation phase breath load should be separately adjusted. The light source and the photodetectors should have been calibrated before experiment is conducted.

The lung simulator drives the air. The two valves are controlled by the phase turning of the lung simulator which keeps in phase between the valves flipping and the lung simulator direction change. When exhalation phase starts, the valves close the inhalation channel and let the air only flows through the exhalation channel towards the mask (the upper part through the two chambers).

The smoked air flows through the photodetector 1, the thickness (concentration) of the smoke will give reading in the photodetector 1 and be continuously recorded. When inhalation phase starts, the valves are flipped to close the exhalation channel and open the inhalation channel. The air flows through the photodetector 2, the thickness of the smoke (if any) will give reading in the photodetector 2 and also be continuously recorded. The calibrated reading from the photodetectors will be compared and the thickness (concentration) of the smoke in the inhaled air can be calculated.

XXI.3 Validation of HADT condensation comparison between steady state and breathing-added situation

As for the experimental validation of the HADT condensation, the setup can be designed as shown in Figure XXI. 3. However, the experiment has not been conducted due to instrument availability.
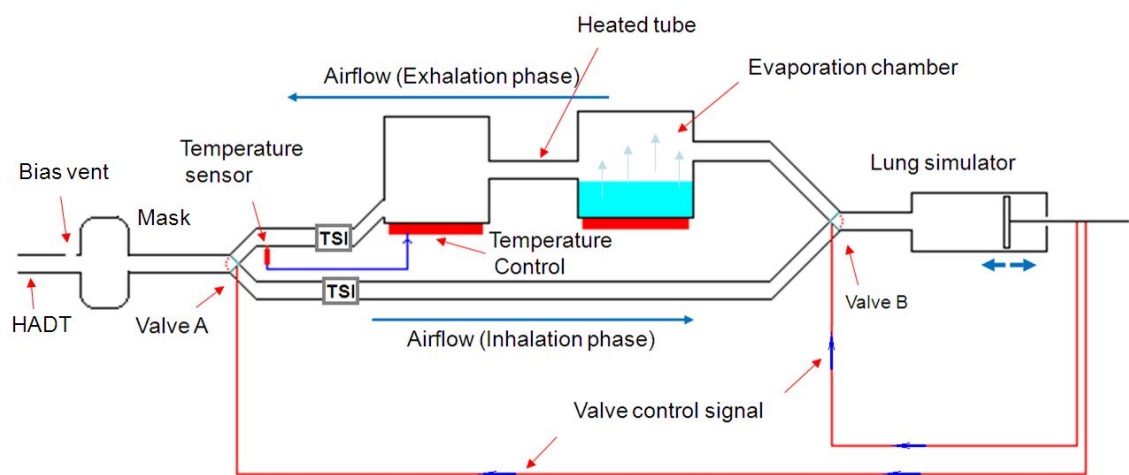
Figure XXI. 3 Experimental setup for validation of HADT condensation with reverse flow

The whole experiment is to validate the reverse flow's influence on the HADT condensation. The purpose of this part of the setup shown above is to obtain an airflow mimicking the thermal properties of exhaled air. That is a 33°C~34°C and fully saturated airflow from the lung simulator to the mask. Ideally, there is another CPAP machine next to it running under steady flow for reference.

Some of the components are same as those used in CO_2 re-breathing validation experiment. The different components and their functions are listed in table below.

Table XXI. 2 Components in dynamic HADT condensation validation experimental setup and their functions

Component	Function
Evaporation chamber	To generate a highly humidified airflow
Heated tube	To keep the temperature of the airflow
Temperature control chamber	To be adjusted so to obtain the required temperature of airflow to the mask
Temperature sensor	To measure the airflow temperature and give signal to control the heating of the temperature control chamber

The air is heated and highly humidified in the evaporation chamber. The specific humidity of the outlet from the evaporation chamber should be higher than the saturated specific humidity at 34°C. The temperature control chamber is adjusted to assure the air temperature at the sensor is 34°C. The airflow temperature all along the way should be no lower than 34°C so to guarantee the airflow saturation at the temperature sensor. The temperature control chamber can also work as a mixing chamber so to provide more stable airflow temperature and humidity under such fluctuating situation. Condensation may occur along the way, condensate collecting sacks may be needed.

Appendix XXII.   Model user instruction

This appendix is a manual of using the Simulink models. These models require MATLAB 2006a or later academic version. The simulation time period should be set as a integer multiple of the breath cycle.

XXII.1   The Fluid dynamic and re-breathing model

The input blocks in this model are shadowed. The "normal" patient's breath load provided in this model is shown below. The patient's breath load and the shape can be adjusted or replaced when necessary.
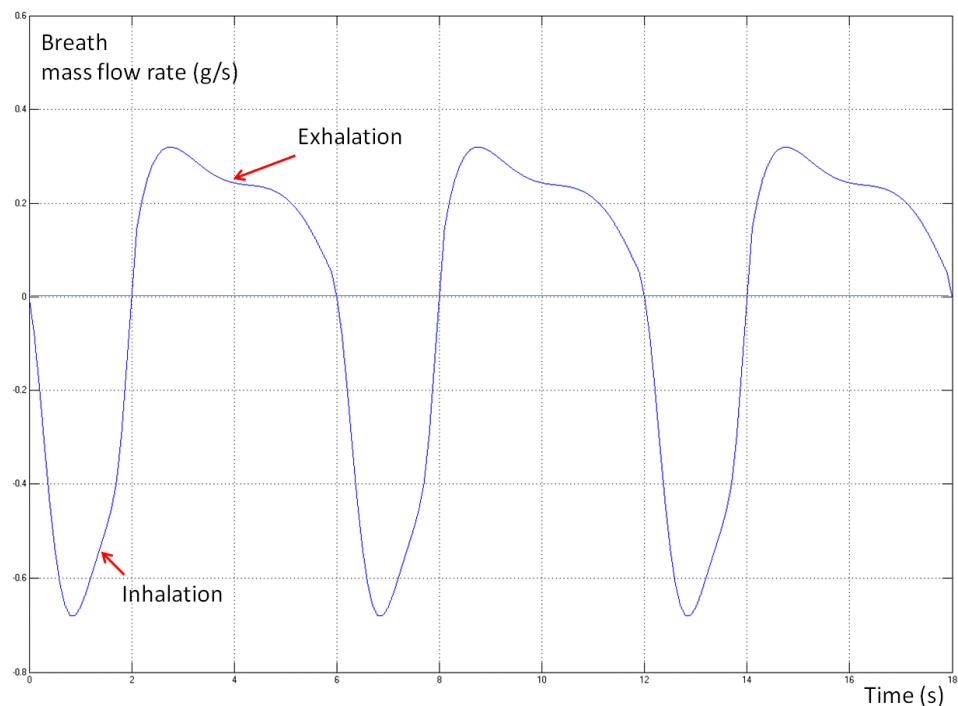
Figure XXII. 1 Patient's normal breath load

The other input blocks and their values are listed in table below:

Table XXII. 1 Fluid dynamic and re-breathing model input blocks and their values

Input block	Value	Condition
Pressure setting	4 ~ 20 cmH$_2$O	Same as CPAP machine pressure settings
Breath magnitude ratio	0	Steady state (no breathing)
	0.663	500 ml breath load
	1	Normal breathing
	2	Deep breathing

Mask capacity ratio	1	Nasal mask
	1.5	Full-face mask
Human nose in-mask space occupancy factor	0	No nose occupancy (with lung simulator)
	1	There is nose occupancy (Test on human breath)

The outputs are Scope or Display blocks which are foreground-colored in blue. They are listed below:

Table XXII. 2 Fluid dynamic and re-breathing model output blocks

Output	Unit	Scope/Display
Breath load	(gram/breath cycle)	Scope
Pressures at ADU outlet, the chamber and the mask	Pa	Scope
Flow velocity in the connecting duct	m/s	Scope
Flow velocity in HADT	m/s	Scope
Backflow (reverse flow)	m	Scope
Backflow (reverse flow) distance	m	Display
Exhaled air level in lumps	Normalized (0~1)	30 scopes for each lump
Exhaled air level in the mask	Normalized (0~1)	Scope
Percentage of exhaled air in next inhalation	Percentage	Display
Percentage of CO_2 in next inhalation	Percentage	Display

XXII.2   The thermodynamic model

The input blocks in this model are shadowed. The patient's breath load and the shape can be adjusted or replaced when necessary except change of breath cycle time for this thermodynamic model.

The input blocks and their values are listed in table below:

Table XXII. 3 Thermodynamic model input blocks and their values

Input block	Value	condition
Breath magnitude ratio	0	Steady state (no breathing)
	0.663	500 ml breath load
	1	Normal breathing
	2	Deep breathing
Mask capacity ratio	1	Nasal mask
	1.5	Full-face mask
Human nose in-mask space occupancy factor	0	No nose occupancy (with lung simulator)
	1	There is nose occupancy (Test on human breath)
Pressure setting	4 ~ 20 cmH$_2$O	Same as CPAP machine pressure settings
Heat element temperature setting	45 ~ 65 °C	Same as the machine heat element temperature settings
HADT tube heating	0 ~ 30 W	Same as the machine tube heating settings
Ambient temperature	14 ~ 33 °C	Validated range
Ambient relative humidity	0 ~ 1	0 ~ 1 represents 0 ~ 100% of relative humidity (e.g. input 0.5 for RH=50%)

The outputs are Scope or Display blocks can be categorized as steady state and dynamic. The steady state ones are red coloured and the dynamic ones are dark-green coloured. They are listed below:

Table XXII. 4 Thermodynamic model output blocks

Output	Unit	Scope/Display
Steady state		
Chamber water temperature	°C	Display
Steady state chamber air temperature	°C	Display
Steady state evaporation rate	kg/s	Display
Steady state chamber air specific humidity	Decimal	Display

Steady state air temperature at HADT lump	°C	30 displays for each lump
HADT lump wall temperature	°C	30 displays for each lump
Gap between lump wall temperature and airflow dew point	°C	30 displays for each lump
Mask wall temperature	°C	Display
Steady state mask air temperature	°C	Display
Dynamic		
Dynamically fluctuating chamber air specific humidity	Decimal	Scope
Averaged dynamic chamber air specific humidity	Decimal	Display
Dynamically fluctuating evaporation rate in the chamber	kg/s	Scope
Averaged dynamic evaporation rate in the chamber	kg/s	Display
Dynamically fluctuating chamber air temperature	°C	Scope
Averaged dynamic chamber air temperature	°C	Display
In-HADT airflow velocity comparison between steady flow and fluctuating flow	m/s	Scope
Dynamically fluctuating air specific humidity at HADT lump	Decimal	Scope
Dynamically fluctuating air temperature at HADT lump	°C	Scope
Dynamically fluctuating condensation/evaporation rate at HADT lump	kg/s	Scope
Net condensation/evaporation rate at HADT lump in a breath cycle	kg/s	Display
Dynamically fluctuating air specific humidity in the mask	Decimal	Scope

Dynamically fluctuating air temperature in the mask	°C	Scope
Dynamically fluctuating condensation/evaporation rate in the mask	kg/s	Scope
Net condensation/evaporation rate in the mask over a breath cycle	kg/s	Display
Averaged specific humidity in inhaled air	kg/s	Display
Averaged temperature of inhaled air	°C	Display

XXII.3 The steady state thermal model

Due to the complexity and size of the thermodynamic model which make the simulation slow, a steady state thermal model is also provided. The input blocks in this model are shadowed.

The input blocks and their values are listed in table below:

Table XXII. 5 Thermodynamic model input blocks and their values

Input block	Value	condition
Mask capacity ratio	1	Nasal mask
	1.5	Full-face mask
Pressure setting	4 ~ 20 cmH$_2$O	Same as CPAP machine pressure settings
Heat element temperature setting	45 ~ 65 °C	Same as the machine heat element temperature settings
HADT tube heating	0 ~ 30 W	Same as the machine tube heating settings
Ambient temperature	14 ~ 33 °C	Validated range
Ambient relative humidity	0 ~ 1	0 ~ 1 represents 0 ~ 100% of relative humidity (e.g. input 0.5 for RH=50%)

The outputs are Display blocks. They are listed below:

Table XXII. 6 Thermodynamic model output blocks

Output	Unit	Number of the display blocks
Steady state		
Chamber water temperature	°C	1
Steady state chamber air temperature	°C	1
Steady state evaporation rate	kg/s	1
Steady state chamber air specific humidity	Decimal	1
Steady state air temperature at HADT lump	°C	30 displays for each lump
HADT lump wall temperature	°C	30 displays for each lump
Gap between lump wall temperature and airflow dew point*	°C	30 displays for each lump
Condensation/evaporation rate at HADT lump	kg/s	30 displays for each lump
Mask wall temperature	°C	1
Steady state mask air temperature	°C	1

* The condensation predicted by dew point is closer to the experimental observation.

References

[1]   Good sleep advice. Why is quality sleep so important?   [cited 12 April 2007]; Available from: http://goodsleepadvice.com/3-whyquality.html

[2]   Sleep-Wake Disorders Center of South Florida Inc. SLEEP WAKE DISODERS. [cited 11 May 2007]; Available from: http://www.sleepwakesfl.com/frontpage.html

[3]   National Institute of Neurological Disorders and Stroke. NINDS Sleep Apnea Information Page 2007 [cited 8 July 2007]; Available from: http://www.ninds.nih.gov/disorders/sleep_apnea/sleep_apnea.htm#What_is

[4]   Lyle D.V. Obstructive Sleep Apnea. 1999 [cited 8 June 2008]; Available from: http://www.aafp.org/afp/991115ap/2279.html

[5]   American Academy of Family Physicians. Sleep apnea.   [cited 21 April 2007]; Available from: http://familydoctor.org/online/famdocen/home/articles/212.html

[6]   Sleep Disorders Center: Sequoia Health Services, Redwood City California. Sleep Apnea.   [cited 7 June 2008]; Available from: http://www.sleepscene.com/apnea.htm

[7]   American sleep apnea association. SLEEP APNEA INFORMATION.   [cited 7 June 2008]; Available from: http://www.sleepapnea.org/info/index.html

[8]   Henry Ford Medical Group. Sleep apnea.   August 2006 [cited 7 June 2008]; Available from: http://www.henryfordhealth.org/body.cfm?id=39639&action=articleDetail&AEProductID=Adam2004_1&AEArticleID=000811&crawl=false

[9]   Dental organization for sleep apnea. Oral appliances.   [cited 7 June 2008]; Available from: http://www.apneadocs.com/pages/Appliances.htm

[10]   21st Century Dental. Sleep Apnea and Snoring [cited 7 June 2008]; Available from: http://www.21stcenturydental.com/smith/sleepapena_tapappliance.htm

[11]   Essig M. Uvulopalatopharyngoplasty for obstructive sleep apnea. 2007 [cited 8 June 2008]; Available from: http://www.ghc.org/kbase/topic.jhtml?docId=hw48958&secId=hw48960

[12]   Essig M. Laser-assisted uvulopalatoplasty. 2007 [cited 8 June 2008]; Available from: http://www.ghc.org/kbase/topic.jhtml?docId=aa75802&secId=aa75802-sec

[13]   Sleep Apnea Surgery Center. surgical solution for adults - Nasal surgery.   [cited 8 June 2008]; Available from: http://www.sleepapneasurgery.com/nasal_surgery.html

[14]   Woodson B.T. Surgical Approaches to Obstructive Sleep Apnea. 2001 [cited 8 June 2008]; Available from: http://healthlink.mcw.edu/article/994957808.html

[15] Australia Innovates. CPAP sleep apnea control - machine to maintain breathing during sleep. [cited 8 June 2008]; Available from: http://www.powerhousemuseum.com/australia_innovates/?behaviour=view_article&Section_id=1030&article_id=10025

[16] The National Heart, Lung, and Blood Institute. How Is Sleep Apnea Treated? [cited 8 June 2008]; Available from: http://www.nhlbi.nih.gov/health/dci/Diseases/SleepApnea/SleepApnea_Treatments.html

[17] Piccirillo JF, Duntley S, Schotland H. Obstructive Sleep Apnea. JAMA. 2000 September 27, 2000;284(12):1492-4.

[18] American Sleep Apnea Association. Sleep apnea information and resources. 1999 [cited 8 June 2008]; Available from: http://www.stanford.edu/~dement/apnea.html

[19] Sun Y-C. CPAP system modelling [Master's degree]: Auckland University of Technology; 2005.

[20] British Thoracic Society, The sleep apnoea trust association. New patient information sheet. [cited 7 June 2008]; Available from: http://www.sleep-apnoea-trust.org/media/patient_empowerment_document.pdf

[21] Crystal G. What is BiPAP? [cited 9 June 2008]; Available from: http://www.wisegeek.com/what-is-bipap.htm

[22] Loube DI. Technologic Advances in the Treatment of Obstructive Sleep Apnea Syndrome. Chest. 1999 November 1, 1999;116(5):1426-33.

[23] Pevernagie D, Masa JF, Meurice JC, Farre R, Marrone O, Rodenstein D. Treatment of obstructive sleep-disordered breathing with positive airway pressure systems. EUROPEAN RESPIRATORY REVIEW. 2007 December 1, 2007;16(106):125-31.

[24] Behbehani K. K. Automatic control of airway pressure for treatment of obstructive sleep apnea. IEEE transactions on biomedical engineering. 10/1995;42 (10):1007-16.

[25] Rauch M. Making CPAP Work. RT for Decision Makers in Respiratory Care 2003 [cited 1 November 2007]; Available from: http://www.rtmagazine.com/issues/articles/2003-06_04.asp

[26] Illinois Department of Public Health, Division of Environmental Health. Illinois Department of Public Health Guidelines for Indoor Air Quality [cited 1 September 2008]; Available from: http://www.idph.state.il.us/envhealth/factsheets/indoorairqualityguide_fs.htm

[27] Carbon Dioxide Information Analysis Center, US Deparment of Energy. Frequently Asked Questions - How much carbon dioxide is exhaled with each breath? . [cited 20 August 2008]; Available from: http://cdiac.esd.ornl.gov/pns/faq_othr.html

[28]   Schettino GPP, Chatmongkolchart S, Hess D, Kacmarek R. Position of exhalation port and mask design affect CO2 rebreathing during noninvasive positive pressure ventilation. Critical Care Medicine 2003 August 31(8):2178-82.

[29]   ResMed. Humidification-Vicious Cycle. 2008 [cited 2008 10 June]; Available from:
http://www.resmed.com/en-us/clinicians/compliance_and_efficacy/humidification.html?menu=clinicians

[30]   Patroniti N, Foti G, Pesenti A. Conditioning of Inspired Gases in Mechanically Ventilated Patients. In: Vincent J-L, ed. *Intensive Care Medicine: Annual Update 2002*: Birkhäuser 2003:p279.

[31]   Guyton AC, Hall JE. Textbook of medical physiology. 10th ed: W. B. Saunders 2000:p441.

[32]   Mador MJ, Krauza M, Pervez A, Pierce D, Braun M. Effect of Heated Humidification on Compliance and Quality of Life in Patients With Sleep Apnea Using Nasal Continuous Positive Airway Pressure. Chest. 2005 October 1, 2005;128(4):2151-8.

[33]   McNicholas WT. Follow-Up and Outcomes of Nasal CPAP Therapy in Patients with Sleep Apnea Syndrome. Monaldi Archives for Chest Disease. 2001 56(PART 6):535-9

[34]   Massie CA, Hart RW, Peralez K, Richards GN. Effects of Humidification on Nasal Symptoms and Compliance in Sleep Apnea Patients Using Continuous Positive Airway Pressure. Chest. 1999 August 1, 1999;116(2):403-8.

[35]   Hayes MJ, McGregor FB, Roberts DN, Schroter RC, Pride NB. Continuous nasal positive airway pressure with a mouth leak: effect on nasal mucosal blood flux and nasal geometry. Thorax. 1995 November;50(11):1179–82. .

[36]   Bacon JP, Farney RJ, Jensen RL, Walker JM, Cloward TV. Nasal Continuous Positive Airway Pressure Devices Do Not Maintain the Set Pressure Dynamically When Tested Under Simulated Clinical Conditions. Chest. 2000 November 1, 2000;118(5):1441-9.

[37]   White DE. Breathing therapy air delivery unit: simulation, design and development [Master's degree]: Auckland University of Technology; 2003.

[38]   Zhen ZF. CPAP mask thermo-fluid dynamic for carbon dioxide and condensation reduction [Master's degree]: Auckland University of Technology; 2005.

[39]   Nakayama Y. Introduction to fluid mechanics. London: Arnold 1999.

[40]   Alden JL. Design of industrial exhaust systems. 3rd. ed. New York: Industrial Press 1959.

[41]   Francis JRDd. A textbook of fluid mechanics for engineering students. London: Edward Arnold 1958.

[42]   1993 ASHRAE handbook: fundamentals. S.I. ed. Atlanta, Ga.: American Society of Heating 1993.

[43]   Douglas JF, Swaffield JA. Fluid mechanics. 4th ed. Upper Saddle River, NJ: Prentice Hall 2000.

[44]   Merritt HE. Hydraulic Control Systems: John Wiley & Sons, Inc. 1967.

[45]   Miller RW. Flow measurement engineering handbook: McGraw-Hill Book Company 1983.

[46]   Newman EV, Merrell M, Genecin A, Monge C, Milnor WR, McKeever WP. The Dye Dilution Method for Describing the Central Circulation: An Analysis of Factors Shaping the Time-Concentration Curves. Circulation. 1951 November 1, 1951;4(5):735-46.

[47]   Cengel YA. Fundamentals of thermal-fluid sciences. Boston: McGraw-Hill 2001.

[48]   Sonntag RE, Van Wylen GJ, Van Wylen GJ. Fundamentals of thermodynamics. 6th ed. New York: Wiley 2003.

[49]   Cengel YA. Heat transfer: a practical approach. 2nd ed. Dubuque, Iowa: McGraw-Hill 2002.

[50]   Cengel YA. Introduction to thermodynamics and heat transfer. International ed. New York: McGraw-Hill 1997.

[51]   Bejan A. Heat transfer handbook. New York: J. Wiley 2003.

[52]   Incropera FP. Introduction to heat transfer. 4th ed. New York: Wiley 2002.

[53]   Ruckenstein E. A Simple Algebraic Method for Obtaining the Heat or Mass Transfer Coefficients under Mixed Convection. Chemical engineering communications. 1980 4(1).

[54]   Ghoshdastidar PS. Heat transfer. Oxford; New York: Oxford University Press 2004.

[55]   Welty JR. Fundamentals of momentum, heat, and mass transfer. 4th ed. New York: Wiley 2001.

[56]   Mills AF. Mass transfer. Upper Saddle River, N.J.: Prentice Hall 2001.

[57]   Rohsenow WM. Handbook of heat transfer. 3rd ed. New York: McGraw-Hill 1998.

[58]   Incropera FP. Fundamentals of heat and mass transfer. 5th ed. New York: J. Wiley 2002.

[59]   Infrared services I. Emissivity values for common materials.   [cited 12, Sept. 2007]; Available from: http://www.infrared-thermography.com/material-1.htm

[60]   Marek R, Straub J. Analysis of the evaporation coefficient and the condensation coefficient of water. International Journal of Heat and Mass Transfer. 2001;44(1):39-53.

[61]   The engineering toolbox. Psychrometric Table of Moist Humid Air Properties [cited 2007 12 April]; Available from: http://www.engineeringtoolbox.com/moist-air-properties-d_1256.html

[62]   Varjão FM, Nogueira SS. Nasal Width as a Guide for the Selection of Maxillary Complete Denture Anterior Teeth in Four Racial Groups. Journal of Prosthodontics. 2006;15(6):353-8.

[63]   Bloomer JJ. Practical fluid mechanics for engineering applications: Marcel Dekker Inc. 2000.

[64]   Erstich E, Milivojevic I. Functional Performance of the FlexFit 407: Nasal CPAP Mask. Test Report: Fisher and Paykel Healthcare Co. Ltd.; 2005.

[65]   Carl N. Stephan MHWS. Predicting nose projection and pronasale position in facial approximation: A test of published methods and proposal of new guidelines. American Journal of Physical Anthropology. 2003;122(3):240-50.

[66]   Ferrario VF, Sforza C, Serrao G. A three-dimensional quantitative analysis of lips in normal young adults. The Cleft palate-craniofacial journal. 2000 Jan;37(1):48-54.

[67]   Sun I. HC600 Chamber Water Usage under Real Ventilation Conditions. Test Report: Fisher and Paykel Healthcare Co. Ltd.; 2006.

[68]   Egan DF, Wilkins RL, Stoller JK, Scanlan CL. Egan's fundamentals of respiratory care. 8th / edited by Robert L. Wilkins, James K. Stoller ed. St. Louis, Mo.: Mosby 2003.

[69]   Doebelin EO. Measurement systems application and design. 5th ed. Maidenhead: McGraw-Hill Education 2003.

[70]   Jeffrey A. Mathematics for engineers and scientists. 6th ed. Boca Raton: Chapman & Hall/CRC 2005.

[71]   The engineering toolbox. Psychrometric Table of Moist Humid Air Properties. 2005 [cited 2007 16 April]; Available from:
 http://www.engineeringtoolbox.com/moist-air-properties-d_1256.html

[72]   Cengel YA. Thermodynamics: an engineering approach. 5th ed. Boston: McGraw-Hill Higher Education 2006.